INCREASING SURGE MARGIN OF TURBOCHARGER CENTRIFUGAL COMPRESSOR AUTOMOTIVE APPLICATION

Hani Mohtar

Ecole Centrale de Nantes

ÉCOLE DOCTORALE

SPIGA

2010

Thèse de DOCTORAT

SPECIALITE: DYNAMIQUE DES FLUIDES ET DES TRANSFERTS

PRESENTEE ET SOUTENUE PAR :

MOHTAR HANI

le 8 Juin à l'école Centrale de Nantes

INCREASING SURGE MARGIN OF TURBOCHARGER CENTRIFUGAL COMPRESSOR AUTOMOTIVE APPLICATION

ELARGISSEMENT DE LA PLAGE DE FONCTIONNEMENT D'UN TURBOCOMPRESSEUR DE SURALIMENTATION AUTOMOBILE

JURY

Président :	M. Gérard BOIS : Professeur - Laboratoire de Mécanique de Lille UMR 8107 ENSAM LILLE - Boulevard Paul Langerin 59655 Villeneuve d'Asq Cedex
Rapporteurs :	M. Georges DESCOMBES : Professeur - CNAM Paris - 292 rue Saint Martin 75141 Paris Cedex 3
	M. Farid BAKIR : Professeur - ENSAM Paris -151 Bd de l'Hôpital 75013, Paris
Examinateurs :	M. Pascal CHESSE : HDR – Responsable de l'Equipe Energétique des Moteurs à Combustion Interne - Ecole Centrale de Nantes - 1, rue de la Noë - 44321 Nantes Cedex 3 France
	M. David CHALET : Maître de Conférences – Equipe Energétique des Moteurs à Combustion Interne - Ecole Centrale de Nantes - 1, rue de la Noë - 44321 Nantes Cedex 3 France

Directeur de thèse : Chesse PASCAL

Laboratoire : Mécanique des fluides UMR CNRS 6598-Ecole Centrale de Nantes

Co-encadrant : David CHALET

Laboratoire : Mécanique des fluides UMR CNRS 6598-Ecole Centrale de Nantes

Acknowledgment

This research project would not have been possible without the support of many people. I wish to express my gratitude to my supervisor, Pascal CHESSE for his supervision, advice, and guidance from the very early stage of this research as well as giving me extraordinary experiences throughout the work. Deepest gratitude are also to the members of the supervisory committee, Associate Professor Dr David CHALET and Professor Jean-François HETET (supervisor during the first year of the thesis).

I gratefully thank the jury members: Professor Gérard BOIS (president), Professor Farid BAKIR and Professor Georges DESCOMBES, for their constructive comments on this thesis, and their very valuable advices.

I owe my deepest gratitude to Dr. Louis LARROSSIERE, for his support without whose knowledge and assistance this study would not have been successful. I would like to thank M. Nicolas BAINES for his advice and guidance.

Many thanks go in particular to Fabrice VIDAL (PSA) and Alain LEBFEVRE (Renault) for their valuable advices in science discussions, and furthermore.

Many thanks go in particular to Michel VIOLLEAU for his help. The turbocharger test bench would not have been existed without him. Many thanks also go to Jérome, Eric and Nicolas (industrial unit of the Ecole Centrale de Nantes), the pleasure working together for the fabrication of the different stabilization techniques.

It is a pleasure to thank those who participated to make this thesis possible: Pierre, Vincent, Sebastian, and Jeremy (internship students).

Special thanks also to Aline LEROCH (Department secretary) for her valuable help which facilitates the many administrative tasks. Thanks to my colleagues in the Internal Combustion Engine Team (EMCI) for their support.

Finally, I wish to express my love and gratitude to my beloved family, for their understanding & love, through the duration of my studies.

Special thanks to my big brother,

Nomenclature

Abbreviations

Abbreviation	Signification
AFR	Air to fuel ratio
BC	Basic Characteristics
BSA	Burst Spectrum Analyzer
DFR	Design flow rate
F	Functioning
FGVs	Flexible guide vane system
FVA	Flow Velocity Analyzer
GR	Groove configuration
GUM	Guide to the Expression of Uncertainty in Measurement
HFR	High flow rate
LFR	Low flow rate
MWE	Map width enhancer
NSs	New swirl system
P	Pinch configuration
PS	Pre-rotation system
RGVs	Radial inlet guide vane system
SG	Swirl generator
SGD	Swirl Generator Device
TPR	Total pressure ratio
TG	Tongue configuration
VIGVs	Variable inlet guide vane system
VGD	Variable geometry diffuser

Greek letters

Greek letter	Unit	Signification
α		Absolute flow angle with the tangential
β		Relative flow angle with the vertical
θ		Vane setting angle
δ		Standard uncertainity
γ		Heat capacity ratio
η_v		Volumetric efficiency
η_f		Fuel conversion efficiency
ρ	Kg/m^3	Density
η_{tt}		Total to total efficiency
δ		Friction coefficient
$\tilde{f}_H = \frac{f_H}{f_{rotor}}$		Helmholtz frequency
ϕ_C		Dimensionless compressor mass flow
ϕ_t		Dimensionless throttle mass flow
ω	rad/s	Helmholtz frequency , angular velocity
ψ		Dimensionless plenum pressure rise
ψ_C		Dimensionless pressure drop across compressor
ψ_t		Dimensionless pressure drop across throttle

Capital letters

Capital letter	Unit	Signification
A	m^2	Area
C	m/s	Absolute velocity
D	m	Diameter
E	J/kg	Energy
Z		Blade number
L	m	Length
V	m^3	Volume
K		Constant
R	mm	Radius
N	rpm	Rotational speed
Q	kg/s	Mass flow rate
P	Bar	Pressure
T	K	Temperature
$\bar{R}$	J/kg/K	Specific gas constant, for dry air
M		Mach number
A_C	m^2	Compressor duct area
A_{th}	m^2	Compressor throttle area
U	m/s	Rotor speed
V_{sw}	m^3	Cylinder swept volume
L_C	m	Equivalent compressor duct length
L_t	m	Equivalent throttle duct length
Q_f	J/kg	Energy available in the fluid per unit mass
W	m/s	Relative velocity
Re		Reynolds number

Small letters

Small letter	Unit	Signification
is		Isentropic
i	°	Incidence angle
b	m	Diffuser height, blade
tt		Total to total
a	m/s	Speed of sound
cr		Critical
a		Air
c		Compressor, corrected
t		Tip, total
th		Throat
h		hub
r	m	radius
p	m, bar	Perimeter, absolute static pressure
s		Entropy, standard deviation
e		error

Subscript

0	Inlet casing inlet, guide vane inlet
1'	Guide vane exit
1	Inducer inlet
2	Impeller exit and diffuser inlet
3	Diffuser exit and volute inlet
4	Inlet volute
5	Inlet exit cone [volute]
6	Volute exit
m	meridional
a	Air
c	Compressor
d	Diffuser, deviation
e	Exit
t	Tip
h	Hub
f	Fluid
th	Throat
atm	Atmospheric
act	Actual
int	Internal
s	Static
is	Isentropic
ref	Reference
cr	Critical
cs	Crank shaft
in	Incidence impeller

fi	Friction impeller
mix	Mixing
i	Impeller, inlet
v	Volute
p	Plenum, pipe

Table of Contents

Introduction

The ever increasingly stringent exhaust emissions legislation and fuel prices are forcing the automotive engine designers to demand increased pressure ratio from the turbocharger compressor, this to ensure complete combustion of the fuel, thereby reducing engine displacement while maintaining or even increasing output power, the so called downsizing. Downsizing has experienced a notable increasing trend in the recent years. For this type of application it is essential to maintain the stable operating range of the compressor as increased pressure is demanded, otherwise inadequate charge air supply will lead to poor combustion, poor specific fuel consumption, reduced power and increased pollutants.

Due to their high efficiencies and high pressure ratio they produce compared to positive displacement compressors, radial centrifugal compressors are commonly used in turbochargers. The turbocharger compressor, in turn, is required to give a broad operating range between surge and choke, and at the same time match the engine speed range, which is very low compared to compressor speed. It is the inherent mismatch of high speed turbochargers to a low speed reciprocating internal combustion engine which provides difficulties for engine designers to produce an optimized combination [Abdullah, 1996].

As it can be shown in Figure I. The compressor map becomes narrower as the compressor pressure ratio increases, i.e. the stable operating range, between surge at low flow rates and choke at high flow rates, decreases. Operation in the unstable condition [surge zone] is undesirable due to the violent pressure pulsations, shaft/bearing noise and vibration which accompany it. Prolonged operation under such severe condition may lead to mechanical failure. On the other hand, choke is related to the occurrence of a sonic condition at a throat section of the compressor stage [throat of the impeller eye [inducer] or at the entry of the vaneless diffuser or at the throat of a vaned diffuser [case of vaned diffuser]], and leads to a rapid reduction in efficiency with only a small increase in mass flow.

For turbocharger compressors, a broad operating range between surge and choke is of such importance that efficiency levels are often sacrificed for flow range.

Although centrifugal compressor instabilities has been widely investigated in the literature, most studies were focused on radial compressors for industrial or aeronautical applications, whose operating condition differs of those of engine applications. Rare investigations have been done to study instabilities in turbocharger centrifugal compressors except in some particular conditions [Chesse et al., 2000 for marine application, and Galindo et al, 2006 for automotive application].

Instabilities in a centrifugal compressor are stall and surge, where centrifugal compressor surge is provoked by a stage stall, which in turn is a collective stall of different compressor elements or a strong stall in one component.

Different studies have been conducted to suppress surge and to compensate for the stable range reduction while increasing pressure capabilities, different experimental techniques including variable geometry techniques, fixed geometry techniques may be considered to be a promising solution. Potential areas for the application of these techniques are the inlet to the discharge of the impeller, diffuser and the volute. However, prior to giving rules which are intended to predict or delay surge in turbocharger compressors, it is necessary to understand instabilities in all compressor components and trying to suppress these instabilities may be a way to suppress stage stall.

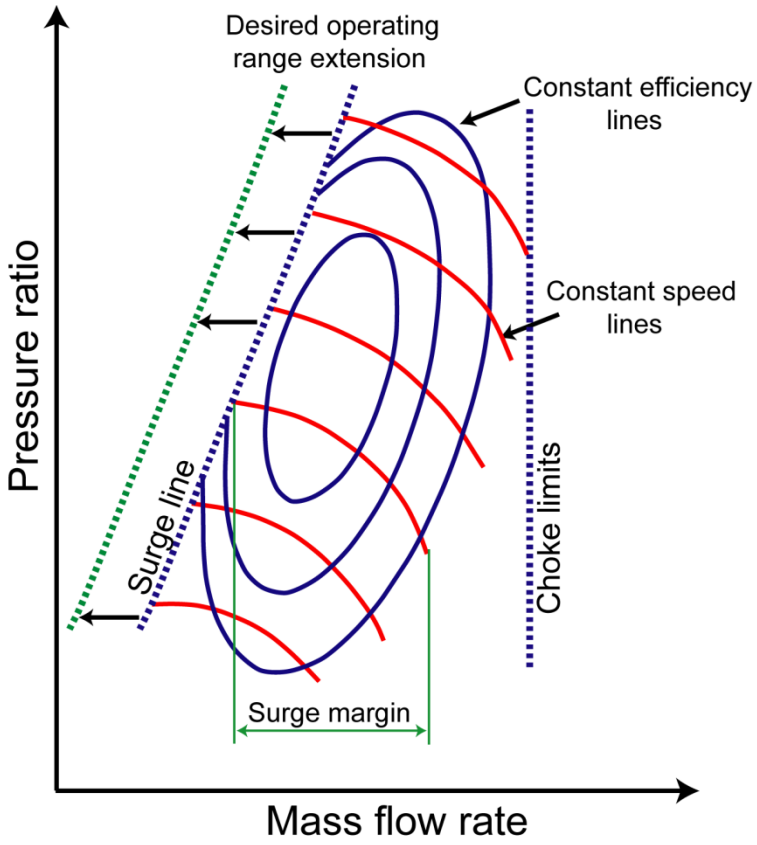

Figure I Schematic of compressor performance characteristic map [Stein, 2000]

The objective of this work is to study and optimize existing fixed and variable geometry techniques commonly used for industrial or automotive applications, to delay local instabilities contribution on system surge, hence increase stable operating range of turbocharger centrifugal compressors. These techniques were tested on a BorgWarner turbocharger compressor, and the possibility of optimizing these techniques was studied. Moreover, proposing different mechanisms to increase the compressor stable functioning while conserving efficiency and taking in consideration cost, manufacturing, packaging, weight addition, and complex control systems addition.

Introduction

Les normes anti-pollution toujours plus sévères et le prix des carburants obligent les ingénieurs de l'automobile à augmenter les pressions de suralimentation délivrées par les turbocompresseurs, afin de d'assurer une combustion complète du carburant tout en réduisant la cylindrée et en maintenant ou même en augmentant la puissance délivrée, technique appelée le [down-sizing]. Cette tendance s'est fortement accentuée ces dernières années. Pour ce type d'application ; il est essentiel de maintenir une large plage d'utilisation du compresseur lorsque une pression plus forte est demandée, sinon un débit d'air inadapté conduira à une combustion incomplète, une consommation spécifique élevée, une puissance réduite et une augmentation des émissions polluantes.

En raison de leur haut rendement et fort taux de compression par rapport aux machines volumétriques, les compresseurs centrifuges radiaux sont couramment utilisés dans les turbocompresseurs. En fonctionnement, le compresseur de suralimentation doit fournir une large plage de fonctionnement entre le pompage et les chocs, et en même temps s'adapter à la plage de régime du moteur qui est beaucoup plus faible que celle du compresseur. C'est cette désadaptation inhérente entre les hautes vitesses d'un turbocompresseur et les basses vitesses d'un moteur à piston qui entraine des difficultés pour réaliser une combinaison optimale [Abdullah, 1996].

Comme indiqué sur la figure 1, le champ compresseur devient plus étroit lorsque le taux de compression augmente, i.e. la plage de fonctionnement stable entre le pompage à bas débit et les chocs à haut débit, diminue. Le fonctionnement dans des conditions instables [zone de pompage] est proscrit en raison de violentes pulsations de pression, bruits de palier et vibrations qui l'accompagnent. Un fonctionnement prolongé dans ces conditions peut conduire à une casse mécanique. De l'autre coté, les chocs sont liés à l'apparition de conditions soniques dans une section du compresseur [col à l'entrée de la roue ou à l'entrée du diffuseur lisse ou aileté] et conduisent à une baisse rapide du rendement pour une augmentation faible du débit.

Pour les compresseurs de suralimentation automobile, une large plage de fonctionnement est d'une telle importance que le rendement est sacrifié au profit de la plage de débit.

Bien que les instabilités des compresseurs centrifuges aient été largement étudiées dans la littérature, la plupart des études sont centrées sur les compresseurs radiaux pour les applications industrielles ou aéronautiques, où les contraintes de fonctionnement sont différentes de celles des applications dans les moteurs à pistons. De rares investigation sont été menées pour étudier les instabilités dans les compresseurs centrifuges de suralimentation, excepté pour certaines conditions particulières [Chesse et al, 2000, pour une application marine, et Galindo et al, 2006 pour une application automobile].

Les instabilités dans les compresseurs centrifuges sont le pompage et de décrochement ; le pompage est provoqué par un décrochement d'étage, qui est un décrochement collectif de plusieurs éléments du compresseur, ou un décrochage fort dans un des éléments.

Plusieurs études ont été conduites pour supprimer le pompage et pour compenser la réduction de la plage de fonctionnement stable tout en augmentant le taux de compression. Différentes techniques expérimentales, incluant les géométries variables et fixes, peuvent être considérées comme des solutions prometteuses. Les domaines d'application pour ces techniques sont : de l'entrée de la roue à la sortie de la roue, le diffuseur, et la volute. Cependant, avant de donner des règles qui sont censées prédire ou repousser le pompage dans les compresseurs de suralimentation, il est nécessaire de comprendre les instabilités dans chaque composant du compresseur. La suppression de ces instabilités peut être une solution pour supprimer le décrochement d'étage.

L'objectif de ce travail est d'étudier et d'optimiser des techniques, fixes ou à géométrie variable, qui diminuent la contribution des instabilités locales sur le pompage du système, et ainsi augmentent la plage de fonctionnement stable des compresseurs centrifuges de suralimentation. Ces techniques peuvent être utilisées pour des applications industrielles ou automobiles. Elles sont testées sur un turbocompresseur BorgWarner. De plus, des nouveaux mécanismes permettant d'augmentant la plage de fonctionnement tout en conservant le rendement peuvent être proposés.

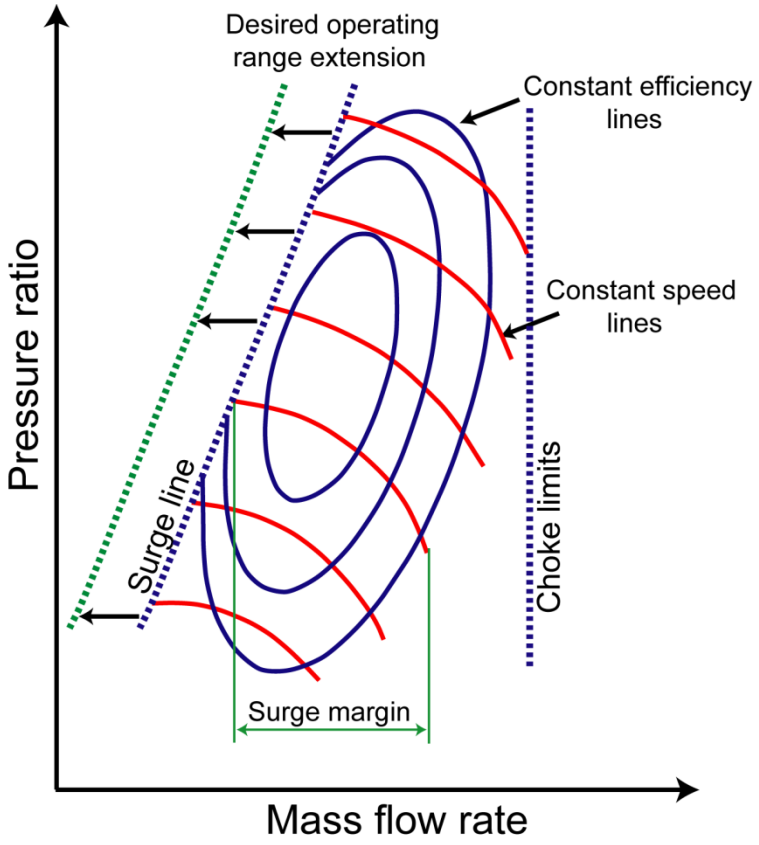

Figure 4-1 Schematic of compressor performance characteristic map [Stein, 2000]

1 Chapter 1: Literature Survey

Chapter 1 begins with a historical review of turbocharging internal combustion engines. In section two, the different air charging systems used to supercharge engines are studied. The downsizing potential, advantages, disadvantages and the current application of these systems are also presented. A more particular interest was evidently done to turbochargers, since they are the subject of this work.

In the third section, the principle of operation of the turbocharger centrifugal compressor, together with an overview of the different one dimensional losses are presented. In section four, we talk about compressor stability analysis, and finally in section five, the different existing techniques to suppress compressor instabilities are studied.

Chapitre 1 : Revue Bibliographique

Le chapitre 1 commence avec une revue historique des moteurs suralimentés. Dans la section 2, les différents systèmes de suralimentation sont présentés. Le potentiel, les avantages et inconvénients du [downsizing] et ses applications actuelles sont également présentés. Une attention particulière est portée sur les turbocompresseurs puisqu'ils sont au cœur de la présente étude. Dans la 3^{ième} section, le principe de fonctionnement d'un compresseur centrifuge est rappelé, et ses différentes pertes sont recensées. La 4^{ième} section est centrée sur l'analyse de la stabilité des compresseurs, et finalement, dans la section 5 les différentes techniques existantes de suppression de ces instabilités sont détaillées.

1.1 Turbocharging internal combustion engines

The primary purpose of supercharging is that, an internal combustion engine of a given size will produce more power if more fuel is made available for combustion. This is limited by the amount of air that is introduced into the engine(1). If the amount of air is compressed to a higher density than ambient prior to entering the cylinder, the maximum power an engine of fixed dimensions can deliver, will be increased. The power delivered by a four stroke engine is shown in equation [1-1]

$$P = \eta_v \rho_a V_{sw} N_{CS} \eta_f E_f \left(\frac{1}{AFR}\right) \quad 1\text{-}1$$

Rudolf Diesel patented his idea for using a supercharger with his compression ignition engine in 1896. Louis Renault, in 1902, patented a system to force-feed the air into a carburettor using a centrifugal blower. Although turbocharging was increasingly adopted after the 2nd World War for large diesel engines in marines, power generation and locomotive applications, they made only slow penetration into the commercial automotive market.

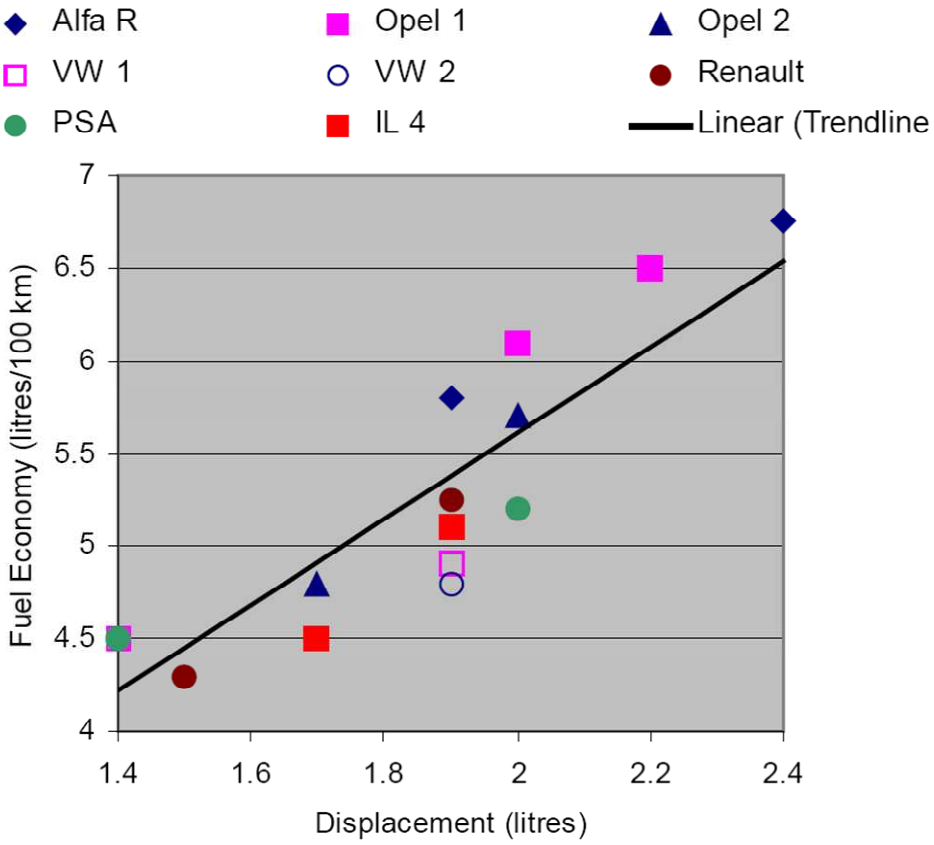

Figure 1-1 Effect of downsizing on diesel engine fuel economy - same vehicle for each engine pair (2)

A second scope of supercharging arises with the oil crises in the 1970s, where increasingly stringent emissions regulations were made. This pushed the industry to turn to turbocharging to the extent that the vast majority of Diesel engines in all sizing ranges are now turbocharged (3). More environmental restrictions arose in 1990 after the Framework convention (4) which preceded the Kyoto protocol in 1997 (5) and the summit of Copenhagen in 2009 (6). These conventions encouraged, and will more encourage the use

of downsized engines and consequently increases number of turbochargers required [Figure 1-1].

Moreover, due to these restrictions, turbocharging gasoline engines is increasingly employed (7), (8), (9) and (10) - after it was limited by the use of high performance sports cars - after overcoming many of the problems associated with pressure charging spark ignition engines with developments in fuel injection systems, combustion chamber design, and electric engine management (3).

1.2 Air charging systems

In this section, a brief description of the different air charging systems is done. Moreover, their downsizing potential, their advantages/disadvantageous and their current application are also presented.

1.2.1 Supercharging

The term supercharging is referred to boosting systems with the compressor driven by mechanical or electrical devices.

❖ Mechanical supercharging

The separate compressor - a positive displacement compressor, or rotary compressor - driven from the power taken from engine provides a compressed air [Figure 1-2]. Most of conventional superchargers employ a positive displacement compressor which has the advantages of rotating at speeds that are reasonably close to engine speeds, and can be driven directly through a simple gearbox from the engine shaft, and a wide range of stable operation. The main drawbacks of the positive displacement are its low-efficiency and low-boost pressure. Moreover, at relatively low boost pressures of about 1.5-2, the supercharger consume 10 to 15% of the engine power at boost pressure of 4 fraction can be as high as 40-50% (3).

Figure 1-2 Mechanical supercharger (11)

❖ Electrically assisted supercharging

The compressor is driven by electric motor. The main advantageous of electrically assisted superchargers is its instantaneous response, its multi mode operation from boosting the engine to recharging the battery (12). However, the serious weight penalty the system imposes, and its complex electrical control system- hence expensive implantation- are still its main disadvantages.

1.2.2 Pressure wave supercharging

Pressure wave supercharging uses wave action in the intake and exhaust systems to compress the intake mixture. An example of a pressure wave supercharging device is the “comprex”, which uses the pressure available in the exhaust gas stream to compress the inlet mixture stream by direct contact of fluid in narrow flow channels (1).

1.2.3 Turbocharging

The term turbocharging refers to using an exhaust gas driven turbine to drive the compressor. Then the turbocharger consists of a compressor, a turbine and are mounted at opposite ends of a common shaft and enclosed in cast housing [Figure 1-3]. Almost radial compressor is used in turbochargers and is driven by the turbine which uses the exhaust gases to produce mechanical work.

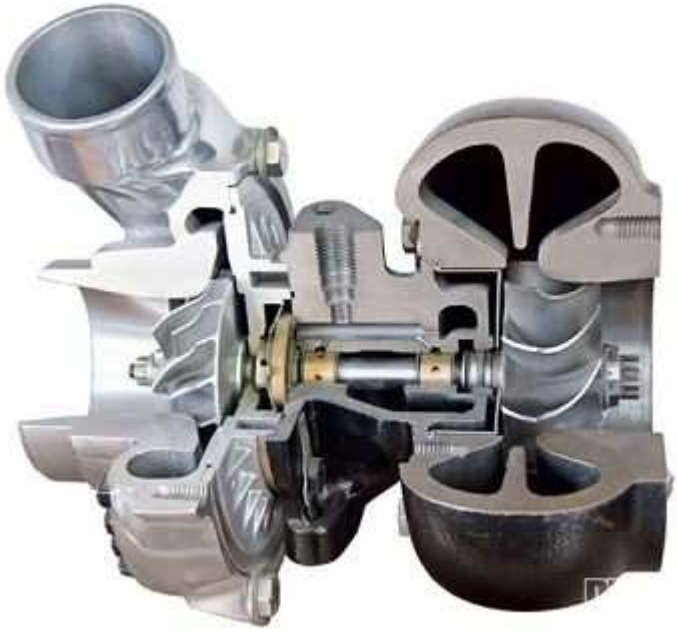

Figure 1-3 Automotive turbocharger (13)

Turbocharger turbines may be radial, axial or mixed flow type. Radial and axial are commonly used in turbocharger. The first mentioned being fitted to small automotive or truck turbochargers, the second to large units applied to large engines-locomotive or stationary and large marine engines. The great advantage of radial inflow turbines is that it maintains a relatively high efficiency when reduced to very small sizes. Moreover, it is simpler and cheaper to manufacture than an axial flow turbine which becomes less efficient as size is reduced due to very short blades and narrow flow passages resulting in high boundary layer blockage (14).

Turbocharging was first reported by Bûchi in 1905 (3). It has been extensively used with diesel engines as a superior boosting system. Recently their application has been extended to cover spark ignition engines [section 1.1].

Pressure ratio developed by turbocharger compressor range from low values for small gasoline engines where the boost pressure is limited to about 2, up to 3.5-4 for vehicle diesel engine that have to operate over a wide flow range, or higher for power generation engines where the width of the operating range can be sacrificed for high boost pressures at design operating conditions. There are also control systems attached to a turbocharger: waste gate for fixed geometry turbochargers, and entry vane controller on fixed geometry turbochargers. Turbocharger speeds can range up to about 300K rpm for very small turbochargers, and as low as 10K rpm for large machines.

From the thermodynamic point of view, the turbocharger system is attractive because it makes use of the exhaust energy - in a typical engine roughly 30 to 40 % of the energy released by the combustion of the fluid appears as energy in the exhaust (15). However, turbocharger performance has been influenced by the mass flow rate of inlet air and engine speed (16), the flow range limitations at the compressor end and to a lesser extent at the turbine range. In addition, it takes time to go from one operating point to another in response to engine demand; this is well known as the turbo-lag.

Various methods of turbocharging have been proposed, these are: single stage turbochargers, two-stage turbochargers and sequential turbochargers.

A. Single stage turbocharging

An ideal single stage turbocharger is a turbocharger with a wide flow range, provides high pressure ratios, high efficiencies at high pressure ratios and a high transient response. Unfortunately, existing single stage turbochargers has the following disadvantages:

1. Slow transient response [turbo-lag]
2. The lack of boost at low engine speed due to low exhaust energy
3. Non ability of high pressure turbocharging due to narrow flow ranges at high pressure ratios, hence a downsizing problematic.

For the first drawback, the causes of the time delay [turbo-lag] in the transient operation of a turbocharged engine can be classified into three groups: mechanical, thermal and fluid dynamic (17). The first two are associated with mechanical, thermal inertia of the turbocharger rotor, and exhaust manifold respectively, and the third cause is fluid-dynamic from the exhaust valve up to the turbine and the compressor outlet to the cylinder (18).

Reduction of rotating inertia has been applied to passenger car engine. Although the inertia of turbocharger of this type is already very small, the high speed operation makes it very important. Two solutions have been identified and acted on, reducing the number of turbine blades makes some improvements, and the use of ceramic for the turbine wheel also reduce the inertia considerably. On a normal turbocharger the nickel based turbine produces 60% of the inertia of the total unit, so the reduction of the reduction obtained is considerable (19).

It is important to note that for truck diesel engine the reduction of rotating inertia is considered as a second effect and comes after the major problem of the lack of air at the beginning of the transient [(19)and (20)]

Techniques like, air injection into the intake manifold at compressor exit [(18) and (16)], or using inlet pre-swirl were effective in increasing the rotational speed of the turbocharger at low engine speed (21).

For the second and third drawbacks, to achieve high pressure ratios with single turbochargers, larger turbochargers can be used, however transient response will be affected due to increase of mass inertia (12). Single turbochargers can be fixed or variable geometry:

- Single stage fixed geometry turbocharger [FGT]

The cheapest and the simplest turbocharger, is currently applied in most diesel and some petrol engines. Its main disadvantages are the three drawbacks mentioned above.

- Single stage variable geometry turbocharger [VGT]

The term variable geometry refers to varying the geometry of the turbine inlet by pivoting nozzle vanes to control the entry angle of the exhaust airflow, hence changing its flow velocity. When the exhaust energy is low [low engine load conditions] the vane is nearly closed to accelerate the turbine and when the exhaust energy is high [high load engine condition], the vane is completely open [Figure 1-4].

The variable turbine nozzle geometry has to a great extent addressed the disadvantages 1 and 2 of fixed geometry turbochargers. It provides low transient response by sudden close down of the variable vane and a variable boost pressure suited to a wide range of engine operating conditions, which improves low speed torque.

The addition of a variable geometry system makes the VGT more expensive than the FGT. VGTs have been used on advanced turbo diesel engines for a few years. The first mass production petrol car that used VTG turbocharging was the 997 Porsche 911 Turbo, which used BorgWarner turbochargers. This is because in petrol cars exhaust temperatures are much higher [than in diesel cars], and this normally has adverse effects on the delicate, moveable vanes of the turbo, BorgWarner engineers however have managed to combat this problem with the new 911 Turbo (22).

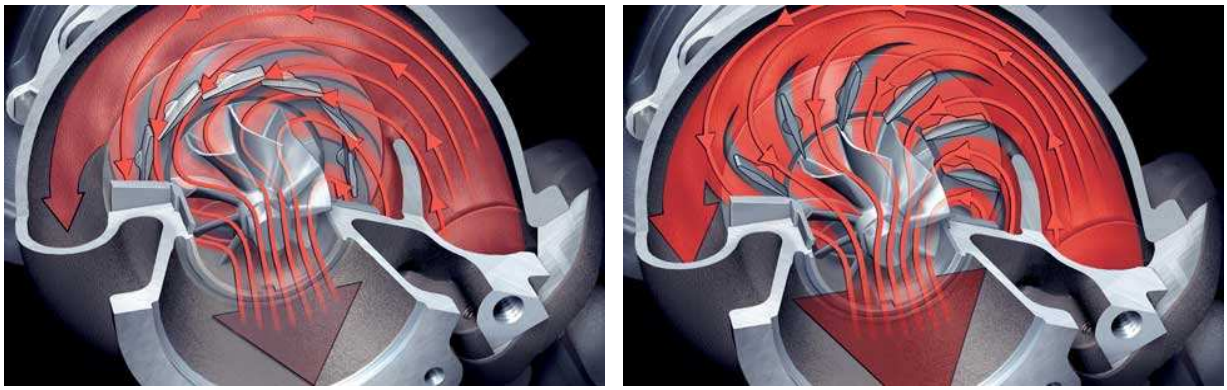

Figure 1-4 Different setting angles of a variable nozzle turbine: at low engine load conditions [to the left] and high engine load conditions [to the right](23).

Using variable geometry technique at the turbine side of the turbocharger has increased - to a great extent - the turbine flow range limitation. However, the flow range limitations at the compressor side [surge line which limits the torque backup for the engine and the choke line which limits the maximum power (20)] still the main problematic for using the single stage for high pressure turbocharging (16).

Suppressing single stage turbocharger compressor limitations, by increasing its margin of stable functioning, permits the use of single stage turbocharger for downsizing applications, which is this work objective.

B. Two stage turbocharging

Two stage turbocharging is a form of multistage turbocharging where two turbochargers are lined up in series. The smaller is close to the engine, is the HP [high pressure] stage and the one further away is the LP [low pressure] stage turbocharger. The compressed air from LP compressor feeds the HP compressor [Figure 1-5].

The two stage turbocharging can overcome the problem with downsizing engines by providing the high pressure necessary for downsizing, and improving the transient and the low load performance of the engine compared to a single stage turbochargers.

Two stage turbocharging cannot match the simplicity of the single turbochargers. It added weight [2 turbochargers, cooling systems, bypasses …] to the engine, a complex control system and has packaging difficulty (12). It is currently used for marine engines, and truck engines, and still not very current for automotive application.

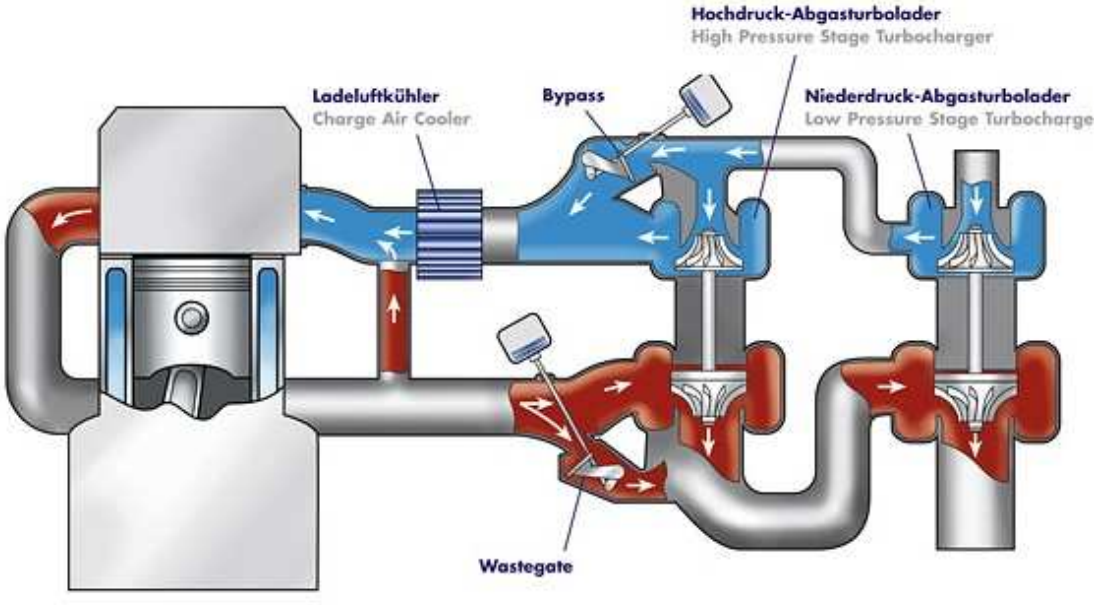

Figure 1-5 BorgWarner 2 stage turbocharger (22)

C. Sequential turbocharging

Sequential turbocharging consists of two differently sized turbochargers positioned in series or parallel with regulated bypass control and inter-cooling system between them.

Sequential turbocharging provides high boost pressures, great turbocharger system efficiency, and higher transient response with smaller HP turbocharging. These are highly favorable for automotive application, however still just used in marine engines (12).

Beside, packaging and weight addition problems, the major difficulty for this system is its complex control system. An advanced electric system is needed.

1.3 Turbocharger centrifugal compressor: principle of operation and aerodynamic losses

A detailed investigation on compressor principle of operation is presented in this section. Moreover, losses through each of the four main compressor components, and their effect on compressor overall performance are also studied.

❖ Energy transfer and compressor efficiency

Consider first Newton's Second Law of Motion applied to a rotating system, the torque developed is equal to the rate of change of angular momentum.

$$\tau = \frac{\Delta(mrC_\alpha)}{\Delta T} \quad \text{1-2}$$

For steady flow process [mass flow is constant], torque can be expressed as:

$$\tau = Q(r_1 C_{\alpha 1} - r_2 C_{\alpha 2}) \quad \text{1-3}$$

In the rotor of a centrifugal compressor, there is work transfer between the fluid and the shaft of the machine. The rate of energy transfer per unit mass flow rate W_{input} is the product of torque and the angular velocity, ω (24).

$$W_{input} = \frac{\tau\omega}{Q} = \omega(r_1 C_{\alpha 1} - r_2 C_{\alpha 2}) \quad \text{1-4}$$

Where $r\omega$ is the blade speed U and r_1, r_2 are radii at impeller inlet and outlet respectively,

Consider the first law of thermodynamic, the work done per unit mass flow is equal to the change of total enthalpy of an adiabatic process. Making these substitutions one obtain the Euler's turbomachinery equation applied between any two points 1 and 2 (24),

$$\Delta h_t = (U_2 C_{\alpha 2} - U_1 C_{\alpha 1}) = h_{1t} - h_{2t} \quad \text{1-5}$$

This equation can be applied to ideal or actual velocity triangle of compressor impeller to deduce ideal or actual enthalpy change. Moreover, this equation is independent of losses in the blade passage (24),

In the other hand, from the velocity triangle at impeller inlet or exit [section 1.3.2], we have,

$$W^2 = U^2 - 2UC_\alpha + C^2 \quad \text{1-6}$$

Substituting in equation 1-5, we will get an alternative form of Equation 1-4.

$$W_{input} = \frac{1}{2}[(C_2^2 - C_1^2) + (W_1^2 - W_2^2) + (U_2^2 - U_1^2)] = \left(h_2 - h_1 + \frac{C_2^2 - C_1^2}{2}\right) \quad \text{1-7}$$

Equation 59, throws the light on the nature of the energy transfer and the mechanism of pressure rise in the compressor. The first term represents the change in absolute kinetic energy occurring in the impeller. The second term represents the change in kinetic energy due to the change on the relative velocity, resulting in a change of static pressure within the rotor. The third term represents the change of energy due to movement of the rotating air from one radius of rotation to another that is the centrifugal energy which raises the static pressure (14).

The efficiency of compressor is one of the most important performance parameters, but often one of the most ill defined and poorly understood [Japikse & Baines, 1997].The efficiency relates the actual work transfer to that which would occur if the working fluid followed an ideal flow process, and can be written as,

$$\eta = \frac{Ideal\ work\ input}{Actual\ work\ input} \qquad 1\text{-}8$$

Actual work can be assessed either by calculation or by direct measurement. Compressor stage isentropic efficiency is computed by the following equation,

$$\eta = \frac{\Delta h_{Euler} - \sum \Delta h_{int}}{\Delta h_{act}} \qquad 1\text{-}9$$

Where the denominator represents the actual input enthalpy change including parasitic works. In addition to the internal losses, the parasitic losses give rise to an increase in the impeller discharge stagnation enthalpy without any corresponding increase in pressure (25).

❖ Compressor components and aerodynamic losses

A turbocharger centrifugal compressor stage comprises rotating and stationary components, it is made up of four principal sections [Figure 1-6].

- **o** Inlet casing [occasionally pre-rotation mechanisms can be used]
- **o** A rotating impeller.
- **o** Vaneless diffuser [variable or fixed geometry], or vaned diffuser [rarely used for automotive application].
- **o** A volute or scroll.

Figure 1-6 shows a 2D schematic of a turbocharger compressor. Stations at inlet and outlet of each component are presented to simplify the losses literature survey.

The contribution of each component of the compressor in compressor pressure rise is shown in Figure 1-7. Stations from 0 to 6 correspond to Figure 1-6 notations.

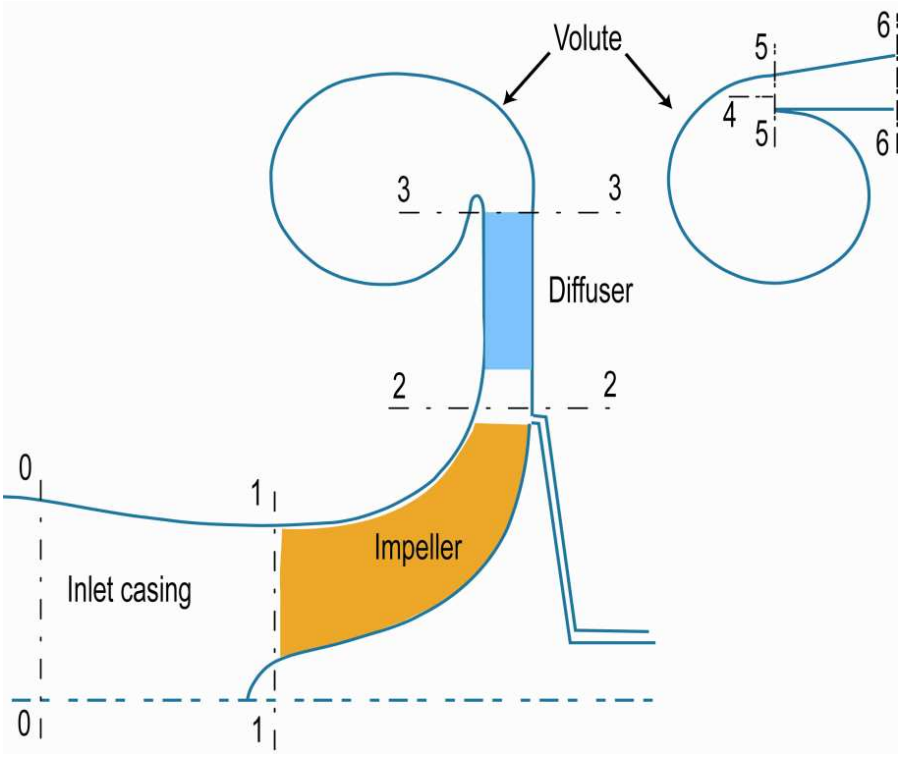

Figure 1-6 2D draw of turbocharger compressor stations

In the inlet casing [process 0-1] the static pressure drops from P0 to P1, due to air velocity increase as it approaches the impeller eye. Energy transfer takes place in the impeller [process 1-2] and its corresponding isentropic compression is designed by 1-2i. The diffuser diffuses part of the kinetic energy at the impeller exit and increases static pressure from P2 to P3. For the pressure rise in the volute, it is considered that no diffusion exists and hence no pressure rise [for this schematic].

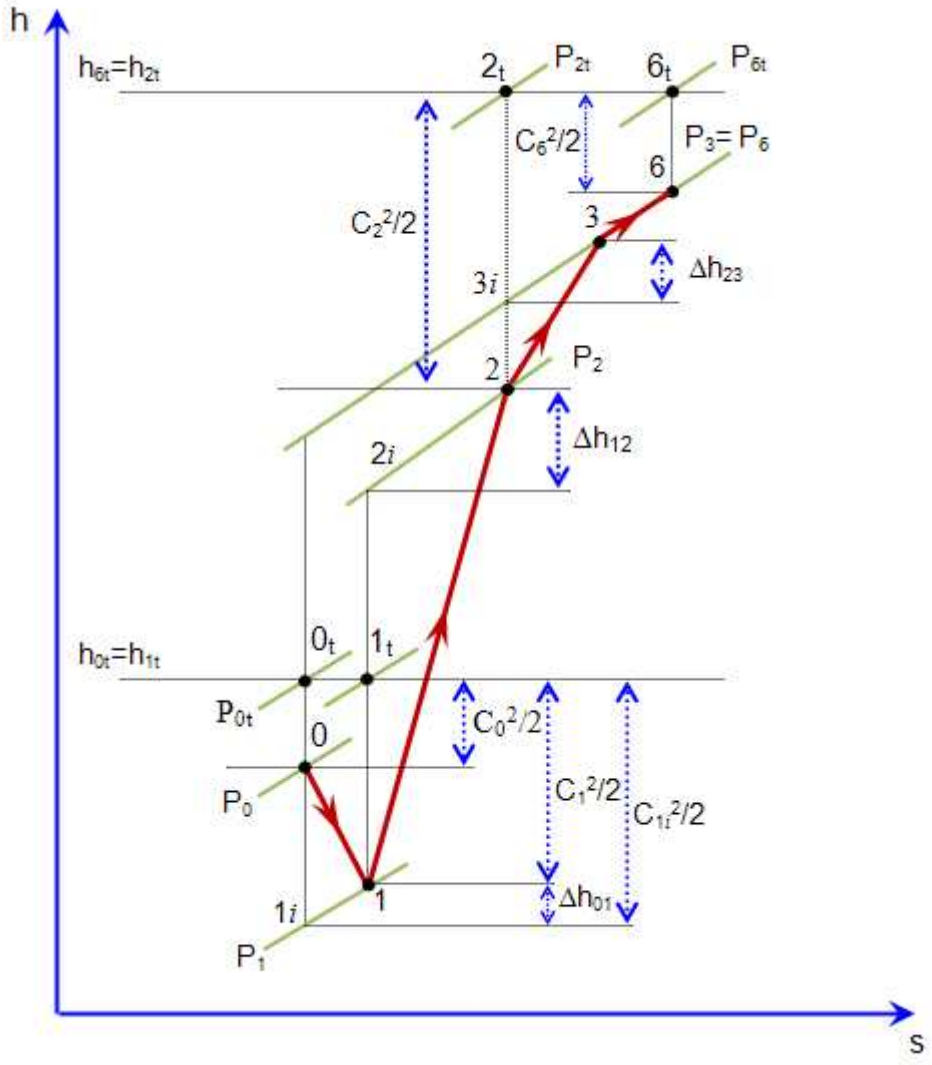

Figure 1-7 h-s diagram for the centrifugal compressor stage

1.3.1 Inlet casing

The function of the inlet casing is to deliver air to the impeller eye with minimum losses and to provide a uniform velocity profile [minimum distortion] at the eye with or without a prescribed level of pre-swirl (14). If the inlet flow is highly distorted the compressor efficiency degrades significantly, first in the impeller and other component downstream due to propagation of undesired flow characteristics (26).

Many Different inlets are employed in centrifugal compressors design. These include a straight inlet, and inlet duct [often curved], a side stream inlet, or they may involve levels of

inlet swirl using either an axial guide vane, radial guide vane or other pre-rotation mechanisms. Impeller inlet considered as an auxiliary element can attain a significant and dominant role in stage performance (27). Due to the packaging constraints which turbocharged engines are submitted in passenger cars, the inlet duct of the turbocharger compressor often requires a 90° bend (28).

Compressor inlet is the most under analyzed component of the centrifugal compressor together with the volute [section 1.3.4]. This is due to high cost of analysis, complex geometry and uncertain gain in performance. This is why one dimensional method is widely used for inlet designs (29). While one dimensional is a simple and cheap method ,however, the flow whithin inlet desgin is by no mean one dimensional [inlet ducts often curved].

In recent years many numerical studies have been conducted on the design of compressor inlets. The impact of inlet profiles of compressor performance was investigated by Ariga et al, 1983 (30), Kim et al, 2001(31), and Engeda et al, 2003(29). According to these studies the flow distortion upstream of the impeller can cause significant efficiency drop and reduce surge margin.

Kim & Koch, 2004 (26) studied numerically two radial inlet models for a centrifugal compressor for industrial application, the intent of their work was to disturb flow as uniformly as possible at the impeller inlet while minimizing pressure losses in the inlet casing [Figure 1-8].

The comparison of aerodynamic performance indicated that the second inlet design outperformed the first inlet design by reducing total pressure loss across the inlet and having more uniformity and less distortion at the end of the inlet vanes for the following centrifugal impeller.

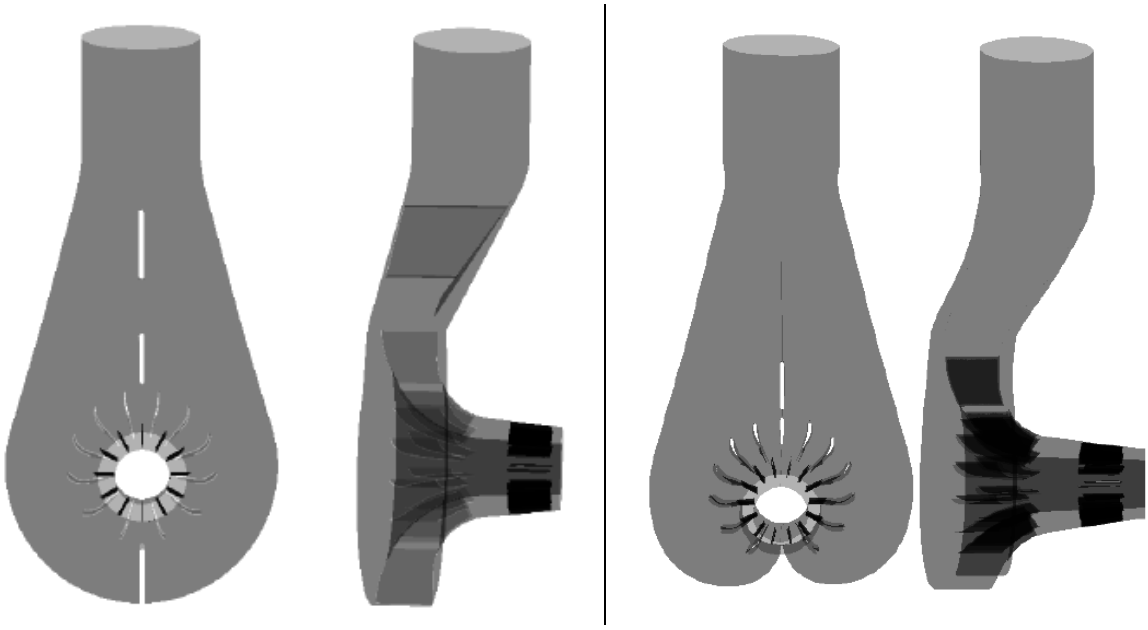

Figure 1-8 Radial inlets 1 [to the left] and 2 [to the right], proposed by Kim & Koch (26)

❖ Inlet casing losses

Enthalpy loss at the inlet casing can be expressed as Watson, 1982 (14)

$$\Delta h_{inlet} = K_{inlet} \frac{C_1^2}{2} \qquad 1\text{-}10$$

Where the inlet enthalpy loss coefficient,

$$K_{inlet} = \begin{cases} 0.05 & simple\ axial\ type\ inlets \\ 0.25 & radial\ inlet, severe\ contours \end{cases} \quad 1\text{-}11$$

Use of inlet guide vanes will inevitably result in more flow losses, values of K_{inlet} ranges between 0.05 [for axial guide vanes with zero setting angle] up to 0.3 and higher depending in the inlet guide vane system.

1.3.2 Impeller

The impeller is the rotating component of the centrifugal compressor, it is the heart of the compressor stage, responsible of the energy transfer process described by Euler turbo machinery [equation 1-12] [proposed by A.D. Leonhard and Albert Euler in 1754, it was first called ‘‘Newton’s Law on Turbomachinery’’. Krain, 2005 (32)].

$$W_{Input} = U_2 C_{\alpha 2} - U_1 C_{\alpha 1} \quad 1\text{-}12$$

Another essential function of the impeller is to decrease the static pressure at the face of the impeller, thus requiring the fluid element at the face of the impeller to flow towards the impeller and subsequently into the impeller (27).

Impeller can be divided into three sections, the first component of the impeller is the inducer that acts as an axial rotor and draws the fluid flow into the impeller in the axial direction, the second component of the impeller is the set of radial blades that energize the fluid and impart mechanical energy to the fluid to increase the fluid total enthalpy and total pressure (33), the third is the impeller discharge. The three components and their effect on compressor performance are developed bellow.

Impeller inducer

Impeller entry section or inducer has a big effect on impeller and hence the overall stage performance.

A design point [best efficiency point], inducer design is optimized to ensure (14):

a. Minimum mass flow inlet Mach number, to avoid shock formation which can lead to boundary layer separation
b. A wide operating range, by avoiding inducer stall at low speeds and preventing premature inducer choke at high speeds. This is determined by the following parameters:
    - Inducer hub to tip radius ratio,
    - Number of blades,
    - Incidence angle, which varies along the inducer leading edge from high values at tip to lower at hub.

Moreover, to ensure a wide range leads again to a desire to minimize the relative Mach number, as the stable operating range between choke and stall decreases significantly as Mach number increase (34).

For turbocharger compressors, the flow arrives at the leading edge with a relative Mach numbers at the tip in the high subsonic or supersonic [for pressure ratio 3:1 and more]. To reduce inlet Mach number, at the tip of the inducer eye at off design points, pre-swirl maybe

used. However, the penalty would be a reduction in energy transfer in the impeller [Euler equation, 1-12]. This point is discussed in the following sections [chapter IV]. Moreover, at off design operation, pre-swirl is also used to decrease incidence angle at inducer leading edge and hence delaying stall [flow separation] at low flow rates.

Impeller hub to tip ratio has a relatively low effect in relative Mach number. Nevertheless, the eye hub maximum and minimum diameter is determined by a number of parameters: inducer stress vibration, impeller manufacturing techniques, number of blade selected,

Velocity triangle at impeller inlet is shown in Figure 1-9. Basic equations that govern the inlet states are, velocity equation [1-13] with uniform axial velocity and no pre-swirl, the inlet velocity triangle is a simple right triangle.

$$W_1^2 = C_1^2 + U_1^2 \qquad 1\text{-}13$$

$$i = \beta_{1b} - \beta_1 \qquad 1\text{-}14$$

Incidence angle, it is defined as the difference between the relative velocity angle and the blade angle, at any impeller eye radius. Note that relations between total and static pressures and temperatures at inducer inlet, are presented in Appendix A.

The incidence angle has a decisive effect on compressor characteristic curves. In theory an ideal incidence should be zero but in practice this is very seldom achieved. In fact many observations indicate values corresponding to a positive magnitude of several degrees (14).

A typical value for incidence, according to Whitfield et al, 1993 [referred to (35)], is approximately -6°. However, Watson, 1982 (14) has q uoted an incidence between 5° and 8° for best efficiency, and Rodgers, 1964 (34) reported -4° to -6° to be the best incidence. Woodhouse, 1948 quoted a value of -4◦ on some Freon compressors and McCutcheon [1978] [referred to (35)] used -10.4◦ and -3◦ at hub and shroud, respectively. Acosta & Bowermann, 1957 (36) reported that the incidence angle at the best efficiency of four tested pump impellers varied between +2° to -0.5° dependin g on the impeller.

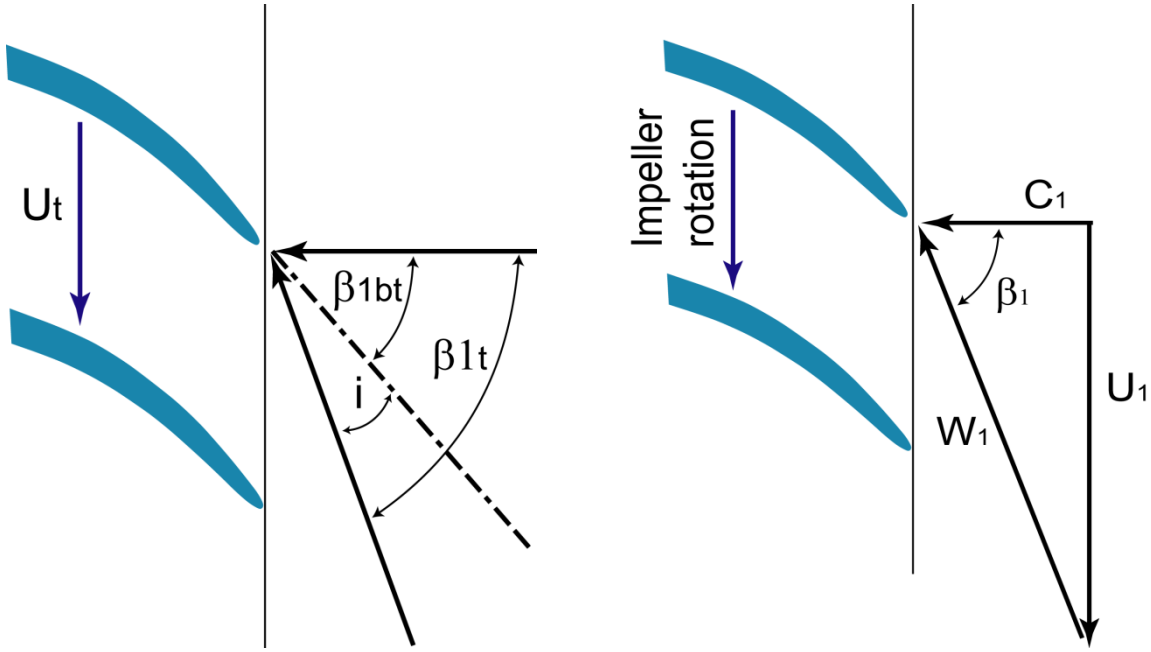

Figure 1-9 Velocity triangle with no swirl at the impeller inducer tip [to the left], and at inducer mean line [to the right]

Finally, in addition to the decisive effect on compressor performance the inducer has, it also plays an important role in determining the level of efficient diffusion which will be attained.

Impeller channel

Designed to direct flow radially to the impeller discharge and to produce additional diffusion. Secondary flows cause low momentum fluid to accumulate on the blade suction side and impeller shroud surfaces (14).

Impeller discharge

The flow at the impeller discharge cannot be perfectly guided by a finite number of blades and it is said to slip leading to the velocity triangles [a perfectly guided flow velocity triangle at impeller discharge, is shown in Figure 1-10]. The body of air passing through the channel between the blades has inertia, and will resist the turning effect of the impeller, the air tends to rotate relative to impeller channel but in the opposite direction (14). The slip factor defined as in equation 1-15 is an empirical attempt to take some account of this phenomenon in a simple one-dimensional treatment of the flow.

The effect of slip is to reduce the magnitude of the tangential component of velocity from that which is ideally attainable. This then has the effect of reducing the delivered pressure ratio and the compressor power consumption [Euler equation].The detrimental [damaging] effect of slip is that the impeller must be larger or run at higher speeds in order deliver the required pressure ratio. This leads to increased stress levels and to increased relative velocities in the impeller, which will then give rise to increased friction losses, and reduced efficiency Whitfield, 1990 (37).

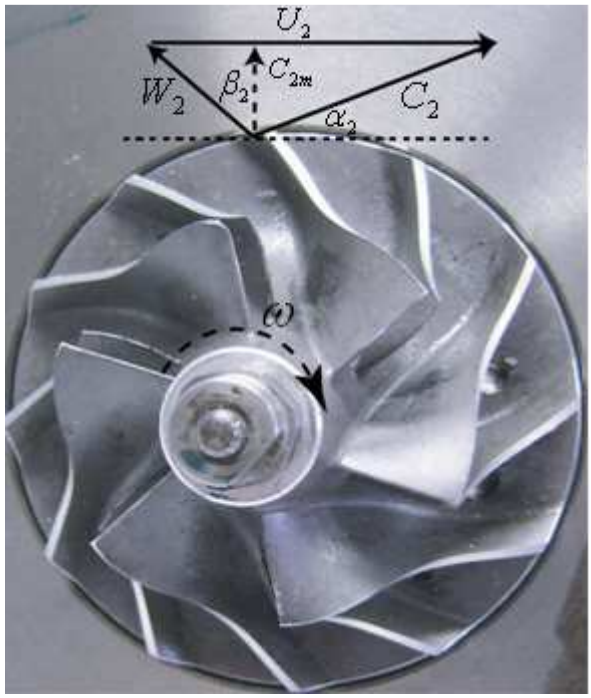

Figure 1-10 Velocity triangle at impeller discharge

Many Attempts have been done to predict the values for the slip factor. At the beginning slip factor depended on spacing between blades, hence having a constant value for a given impeller design. The variation of slip factor with mass flow rate has been investigated later. A

list of slip factor empirical models, proposed in the literature, is presented bellow. Figure 1-11 helps to clarify empirical models [1-15 to 1-29].

$$\sigma = \frac{C_{2\alpha}}{C_{2b\alpha}} \quad 1\text{-}15$$

o Stanitz model

$$\sigma = 1 - 0{,}63\frac{\pi}{Z} \quad 1\text{-}16$$

Stanitz model has a constant value for a given impeller design. It was considered to be satisfactory for blade angles in the range -45°< β'_{2b}< +45°(37).

o Stodola model

$$\sigma = 1 - \frac{\pi}{Z} sin\beta'_{2b} \quad 1\text{-}17$$

$$\beta'_{2b} = \frac{\pi}{2} - \beta_{2b} \quad 1\text{-}18$$

Stodola model is applied for a radius ratio of $(r_{1t}/r_{\ 2}) < 0{,}6$ and a blade number Z>12. Good results were obtained for: 45° < β'_{2b} < 60°.

Stodola model is generally used for blade numbers between 24 and 32. For less blade number the model proposes the following equation:

$$\sigma = 1 - \frac{\pi}{Z\frac{C_{2b\alpha}}{U_2}} sin\beta'_{2b} \quad 1\text{-}19$$

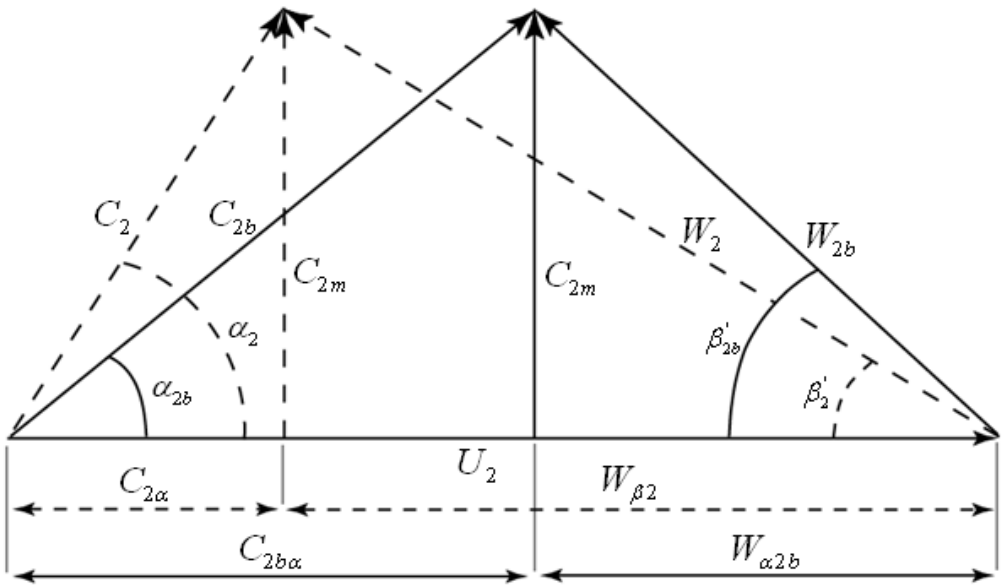

Figure 1-11 Velocity triangle at compressor outlet

o Eckert model

$$\sigma = \frac{1}{1 + \frac{\dot{h}}{h}\frac{\pi sin\beta'_{2b}}{2Z\left(1 - \frac{r_{1t}}{r_2}\right)}} \quad 1\text{-}20$$

Where,

$h^*/h = 0.85$ pour $\beta'_{2b} < 90°$

$h^*/h = 0.70$ pour $\beta'_{2b} \geq 90°$

o Balje model

It was developed for radial compressors, aviation application. See equation 1-21,

$$\sigma = 1 - \frac{Z}{Z + 6.2\left(\frac{r_{1t}}{r_2}\right)^{2/3}} \quad 1\text{-}21$$

o Kazandjane model

$$\sigma = \frac{1}{1 + \frac{2}{3}\frac{\pi}{Z}\frac{1}{1 - \left(\frac{D_{1t}}{D_2}\right)^2}} \quad 1\text{-}22$$

o Traupel model

$$\sigma = 1 - (1 - \sigma_{20})\frac{20}{Z} \quad 1\text{-}23$$

Where σ_{20}, represents the slip factor for a number of blades, Z=20.

o Buseman model

Approximated by Weisner by

$$\sigma = 1 - \frac{\sqrt{(sin\beta'_{2b})}}{Z^{0.7}} \quad 1\text{-}24$$

o Augnier model (38) using the formulation of [Weisner, 1967]

$$\sigma = 1 - \frac{\sqrt{(sin\beta'_{2b})}\ sin\alpha_{s2}}{Z^{0.7}} \quad 1\text{-}25$$

$$\varepsilon = \frac{r_{1m}}{r_{2m}} \quad 1\text{-}26$$

Which holds up to the limited radius ratio,

$$\varepsilon = \frac{\sigma - \sigma_*}{1 - \sigma_*} \quad 1\text{-}27$$

Where

$$\sigma_* = (19\deg + O.2\beta'_{2b}) \quad \text{1-28}$$

When radius ratio exceeds the limiting value, a corrected slip factor is defined by

$$\sigma_{cor} = \sigma\left[1 - \left(\frac{\varepsilon - \varepsilon_{limit}}{1 - \varepsilon_{limit}}\right)^{\sqrt{\beta'_{2b}}/10}\right] \quad \text{1-29}$$

ε = impeller mean line radius diameter

α_{s2}= stream line slope angle with axis [90° in the cas e of tested turbocharger compressor]

❖ Impeller losses

Losses in the impeller can be divided into:

A. incidence losses
B. skin friction losses
C. recirculation losses
D. leakage losses
E. disk friction
F. shock losses
G. Blade loading
H. Mixing losses

These losses are divided into parasitic and internal losses [(25) and (24)]. Where parasitic losses are assumed to be disk friction losses, recirculation losses, and leakage losses.

A. Incidence losses

The losses due to incidence onto the rotor play an important role in shaping the compressor characteristics. Only at one operating point, the fluid will move smoothly into the passages of bladed component, at other operating conditions an angle of incidence will exist.

Since incidence losses do not usually coincide with zero with the zero incidence condition (39), the objective of an incidence loss model is to find the incidence angle at which minimum losses occur besides predicting losses due to incidence. There exist several methods of modeling incidence losses. Of the models available in the literature those due to Wallace in 1958 and NASA 5 [[Futral & Wasserbauer, 1965] referred to Grandahl, 1998 (40)] are most widely used. A comparative study of these two models is given by Whitfield & Wallace, 1973 (41). It is worth to mention that the two loss models were first used for inflow turbines and then applied to centrifugal compressor.

Here are the two models in more details:

1. Referred to as NASA loss model proposed by Futral & Wasserbauer, 1965 and applied to centrifugal compressors by Galvas, 1973 (42). It assumes that the loss is given by the tangential component of relative kinetic energy destroyed. This model was reported in Watson, 1982 (14) and Whitfield & Wallace, 1973 (41) .

If the optimum approach flow angle β_{1opt} is defined as that at which there is no change in tangential component of velocity [Figure 1-12], then the incidence loss is considered to be, in terms of an enthalpy change (39):

$$\Delta h_{inc} = \frac{W_i^2}{2} \qquad 1\text{-}30$$

Where

$$W_i = W_1 sin(\beta_1 - \beta_{1opt}) \qquad 1\text{-}31$$

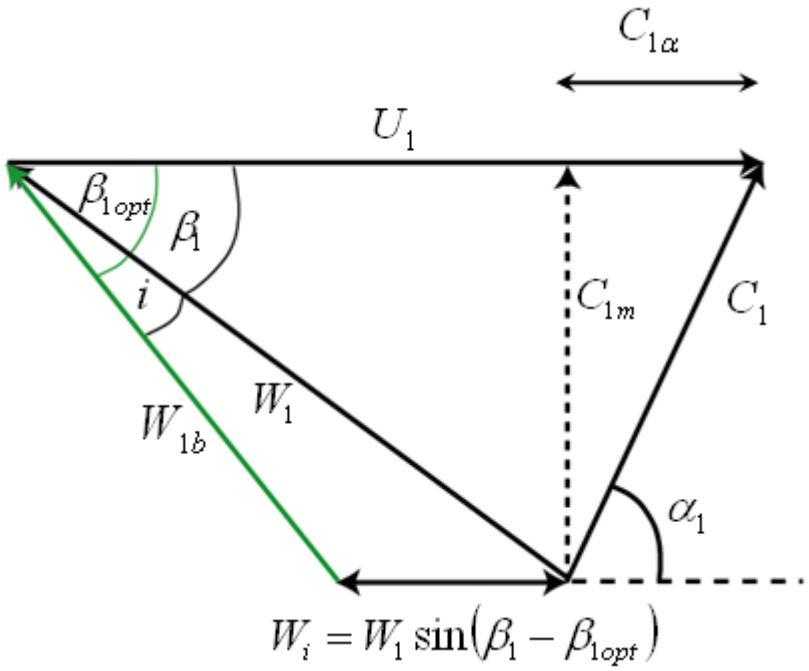

Figure 1-12 Incidence losses due to NASA model

2. A constant pressure incidence model reported by Whitfield & Wallace, 1973 (41) where it is assumed that the flow just inside the blades has adapted to the blades via a constant pressure process. Presented as a function of entropy gain:

$$\Delta s = \bar{R}\frac{\gamma}{\gamma - 1} ln\left[\frac{-1\sqrt{\left[1 + 4F_R^2 M_1^2\left(\frac{\gamma - 1}{2}\right)\left(1 + \frac{\gamma - 1}{2}M_1^2\right)\right]}}{2F_R^2 M_1^2\left(\frac{\gamma - 1}{2}\right)}\right] \qquad 1\text{-}32$$

Where

$$F_R = \frac{A_{1Cos\beta_1}}{A_{1'Cos\beta_{1'}}} \qquad 1\text{-}33$$

And $\beta_{1'}$ is the angle of flow just inside the blade.

Watson, 1982 (14) concludes that for centrifugal compressors, the differences between the two models are small. According to Whitfield & Wallace 1973 (41), the main difference lies in

the prediction of the incidence angle at which zero loss occurs. For Wallace model, zero loss is predicted when the flow angle at the inlet equals the blade angle. Noting that, the use of NASA model leads to a loss varying with the square of the mass flow, symmetrical about the design flow (40).

Some authors like Conrad et al, [1995] [referred to (25)] and Augnier, 2000 (43), consider the loss to be a proportion of the change in kinetic energy associated with tangential component of velocity.

$$\Delta h_{inc} = \frac{K W_i^2}{2} \qquad 1\text{-}34$$

Where K in considered between 0,5 and 0,7 by Conrad et al and 0,4 by Augnier.

Augnier, [1995] has applied equation 1-34 at hub, shroud and mean surfaces. The overall incidence loss in then combined in a weighted average, with the mean stream line values weighted 10 times as heavy as hub and shroud values. He considers that at positive incidence angles, equation 21 underestimates the entrance loss.

Finally, Hammoud et al,1997 (44), presented incidence losses in function of power loss as:

$$P_{in} = K_{in} \frac{\pi\sqrt{Z}}{A_1} \int_{r_{1h}}^{r_{1sh}} W_1^2 r \sin^2 i \, dr \qquad 1\text{-}35$$

$$\text{With } K_{in} = \begin{cases} 2 \; if \; i < 0 \\ 1 \; if \; i \geq 0 \end{cases} \qquad 1\text{-}36$$

B. Skin friction losses

According to Augnier, 2000 (43), Boyce, 2003(33), and Watson, 1982 (14), skin friction losses are typically the greatest, and are a function of the Reynolds number, surface finish, and flow rate.

Ferguson, 1963 [referred to (40)] defined loss due to friction as:

$$\Delta h_{fi} = C_f \frac{l_{hyd}}{D_{hyd}} \frac{W_1^2}{2} \qquad 1\text{-}37$$

Augnier, 1995 (38) and Jansen, 1979 (45) proposed some changes to Ferguson formula,

$$\Delta h_{fi} = C_f \frac{l_{hyd}}{D_{hyd}} \overline{W}^2 \qquad 1\text{-}38$$

Where

$$\overline{W} = \begin{cases} \dfrac{(W_1^2 + W_2^2)}{2} \; [Augnier, 1995] \\ \dfrac{(C_{1t} + C_2 + W_{1t} + 2W_{1h} + 3W_2)}{8} \; [Jansen, 1979] \end{cases} \qquad 1\text{-}39$$

C_f is the surface friction loss coefficient , l_{hyd} is the mean channel length and D_{hyd} is the mean hydraulic channel diameter.

Where the mean hydraulic channel diameter,

$$\mathrm{D_{hyd}} = \frac{4\mathrm{A}}{\mathrm{p}} \qquad 1\text{-}40$$

Where the cross section area A and perimeter p are mean values for the passage. The mean hydraulic diameter $\mathrm{D_{hyd}}$ corresponds to a circle with area A and perimeter p. The mean channel length (46)

$$l_{hyd} = \frac{1}{4} 2\pi \, (r_2 - r_1) \qquad 1\text{-}41$$

The friction loss is actually calculated for constant area pipes of circular cross section. The friction loss coefficient C_f is defined by Watson, 1982 (14):

$$C_f = 4f \qquad 1\text{-}42$$

Where the friction factor f depends on the Reynolds number. Many different formulas for the friction factor have been published, see e.g. Ferguson, 1963 or White, 1986 [referred to (40)].

The skin friction coefficient can be computed from an empirical correlation of pipe friction factors for laminar, transitional and turbulent flow including surface roughness effects given by Chlichting, 1979 .

$$C_f = C_{f_0}\left[1 + 0.075Re^{0.25}\sqrt{\frac{D_{hyd}}{2r_c}}\right] \qquad 1\text{-}43$$

Where r_c is the mean radius of curvature of the flow path, Re is the Reynolds number. The skin friction coefficient C_{f_0} for smooth-walled straight pipes C_{f_0} is calculated from the Prandtl universal law$[Re > 3000]$.

$$\frac{1}{\sqrt{C_{f_0}}} = 1.74log\left(Re\sqrt{C_{f_0}}\right) - 0.4 \qquad 1\text{-}44$$

C. Recirculation losses

Recirculation losses account for the backflow into the impeller exit. The backflow is caused by an increased exit flow angle that then results in flow recirculation causing energy to be returned to the impeller and has an approximately 2 percent effect on the compressor performance at design conditions.

Enthalpy drop due to flow recirculation as calculated by Abdullah, 2006 (46), Oh et al, 1997 (25), and Augnier, 1995 (38),

$$\Delta h_{rc} = \begin{cases} 0.02\sqrt{tan\alpha_2 D_f^2 U_2^2} & [Abdullah, 2006\,] \\ 8 * 10^{-5} sinh\,(3.5\alpha_2^3) D_f^2 U_2^2 & [Oh\ et\ al, 1997\,] \\ U_2^2\left(0.5D_f - 1\right)\left[{}^{W_{\theta 2}}/_{C_{2m}} - 2cot\beta_{2b}\right] & [Augnier, 1995\,] \end{cases} \qquad 1\text{-}45$$

Where D_f is the diffusion factor [ratio between impeller exit and inlet relative velocities].

D. Clearance losses

Clearance losses account for the flow that escapes the compressor flow path through the clearance gap between the impeller blades and the exterior shroud. and has an approximately 1,5 percent effect on compressor performance at design conditions.

Watson, 1982 (14) found that the clearance loss of a centrifugal compressor can be approximated by

$$\Delta\eta_{cl} = K_c \frac{l_{cl}}{b} \quad 1\text{-}46$$

Where l_{cl} is the axial clearance, b is the impeller tip width, and K_c is equal to 0,3 .Liazid et al, 2002 (47) obtained a correction factor $K_c\ of\ 0{,}4$.

E. Disk friction losses

Disk friction losses limit the torque coefficient and depend on different flow regimes and roughness of the impeller finish. The torque coefficient for the friction work is split between the disk and the impeller housing and has an approximately 1,5 percent effect on the compressor performance at design conditions.

Enthalpy drop due to dick friction [Galvas, 1973 (42)]

$$\Delta h_{disk} = 0.01356 \frac{\rho_2}{Q R_e^{0,2}} U_2^3 D^{\frac{3}{2}} \quad 1\text{-}47$$

$$R_e = \frac{U_2 d_2 \rho_{01,rms}}{\mu_{00}} \quad 1\text{-}48$$

F. Shock losses

Shock losses account for the Mach number at the throat approaching 1. Since shock losses are irreversible and source of entropy change, entropy creation is due to heat conduction and high viscous normal stresses within the wave shock [Denton, 1993 (48)].

Shapiro, [1953] [referred to (48)] derived the entropy equation across a plane normal shock wave as:

$$\Delta s_{shock} = C_v \frac{2\gamma(\gamma-1)}{3(\gamma+1)^2}(M^2-1)^3 + \Theta(M^2-1)^4 \quad 1\text{-}49$$

Where M is the upstream Mach number. Equation 1-49 is applicable for oblique shock waves provided M as the component of Mach number perpendicular to the shock front.

G. Blade loading losses

Blade losses account for the blade-to-blade pressure gradient that produces secondary flows that potentially lead to stall.

Enthalpy losses due to blade losses are given by Rodgers, 1987 (49) as,

$$\Delta h_{bl} = \frac{C_{\alpha 2}^2}{X_s} \quad 1\text{-}50$$

Where

$$X_s = \frac{ZL_R}{D_2} \quad \text{1-51}$$

The amount of diffusion which can be achieved in a blade passage is limited by the process of boundary layer growth and stall.

H. Mixing losses

Mixing process in centrifugal compressor can be produced in two different compressor stations. Mixing of the blade wake flows with the free stream flow also known as wake mixing loss, and mixing of the distorted meridional velocities known as blockage losses (38).

Denton [see Appendix 3 in Denton,1993 (48)] explained briefly the entropy production due to mixing out of a wake behind a trailing edge [wake mixing losses]. Moreover, Augnier, 1995 (38) and Johnston et al, 1966 (50) presented the wake mixing losses in terms of enthalpy losses.

Enthalpy losses due to wake mixing as presented by Johnston et al (50),

$$\Delta h_{mix} = \frac{1}{1 + tan^2\alpha_2}\left(\frac{1 - \varepsilon_{wake} - b^*}{1 - \varepsilon_{wake}}\right)^2 \frac{C_2^2}{2} \quad \text{1-52}$$

Where $\varepsilon_{\text{wake}}$ is the wake fraction of blade to blade space, and b^* ratio of vaneless diffuser inlet width to impeller exit width.

1.3.3 Diffuser

Radial diffusers can be classified as vaneless, vaned and low solidity vaned diffusers. The vaneless diffuser is widely used in automotive turbochargers because of the broad operating range it offers. Moreover, it offers a shock free deceleration, a simple construction and is more tolerant to erosion and fouling than the vaned diffusers. However, the vaneless diffuser needs a large diameter ratio because of its low diffusion ratio. Generally the vaneless diffuser demonstrates lower pressure recovery by as much as 20% and lower stage efficiency by 10% compared to a conventional vaned diffuser (51).

Fixed vaned diffuser creates a throat and the increased blockage reduces the flow range by stalling at reduced flows and by choking at higher flows. This is because fixed vanes cannot deal with the changing flow angle as the flow rate at any speed changes from its optimum value. Moreover, high velocity at throat increases friction loss, increases diffusion loss downstream and consequently reduces pressure recovery. On the other hand a higher compressor stage efficiency than that produced by a vaneless diffuser may be reached by carefully designing the fixed diffuser vanes to control the diffusion process.

❖ Role of vaneless diffuser and its effect on the compressor performance

The role of the diffuser is to convert the kinetic energy leaving the impeller into a static pressure rise. Kinetic energy leaving the impeller is equivalent to 40 to 50% of energy input to the fluid [(27) and (52)]. Diffusers convert kinetic energy to pressure rise by one or both of the two principle techniques [case of diffuser with constant width].

- Decrease in the radial velocity component, C_{2m} : According to continuity equation, and due to the increase in flow passage area from impeller exit to diffuser inlet [the area of flow in the radial direction is directly proportional to the radius].

- Decrease in tangential velocity component, $C_{2\alpha}$: According to the conservation of angular momentum principle [neglecting friction losses], $rC_{\alpha} = constant$, hence the tangential component decreases from impeller tip to diffuser exit in inverse proportion to the radius.

In the vaneless radial diffuser the air follows an approximately logarithmic spiral path. For an incompressible fluid this path can be described by Figure 1-13,

$$tan^{-1}\left(\frac{C_{2m}}{C_{2\alpha}}\right) = Constant \qquad 1\text{-}53$$

There are a few vaneless diffuser designs possible. Vaneless diffuser configurations can be pinched or unpinched. The pinch means that diffuser height is decreased compared to the rotor trailing edge height from the shroud or the hub or from both walls Figure 1-14, this abrupt area reduction takes place at the diffuser inlet to stabilize the flow coming out of the impeller. Moreover, vaneless diffusers consist of two radial walls that may be parallel, diverging, or converging.

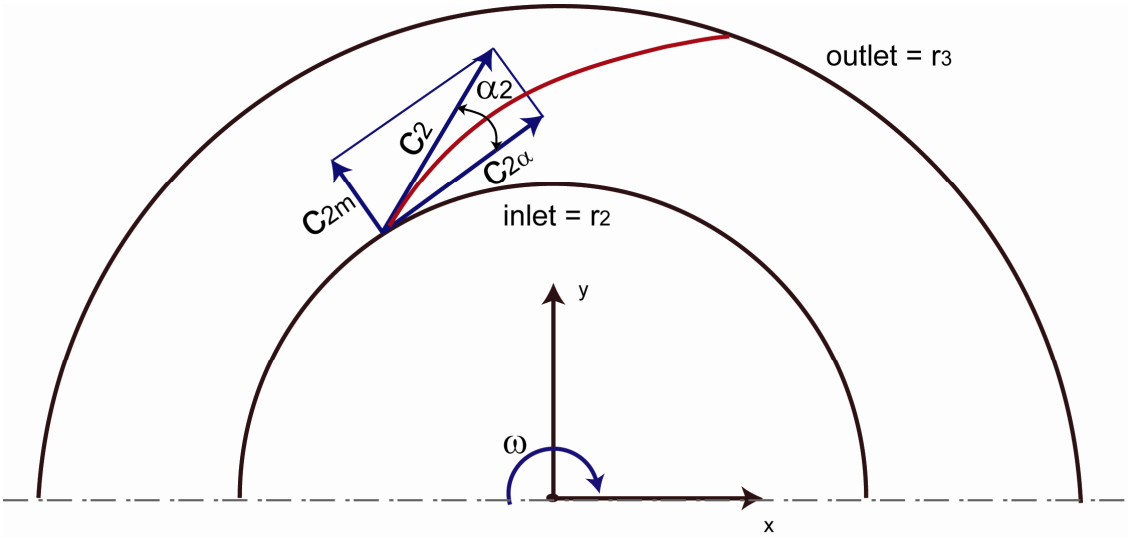

Figure 1-13 Vaneless diffuser geometry

The flow in the diffuser begins as a mixture of core and boundary layer flows, eventually the boundary layers develop and merge together.

The two most important geometrical design criteria affecting the diffuser performance are the channel height b and the diffuser outlet/rotor outlet ratio r_3/r_2. Another important parameter is the diffuser inlet critical angle α_{cr} in which reverse flow occurs. Inlet reverse flow has been linked in many studies to the possible occurrence of rotating stall [C page 56].

Different researchers have investigated the influence of inlet flow conditions and geometries of vane less diffuser on critical flow angle. Senoo et al, 1977 (53) divided the parameters which influence the critical inlet flow angle into:

- Ratio of width to inlet radius of diffuser, b/r_2
- Exit to inlet diffuser radius ratio, r_3/r_2
- Distortion of inlet main-flow

- Inlet Mach number, M_2
- Reynolds number,
- Inlet boundary layer thickness
- Variation of diffuser width with respect to radius.

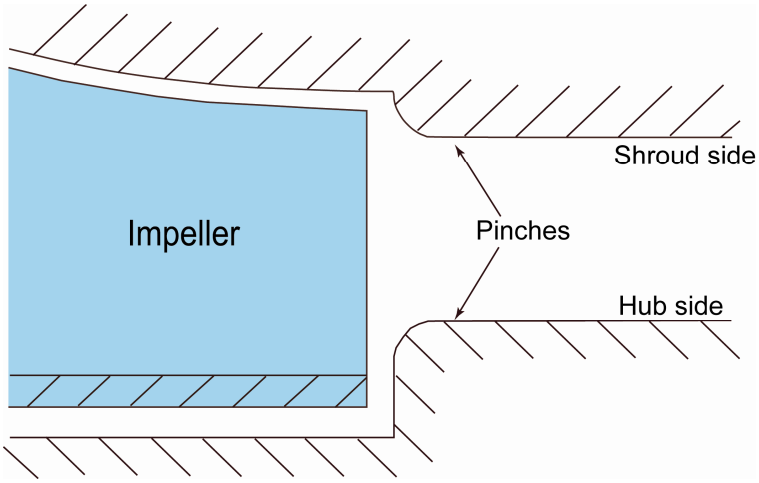

Figure 1-14 Shroud and hub pinched diffuser

Senoo et al (53) concluded that, the most significant influence on the critical reverse flow angle is the diffuser width to radius ratio, b/r_2 , a purely geometrical parameter. Senoo & Kinoshita, 1978 (54) predicted the diffuser critical angle at which the onset of rotating stall can be expected [Figure 1-15]. Note that the curve of Figure 1-15 applies for long diffusers and moderate Mach numbers.

According to Van den Braembussche et al, 1980 (55) the critical inlet flow angle was found to be higher with the lower diffuser inlet width/radius ratios. Van den Braembussche showed that Senoo's prediction of the critical diffuser inlet flow angle agreed well with experimental data if a Reynolds number correction was applied.

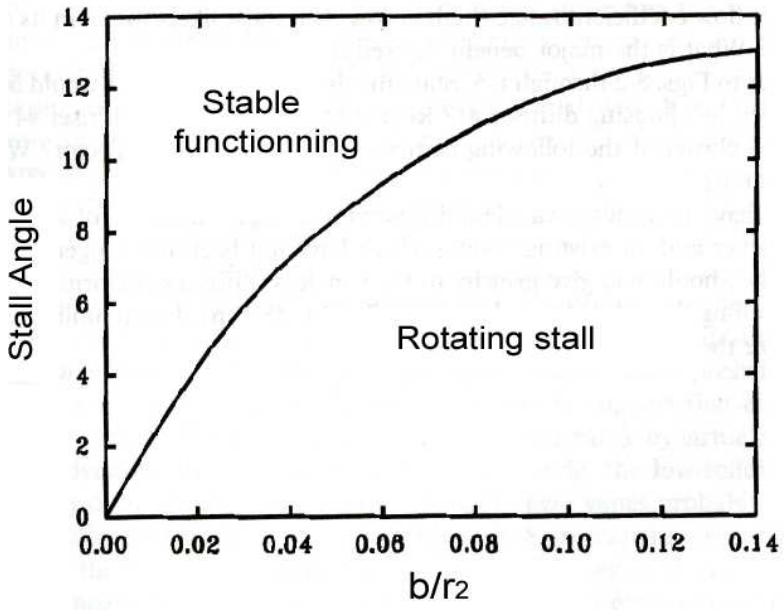

Figure 1-15 Diffuser stall critical angle as predicted by Senoo & Kinoshita, 1978 (54)

Disagreements and contradictions still exist towards how many factors and which factors should be taken into consideration towards the prediction of critical angle.

❖ Vaneless diffuser losses

The vaneless diffuser pressure losses are skin friction and exit losses of kinetic energy (54), with skin friction having the greatest effect it increases as the direction of swirl flow becomes closer to the circumferential direction [flow rate decreases], while exit loss increases with flow rate. Skin friction in diffuser can be modeled in a similar manner as in the impeller.

$$\Delta h_{fd} = C_h \frac{l_{hyd}}{D_{hyd}} \frac{C_2^2}{2} \qquad 1\text{-}54$$

In early publications [Stanitz, 1952 (56)] the coefficient of friction f was found to vary with radius. In particular the value was considered very high at the entry of the diffuser. However, Augnier, 2000 (43) explains that as the vaneless diffuser radius increases the skin friction also increases. Watson, 1982 (14) considered that if the diffuser entry losses are correctly accounted for [particularly, mixing losses at impeller tip], reasonable results can be obtained by using a constant value of the coefficient of friction. Johnston et al, 1966 (50) uses a constant value between 0.005 and 0.001 for the friction factor.

Stanitz, 1952 (56) developed an analysis method to predict the performance of vaneless diffusers. He assumed one dimensional compressible flow with friction, heat transfer, and area change in vaneless diffuser,

$$\Delta h_{fd} = C_p T_{2t} \left[\left(\frac{P_3}{P_{3t}} \right)^{\frac{\gamma-1}{\gamma}} - \left(\frac{P_3}{P_{2t}} \right)^{\frac{\gamma-1}{\gamma}} \right] \qquad 1\text{-}55$$

Vaned diffuser exhibits energy destruction losses associated with skin friction, incidence angle, blockage, wake mixing, and choking that are very similar to the impeller conditions. More about vaned diffuser losses can be found in (43).

1.3.4 Volute

The volute is the second static main compressor component, it is typically cast, therefore expensive to manufacture, not practical to change. It can be overhung or symmetric [Figure 1-16]. Due to installation constraints, overhung volutes are commonly used in centrifugal compressors and for turbocharger applications (24).

Volute has two functions: collection and diffusion. It must collect and transport the fluid to the downstream system. It also raises the static pressure by converting kinetic energy to potential energy [static pressure]. Diffusion is more effective for the kinetic energy associated with the tangential velocity, accomplished by increasing the cross-sectional area in the volute. But there is often an efficiency loss arising from the inability of the volute to convert the kinetic energy associated with the radial component of the velocity out of the diffuser. This effect is compounded when a vaned diffuser is used, as the vanes create a more radial flow into the diffuser.

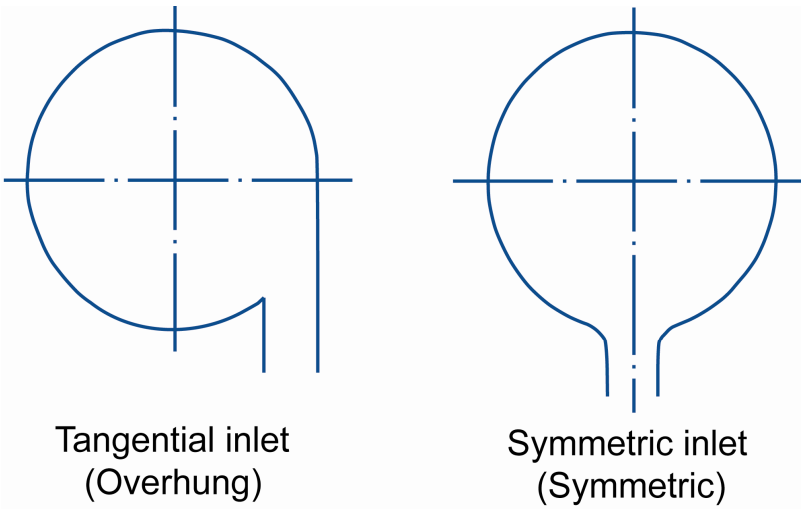

Figure 1-16 Overhung and symmetric volutes

The design of the volute not only impacts the compressor efficiency but also influences the operating range [(57) and (58)]. Little research has been done to understand the flow in volutes of centrifugal compressors, most of work done on volutes was on radial flow pumps where the effect on the performance is strong due to the direct interaction impeller – volute with no diffuser.

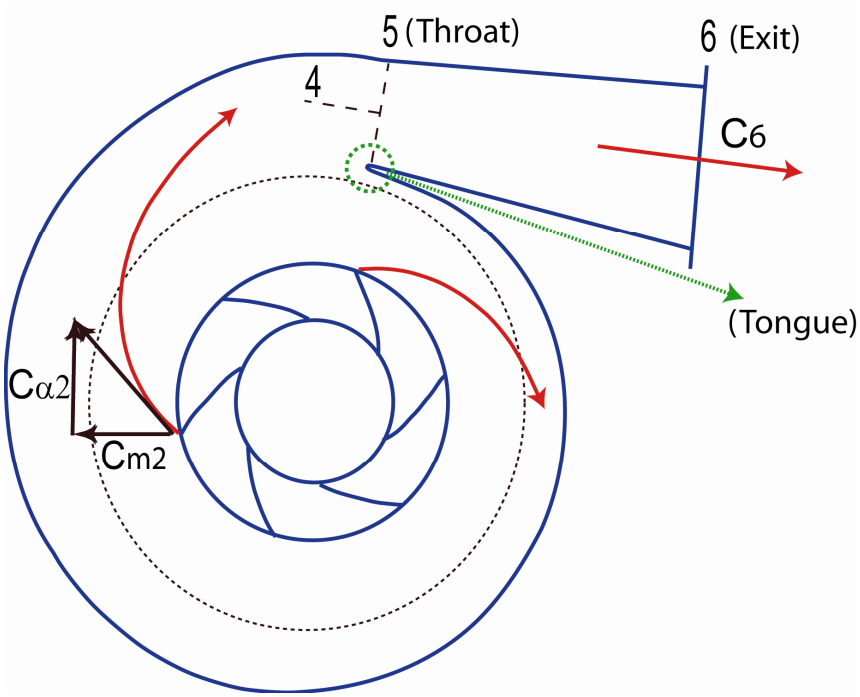

Figure 1-17 Volute flow conditions

The volute is often designed according to one-dimensional calculation (59). After calculating the tangential and radial velocity at diffuser exit, the process in the volute can be understood by using conservation of mass and conservation of angular momentum. At design point, the tangential speed leaving the impeller, and therefore the tangential velocity leaving the diffuser, is approximately constant [$C_{\alpha 3}$ = constant along a speed line]. The effective velocity of air passing the volute throat will depend on the mass flow and the local flow area (24). In

this way, at design point the static pressure is constant around the conference [Figure 1-17].

$$C_6 = \frac{Q}{\rho_6 A_6} \qquad 1\text{-}56$$

At flow rate higher than the design point $C_{\alpha 3} < C_6$ flow must accelerate through the volute and as a consequence the pressure decreases. At flow rates lower than the design point flow rate, $C_{\alpha 3} > C_6$flow will diffuse in the volute and a pressure increases.

At off design operation, the volute generates a circumferential variation of the static pressure at the impeller outlet imposing periodic outlet conditions, and can be noticed even at the leading edge of the impeller blades. The main consequence is an unsteady impeller flow with a circumferential variation of mass flow and blade loading [(60) and (61)]. This causes pressure, velocity and flow angle oscillation in the diffuser and in the impeller blade passages, which lead to a decrease in efficiency and additional noise (58).

The volute circumferential pressure distribution propagates upstream and imposes periodic outlet conditions on the impeller. The impeller exit flow shows a strong variation of the flow angle and total pressure. The potential flow assumption is no longer acceptable. This means that any prediction method should account for this strong interaction between the impeller and the volute.

As mentioned before, the volute is often designed according to one dimensional calculation in which the flow in the volute is assumed to be frictionless and compressible (59). However, due to Xu et al (62) traditional volute design is based on two-dimensional analysis, and the emphasis is on collection and less on the diffusion function. There is little published material with respect to the detailed design of volutes, and the procedure is largely one of experience based on previous designs and tests.

❖ Overall volute performance and effect on the performance of the compressor

According to Ayder, 1993 (58) there are five key geometrical parameters that affect the overall performance of the volute.

A. Circumferential variation of the cross sectional area
B. Shape of the cross-section
C. Radial position of the cross section
D. Position of the volute inlet
E. Tongue geometry

A detailed literature survey of the effect of the different geometrical parameters on the volute performance is reported by [Reunanen, 2001 (59)]. Note that a very few studies have been conducted on centrifugal compressor volutes, and much lesser on small turbocharger compressor. Hence, it is necessary to understand the effect of the different geometrical parameters on compressor performance, and how we can improve its performance.

A. Circumferential variation of the cross section

Stiefel, 1972 (63) shows that the area of the cross section of the volute has a major influence on the shape of the performance map and on the stable operating range of the compressor. The use of smaller volutes shifts the operating map towards lower flow and narrows the range of operation. Moreover, author claimed that the best compressor efficiency is achieved when the volute cross sectional area is 10 to 15 % smaller than the area calculated according to frictionless losses.

Cumpsty, 1989 (64) analyzed the results of Stiefel (63) , presented in Figure 1-18. He considered that the reason why the maximum efficiency of the compressor does not exist at volute design is due to radial energy dissipation and not due to frictional losses. This can be explained in the same figure where using bigger volutes has relaxed the uniform pressure in the circumferential direction hence flow outside the diffuser can turn toward the circumferential and the radial component is no longer wasted.

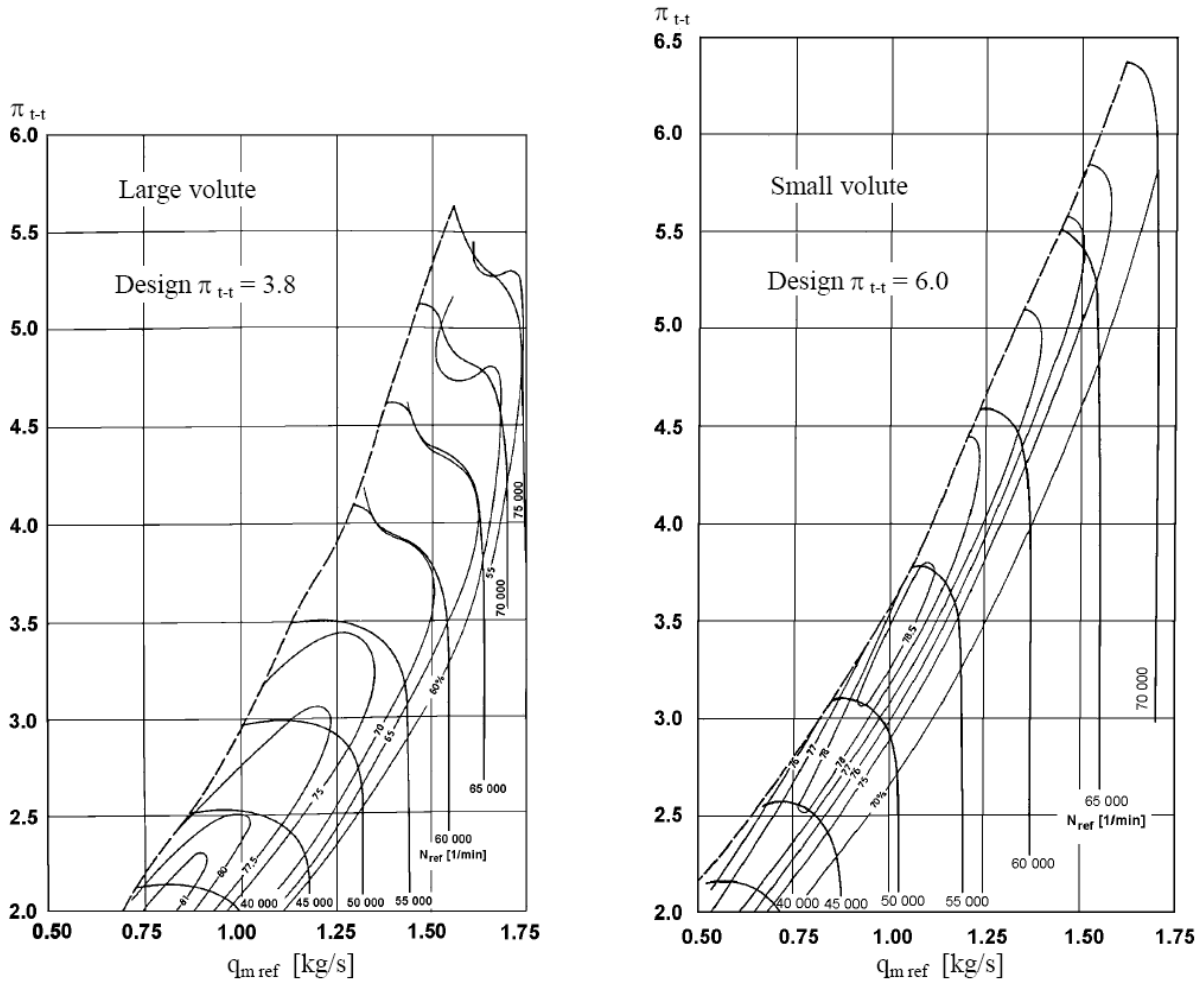

Figure 1-18 Effect on compressor pressure ratio and isentropic efficiency of two different volutes (64)

Since the flow in the volute contains an appreciable swirl and kinetic energy, process of collection must be done with minimum losses (24), for that reason a careful attection should be given to volute cross section variation.

The possibility of testing bigger section volutes on small turbocharger compressor will be interesting. If this proves the shift of high efficiency regions, it will be interesting to think of a variable geometry technique to vary volute section area. Taking in consideration that such a technique is complex and add difficult to manufacture.

B. Shape of the cross section

Ayder, 1993 (58) reported that the shape of volute cross section should be symmetric. Unequal high and width of the volute causes additional losses due to acceleration and deceleration of the swirl velocity inside the volute.

Mishina & Gyobu, 1978 (65) have showed that the effect of cross section shape on the total pressure loss through the volute, is relatively small, with circular cross sections having the lowest loss and the rectangular the highest losses.

C. Radial location of the cross section

The radial location of the cross-section has a strong influence on the performance of the volute. According to the conservation of angular momentum, the tangential velocity in a swirling flow is inversely proportional to the radius.

Mishina & Gyobu, 1978 (65) showed that the radial location has a great effect on volute losses with volute channels located at small radii create higher losses.

Ayder [1993] showed that the reduction in the radius of the volute channel causes re acceleration of the fluid, and partially destroyed the static pressure increase in the diffuser

D. Position of the volute inlet

The effect on the overall compressor performance of tangential and symmetrical inlet was investigated by Hübl, 1975 [referred to (59)]. As it can be seen in Figure 1-19, tangential inlets give higher efficiency than symmetric ones.

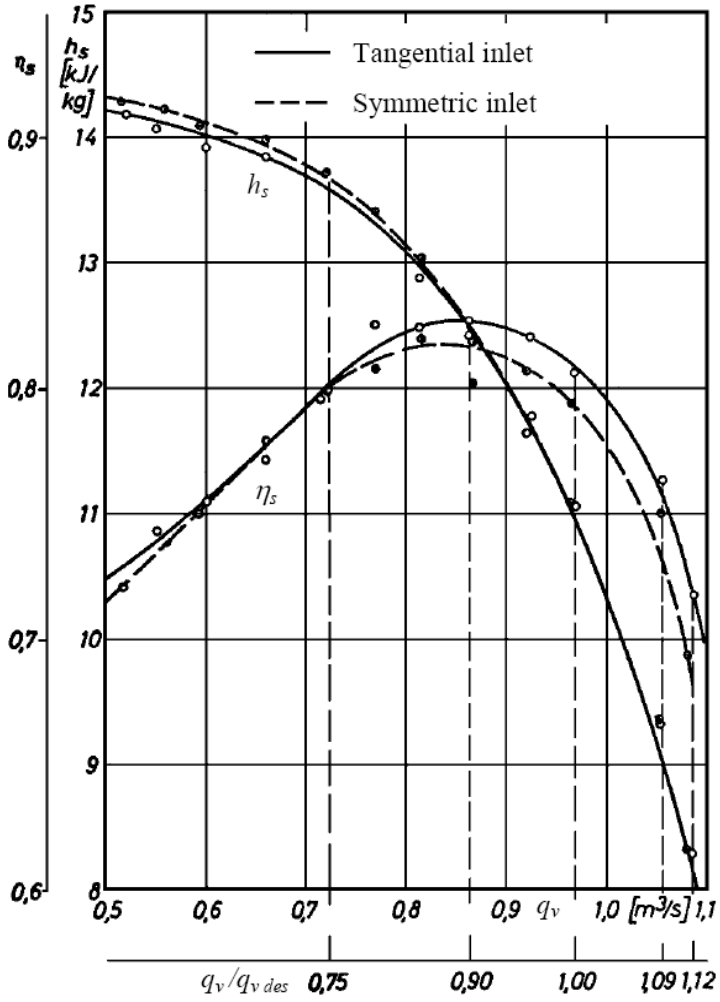

Figure 1-19 effect of symmetric and tangential inlet on the compressor performance (59)

E. Tongue geometry

For improving volute design, it is important to understand the flow structure around the volute tongue where pressure loading is extreme. Tongue region has been widely investigated in radial flow pumps where the effect on the performance is strong due to the direct interaction impeller – volute with no diffuser (59). However, very few investigations were done on centrifugal compressor, and still fewer in small compressors.

The leading edge of the tongue is analogous to that of an airfoil, it can be round or sharp. A sharp leading edge has low blockage but is sensitive to angle of attack; while a well-rounded leading edge has large blockage but it is insensitive to incidence, forces secondary flow center away from the tongue area, and produces high losses near the tongue area.

A better understanding of the influence of the tongue has been explained by [Xu & Müller, 2005 (62)] using three-dimensional analysis. It is shown that the round tongue provides the improved pressure coefficient at high flow as compared to the sharp tongue. However, the absolute peak pressure recovery is attained with the sharp tongue, at a loss of range.

Lipski, 1979 (66) considered that the pump head efficiency is strongly dependant on the position and shape of the tongue. In addition, the force on the tongue becomes zero at point of maximum efficiency. Author proposed adjusting tongue angle and length to control pump performance, and suggested that the tongue should be shortened if an increase in the efficiency at off design conditions is required [especially at high flow rates].

Figure 1-20 Volute modifications with exit turning about the axis (67)

Dean, 1973 (68) reported that modification of volute tongue are likely to have minimal effect on the flow, and that most pressure distortion is produced by the abrupt turning in the exit passage. Author recommended that the exit turning should curve about the axis for quite a distance downstream the tongue to limit the loading in the tongue or cutwater area. This point was proved numerically by Ji et al, 2007 (67) [Figure 1-20].

The tongue length and angle were studied by Lipski, 1979 (66) and Dong et al 1997 (69). The first proposed a movable and adjustable tongue and proposed controlling tongue angle in function on operating point. The later studied the effect of retracting and rounding the volute tongue on the centrifugal pump performance. As it can be seen in Figure 1-21, pump head was increased at low and high flow rates when retracting the tongue. Moreover, Dong et al (69) reported a noise decrease due to tongue moved away from the impeller.

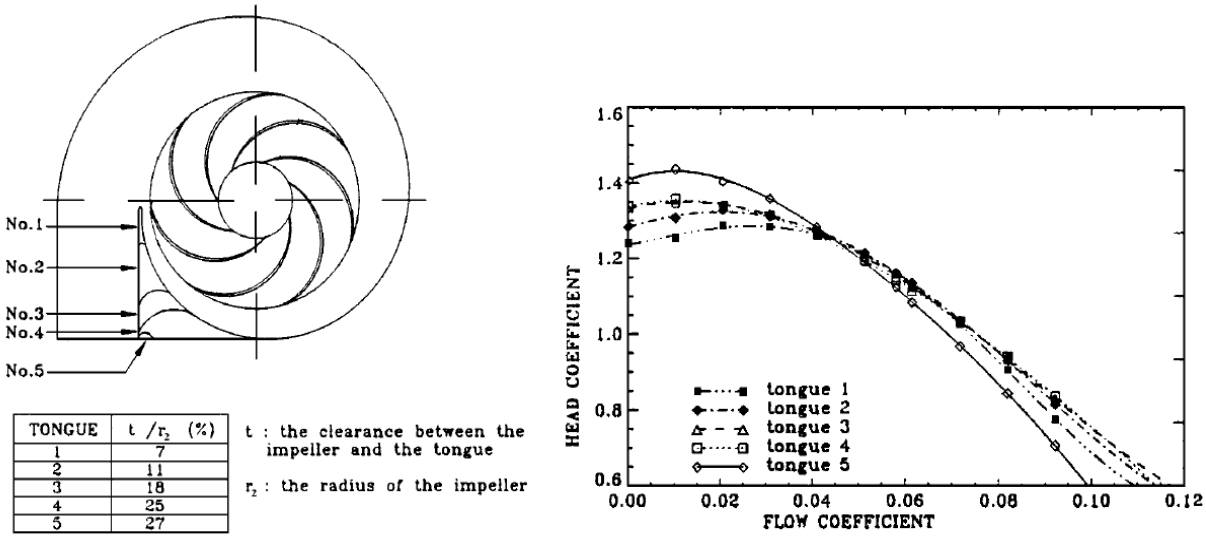

Figure 1-21 Effect of the different tongue shapes on the overall performance of the pump (69)

Finally, Yadav & yahya, 1980 (70) found that the volute performance was strongly dependent on the tongue area at low and high inlet swirl angles. Hence it is important to understand the flow structure around the tongue for improving volute design.

❖ Volute losses

Watson, 1982 (14) defined the energy losses in the volute as the results of destruction of kinetic energy at the diffuser exit due to turbulent mixing, as the flow enters the collector. He assumed that the loss is about half of the kinetic energy leaving the diffuser. Cumpsty, 1989 (64) explained losses due to the inability of the volute to use the radial kinetic energy out of the diffuser and assumes this loss to lie between 2-5 points of efficiency.

$$0.02 \leq \Delta\eta_{volute} \leq 0.05 \qquad 1\text{-}57$$

Japikse & Baines, 1997 (24), and Augnier, 2000 (43) offered a simple one dimensional method for the prediction of volute total pressure loss and static pressure recovery. They divided losses into, skin friction losses, meridional velocity head losses, tangential velocity head losses and exit cone losses. Figure 1-17 shows the basic volute geometry and the station number employed.

Skin friction losses

Because of the velocities are small, frictions on the wall of the volute does not generate much loss and their contribution is small compared to that generated by the long narrow passage upstream where velocities are much higher [Cumpsty, 1989], this was proved experimentally by Brown and Bradshaw [1946] [referred to Cumpsty, 1989].

Only the tangential velocity is presented in the equation, since it is assumed that the kinetic energy associated with the radial velocity is lost due to swirling inside the volute, [Ayder, 1993 (58)].

$$\Delta P_{fv} = C_f \frac{L_{hyd}}{D_{hyd}} \frac{C_{\alpha 4}^2}{2}$$
$$L_{hyd} = \frac{\pi(r_4 + r_5)}{2} \quad \text{1-58}$$
$$D_{hyd} = \sqrt{\frac{4A_5}{\pi}}$$

Where C_f friction coefficient can be found from Moody's chart.

Meridional velocity head loss

As mentioned above, meridional velocity assumed to be totally lost, According to Japikse & Baines (24) this is pessimistic since some of the meridional velocity can be used in the downstream element, the loss component can be written as,

$$\Delta P_{mv} = \rho \frac{C_{m4}^2}{2} \quad \text{1-59}$$

Tangential velocity head loss

Part of the tangential velocity head is expected to be lost when the area and mean radius variation in the circumferential direction forces a change in angular momentum.

$$\Delta P_{tv} = \frac{\rho}{2}(C_{\alpha 4} - C_5)^2 \quad \text{1-60}$$

Exit cone loss

The performance of the cone matches that of an optimized ideal conical diffuser. Losses can be expressed as,

$$\Delta P_{tv} = K_e \frac{\rho}{2}(C_5 - C_6)^2 \quad \text{1-61}$$

Where K_e is the exit cone loss coefficient, it ranges from 0.15 for exit cones with opening angle about 10° up to 1.1 for angle 60° (59).

Finally the overall total pressure loss of the volute is obtained by adding the different losses together,

$$\Delta P_{totv} = \Delta P_{fv} + \Delta P_{tv} + \Delta P_{mv} + \Delta P_{ev} \quad \text{1-62}$$

These equations presents a simple one dimensional model for a volute, however, a more detailed one dimensional model has been studied by [Traupel, 1966 referred to (24)] and his work give quite realistic results and has been used for design (24).

It worth noting that due to Van den Braembussche (61), swirl is the main source of losses in a volute. Optimum volute performance requires minimum radial velocity at impeller exit. Simultaneous optimization of the impeller and the volute is recommended. Moreover, volute losses are likely to be higher for compressor with a vaned diffuser than with an annular diffuser, as a larger part of the total kinetic energy at the outlet of the vaned diffuser is in the radial direction.

Most volute studies have been performed on existing geometries and were mostly based on the pump Van den Braembussche R.A, 2006 (61). Very limited literature in the turbocharger compressor volute has been reported in the open literature. Accept the work done by Eynon & Whitfield, 2000 (57) on the volute of a turbocharger centrifugal compressor. Authors studied the effect of volute on the overall turbocharger compressor performance, and show that the volute performance is a function of inlet flow angle and that it plays a significant role in setting both the best efficiency flow rate and the operating range of the compressor.

A very few information available for the guidance of the volute design and design parameters influences of the performance on turbocharger compressor design. Hence, this subject is not well studied yet and more research in this field is needed.

1.4 Centrifugal compressor instability

Compressor performance is typically characterized by the pressure ratio, efficiency, mass flow, and energy addition. Stability is also, however a performance characteristic. It is related to the response of the compressor to a disturbance which perturbs compressor operation from a steady operating point. If the disturbance is transient, the performance is considered stable if the system returns to the original point of operational equilibrium. The performance is unstable, if the response is to drive operation away from the original point.

There are two areas of compressor performance that relate to stability, one deal with operational stability, the other with aerodynamic stability. Operational stability: Is concerned with the matching of performance characteristics of the compressor with a downstream flow device such as throttle, turbine or jet nozzle. Aerodynamic stability is concerned with the limitation of steady state operation due to stall and surge (71). Instability phenomena in centrifugal compressors have been the focus of many studies [Emmons et al, 1952 (72), Toyoma et al, 1977(73), Stenz, 1980 (74), and Greitzer, 1976 parts I and II (75) and(76)]. Greitzer, 1981 (77) have done a review of aerodynamic instabilities found in compression systems.

Since the aim of this work is to delay turbocharger compressor surge, and the occurrence of surge is a result of the stalling of some component or combination of components (71). Then a thorough introduction to stall in each component is needed prior to giving rules which intends to predict or delay surge.

Stall in each of compressor components and system surge are developed in the following section.

1.4.1 Stall

The earliest report on stall [dynamic stall] appears in the work of Cheshire [1945], which is a history of centrifugal compressor development in Britain in the 2nd World War (71). Japikse & Baines, 1997(24) defined stall as: *when stream lines adjacent to the wall is insufficient to overcome the adverse pressure gradients and the shear stress along the wall*. When these *viscous shear effects and adverse pressure gradients are sufficient to reduce the fluid velocity to zero, it is forced to deviate from the surface and fluid is said to be stalled* Figure 1-22.

Then stall is referred to flow separation. It can be created either by 2D boundary layer separation [example: simple stall of an unswept aircraft wing] or a 3D skewed boundary layer separation [example: duct bends] (24).

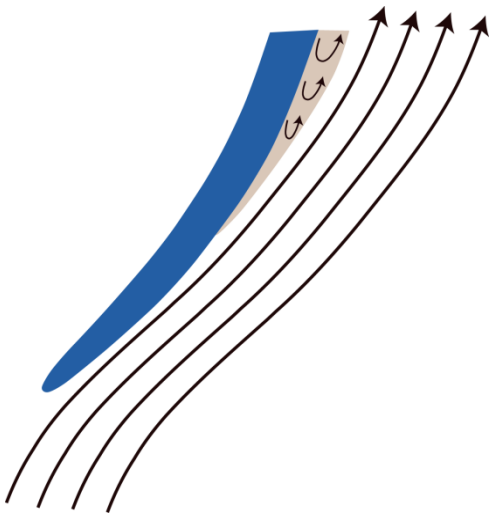

Figure 1-22 Flow separation

Stall can also be regarded as the cessation of a continued rise in static pressure recovery in the diffuser or impeller (71).

Stall phenomena may be of a steady [static] or dynamic [rotating nature]:

1. Static [steady]: stationary and can be associated with a fixed location in the compressor.
2. Dynamic [rotating]: consists of zones of stalled passages [local region of stagnant flow, often called stall cells] covering a small number of blades and rotating in the absolute direction of rotor rotation [Figure 1-23]. They usually have a constant rotational speed between 20 and 80% of the rotor rotational speed: larger cells rotate at a lower rotational speed than small cells (77). While many studies have been done to study the effect of rotating stall, details of stalled flow [example: number of stall cells, their speed relative to impeller ...], but this subject is far from being completely understood (71).

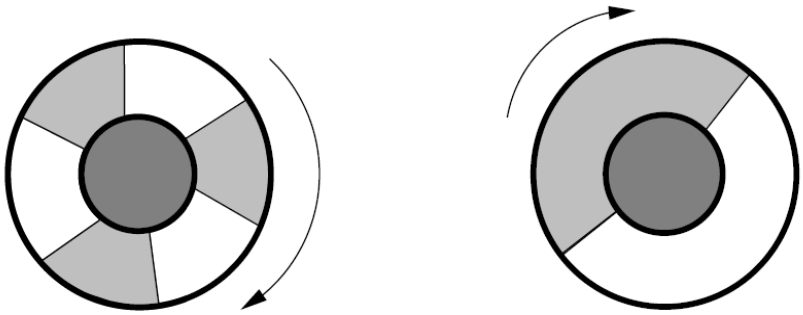

Figure 1-23 Rotating stall cells (78)

Rotating stall introduces a gradual or abrupt drop of the pressure rise as depicted in Figure 1-24. Moreover, rotating stall can introduce hysteresis into the system, implying that the flow rate has to be increased beyond the stall initiation point in order to bring the compression system out of its stalled operating mode (77). For rotating stall, the pressure ratio fluctuation frequencies are of the same order as the rotor frequency.

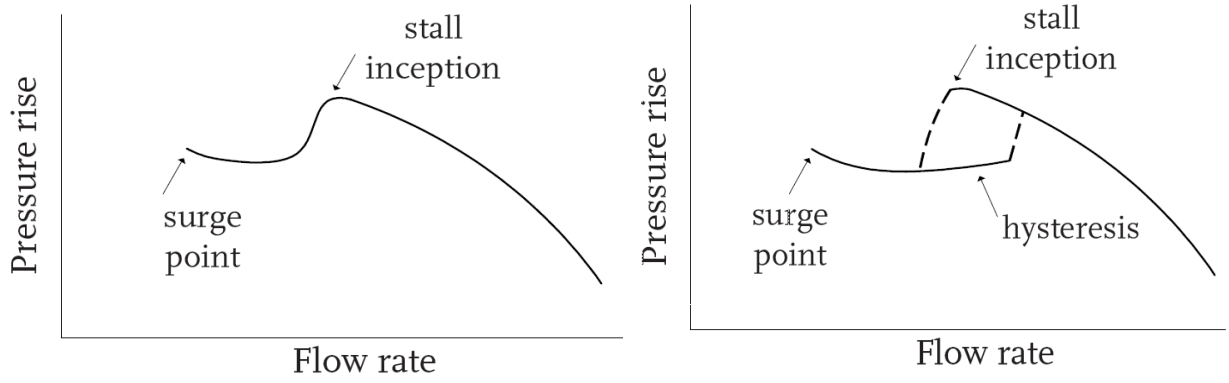

[a] Gradual stall

[b] Abrupt stall with hysteresis

Figure 1-24 Compressor map in the presence of rotating stall (79)

Given its distorting effect, stalled flow in a centrifugal compressor deteriorates performance and efficiency due to thickening of the boundary layer. Moreover, it is accompanied by loss in total pressure, and it limits operating range [Kammer et al, 1985 (80) and De Jager, 1995(81)].

Stall occurs in rotating and stationary blade rows and in both axial and centrifugal compressors. Stall also occurs in turbines, and when this happen losses increases significantly.

❖ Stall in each component of the centrifugal compressor

This section presents a literature survey of static and rotating stall in each of the compressor components.

A. Inducer stall

When the mass flow rate through the compressor is gradually reduced at constant speed, the axial component of the absolute velocity decreases, thus increasing the incidence angle of the air approaching the leading edge of the inducer. Beyond a critical incidence angle the flow can no longer adhere to the suction side of the inducer blade [Figure 1-25]. Flow separation from the surface creates a stall condition subsequently encouraging reversal flow. Inducer stall may contribute to surge, particularly at high pressure ratios, but can exist at normally stable operating condition (14).

Another cause of Inlet separation is the shock wave at or near the throat of a transonic impeller (24).

Besides Watson, 1982 (14), dynamic stall has also been observed in the inducer by Ariga et al, 1983 (30), who refers inducer stall to rotating stall and considered that cells [small recirculation] rotate in the opposite direction of rotor rotation.

While in Kammer et al, 1985(80), the inducer stall is considered non-rotating, and the stall type in the other two components [impeller and diffuser] is rotating stall. Moreover, authors considered that inducer can tolerate only a certain fraction of reverse flow and can therefore cause compressor surge.

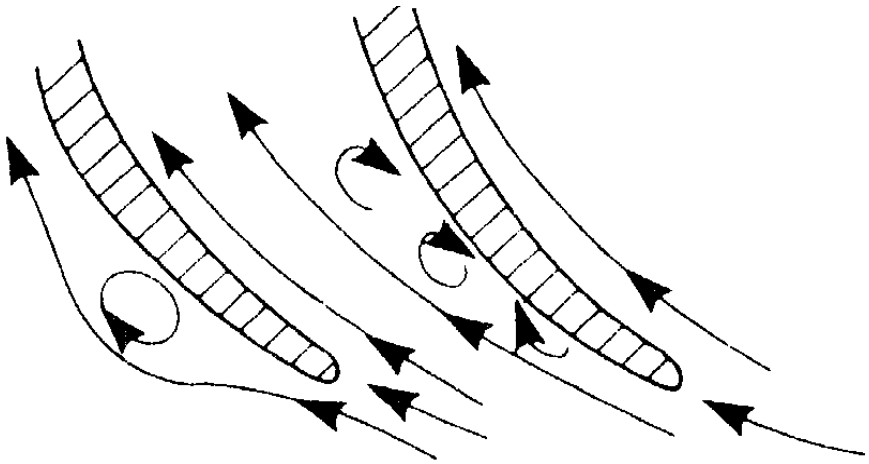

Figure 1-25 Flow separation in the inducer (14)

Parameters suited as stall criteria in the inducer are: incidence angle, deceleration ratio W_{th} / W_1 and pressure rise (80). Moreover, inducer stall can be detected experimentaly by inserting a thermocouple near the shroud or by carefully monitoring the tip static pressure in that region. Thermocouples will read high temperature values due to backflow.

B. Impeller stall

Flow can separate in the impeller passage, as it turns from the axial to radial direction, due to Coriolis forces. These forces acts differently on different impeller stream lines depending on their velocities. The high velocity stream lines tend to separate from low velocity stream lines, which generates secondary flows and subsequently flow separation [Figure 1-26] (24).

Separation also occurs at the suction side of the blade in the radial direction of the impeller which leads to the formation of wake (14). At least one instant of dynamic stall in the radial part of the impeller has been reported by Abdelhamid & Bertrand, 1980 (82) .

To end this part, note that to predict stall onset in the impeller, the velocity ratio and diffusion factor are used (80).

C. Diffuser stall

Diffuser stall can be observed in vaned as well as vaneless diffusers.

- Vaneless diffuser stall

As a steady stall mode, two-dimensional or three dimensional separations can occur in vaneless diffuser, with three dimensional or skewed are very common and the existence of two-dimensional is highly improbable (24).

Watson, 1982 (14) explained vaneless diffuser steady stall as: *The most common separation flow in the vaneless diffuser is caused by the local reversal of flow normally occurring on the shroud side of the diffuser wall and is very much influenced by the flow leaving the impeller. To conserve angular momentum, the flow in a parallel walled vaneless diffuser tries to maintain a constant flow angle [equation 1-53]. However, due to compressibility and viscosity effects the stream line close to the wall have less kinetic energy and follow a path of less reduced spiral angle until eventually they are swept back to the impeller. This back flow is diffuser stall*

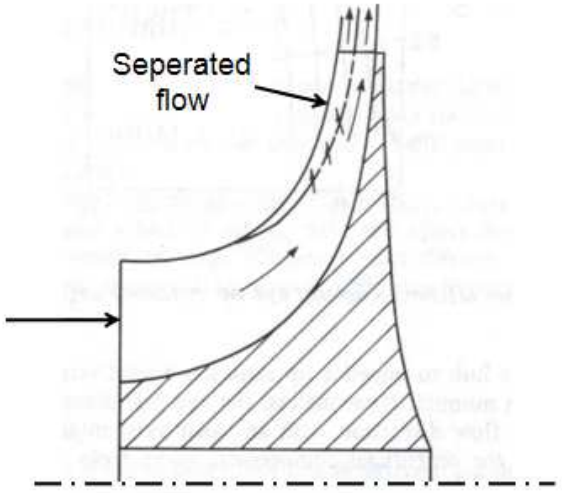

Figure 1-26 Flow separation in the impeller (14)

Diffuser is by far the most component of centrifugal compressor to suffer problems of rotating stall (24).Diffuser rotating stall is problematic because the amplitude of pressure fluctuation it causes is larger than that during impeller rotating stall.

Many studies were carried out with both theoretical and experimental methods on rotating stall in vaneless diffusers. [Jansen, 1964 (83), Senoo et al, 1977 &1978 (53) & (54), Frigne, et al, 1985 (84) , Dou et al, 1998 (85), Ljevar, 2006 & 2007 (86) & (87), Ferrara et al, 2004 (88), and Gao et al, 2007 & 2009 (89) &(90)].

Still, there are controversies on which factor indeed causes the occurrence of rotating stall. Some authors relate diffuser stall [flow break down] to the effects of boundary layers separation [(83) and (53)], while others think that the inviscid core flow is the possible reason (85), and still other researchers believe that the interaction between the core flow and the boundary layer is responsible for rotating stall (84). However, most of these studies agree on that rotating stall occurs when (90),

1. The absolute inlet flow angle reaches a critical value α_{cr} [where, critical angle depends on diffuser geometry and aerodynamic parameters]
2. Three dimensional boundary layer separations.

Moreover, these studies agreed that, stall cells rotate in the diffuser at a fraction of the impeller rotational speed, and that the number of stall cells present is also influenced by diffuser geometric parameters as well as flow parameters. Moreover, generated instabilities can be measured over the whole axial width of the diffuser (89) .

Finally, effect of impeller on vaneless diffuser stall has been investigated by Tsujimoto et al, 1996 (91) who studied impeller blade angle influence on instability of vaneless diffuser. He concluded that upstream impeller had no influence on rotating stall in diffuser. However, analysis carried out by Ljevar et al, 2006 (86) showed strong influence of impeller on diffuser stall.

- Vaned diffuser stall

Vaned diffuser stall occurs when the air incidence angle at the diffuser vane inlet reaches a critical angle, in a similar way as the inducer stall (14). Many investigations have been done on stall in vaned diffuser [see Elder & Gill, 1984 (92)].

D. Volute stall

Very few studies have been done on stall in volute instabilities. The simple overhung volute becomes essentially a wrapped-up conical diffuser, with swirling flow which might enters into a stall mode either ordinary or skewed. Stages have been diagnosed where stage stall and surge were found as soon as the volute changed over from accelerating to diffusing mode (24). Fischer, 1988 (93) observed that in compressors with vaneless diffuser the volute tongue sets up a circumferential disturbance that gives to a non uniform pressure field in the inducer, which can cause premature stalling, eventually leading to surge.

The instability of the tongue zone was also reported by Hillewaert et al, 1999 (94) who developed a numerical code to study impeller volute interaction and concluded that at high mass flow rate the strongest static pressure distortion is located around the tongue zone which creates a separated flow into the exit cone onto the suction side of the tongue. Yadav & yahya, 1980 (70) observed a flow separation at high inlet swirl angles near the volute tongue as well as in the exit diffuser.

From few investigations on volute instabilities, we can conclude that volute instability may have a decisive effect on stage instability, however it is the least researched instability in centrifugal compressors. A thorough study is needed to better understand volute instability effect on stage stall and eventual system surge of turbocharger compressors.

❖ Stage stall

In previous section, component stall has been presented. It was indicated that many stall types can exist without stage stalling. It is possible for several components to stall without the entire stage stalling.

A compressor stage enters a stage stall when:

- o One of its components enters a strong stall
- o A number of elements together collectively stall

Stage stall is the condition where the basic flow characteristics of the stage alone are no longer stable so that the overall head versus flow rate is no more stable [positive or zero slopes] (24).

$$\left.\frac{\partial \mathrm{TPR}}{\partial \mathrm{Q}}\right]_{\mathrm{N}} \geq 0 \qquad \text{1-63}$$

The two main components -impeller and diffuser- of the centrifugal compressor may stall individually or simultaneously. Stall in one component by itself may not be enough to cause the whole stage to stall (3). When there is a very strong stall in one component or when several components together stall the stage cannot operate stably and the phenomenon is described as stage stall. When the stage stall becomes periodic and grows to a large amplitude, the system [comprising inlet ducting, inlet guide vanes, rotors, stators or diffusers, and any pressure recovering exhaust system] can become exiting. This system instability is described as surge. De Jager, 1995 (81) considered that surge can only occur if both the components stall simultaneously.

After studying stall in each compressor component, and the contribution of each component stall on overall stage stall. In the coming part, system surge will be explained.

1.4.2 Surge

Surge is a self-excited cyclic phenomenon, affecting the compression system as a whole, characterized by large amplitude pressure rise and annulus averaged mass flow fluctuations. Even flow reversal is possible. The occurrence of surge is a result of the stalling of some component or combination of components such that continued reduction of flow rate makes the entire system unstable and causes surge (71).

The essential differences between rotating stall and surge are that the average flow in pure rotating stall is steady in time, but the flow has a circumferentially non-uniform mass deficit, while in pure surge the flow is unsteady but circumferentially uniform. Because it is steady, rotating stall may be local to the compressor or to parts of the compressor. Due to its unsteadiness, surge involves the entire compression system. So, the phenomena can be regarded as distinct. On the other hand, both phenomena are natural oscillatory modes of the compression system, with surge corresponding to the lowest [zero] order mode, and thus they are related (81).

Surge results in considerable loss of performance and efficiency. Furthermore, the power level of the pressure oscillations can approach that of the compressor itself, inducing large mechanical loads on the entire compression system (79).

Surge frequency and amplitude are dictated by the size and the volume of the installation before and after the compressor, their flow characteristics and compressor speed (14). One can distinguish four types of surge based on the amplitude and frequency of the associated oscillations, these are: mild surge, classic surge, deep surge, and modified surge [De Jager, 1995]. The terminology is not unique, e.g., in [Williams et al, 1993 (78)] the term classic surge is used for phenomena that are termed here modified surge [Figure 1-27]. Figure 1-28 shows difference between deep and mild surge.

For mild and classic surges, there is no flow reversal. However, periodic pressure ratio fluctuations are small for mild surges whereas they are larger for classic surges [Vishwanatha & Ramesh, 2007 (95)]. The frequency of mild surge fluctuations is often close to the natural frequency of the compression system [Fink et al, 1991 (96)] i.e., the resonance frequency of the compressor duct and the volume connected to the compressor [called plenum] (64). A mix of classic and rotating stall is called modified surge. Deep surge is the most severe form of surge and it is associated with low frequent, large amplitude oscillations and negative flow rates [back flow] during a part of the surge limit cycle (79). If an automotive turbocharger is driven in deep surge cycles for too long the turbo charger will break down (97).

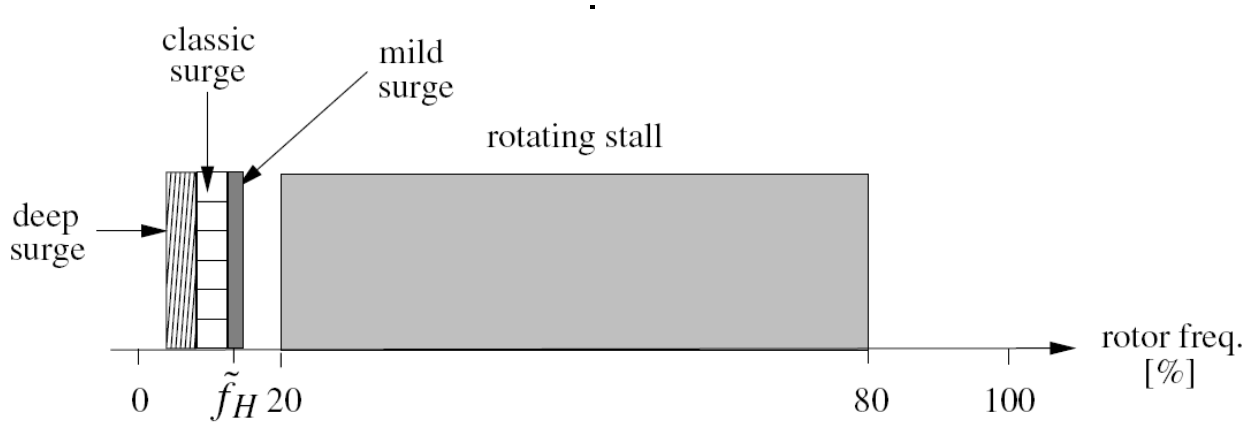

Figure 1-27 Frequencies of several types of aerodynamic flow instabilities with scaled Helmholtz frequency (78)

An example of such a limit cycle oscillation is shown in Figure 1-28. A transition from mild to deep surge is studied in Ribi & Gyamathy, 1993 (98).

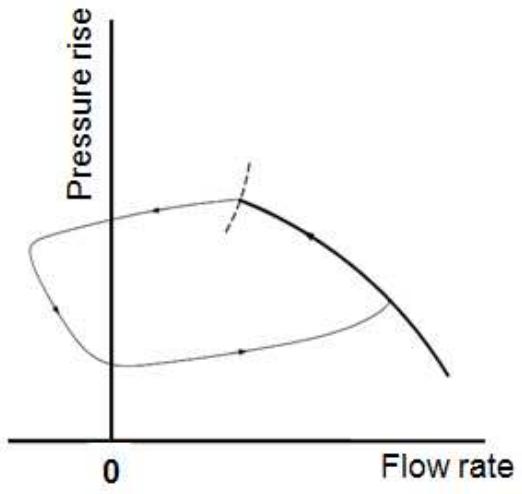

Figure 1-28 a typical deep surge cycle (79)

In the literature, various models can be found that describe rotating stall or surge, as first proposed by Emmons et al, 1952 (72) then progressed through many development and modification stages [(75) &(76)], the present models for the prediction of performance characteristics during the compressor unstable flow regime are still relying on empirical data and experience (35). Greitzer [(75) & (76)] showed that the value of a parameter B [system impedance], largely determines whether, upon onset of instability, the system will settle into a stable rotating stall or enter a surge cycle [Figure 1-29]. Where B is defined as:

$$B = \frac{U_t}{2\omega L_c} = \frac{U_t}{2a}\sqrt{\frac{V_p}{A_c L_c}} \qquad 1\text{-}64$$

$$\omega = a\sqrt{\frac{A_c L_c}{V_p}} \qquad 1\text{-}65$$

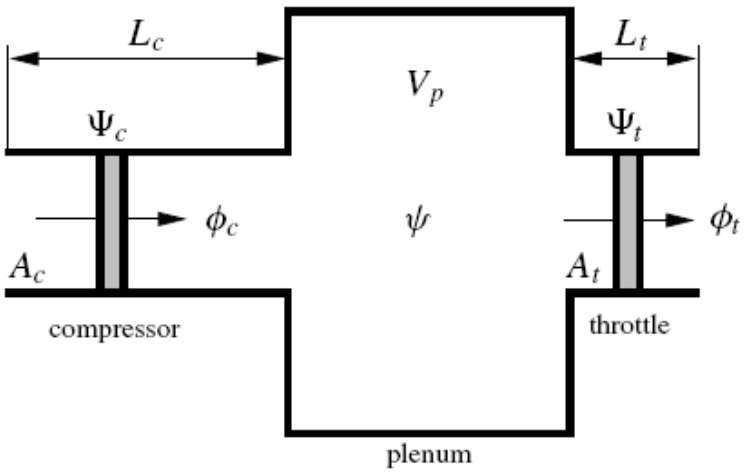

Figure 1-29 Surge model for compression system (40)

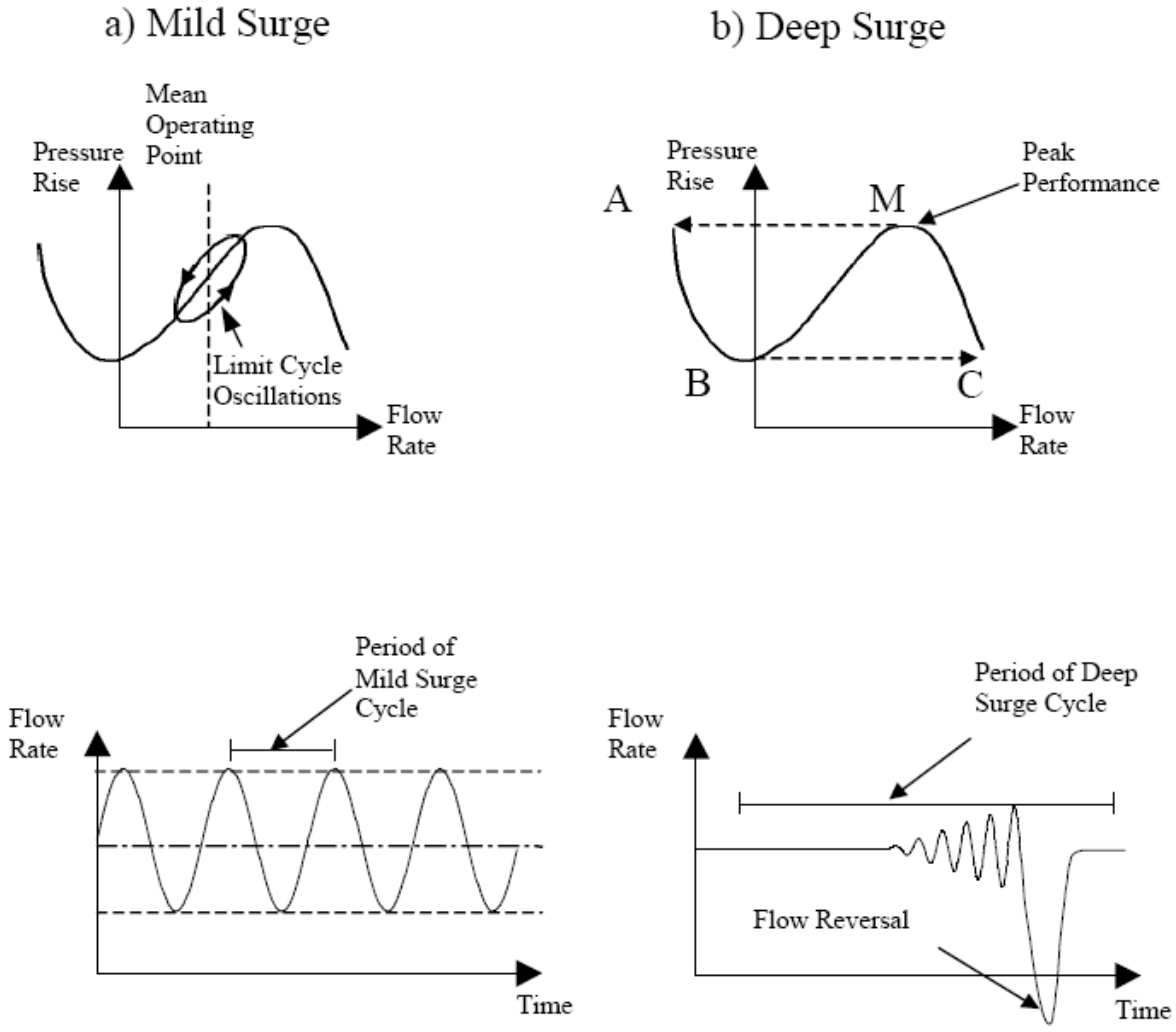

Figure 1-30 Schematic of Mild and Deep Surge Cycle (99)

Note that, the application of Greitzer model to centrifugal compressor was first proposed by Hansen et al, 1981(100). A comprehensive overview can be found in (40), see also (101).

Surge has been the subject of numerous studies and the interested reader can be referred to countless publications. See for example [(71), (102), (96),(81),(98),…].

1.5 Techniques to suppress surge in centrifugal compressors

The main aim of any surge suppression technique should emphasize the ability to delay, or better still eliminate, the tendency for stall to develop in any component (35).

Various techniques have been proposed in order to extend the stable range of a centrifugal compressor. These techniques can be variable or fixed and are listed in increasing order of complexity [and therefore decreasing order of acceptability] for each case. A literature survey of each of these techniques is covered in this section.

1.5.1 Variable geometry techniques

The basic velocity triangles have limitations which are too restrictive for wide range compressor applications. Therefore, the desires to change these velocity triangles beyond that which is normally practical, one must use adjustable or variable geometry. Variable geometry can be used at the inlet of a stage [impeller inlet], in the diffuser, or the volute [not yet used for automotive turbocharger compressor applications].

A great advantage of variable geometry techniques is their ability to reduce the surge flow limit without adversely affecting compressor performance at the design point. It meets this requirement as they remain inactive when design point peak efficiency is required and used only when surge is imminent.

In this section, we will introduce the different variable geometry techniques to limit onset and development of stall, in centrifugal compressors [different applications] studied in the literature. The different geometry techniques proposed and tested to suppress surge are presented in increasing order of complexity.

1.5.1.1 Techniques for imparting swirl at compressor inlet

Variable inlet guide vanes are popularly used for flow control, and they work by one of two principles (27):

- Throttle the inlet [using simple throttles or inefficient guide vanes] and relocating the operating point of the compressor by changing inlet density.
- Change the inlet swirl, this is the more efficient approach. In which the compressor in unloaded according to the Euler equation of turbomachinery.

Pampreen, 1993 (71) explained the effect why imparting swirl at the compressor inlet cause a shift of the surge line to lower flow rates, when imposing positive swirl or prewhirl [in the direction of rotor rotation] or to higher flow rate when imposing negative or counter swirl [in the opposite direction if rotor rotation].

For sign velocities employed in this work, the components of velocity in the rotor direction of rotation are positive and those on the opposite direction are negative.

In case of positive swirl surge line shifts to lower flow rates by decreasing the incidence angle at which surge occurs to a lower value of flow rate. This is illustrated in the vector diagram of Figure 1-31. The solid line vectors show the velocity triangle of zero swirl at an inlet relative flow angle β for a given rotor linear speed U. With positive swirl, the same value of inlet relative flow angle occurs at a lower value of axial velocity. This means that stalling incidence angle will occur at a lower value of mass flow, or flow coefficient and thus provide a wider stable operation (71).

In case of negative swirl, surge line shifts to higher flow rates by increasing the incidence angle at which surge occurs to a higher value of flow rate. With negative swirl, the same value of inlet relative flow angle occurs at a higher value of axial velocity. This means that stalling incidence angle will occur at a higher value of mass flow or flow coefficient and thus provide a narrower stable operation.

Theoretically, when providing prewhirl [pre rotation in the impeller rotation direction], the specific work developed by the machine reduces due to Euler's equation [equation 1-12]. If the pre-rotation is applied in the opposite to impeller rotation direction, the specific work developed by the compressor increased. However, experimental results shows that the specific work cannot be increased further when the inlet guide vane angle is beyond -20°(103) . Shouman & Anderson, 1964 (104) reported this angle to -15°.

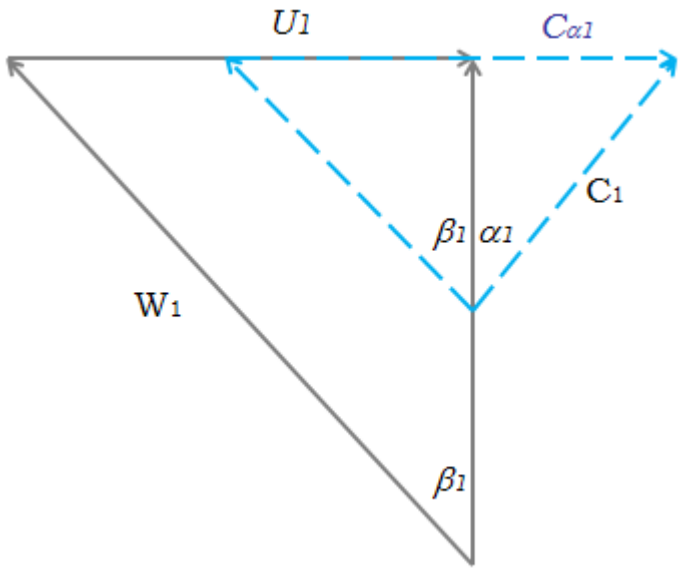

Figure 1-31 Inlet velocity diagram showing reduction in inlet velocity due to positive swirl (71).

Swirl at impeller inlet can be imparted using one of the following techniques:

A. Variable axial guide vanes
B. Radial axial guide vanes
C. Flexible guide vanes
D. Other swirl generators

The effect of inlet swirl at the compressor inlet has been widely investigated [Rodgers,(34),(105), &(106)] for small gas turbines. Whitfield et al, 1975 (107), Simon et al, 1987, and Najjar & Akeel, 2002 (108), for process compressors. Kyrtatos et al, 1980 (109), Watson, 1982 (14), Whitfield et al, 1975, 1998 [(107) &(110)], Ishino et al, 1999 (111) , Nikpour, 2004 (112), and Galindo, 2006 (113), for turbochargers, and yet it remains little used in the turbocharger application. Elder & Gill, 1985 (114) attributed this lack of interest to increased costs, noise and icing problem, particularly at high speeds.

A. Axial guide vanes

Variable inlet guide vanes [VIGV] have been used in centrifugal compressors for blowers, in gas turbines for electrical power generation, and in gas engines for automotive propulsion, and yet not used in the automotive turbocharger application. At the beginning the principle was used for power regulation and not necessarily for surge line improvement. However, the experimental data show that significant shifts can be made in centrifugal compressors surge line with inlet guide vanes (71).

Whitfield et al, 1975 (107) showed experimentally that compressor stable operation can be extended to low flow rates when imparting positive swirl. Moreover, author studied the effect of different prewhirl distributions on the compressor performance, supported by experimental results carried out on radially bladed impeller, produced results indicated that the forced vortex gives the best favorable velocity distribution at inducer inlet and free vortex the most undesirable.

Ishino et al, 1999 (111) developed a variable AGVs [Axial Guide Vane system] for a small centrifugal compressor of automotive turbocharger. The effect of different positive AGVs setting angles on the compressor performance has been investigated. They concluded that AGVs was effective in improving surge limit, and in improving compressor efficiency at middle and low flow rates, with the effect of efficiency becoming greater at high pressure ratios. Moreover, the effect of including a center body to the AGVs was also studied. Results showed that center body improves efficiency at high flow rates by preventing flow passing through the center hole.

Uchida et al, 2006 (115) investigated the effect on surge limit of a turbocharger compressor using a variable AGVs. Figure 1-32 shows the effect of a +80° AGV setting angle compared to 0° AGV setting angle, on compressor compression ratio. As it can be seen, accompanied to the surge line improvement, high pressure losses are obtained. This can be explained by pressure drop through the AGVs and the positive pre-rotation [Euler equation].

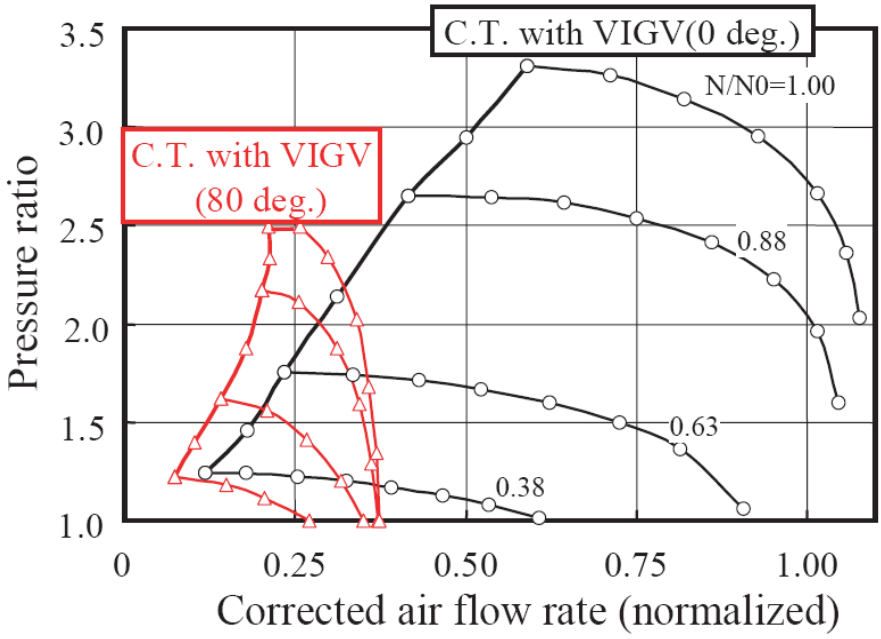

Figure 1-32 Positive swirl effect on compression ratio [Uchida et al, 2006 (115)]

Flow in centrifugal compressor with AGVs is numerically simulated and analysed by Xiao et al, 2007 (116) . After confirming performance cuves shift to low and high flow rates when imarting positive and negative swirl, respectively. He concluded that at high positive guide vane angles, back flow regions are found in front of the suction surfaces of splitter blades at high flow rates, while at low flow rates, seperation exists on the suction side of the main blade.

Gopalakrishnan & Rangaswamy, 1974 (103) studied experimentaly the influence of imparting postive swirl using AGVs at the inlet of a blower centrifugal impeller. He concluded that a pre-rotation in the region of 7° to 20° in the dire ction of rotor rotation, improves the performance of the blower. While, high pre-rotation angles amounted to high pressure losses in the suction duct of the blower. Gopalakrishnan & Rangaswamy (103) did not give any describtion of the tested AGV system.

AGVs for industrial centrifugal compressor has been improved using a combination of numerical and experimental analysis by Coppinger & Swain, 2000 (117). Authors proposed some important improvements in order to minimise pressure losses throught the guide vane system while inducing large swirl angles.

Rodgers, 1964 (34) evaluated the feasibility of regulating inlet guide vanes to improve the stability limit of a centrifugal compressor with vaneless diffuser, he arrived at the conclusion that significant changes in surge characteristic may be obtained through inlet guide vane regulation, provided the vaneless diffuser is not operated near its stability limit.

Rodgers, 1990 (106) investigated the use of AGVs in a single stage centrifugal compressor with vaned diffuser, he concluded that AGVs regulation increased impeller stability, this permitted the diffuser to operate stalled, and this provide the compression system stability remained in the negative slope.

Steinke & Crouse, 1967 (118) invesitgated the effectiveness of variable AGVs to control flow at the rotor inlet for gas turbine application. After studying different veloctiy distributions at rotor inlet, authors concluded the potential of improving surge limits with varibale AGVs.

The effect of different vane profiles of an AGVs on the overall performance of a centrifugal compressor has been investigated by Najjar & Akeel, 2002 (108).

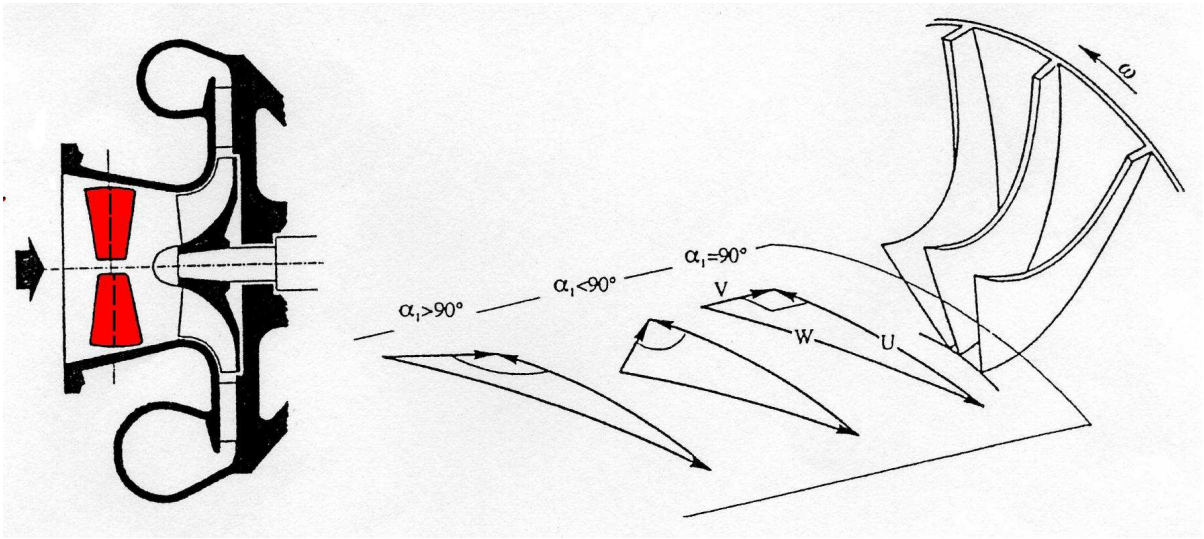

Figure 1-33 Imparting positive and negative swirl using VIGVs (21)

As it can be seen, the AGVs has been tested for different compressor application for the goal of improving surge margin. Authors agreed on the following:

- Positive setting angles move surge line to low flow rates, by decreasing incidence losses at impeller inlet at low flow rates.
- Efficiency slightly increases at middle and low flow rates, at positive setting angles.
- AGVs create high pressure losses, particularly for high setting angles and at high speeds and flow rates.

Although positive AGV setting angles have shown their ability to improve surge line, and slightly increase efficiency at middle and low flow rates. However, this technique is still not used for turbocharger applications. This is due to packaging difficulties, complex manufacturing and control, hence additional cost.

Moreover, it is worth noting that, very few studies have been done on the effect of high negative swirl imparted by AGVs on compressor performance and surge line limits.

Positive and negative AGV setting angles are shown in Figure 1-33 and Figure 1-34.

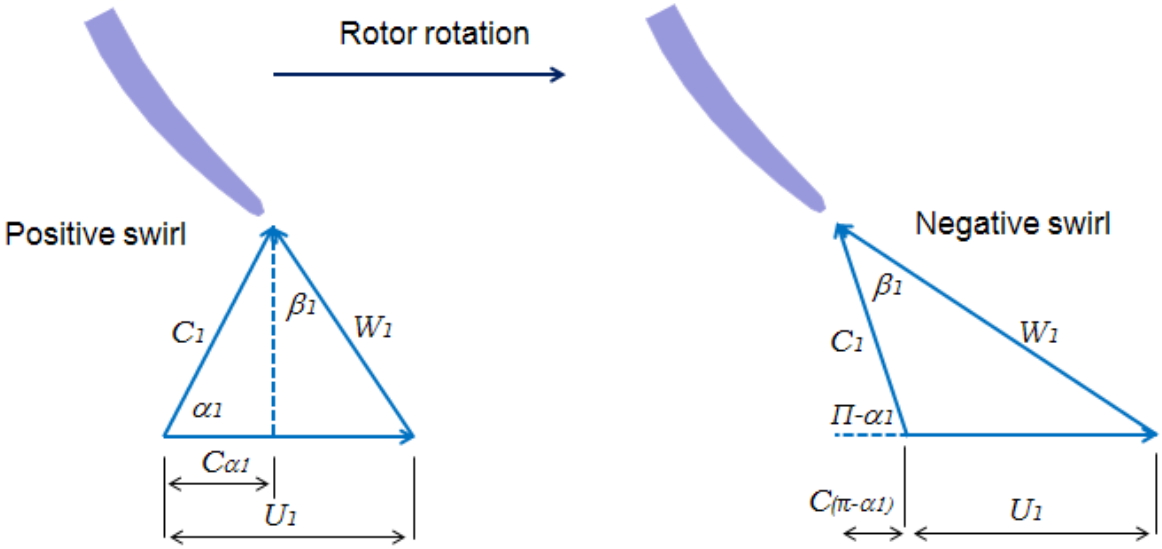

Figure 1-34 Nature of positive and negative swirl

B. Radial guide vanes

The radial arrangement is when guide vanes are installed in the radial inlet duct, perpendicular to the compressor axes [Figure 1-35]. With the radial guide vanes, the swirl is initiated in the radial plane and then turned through into the axial direction.

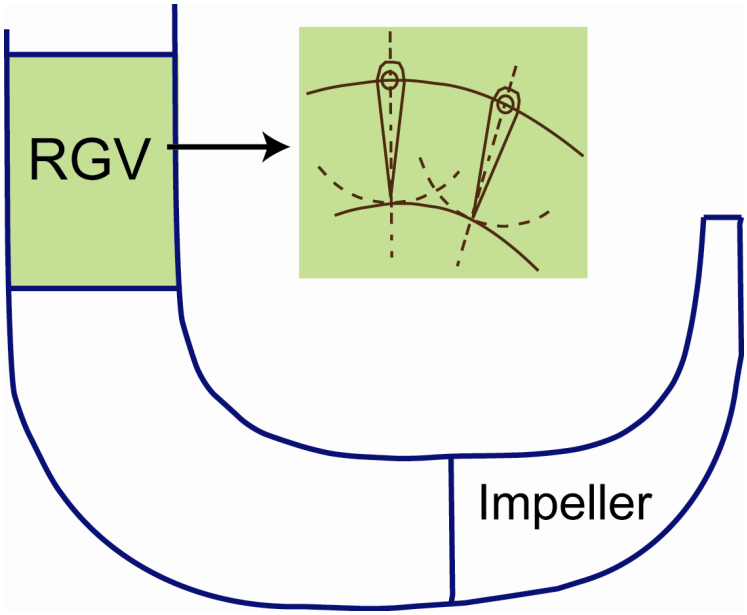

Figure 1-35 RGV configuration

Rodgers, 1977 (105) used a combination of backswept impeller with variable inlet guide vanes, showed that application of positive inlet swirl [Angle 40°] provides a significant shift of the surge line to reduced flow rates [Figure 1-36], while the application of 'small' negative inlet swirl [Angle -13°] moves the surge line to hi gh flow rates. The improvement of operating range, particularly at high pressure ratio, was accompanied with efficiency drop at the different rotational speeds, unless a slight increase at high flow rates when applying he small negative swirl.

For turbochargers for an automotive application, Schulte et al, 2004 (119) studied a compact SGD [swirl generator device] that can be installed in the reduced space allocated in the vehicle. High negative SGD angle improves surge line while small negative angles move surge line to high flow rates [25% of surge line improvement at -60°]. In the other hand positive angles slightly move surge line to low flow rates. The surge increase at high negative angles was accompanied with efficiency losses. However, some efficiency increase was obtained at low flow rates when imparting positive swirl.

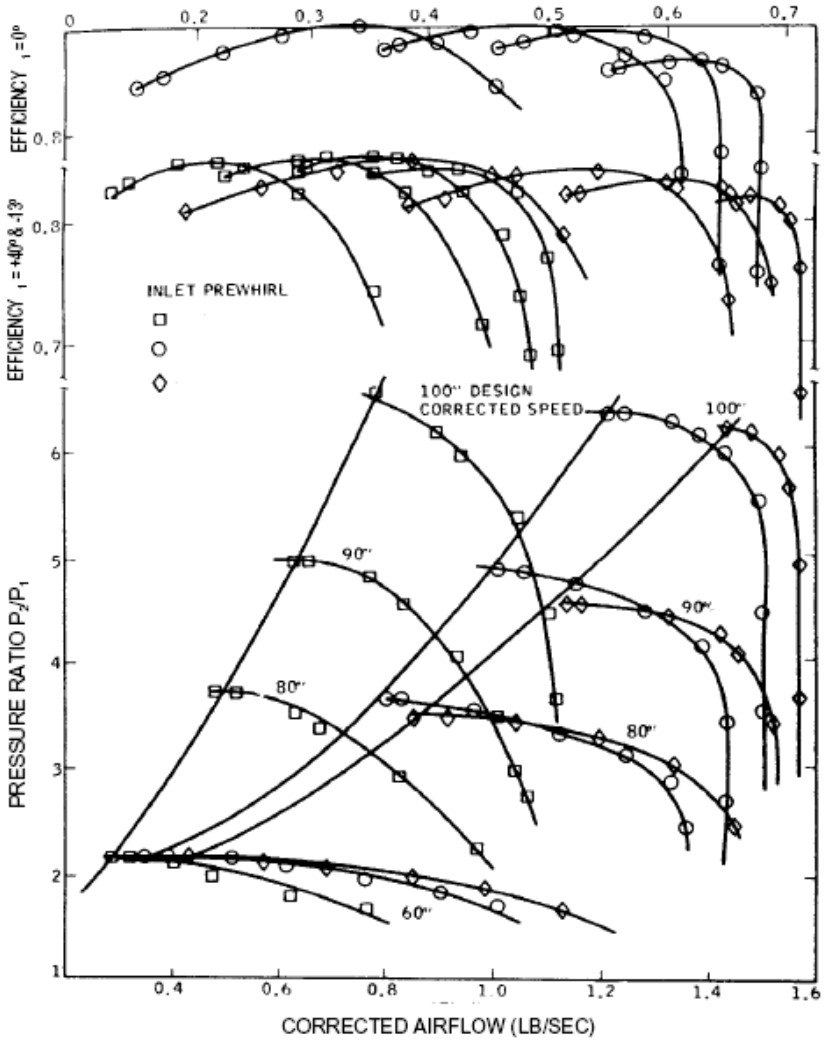

Figure 1-36 Effect on compressor compression ratio and efficiency of RGVs (105)

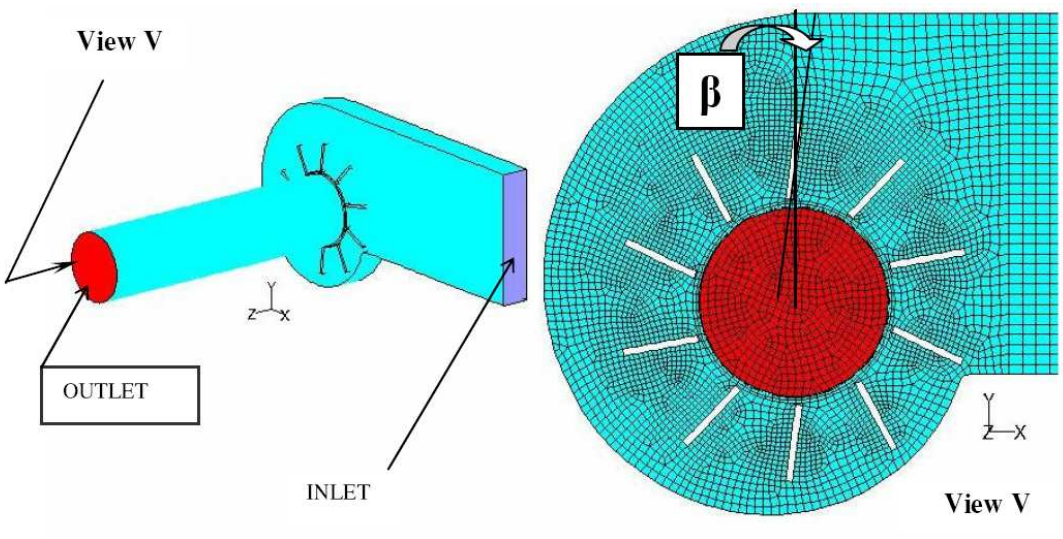

Figure 1-37 Radial swirl generator studied by Schulte et al, 2004 (119)

Noting that the SGD system of Schulte et al, 2004 (119) was first patented by Kindl et al, 2006 (120).

Based on the configuration of Schulte & al (119), Galindo, 2006 (113) has studied a 10 blade SGD system, the system was fabricated from hard plastic material. Author had the same conclusion of Schulte that negative angles were best for moving surge line to low flow rates. He explained the surge line shift with negative swirl by the increase of relative velocity in one hand, and the decrease of the incidence angle with respect to axial configuration in the other hand. Moreover, Galindo recommended small negative swirl angles since it increases compression ratio compared to basic characteristics, which is not the case when imparting positive swirl.

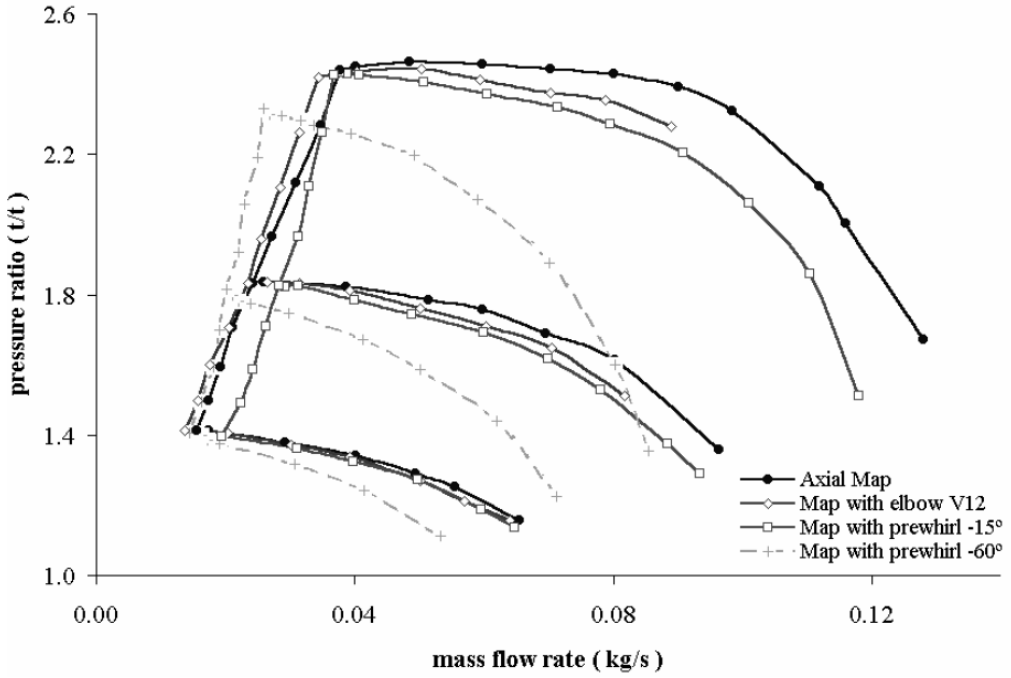

Figure 1-38 Effect of negative SGD angles on compressor performance [Schulte et al, 2004(119)]. Pressure losses in the SGD system are included in the map

Finally, very few investigations have been done on the application of RGVs on automotive turbocharger applications. The system still has some major drawbacks

- RGVs cannot obtain zero swirl. Since the curved duct imparts swirl even if the radial vane angle is zero.
- Packaging difficulties, and additional control systems, hence more expensive.

C. Flexible guide vanes

Flexible guide vanes [FGV] produce flow vectoring in the direction of rotation of the rotor [positive swirl], and deform under the effect of flow velocity. It consists of a fixed area connected with support section and an adjustable or deformable area, sometimes connected with circular adjusting section [Rudolf et al, 2006 (121). FGVs has been applied to industrial centrifugal compressor, it was presented as a smart inlet guide vane for their ability to act as high-response actuators and provide proportional control [Willimas & Cornelius, 2006 (122)].

The application of flexible guide vanes to turbochargers was first proposed by Wimmer & Steindl in 2004(123) then Rudolf et al in 2006 (121). However, their effect on the compressor performance was not presented.

The FGVs proposed by Rudolf et al (121) is presented in Figure 1-39. The system consists of 4 flexible vanes, fixed from end and can be regulated from the other end. The disadvantageous of this system is its complexity and consequently its cost which is inacceptable in a very cost sensitive car market. On the other hand this system can offer another view to the pre rotation systems at compressor inlet since it 'can' offer a well distributed angle in contrary with axial or radial systems. However, for this a very well studied system has to be done.

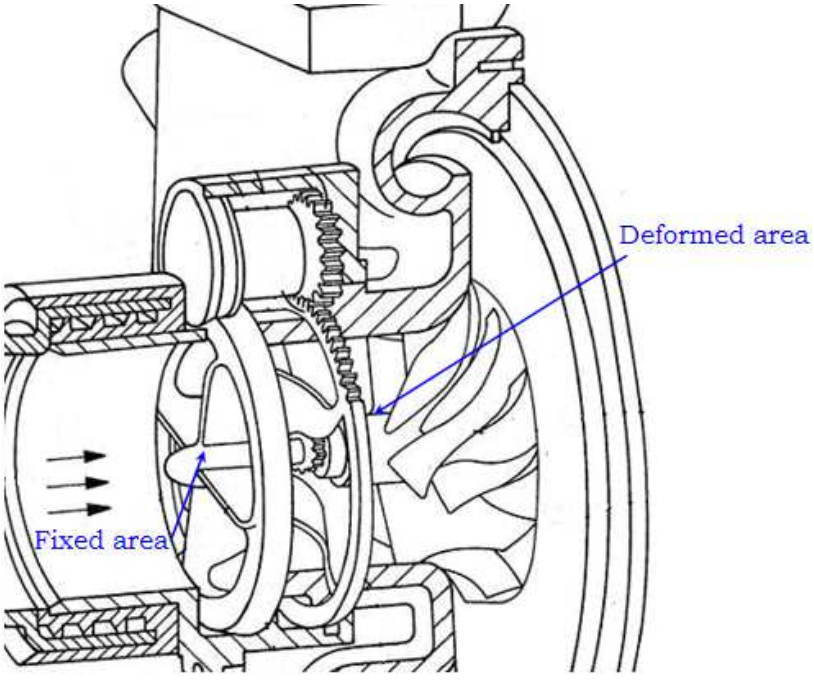

Figure 1-39 Flexible guide vane system (121)

Although FGVs has been recently used for automotive application, and in spite of the two inventions of Wimmer et al (123), and Rudolf et al (121), no public studies on the application and effect on performance of the FGVs on turbocharger compressors were found.

This work contributed in presenting the effect of FGV on an automotive turbocharger compressor performance and stable functioning.

D. Other swirl generators

Whitfield & Abdullah, 1998 (110) investigated the application of high inlet swirl through the use of a variable geometry volute at the compressor inlet. The proposed technique was advantageous in surge suppression by producing high swirl angles efficiently. However, a major disadvantage of this configuration is the place it takes and its need to have a dual entry, which is a major constraint for automotive application [Figure 1-40].

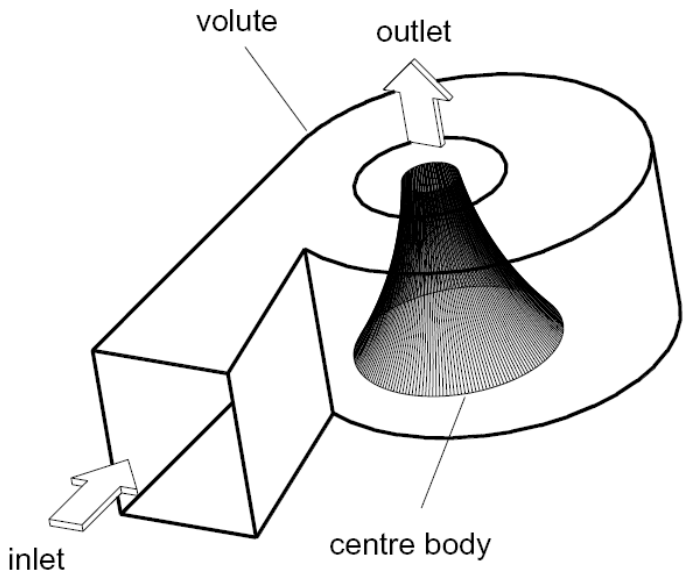

Figure 1-40 Working principle of the volute swirl generator (35)

Some of the patented swirl generators [Barker, 2005 (124) and Mcdonald, 2004 (125)] are presented in Figure 1-41 and Figure 1-42. It is assumed that these generators can be used for turbocharger for automotive application. The two swirl generator are almost similar, they are composed of two inlets, when swirl is needed the valve of the inner tube closes and the vanes between the two tubes impart swirl to the fluid entering the impeller, when swirl is not needed [ex. high flow rates] valve opens and the biggest part of the fluid enters the main entry.

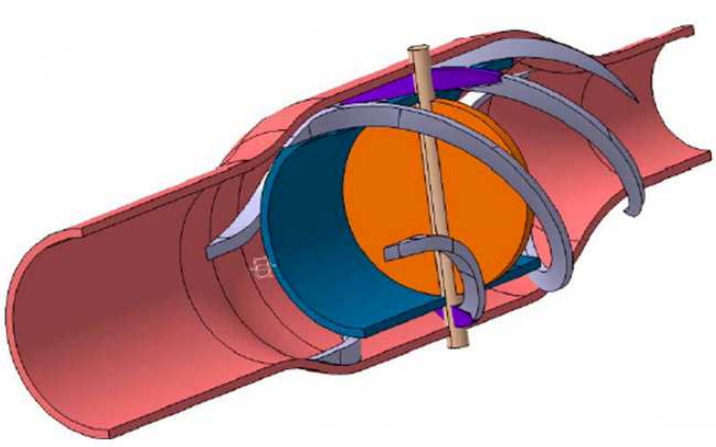

Figure 1-41 Swirl generator developed by Ford (124)

Results obtained from the Barker's swirl, were not presented in [Barker, 2005 (124)]. However, the new swirl generator is believed to efficiently increase the operating range of the compressor, up to 20% according to computational fluid simulation [CFD] (126).

Results obtained when installing Mcdonald swirl generator [Figure 1-42] are shown in Figure 1-43. Compressor efficiency and compression ratio at blade angles 0°, 50°, and 70° [blade angle is 8 in figure], are presented. Some small changes to surge line was obtained, together with efficiency increase at low speeds. Notice that, the zero swirl was not compared to straight tube inlet characteristics. However, this comparison is very interesting to find out the effect of system impedance change when installing the proposed system. Moreover, efficiency was presented at one speed line which is not sufficient.

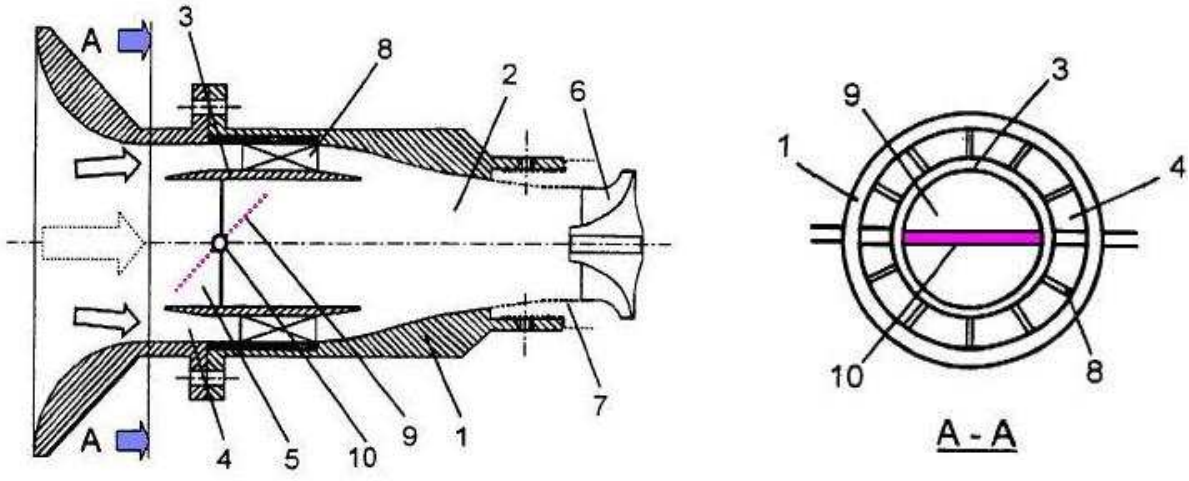

Figure 1-42 Inlet swirl vanes with inner sleeve and shut-off valve [Mcdonald, 2004]

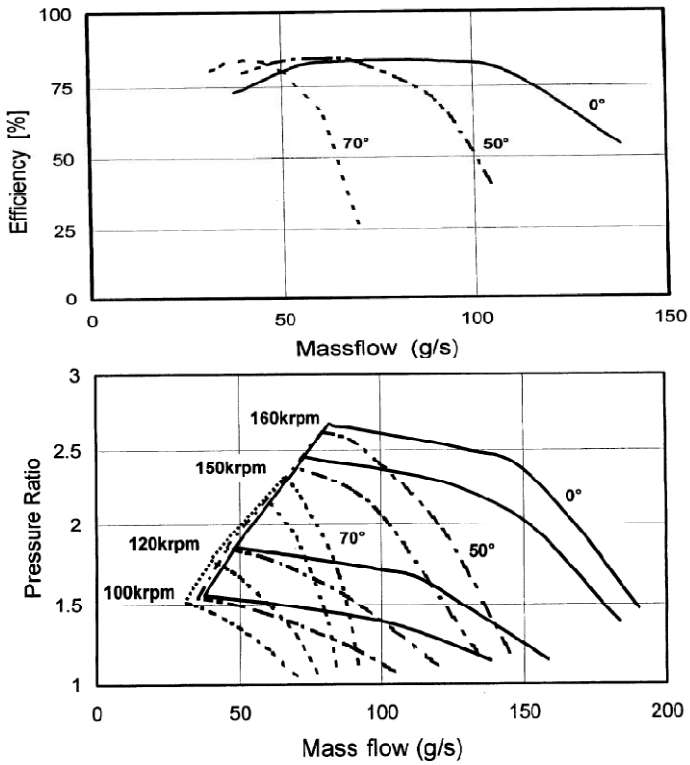

Figure 1-43 Results obtained when using Mcdonald swirl generator (125)

The presented swirl mechanism would add substantially to the total cost and complexity to a turbocharger unit. Moreover, with the reduced space allocated in the vehicle these techniques can be difficult to install.

The feasibility of these generators, therefore, needs to be assessed further from a cost point of view, and from its ability to be operated automatically when located on an engine.

1.5.1.2 Variable geometry diffuser

The different techniques proposed or tested in the literature to vary the geometry of vaneless and vaned diffusers are presented in this section

- Vaned diffuser

The incentive for the application of vaned diffuser, which in theory can reduce the friction losses by reducing the long flow path usually associated with the vaneless type, has been the demand for high efficiency at high Mach numbers. A typical vaned diffuser consists of two parts, a semi-vaneless space where the free vortex type flow changes to a straight channel flow, which is diffused from the vane throat to outlet

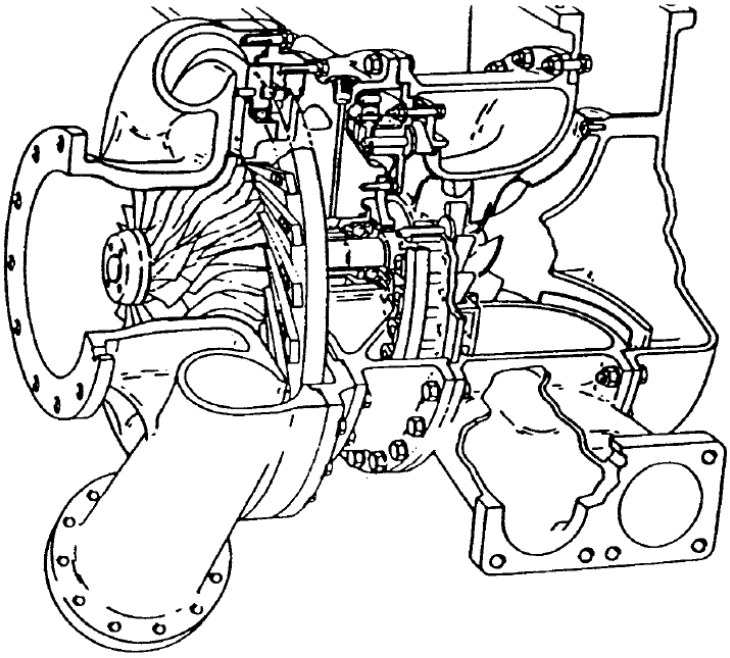

Figure 1-44 the variable geometry diffuser tested by Berenyi et al, 1979 (127)

Simon et al, 1978 (128) and Zhou et al, 2008 [referred to (35)] used aerodynamically shaped diffuser vane profiles and adjusted them in conjunction with variable inlet swirl vanes for industrial compressor applications. They showed that the simultaneous adjustment of the inlet guide vanes and diffuser vanes provided expansion in the operating range and efficiency improvements over the entire range of the compressor [Synergy effect].

Harps et al, 1979 (129) and Berenyi et al, 1979 (127) described an arrangement where the vanes were pivoted close to the leading edge and the vane angle set by pins sliding in slots along the chord of the vane. The vane pivot position was chosen so that the diffuser throat area was maximized at the minimum stager angle to allow a high choked flow rate [Figure 1-44]. Conclusions from these two studies were highly in favour of the variable diffuser design for improving surge and pressure ratio requirement when used with backswept impeller.

Chapman et al, 2003 (130) reported a numerical study on the effect of variable vaned diffuser on turbocharger compressor performance. He concluded that the incidence plays the major role in determining the range of the diffuser, with 10° setting angle giving best efficiency and pressure recovery and choke margin of stage was increased. Chapman et al, 2007 (131) developed a variable vaned diffuser [Figure 1-45]. The variable system can be rotated in real time to increase the operating range of the turbocharger under loading conditions.

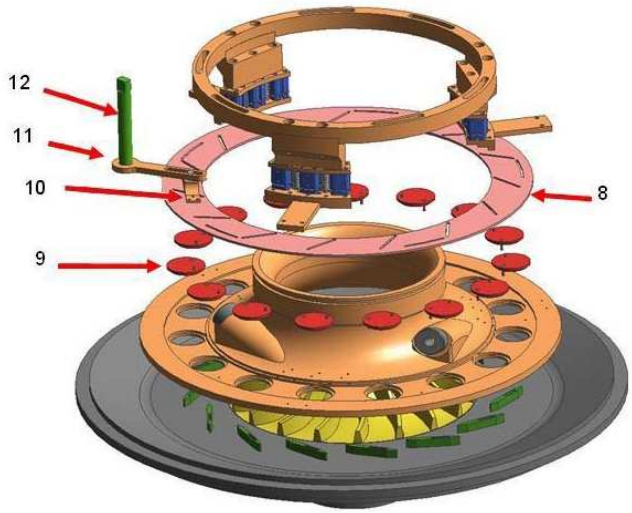

8	Groove ring
9	Vane washer
10	Rotation connection
11	Shaft arm
12	Turning shaft

Figure 1-45 Variable diffuser geometry (131)

A new variable geometry diffuser whose vanes can be put in and out at the diffuser passage was developed by Tange et al, 2003. The system has moved surge line to high flow rates, while very slightly moving choke line to high flow rates, and conserving efficiency with respect to vaneless diffuser. The advantage of their system is a torque improvement by the variable geometry diffuser at low engine speeds.

Regardless the good results obtained by variable vaned diffusers, economic analysis for gain versus payoff should be done. Moreover, noise production due to small distance between impeller blade trailing edge and diffuser leading edge still a problematic of this technique [salvage, 1999 (132)]

❖ Vaneless diffuser

Whitfield et al, 1976 (133) stimulated the application of variable vaneless diffuser wall by introduction of a series of alternative wall plates. Effects of these arrangements on the compressor map include the shifting of peak pressure ratio to lower flow rates and broader operating range.

Whitfield & Sutton, 1989 (134) conducted an investigation on effects of the flexible diffuser and sliding throttle ring on the compressor performance [Figure 1-46]. Although a truly variable geometry diffuser was not used in this study, plates simulating the two mechanisms were designed and tested [The design and testing of these variable geometry devices is fully reported by Leonard, 1989 [referred to (134)].

Figure 1-46 shows various combinations of the plates simulating a flexible diffuser and sliding throttling ring. As in the earlier work of Whitfield et al, 1976 (133), peak pressure ratio was again moved to lower flow rates together with improvements in the pressure ratio and efficiency at the near surge flow rates.

Whitfield & Sutton, 1991 (135) studied the different existing techniques to improve turbocharger compressor surge margin, and stated that the use of variable geometry compressor with a variable geometry turbine leads to a considerable increase in low speed torque without incurring the danger of compressor surge.

Due to more available space, more studies on different techniques for varying the geometry of a vaneless diffuser for industrial applications have also been studied [see Nestiel, 2002 (136)].

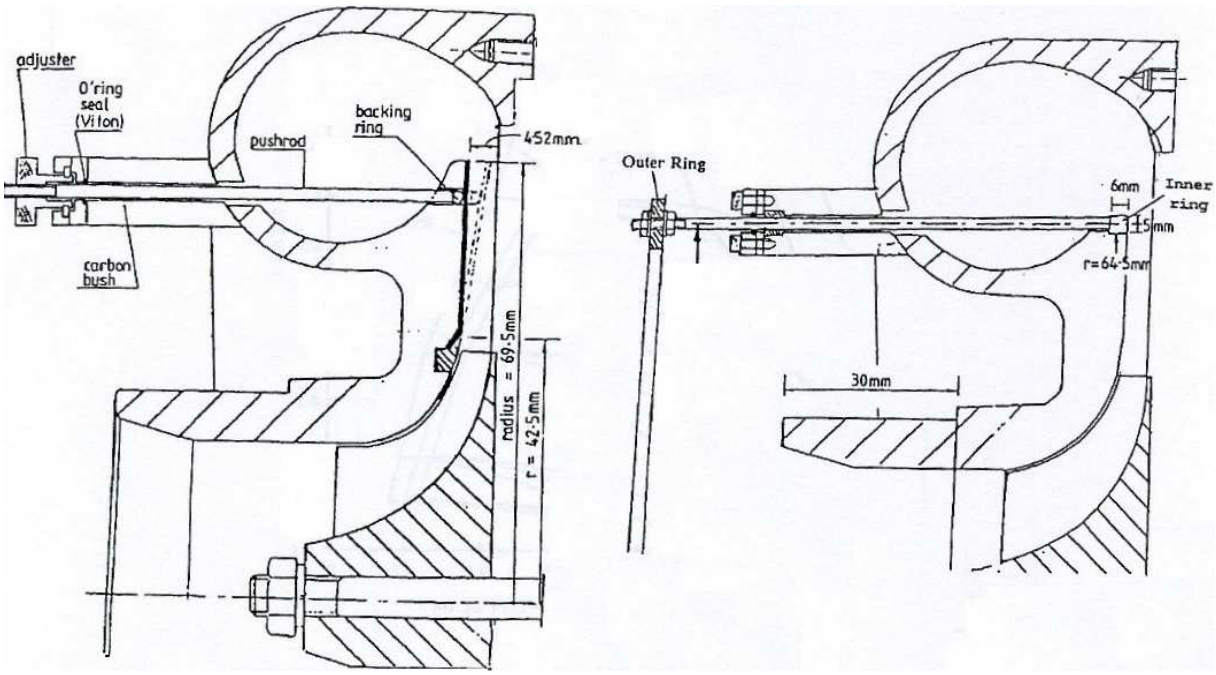

Figure 1-46 housing with polymer disc [left] and a sliding ring [right]. (134)

1.5.1.3 Variable volute geometry

Lipski, 1979 (66) has made experiments in a single stage centrifugal pump equipped with a movable and easy changeable tongue [Figure 1-47]. According to Lipski, pump head and efficiency depend on the position and shape of the tongue. Moreover, Lipski suggested that the pump could be controlled by adjusting tongue angle and length as the operating point changes.

Variable volute geometry techniques for centrifugal compressor applications have not been studied yet. This may be due to the difficulty of this technique and it complexity particularly for automotive turbocharger applications.

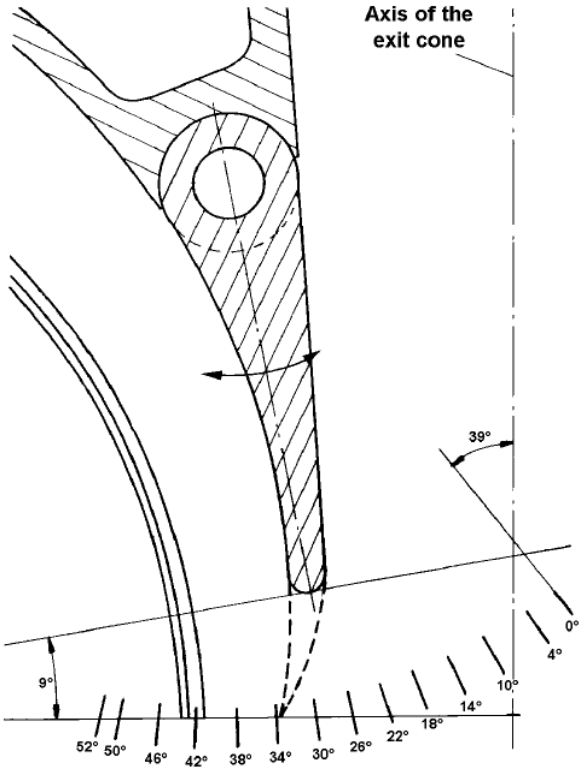

Figure 1-47 Movable and changeable tongue of the pump volute tested by Lipski, 1997 (66)

1.5.2 Fixed geometry techniques

The term fixed geometry techniques is used to explain techniques which alter the internal flow state without using variable geometry systems. Several techniques have been recommended that would affect the stable operating range of the impeller by modifying its basic flow states. One of the techniques most commonly employed today is casing treatment.

Here are the existent fixed geometry techniques in an increasing order of complexity.

1.5.2.1 Casing treatment

The benefits of casing treatment seem to have been discovered more or less around 1970. The discovery occurred on a transonic fan and this type of machine was used for many of the subsequent studies mainly at NASA Lewis. It was mainly applied to axial compressors and is usually installed in the casing over the rotor tip (64).

Casing treatments include grooves, slots or even holes cut in the compressor housing, and offer a low cost means of range extension, but their effectiveness is not always guaranteed (3). The design of the slots grooves or holes remains experimental [Eynon et al, 1996 (137)] however their location can be estimated by one dimensional model. Moreover, slots are normally concentrated in the inducer region of the impeller, although some authors apply casing treatments at the rotor tip side [(138) & (139)].

Jansen et al, 1980 (138) experimented with groove cut in the extended back face of the impeller adjacent to the entries of the diffuser passages, and Amann, 1975 (139) introduced a casing modification downstream of the impeller tip. Measurements on their test compressor showed that the flow reversal accompanying the surge occurred somewhere between the

impeller tip and the diffuser vane leading edge. So the location of this slot was chosen such that it would provide a flow relief path for the fluid backflow. A substantial increase in the flow range to be affected by the slot was obtained.

One of the problems in deciding on the usefulness of casing treatment, and in speculating how best to design it, is the ignorance which exists regarding the flow in the region which is most often critical, the end wall region near the blade tip

There has been little application of end wall treatment to industrial centrifugal compressor in the 70s, but a program of tests on two compressors has been reported by Jansen et al, 1980 (138). A total of thirty different ideas were tried to delay stall and, as the paper makes explicit, most were unsuccessful. The paper (138) describes those who were successful and interesting.

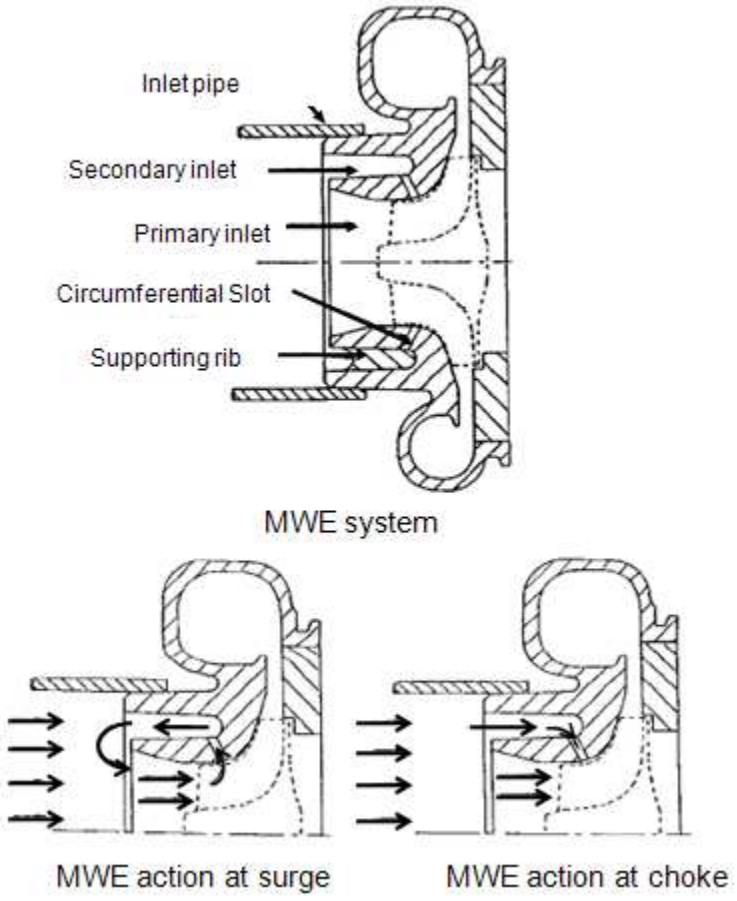

Figure 1-48 Fisher's Map width enhancement system (93)

Magdougal & Elder, 1982 (140) describe the design and testing of 2 types of casing treatment applied to a turbocharger centrifugal compressor with radial and backswept impellers, a grooved and a slotted configuration. Grooved configuration was more successful with 28% increase of surge margin.

Casing treatment with the slotted cover proposed by Fischer, 1988 (93) still the most successful for turbocharger applications. This grooved or slotted cover, referred to as Map Width Enhancer [MWE], helps to improve the surge margin by recirculating the reverse flow to the impeller inlet when surge is eminent due to decoupling the inducer from the pressure

field created by the volute, and improves the choke line by allowing additional air into the compressor through the same slot [Figure 1-48].

The mechanism is simple and cost effective and requires minimal changes to the installation, and it showed a real improvement in the stable operating region of the compressor, this improvement was verified with engine testing [figure 2-45].

Eynon et al, 1996 (137) studied the nature of flow structure through the inducer bleed slot for a particular MWE design. He concluded that the flow reversal through the slots commences at flow rates near to that at which peak efficiency occurs.

The MWE technique has been tested by other researchers and the results announced correlate with those of Fischer [(112) & (141)]. Authors explain the surge line improvement by the considerable amount of positive swirl [In the direction of rotor rotation] produced by the recirculating flow at the impeller inlet.

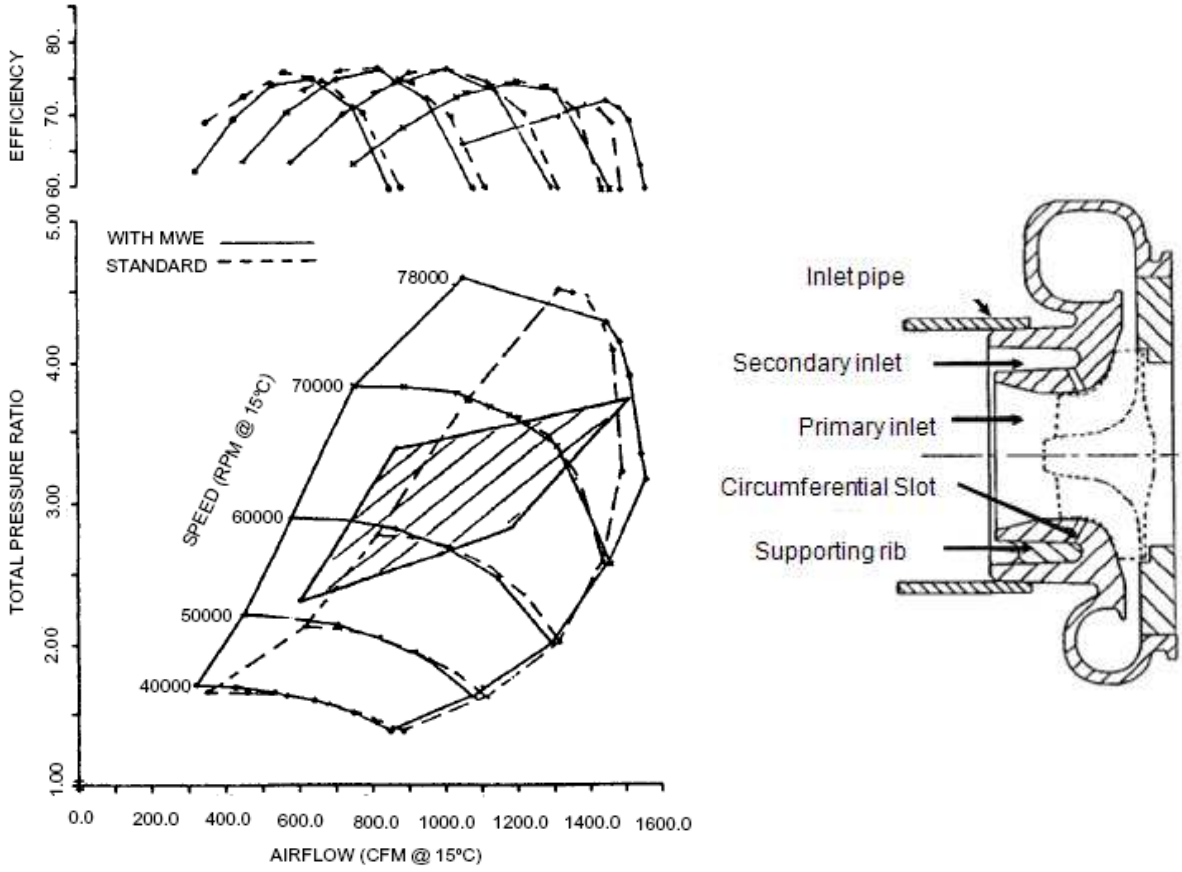

Figure 1-49 Effect of the MWE system [to the right] on an 140mm impeller engine requirement (93)

However, others consider that introducing negative swirl to the recirculating flow, by installing vanes in the cavity in order to control the swirl flow in recirculation, is more effective in improving the surge margin with no efficiency reduction (142). See Figure 1-50.

Much work has been carried out to optimize the conventional MWE system proposed by Fischer. These include bleed slots [or grooves] locations, percentage of open area, their depth and width. Moreover, the significance of the length of the inner tubular wall, L [figure 2-47] has been also investigated.

Extending the length of the inner tubular wall with respect to conventional MWE tubular wall length [In conventional MWE structure, L/Di do not exceed 0.5 (143)] results in proportional improvements to surge margin (112), this improvement is more significant when L/Di>0.9 (143). The MWE pipe length was optimized to get 15% of surge improvement. However, this improvement was accompanied with efficiency drop [Figure 1-52].

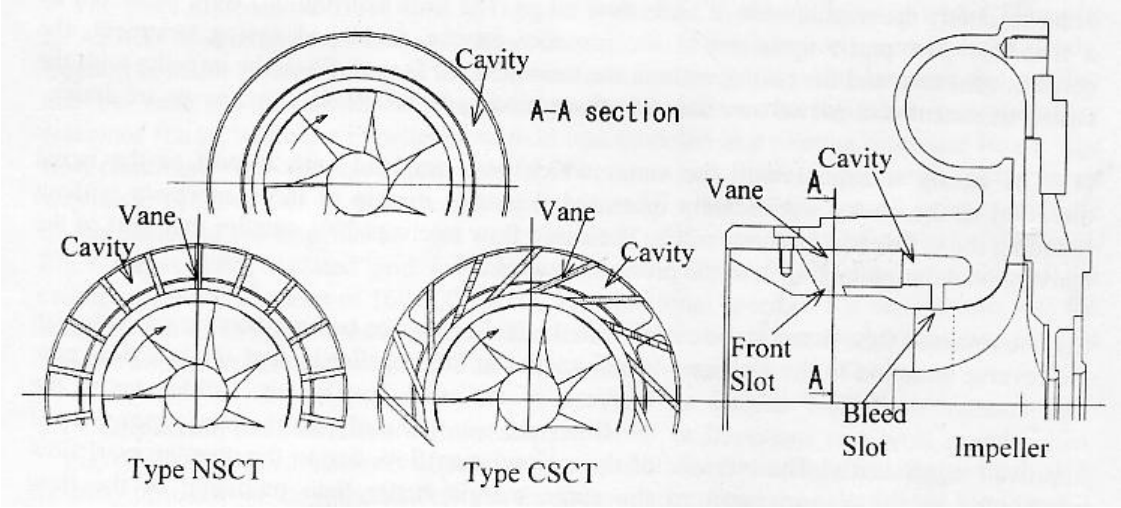

Figure 1-50 Different MWE tested in [Yamaguchi et al, 2002 (142)], with type CSCT introducing negative swirl at the compressor inlet

Very few studies were done on holes which were proposed to replace grooves and slots [Figure 1-51]. The advantageous of holes is that it can be closed and opened; hence a variable geometry can be added. However, their effect on compressor performance has not been tested yet.

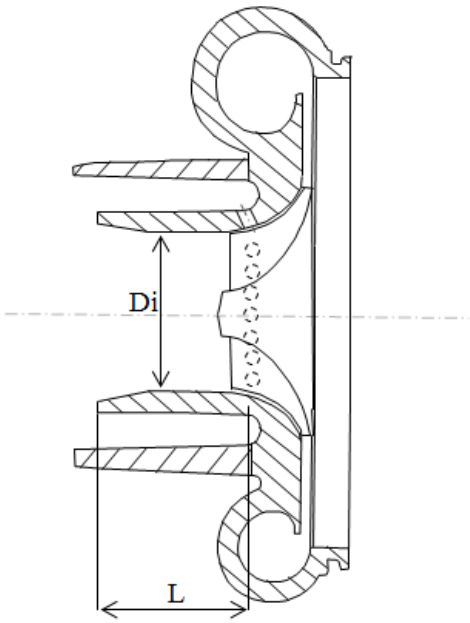

Figure 1-51 2D draw of an MWE system with holes

As mentioned above, MWE system is a simple, cheap and provided good result in increasing surge margin while conserving efficiency. However, this system has not yet applied to automotive engines. A major drawback of MWE is an "intake roar" or noise, the aftermarket filter lets too much noise through to the occupants of the car. Still researches are going on to overcome this problematic. Moreover, dimensioning the MWE needs hard work [CFD and experimental analysis] and this is not yet done.

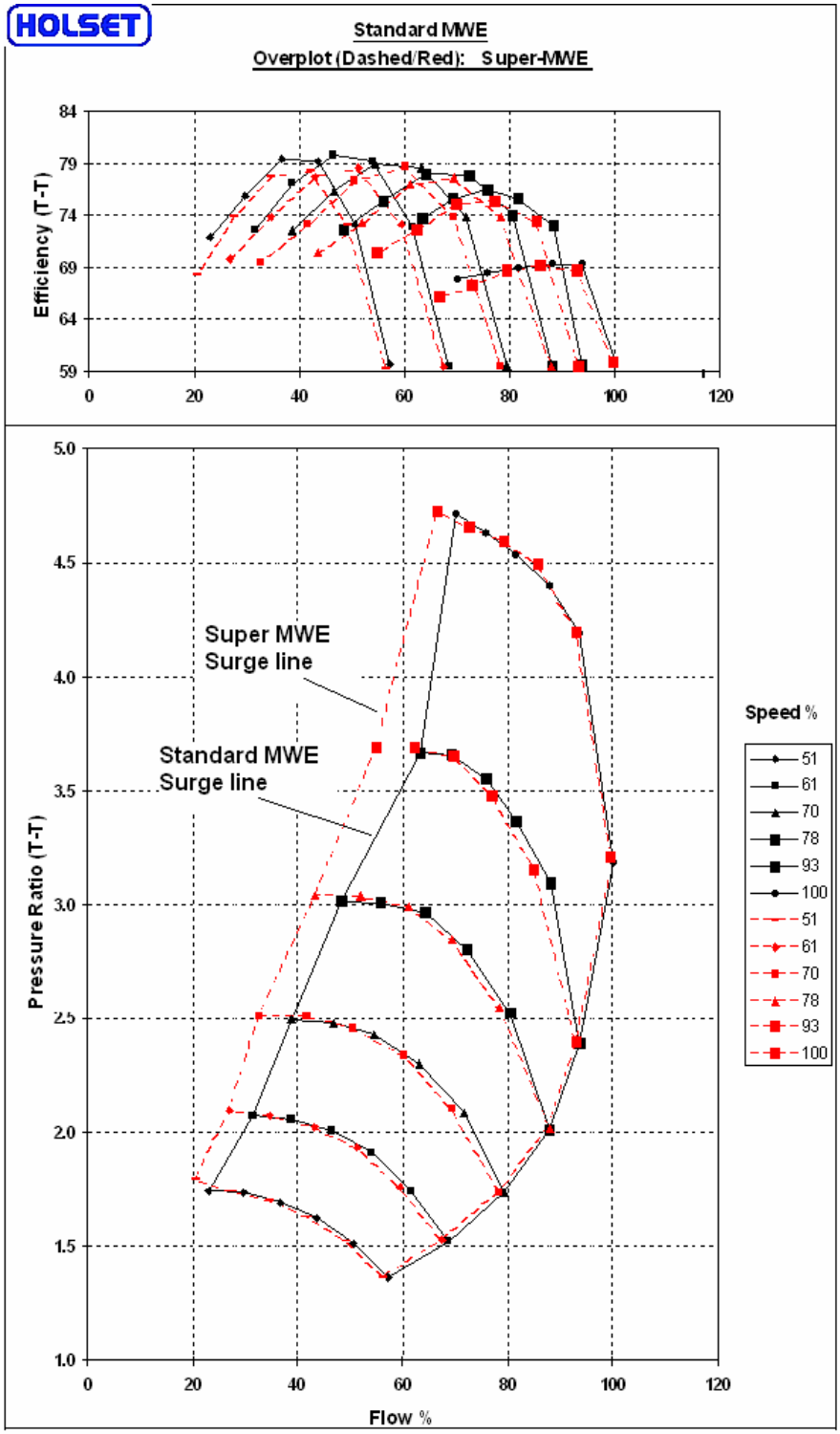

Figure 1-52 Super-MWE compared to conventional MWE (112)

1.5.2.2 Backswept impeller

The operating range is also improved by adopting backswept impellers [(129), (127) & (3)]. Introduction of backsweep to increase range also brings with it a substantial stresses in the blades due to the necessity to increase the rotational speed to obtain a given pressure ratio (3) [Figure 1-53].

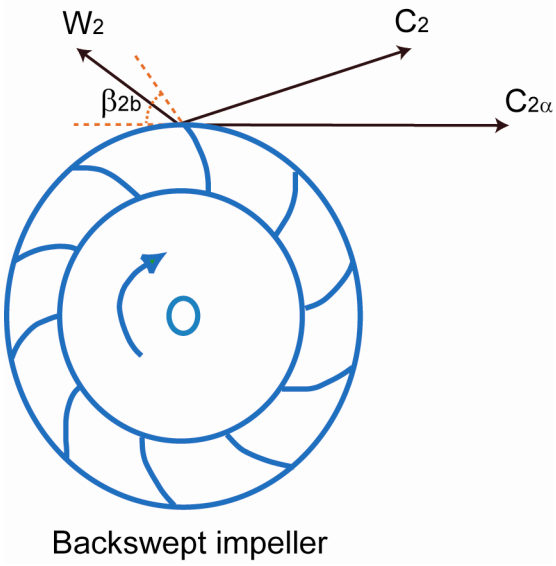

Figure 1-53 velocity triangle at the exit of a backswept impeller

Despite the accompanying increase in inlet relative Mach number, the use of large backsweep also ensures that the velocities into the diffuser are not too high and this leaves the impeller leading edge incidence as the factor most likely to trigger surge. If, however, the inlet pre-swirl mechanism is in effect at the same time, the effect on inlet relative Mach number may be reduced (35). Effect of backswept on compressor efficiency and stability is shown in Figure 1-54

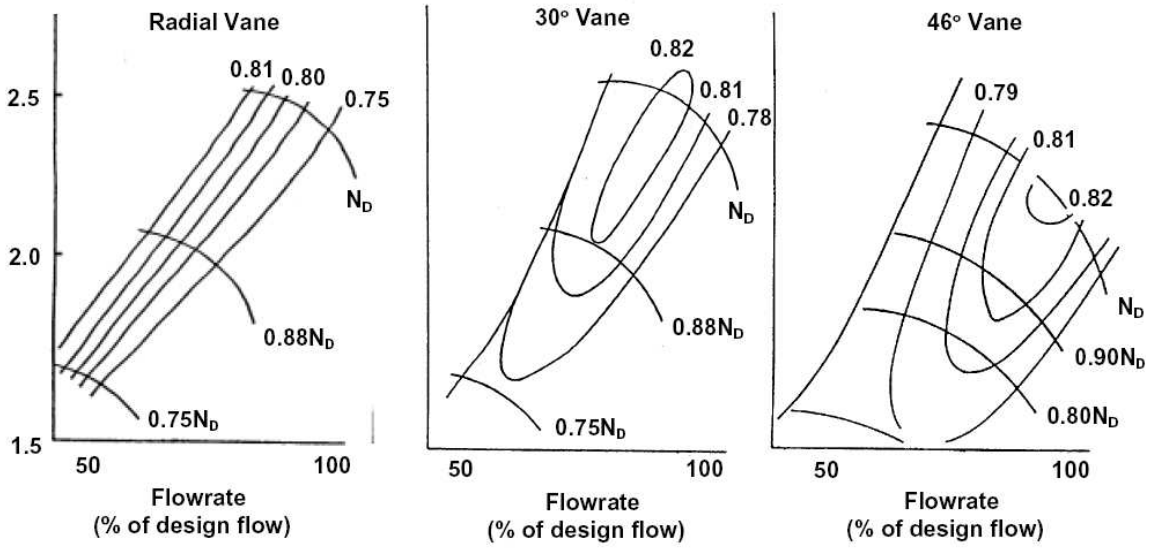

Figure 1-54 Influence of sweepback on efficiency and stability (144)

1.5.2.3 Diffuser

❖ Vaneless diffuser

Instabilities in vaneless diffusers was discussed in section [1.4], and it was mentioned that rotating stall in diffusers occurs when the absolute inlet flow angle reaches a critical value, α_{cr} and because of three boundary layer separation. Hence to suppress diffuser instabilities one has to increase inlet diffuser angle, and delay the occurrence of reversed flow.

The literature review in this section treats the suppressing stall in centrifugal compressors for industrial applications [in most cases]. Fixed techniques to suppress stall onset are rarely investigated for turbocharger compressors. For industrial compressor applications, the ultimate goal of the industry, which emphasizes reliability, is to adopt an effective, but simple system to avoid flow instabilities. Thus there is a strong need to find a passive but simple method for stall control.

Devices developed to increase inlet diffuser angle.

To increase diffuser inlet angle, one has to decrease tangential velocity, increase radial component, or the two at the same time.

We begin with literature review of existing fixed geometry techniques to increase radial velocity, then after we talk about radial velocity reduction techniques.

Abdelhamid, 1980 (82) has introduced sharp edge throttle rings at the exit of the diffuser, reducing the diffuser exit width and hence increasing radial component [Figure 1-55]. The use of the throttle rings had stabilizing effect at low flow rates where the compressor was normally subject to flow oscillations. However, the use of throttle rings in normal operating range led to a reduction in overall efficiency.

Yingkang et al, 1987 (145) has studied five vaneless diffusers with a constant inlet height and varying wall taper. Diffuser performance was not seen to be very sensitive for the blade number and the outlet sweep angle. A small amount of wall convergence was seen to be beneficial for the performance of the vaneless diffusers. Convergent diffusers suppressed the flow reversal toward the diffuser outlet. Wall convergence also improved the radial velocity distribution.

Pinched diffusers were also used to increase radial velocity. Turunen-Saaresti et al, 2006 [referred to (146)] have studied numerically and experimentally various pinch configurations. The pinch was found to improve the efficiency, but only one configuration was measured. The velocity at the diffuser was more radial with the pinched diffuser. This is due to diffuser area decrease.

Turunen-Saaresti et al, 2009 (146) have studied experimentally different pinch configuration at the shroud and hub sides. He concluded that pinch on the shroud side was the best, and recommended small amount of pinch for better diffuser performance. Moreover, he concluded that highly pinched diffusers increase rotor efficiency. However, he did not mention any effect of pinch on surge line improvement.

Nikpour, 2004 (112) reported that the diameter and depth of the diffuser recess [Figure 1-56] can be optimized to improve compressor stability at surge and thereby increase surge margin. Figure 1-56 shows the effect of diffuser recess diameter on performance show that the larger recess diameter has resulted in improvements of up to 9% in surge margin. Nikpour has conducted a CFD study to understand the mechanism of flow changes due to recess geometry changes. He concluded that the presence of the recess has set up a region

of strong secondary flow recirculation at the trailing edge of the impeller. The recirculation region acts as an aerodynamic pinch which reduces the flow area locally therefore accelerating the flow and help stabilizing the near surge flow condition.

The stable operation range of the vaneless diffuser has been studied in [Jansen, 1964 (83)]. Jansen has calculated the operating range of a vaneless diffuser with two different inlet width-radius ratios, 0.125 and 0.08. The stable operation range of the vaneless diffuser was at the higher inlet flow angle [calculated from the radius] with the wider diffuser. However, Jansen states that the effect of the diffuser width can be adverse and the overall effect of decreasing the diffuser width is beneficial.

According to [Van den Braembussche et al, 1980 (55)] the critical inlet flow angle was found to be higher with the lower diffuser inlet width/radius ratios.

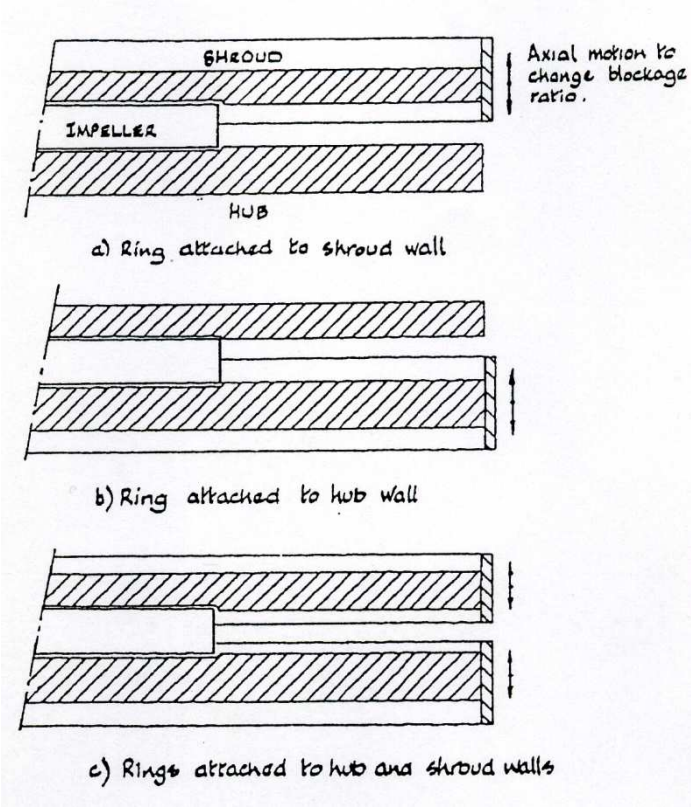

Figure 1-55 Diffuser throttle ring (82)

A simple passive mechanism reported to decrease tangential velocity and increase radial velocity and very effective to suppress to suppress rotating stall is mounting radial shallow grooves on the diffuser walls, these grooves were also called swirl breaker or J-grooves (147).

Kurokawa et al, 1998 (147) explained theoretically the effect of these grooves, he concluded that using J-grooves increases diffuser inlet angle by two mechanisms which have the same weight of contribution.

- A significant decrease in the tangential velocity due to mixing between the main flow and the groove flow.
- An increase in meridional velocity of the main flow due to reverse flow in the grooves.

CFD analysis was conducted by Gao et al, 2009 (90) showed that the inlet flow angle especially that near the wall is significantly increased due to the groove inward flow. This increase is due to a decrease in the tangential velocity but also an increase in the radial velocity. Gao et al (90) concluded that grooves should be mounted at the separation zone in the diffuser walls and that the radial separation range determines the groove length.

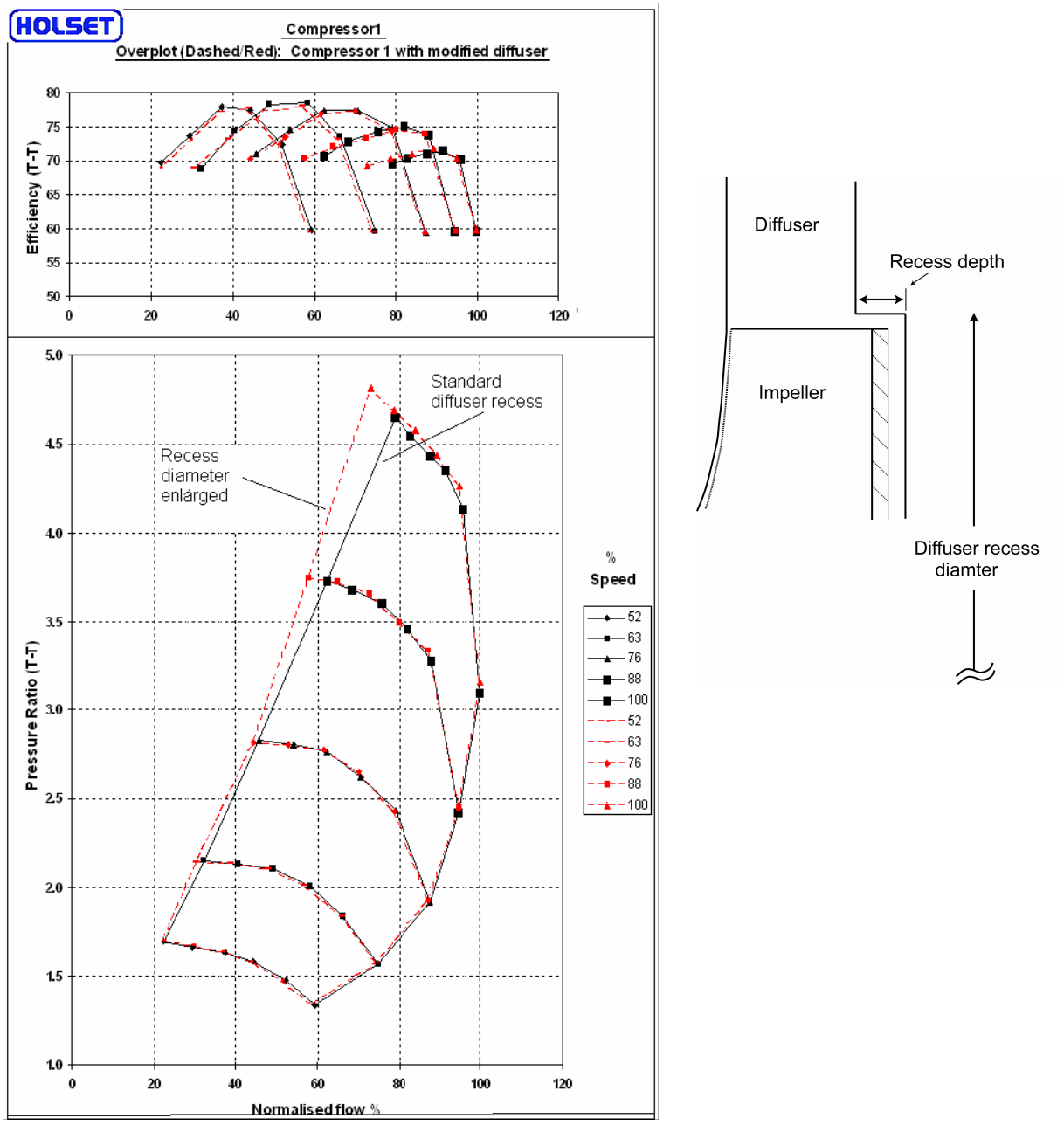

Figure 1-56 Effect of diffuser recess on performance [to the left], enlarged view of impeller tip-diffuser inlet where diffuser recess [to the right] (112)

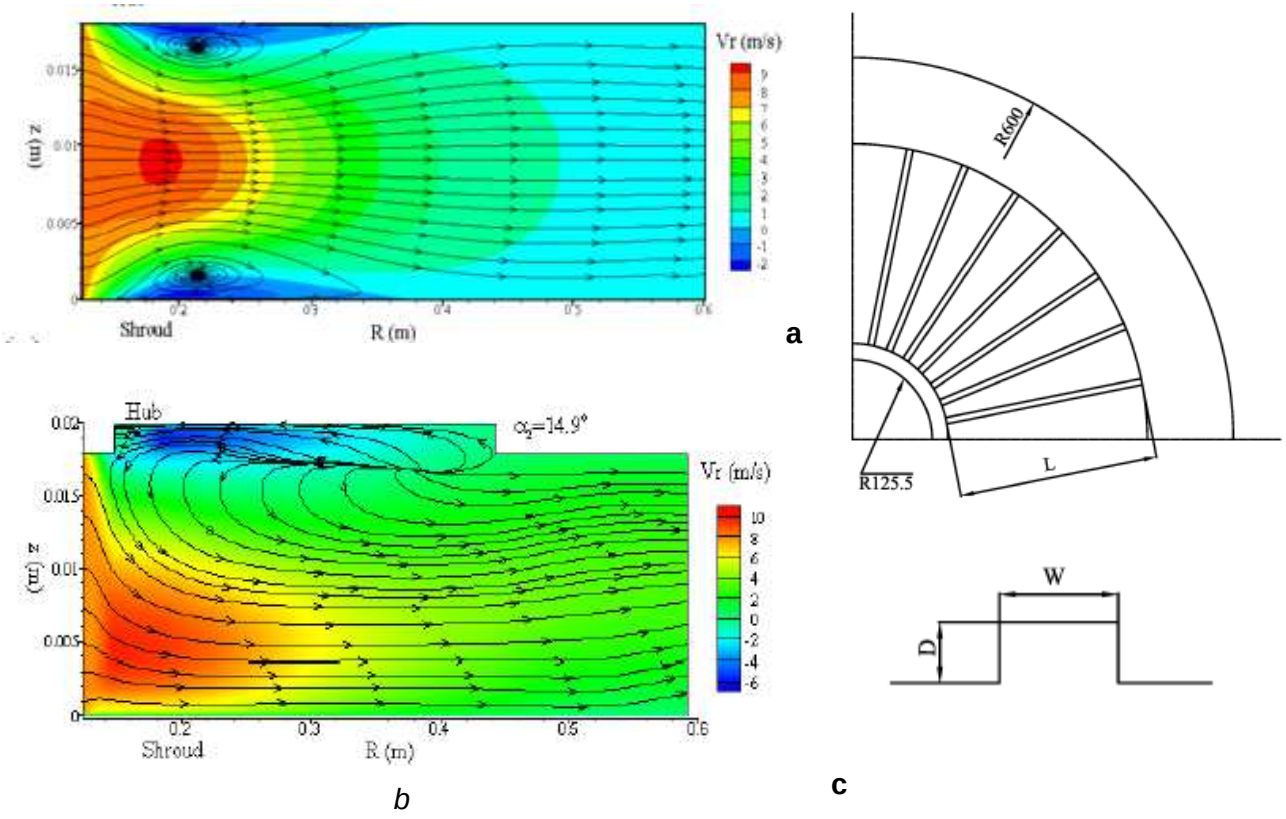

Figure 1-57 a] Stream lines and radial velocity countours without grooves, b] with grooves and c] schematic diagram of radial grooves [J-grooves], (90)

Moreover, Gao et al (90) showed that the diffuser operation range is increased from the original stall critical angle 14.9° to 9.5°, which means that the stall flow angle is decreased by about 36%. The reasoning behind this considerable effect can be found by inspecting the flow field distributions with the existence of grooves is shown in Figure 1-57, which shows the radial distribution of the tangential velocity around grooves. As it can be seen, the original large reversed flow regions on both sides of the smooth diffuser [Figure 1-57a] are all blown away [Figure 1-57b]. The flow near the hub side is sucked or driven into the groove, moves towards diffuser inlet, then flows down along the wall, and reenters the main flow.

It worth to mention that, shallow grooves parallel to impeller axis were used by Kurokawa et al, 1998 (147) to suppress recirculating flow at impeller inlet.

Despite all of the above-mentioned published literature and ongoing researches on suppressing instabilities in vaneless diffuser, there remain many investigations to be done and many questions to be answered.

1. The use of J-grooves for turbocharger application was not studied, and that of pinches or throttle rings was not thoroughly investigated.
2. What is the effect on turbocharger compressor performance and surge line of J-grooves, and if these mechanisms are advantageous in suppressing instabilities without efficiency sacrifices.
3. What is the effect of J-grooves at compressor high flow rates, and choke line.

4. Unless the CFD analysis done by Gao et al (90), and theoretical study of Kurokawa et al (147) the influence of groove geometry parameters [Depth, number, length and width of grooves] were not thoroughly studied in the literature.

This work presents trends to answer these questions

Devices developed to delay occurrence of reversed flow.

Among the devices used to delay occurrence of reversed flow, Senoo et al, 1983 (52) showed that using a small-solidity cascade in a centrifugal blower impeller with backward-leaning blades, delay occurrence of reversed flow and consequently provides a wide range of stable functioning. Senoo showed a better pressure recovery when using a the circular cascade diffuser than that of a vaneless diffuser.

- Vaned diffuser

In addition to flow range reduction, the complexity of installing vanes in the very small width diffusers of the turbocharger compressors, and its cost of manufacturing makes this technique not applied for automotive applications.

1.5.2.4 Air injection

Kyrtatos & Watson, 1980 (109) note that the pre-swirl at inducer inlet can be generated by tangential air jets in the compressor inlet. But according to their results the air jet will typically use 20-40% of the compressor inflow near surge, implying that a large increase in turbine power is required to drive the compressor. The effect of tangential air injection at the inducer inlet is shown in Figure 1-58.

Moreover, air injection can be introduced in the diffuser section, a study of its application has been conducted by Shoch, 2003 (148). Significant improvements to the surge line have been reported.

Applying air jet at the turbocharger compressor has not been applied to automotive turbochargers; its application was restricted to industrial applications.

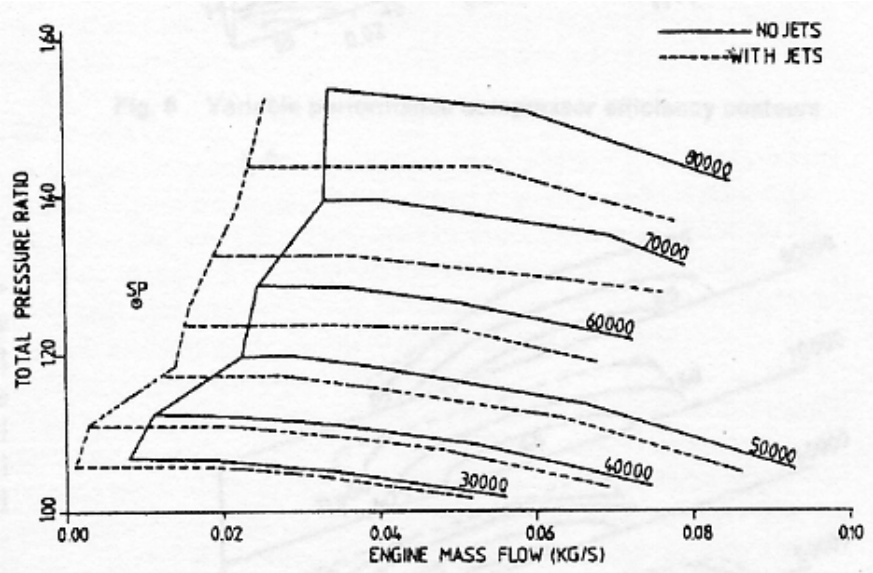

Figure 1-58 Effect on compressor compression map of imparting pre-swirl aerodynamically, (109)

1.5.2.5 *Other fixed* geometry techniques

Some more fixed geometry techniques are studied in the literature, these techniques are almost complex, and take no consideration of packaging problems, therefore their application is not evident in automotive market. We take as example the system proposed by Mcdonald, 2004 (125). System functioning can be understood from Figure 1-59. When no swirl is need, Valve 1 will open, and 2 will close. When swirl is needed, valve 2 is close and 1 is open. No results have been presented to show the effect on the compressor performance of such a system.

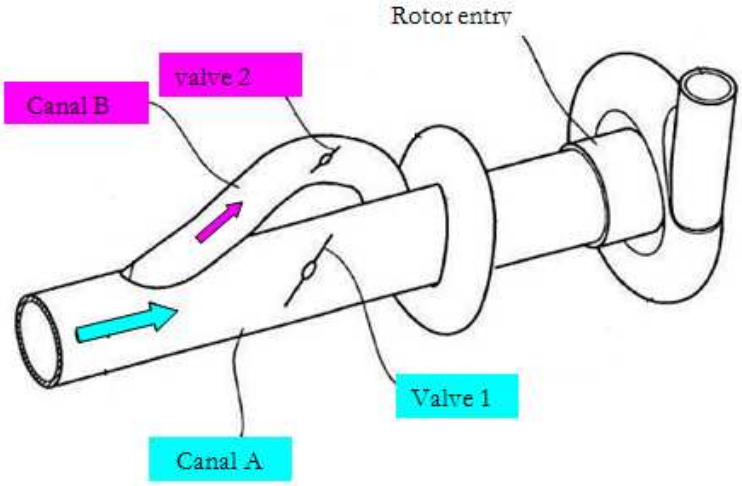

Figure 1-59 A fixed geometry swirl generator (125)

1.5.3 Synergy effect of fixed and variable geometry techniques

Synergy is the possibility of adding the fixed and geometry techniques, or variable geometries at different compressor sections.

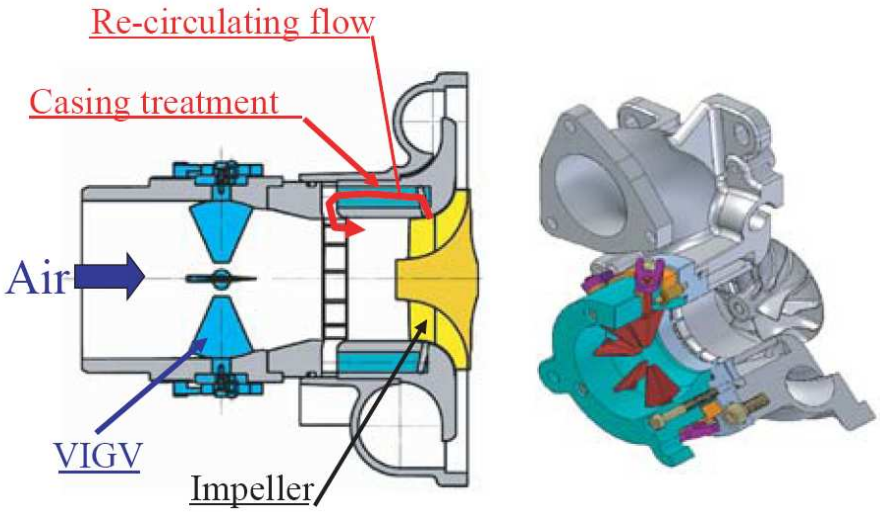

Figure 1-60 The structure of compressor with an MWE coupled with VIGVs (115)

The only synergy effect studied in the literature is the combination of an MWE system with an AGVs. This was studied by [Uchida et al, 2006 (115)]. As it can be seen the AGVs was installed upstream of the MWE system [Figure 1-60]. It was found that the surge line has been reduced significantly, reaching a 55% of reduction compared to a conventional compressor.

The same coupling was proposed by Anthony, 2006 (149). Author proved a significant increase in surge margin while using the MWE system coupled with a AGVs at θ=+20° setting angle [Figure 1-61]. The effect on compressor efficiency showed a slight efficiency decrease compared to conventional MWE.

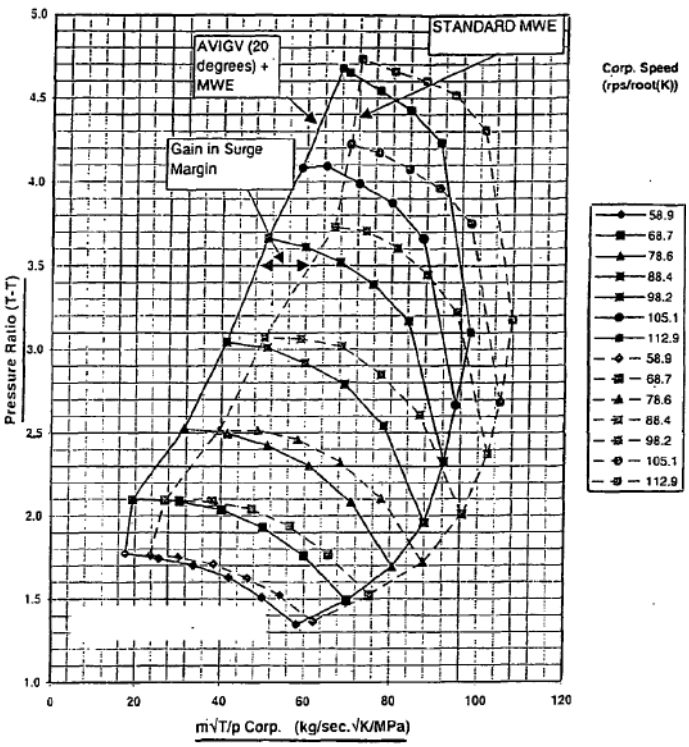

Figure 1-61 Effect on the surge margin using an MWE coupled to AIGVs at +20°(149)

Despite the surge line improvement presented by the two authors, this synergy is complex, expensive and takes little consideration on packaging constraint. A more complete study on the effect of this synergy has to be done to prove the effectiveness.

Moreover, the advantageous of coupling a variable geometry diffuser with techniques to suppress instabilities at impeller inlet [pre rotation mechanisms] or instabilities in the impeller [casing treatments] are not yet studied. Even if this combinations adds complexity to turbochargers, but some good surge line improvements can be predicted due to delaying stage stall – due to suppressing instabilities in two components.

Still more study has to be done to investigate the impact of synergy effect on surge line, and if the gain benefits in performance and surge line improvement can overcome the complexity of the two variable geometry techniques and its high cost [Complex control systems, packaging difficulty, weigh addition, manufacturing complexity all this leads to expensive implementation].

2 Chapter 2: Experimental facilities, instrumentation and uncertainty analysis

Experimental facilities used in this work are presented in this chapter. The three test facilities used for this work are: Overall compressor performance test facility [turbocharger test facility], a local measurement test bench [LDA test facility], and pressure losses test bench, are described in the first section of this chapter. Moreover, Instrumentations of the different test facilities are also briefly described.

On approaching surge varying pressure fluctuation exists. Pressure fluctuation of different frequency also develops when a compressor component stalls. Section two, describes the method used to detect tested compressor surge and rotating stall [mild surge].

Still with the careful selection of the instrumentations [accurate, proper location…], the level of their accuracies is limited. This brings the needs to implement the uncertainty analysis on the instrumentations. Uncertainty analysis is done in the last section of this chapter.

Chapitre 2 : Installations expérimentales, instrumentation et incertitude de mesure

Les 3 installations expérimentales utilisées dans ce travail sont présentées dans ce chapitre :

- *un banc d'essais de turbocompresseurs à air chaud permettant la mesure des champs de fonctionnement des compresseurs*
- *une installation permettant la mesure locale d'écoulement [LDA]*
- *un banc de test de perte de charge*

L'instrumentation de ces 3 bancs d'essais est présentée brièvement.

A l'approche du pompage, différentes fluctuations de pression apparaissent. De même lorsqu'un des composants du compresseur décroche, certaines fréquences apparaissent. Le paragraphe 2 décrit la méthode appliquée pour détecter le pompage du compresseur et le décrochement tournant [pompage moyen].

Bien que l'instrumentation de mesure ait été sélectionnée et installé avec soin [précision, positionnement correct…], le niveau de précision est limité. Ceci entraîne le besoin d'une analyse des incertitudes, qui est effectuée dans le dernier paragraphe de ce chapitre.

2.1 Turbocharger test facility

Turbocharger test facility was used to determine the overall compressor performance. The turbocharger test rig located at the Laboratory of Fluids Mechanics at the Ecole Centrale de Nantes is shown in Figure 2-1 and Figure 2-2. The overall compressor performance parameters and surge line detection, were measured in this facility.

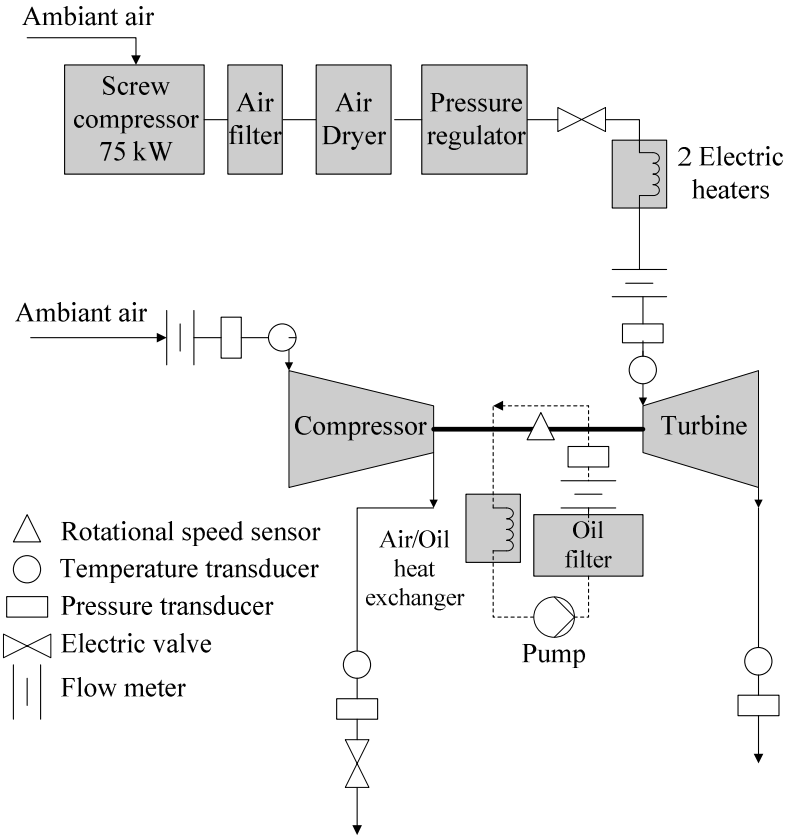

Figure 2-1 Scheme of the installation

The turbine was driven by two electric heaters [18KW each], which allow the regulation of the turbine inlet temperature. An electric vane controls the turbine expansion ratio and air mass flow at the turbine inlet. Air was drawn through the test rig by a screw compressor with maximum pressure of 7.5bar and maximum flow rate of 0.24 m^3/s. The compressed and continuous air is filtered using a 405 CF carbon filter and dried before the turbine inlet. Air is then exhausted outside by an extractor fan. A pressure regulator is added to the turbine inlet line to avoid pressure overshooting.

In the compressor side, air is filtered at the compressor entry. At compressor outlet, an electric vane controls the pressure ratio and air mass flow. Air is then exhausted outside by an extractor fan [it joins the same exit turbine circuit].

An oil pump lubricates the turbocharger. A heater and cooler were used to regulate oil temperature.

During this work, another turbocharger test facility was also used. The main difference between the two test facilities is the ducting at compressor entry - delivery lines. Moreover, a 144 KW heater [Figure 2-3] installed in the second test bench.

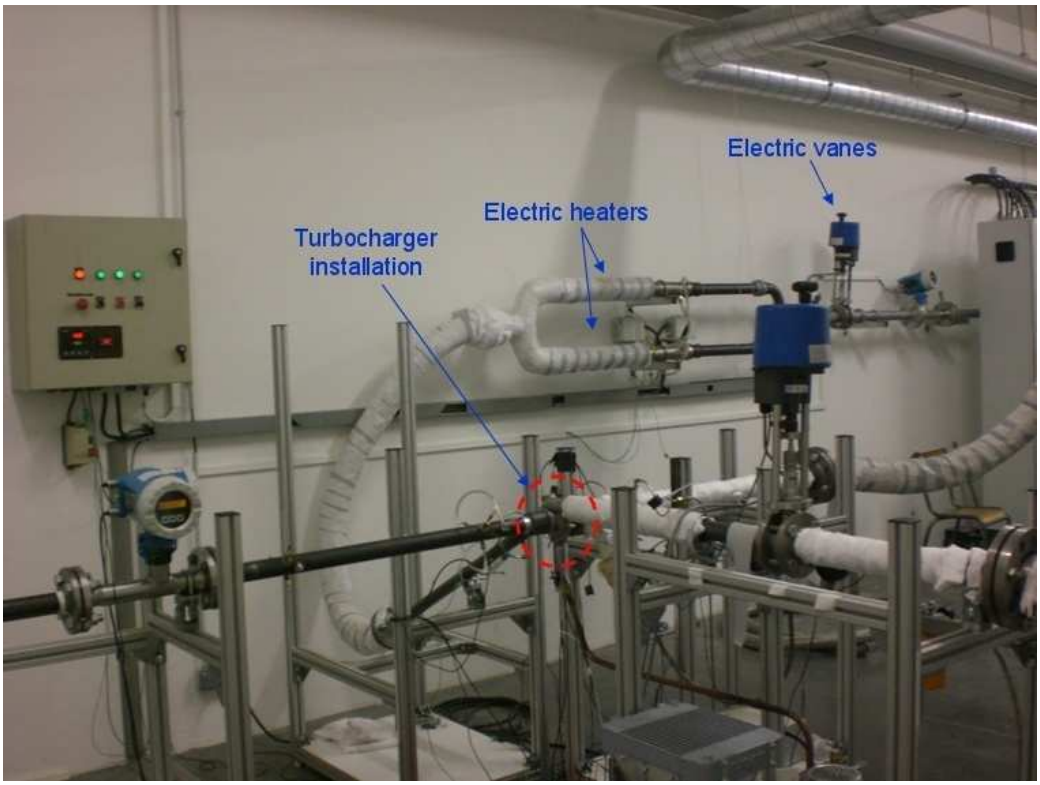

Figure 2-2 overall compressor performance test facility

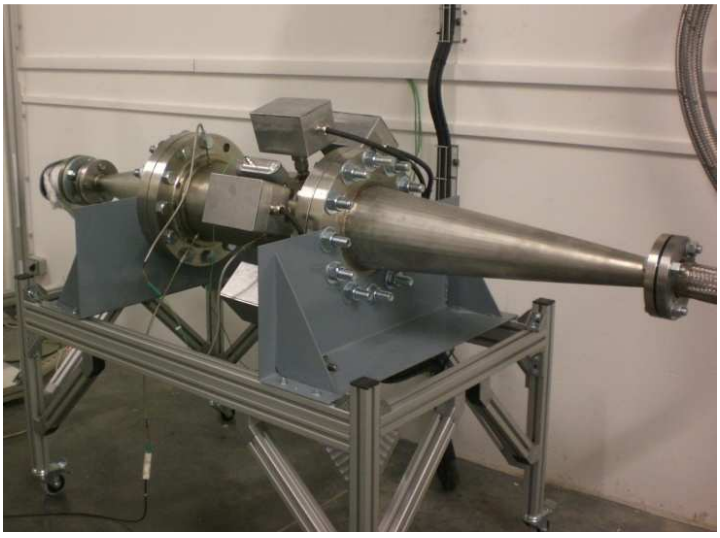

Figure 2-3 144KW heater

- Measurement system in turbocharger test facility

  In Figure 2-4 an isolated compressor is shown with the location of the transducers used for the performance measurements.

  The different transducers used for the performance measurement are presented bellow. Moreover, manufacturer specification of each transducer is presented in Table 2-1

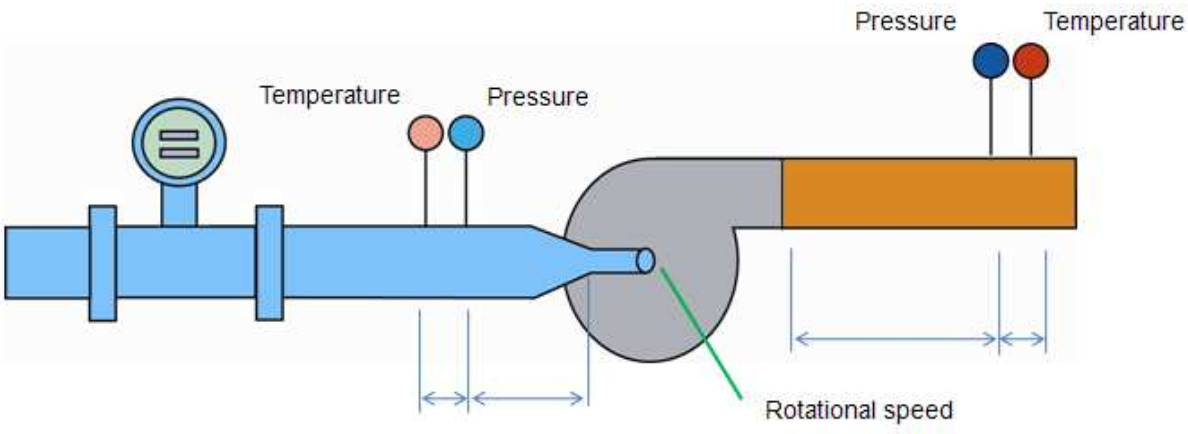

Figure 2-4 Transducers installation on the compressor test bench

- Mass flow rate was measured by a thermal mass flow meter, a Proline t-mass 65F [Figure 2-5 c]
- Rotational speed was measured by means of an inductive sensor [Figure 2-5 a]
- Temperature was measured using K type thermocouples located in the compressor entry and delivery lines,
- Piezoresistive sensors were installed to measure inlet and outlet static pressures,

a

b

c

Figure 2-5 a] inductive sensor for rotational speed measurement [PICOTURN], b] Piezoresistive sensors for static pressure measurement [Sensor technics] c] Proline t-mass 65 flow meter.

Sensor	*Type*	*Calibrated range*	*Accuracy, Δ*	*Uncertainty, δ*
Temperature [T]	K type thermocouple	0-1000℃	±1℃	$\left(1/\sqrt{3}\right)$
Pressure [P]	piezoresistive relative pressure sensor (Sensortechnics)	0-100mbar	±0.1mbar	$\left(0.1/\sqrt{3}\right)$
		0-350mbar	±0.35mbar	$\left(0.35/\sqrt{3}\right)$
		0-1bar	±1mbar	$\left(1/\sqrt{3}\right)$
		0-2bar	±2mbar	$\left(2/\sqrt{3}\right)$
		0-5bar	±5mbar	$\left(5/\sqrt{3}\right)$
Rotational speed [N]	Inductive sensor (PICOTURN)	0-200000 tr/min	±200 tr/min	$\left(200/\sqrt{3}\right)$
Air mass flow rate [Q]	Thermal mass flow sensor (Proline t- mass65)	0-0.005kg/s	±0.00075kg/s	$\left(0.00075/\sqrt{3}\right)$
		0.005-0.25kg/s	±1.5%.Q kg/s	$\left([1.5\% * Q]/\sqrt{3}\right)$

Table 2-1 Manufacturer specification for each sensor

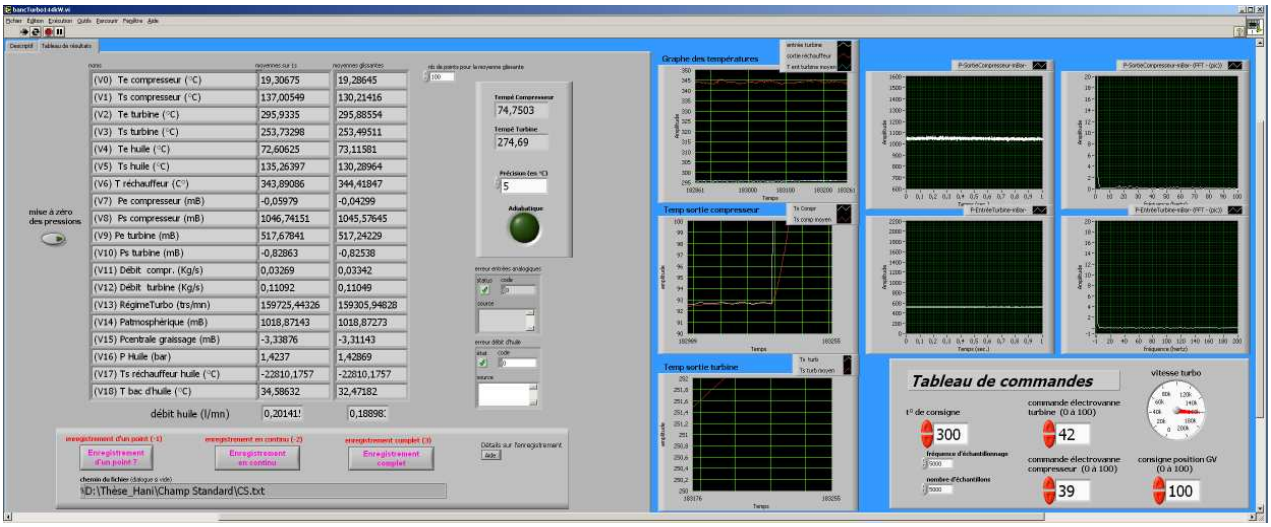

Figure 2-6 used LabView, screenshot

All transducer signals are connected to a 'NATIONAL INSTRUMENT' data acquisition Plug-in board in the measurement computer. A 'LabView' based data acquisition system is used to measure, monitor and store all the available measurement signals [Figure 2-6].

2.1.1 Compressor performance map

Compressor performance maps present compressor characteristics at different operating points. It includes the following calculated parameters:

1. Total to total pressure ratio, TPR[equation,2-15]
2. Corrected mass flow rate, $\mathrm{Q_c}$ [equation, 2-1]
3. Corrected rotational speed, N_c [equation,2-2]
4. Total to total isentropic efficiency, η_{tt} [equation,2-14]

The definition of the non-dimensional pressure rise, mass flow, rotational speed and total to total efficiency is detailed bellow.

- Corrected mass flow rate

$$Qc = Q\sqrt{\frac{T_{1t}}{T_0}}\frac{P_0}{P_{1t}} \qquad 2\text{-}1$$

Where T_0 is the reference temperature (= 298K), and P_0 is the reference pressure (=1bar)

- Corrected rotational speed

$$Nc = N\sqrt{\frac{T_0}{T_{1t}}} \qquad 2\text{-}2$$

- Inlet and outlet absolute velocity

$$C_1 = \frac{QRT_{1s}}{P_{1s}A_1} \qquad 2\text{-}3$$

$$C_2 = \frac{QRT_{2s}}{P_{2s}A_2} \qquad 2\text{-}4$$

1 and 2 are the point measures at compressor and outlet

Where inlet and outlet section areas

$$A_1 = \pi r_1^2 \quad and\ A_2 = \pi r_2^2 \qquad 2\text{-}5$$

- Inlet total temperatures

$$T_{1t} = T_{1s} + \frac{C_1^2}{2Cp} \qquad 2\text{-}6$$

- Outlet total temperatures

$$T_{2t} = T_{2s} + \frac{C_2^2}{2Cp} \quad \text{2-7}$$

- Inlet and outlet static pressure

$$P_{1s} = P_{atm} - p_{1s} \quad \text{2-8}$$

$$P_{2s} = P_{atm} + p_{2s} \quad \text{2-9}$$

- Inlet and outlet total pressures $(\gamma = cst)$

$$P_{1t} = P_{1s}\left(\frac{\mathrm{T_{1t}}}{\mathrm{T_{1s}}}\right)^{k} \quad \text{2-10}$$

$$P_{2t} = P_{2s}\left(\frac{\mathrm{T_{2t}}}{\mathrm{T_{2s}}}\right)^{k} \quad \text{2-11}$$

$$k = \frac{\gamma}{\gamma - 1} \quad \text{2-12}$$

- Outlet isentropic temperature

$$T_{2i} = \mathrm{T_{1t}}\left(\frac{\mathrm{P_{2t}}}{\mathrm{P_{1t}}}\right)^{1/k} \quad \text{2-13}$$

- Total to total efficiency

$$\eta_{tt} = \frac{T_{2i} - T_{1t}}{T_{2t} - T_{1t}} \quad \text{2-14}$$

- Total pressure ratio

$$TPR = \frac{P_{2t}}{P_{1t}} \quad \text{2-15}$$

The basic compressor performance map presented in Figure 2-7. Figure shows compressor characteristics for a straight inlet compressor, and a turbine inlet temperature of 150°.

The mild surge zone corresponds to a zone where high frequency pressure fluctuation is encountered. The frequency of outlet pressure at this zone is around 70Hz [section 2.1.2], and operating points at the deep surge inception have an outlet pressure frequency of 20Hz [section 2.1.2].

The surge line presented [dotted line in blue] in the compressor performance map represents operating points close to the deep surge inception line [dotted line in red], such that no surge was incepted [Figure 2-7]. In this way the minimum stable mass flow was measured using the Proline t-mass flow meter.

For the rest of this work, “minimum stable mass flow line” will be noted as the surge line. Moreover, the choke line is considered as the intersection of the iso-speed curve at an efficiency of 0.6 (93).

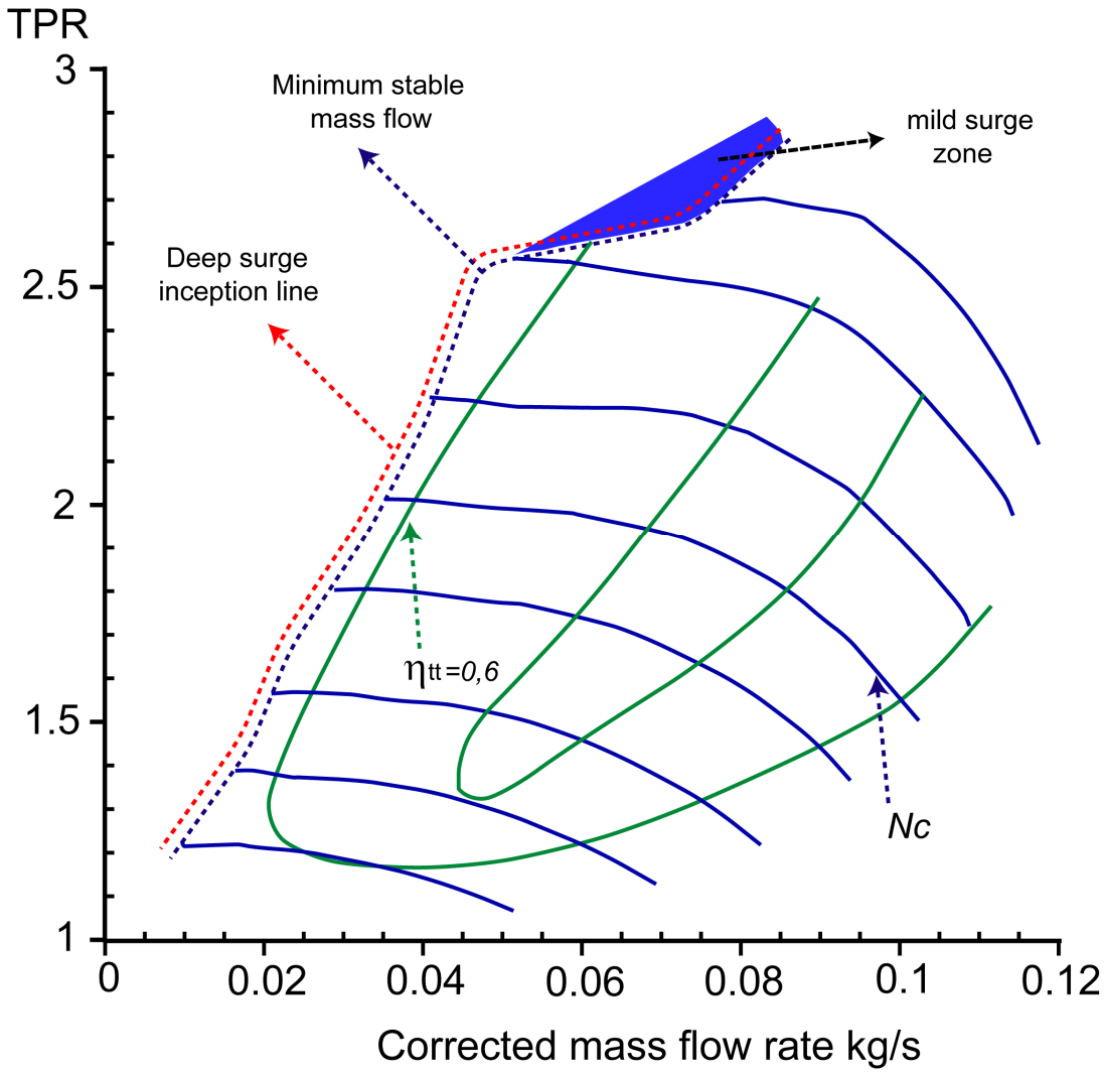

Figure 2-7 Compressor basic characteristics

Compressor total pressure ratio and isentropic efficiency as function of corrected mass flow rate were obtained by gradually reducing the compressor flow rate by the mean of an electric valve located at the compressor entry while maintaining the electric valve at the turbine entry at constant position.

For a constant turbine valve opening, compressor operation points were measured from high flow rates to surge line. To have precise and smooth pressure ratio curves, big number of points was measured. However, for efficiency line, it was presented at a constant speed line, these speeds were chosen before testing, so that big number of points were measured around the chosen speeds. This because, compressor exit temperature takes long time to stabilise compared to compressor pressure exit.

Tecplot 360 was used to trace compressor map, it allows presenting iso-speed and iso-efficiency lines in a same graph. Measured data is added to Tecplot, which traces iso-speed pressure line using interpolation (150). Total to total efficiency at the chosen constant speed was extracted and plotted using Excel.

Experiments were repeated several times to ensure results, and to improve possible factors that can influence results [APPENDIX C].

2.1.2 Surge limit detection

A clear definition of the surge line is very necessary for this work, an objective and reliable method had to be found. Different methods have been proposed in the literature to detect surge limit onset, these are:

1. Instabilities of compressor operating variables
2. Audible effects
3. Important gas temperature increment at compressor inlet
4. Frequency analysis of the instantaneous variables of Pressure, temperature, air mass flow and rotational speed [(113) &(151)].
5. Sound and casing vibration measurements. It was shown that acoustic signal features exhibit a good correlation with operating conditions (152).

For the first three factors, the experimental test surge detection is usually carried out by an expert operator who decides when the compressor surge has started, and this has two main disadvantages: the compressor behavior is classified on the basis of a subjective criterion, and it is not possible to automate turbochargers testing with a sufficient level of reliability (151).

Moreover, for point 3, standard temperature and pressure measurements done at the inlet and outlet paths did not reveal the onset of flow anomalies, however the signal obtained from the unique sensors embedded in the compressor flow path exhibited appreciable correlation with surge behaviour [Menon et al, 2006 (151)]

On the other hand, the last two factors [points 4 and 5] are objective criterion for surge detection, and are used for active surge control in automotive engines.

For point 4, vibration or acoustic measurements can be correlated to aerothermodynamics operating condition methods for diagnosing the presence of unstable operation by means of least intrusive measurements. Sound and casing vibration measurements are used for this purpose. It was shown that acoustic signal features can be extracted, that exhibit a good correlation with operating condition [Aretakis et al, 2004 (152)].

This work draws its basis from Galindo et al, 2006 (113) , who detected surge limits were via a frequency based criterion, by analysing four different variables using a simple algorithm based on the frequency analysis of the instantaneous variables to determine the unstable behaviour.

Significant variations of the turbocharger compressor operating variables [pressure, air mass flow, and rotating speed] are encountered when the surge phenomenon appears. Galindo found that the most sensitive to surge was the downstream pressure. When surging, the pressure spectrum showed higher low frequency contents than in stable operation. The main frequency peak, which described the surge phenomenon fairly accurately, depends on the compressor size, the installation arrangement, and operating conditions [(113) & (153)].

In order to extract the frequency contents of the instantaneous variable, the discrete-time Fourier series was used. Due to Galindo, this approach was preferable to other algorithms because of its high performance.

For this work then, surge limits were detected via a frequency based criterion, in the pressure spectrum -analyzing the pressure downstream of the compressor. Compressor outlet pressure was measured with a sampling frequency of 1 KHz. The pressure signal was transformed using FFT. The frequency peak which describes the surge was about 20Hz, and that of mild surge [or rotating stall] was about 70Hz [Figure 2-8]

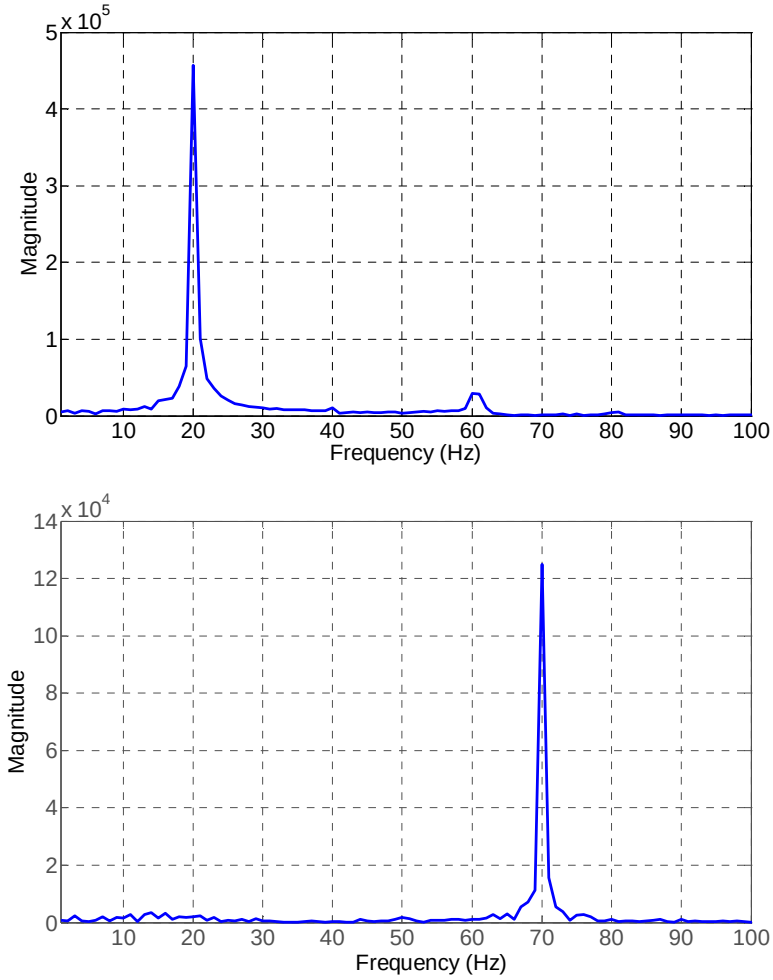

Figure 2-8 Surge [top] and mild surge [bottom] frequency for the tested compressor

2.2 Pressure loss test facility

Pressure loss test facility was used to determine pressure losses through the different tested pre rotation mechanisms [Figure 2-9]. The effect on compressor performance and surge line of these mechanisms are studied in chapter IV.

The methodology to obtain the pressure loss caused by the different swirl generators was similar to that used by Galindo et al, 2006 (113), it was adapted here to the different swirl generator systems [equation, 2-16]. The method is detailed in section 4.1.3.

$$\Delta P_{SG} = \Delta P_{AB\ with\ SG} - \Delta P_{AB\ without\ SG} \qquad 2\text{-}16$$

The different transducers used to measure variables needed to calculate pressure losses, are shown in Figure 2-9, and presented bellow,

- Air mass flow rate: Proline t-mass 65 for mass flow rate,
- Inlet and outlet static pressures: piezoresistive,
- Inlet and outlet temperatures: K type thermocouples.

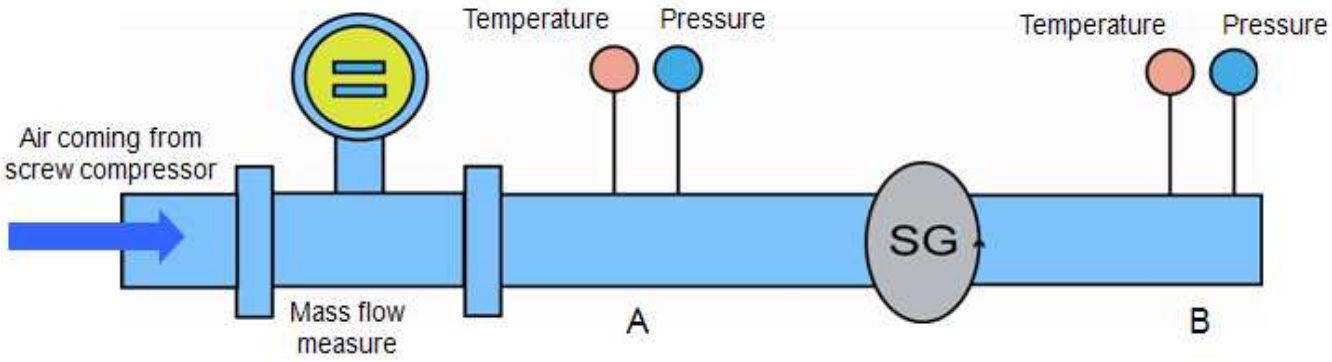

Figure 2-9 Schematic of pressure loss test bench

2.3 LDA test facility

This section describes the experimental setup of Laser Doppler Anemometry installed at internal combustion engine team at the Ecole Centrale de Nantes. A brief introduction about LDA theory, the basic settings, adjustment and some descriptions of analysis software are given.

LDA test measurements were conducted to study flow structure at the downstream of the stabilization systems. Axial and vertical velocities were investigated at different setting angles and diameters.

The two most common flow velocity measurement devices used in industry and universities are laser Doppler anemometry and hot-wire anemometry. Even if Pitot static probes are less expensive and give accurate and reliable measurements, but their measures in regions where flow in highly turbulent are inaccurate.

A laser Doppler anemometer measures the velocity at a point in a flow using light beams. It senses true velocity component, and measures that component in a sequence of near instantaneous samples [Devenport, 2006 (154)]. This way of measure has advantages and disadvantages cited in Table 2-2.

LDA advantages	LDA disadvantages
Does not disturb flow [like pitot tube does]	Expensive
Used in flow of unknown direction	Need of transparent flow
Accurate measurements in unsteady and turbulent flows where velocity is fluctuating with time	Don't give continuous velocity signals

Table 2-2 Advantages and disadvantages of LDA measurement system

❖ Basic principles

As indicated by the name Laser Doppler Anemometry, the Doppler effect plays an important role in LDA, since the technique is based on Doppler shift of the light reflected [and/or refracted] from a moving seeding particle.

Doppler effect: The principle is illustrated in Figure 2-10, where the vector U represent the particle velocity, and the unit vectors e_i and e_s describe the direction of incoming and scattered light respectively.

According to the Lorenz-Mie scattering theory, the light is scattered in all directions at once, with the highest intensity of scattered light will be on the forward side [forward scatter] of the particle, i.e. in the direction away from the incident light. Much less light is scattered in other directions. However, positioning the receiver for forward scatter requires the receiver to be opposite to the light source. Then it is more convenient to use the back-scattered light, because this allows integration of transmitting and receiving optics in a single head. This is simpler for maintaining alignment among multiple velocity components.

Consider only the light reflected in the direction of the receiver. The incoming light has the velocity *c* and the frequency f_i, but due to the particle movement, the seeding particle "sees" a different frequency f_p, which is scattered towards the receiver. From the receiver's point of view, the seeding particle act as a moving transmitter and the movement introduce additional Doppler-shift in the frequency of the light reaching the receiver.

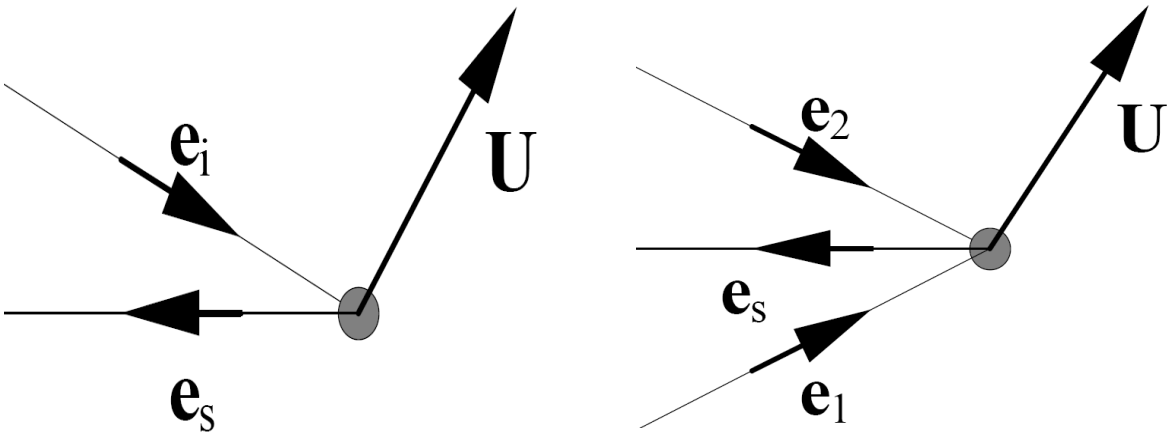

Figure 2-10 scattering light from moving seeding particle

Note that, the best scattering signals are obtained when the particle diameter is several times the wavelength. However, the particles must be small enough to follow the flow.

❖ Laser Doppler Anemometer System

A "One-component dual-beam system" is shown in Figure 2-11. One component because it measures one specific velocity component [U in the diagram]. Dual beam because it uses two laser beams of equal intensity. The beams are generated from a single laser using a half silvered mirror [the 'beam splitter']. They are then focused using a lens [called the sending lens]. The lens also changes the direction of the beams causing them to cross at the point where they are focused. The region where the beams intersect is where the velocity measurement is made. It is called the measurement volume.

The interference of the light beams in the measurement volume creates a set of equally spaced fringes [light and dark bands] that are parallel to the bisector of the beams [Figure 2-12]. A measurement is made when a tiny particle being carried by the flow passes through these fringes. As it does so the amount of light received by the particle fluctuates with the fringes. The amount of light scattered [i.e. reflected] by the particle therefore also fluctuates. The frequency of this fluctuation is proportional to the velocity of the particle normal to the fringes.

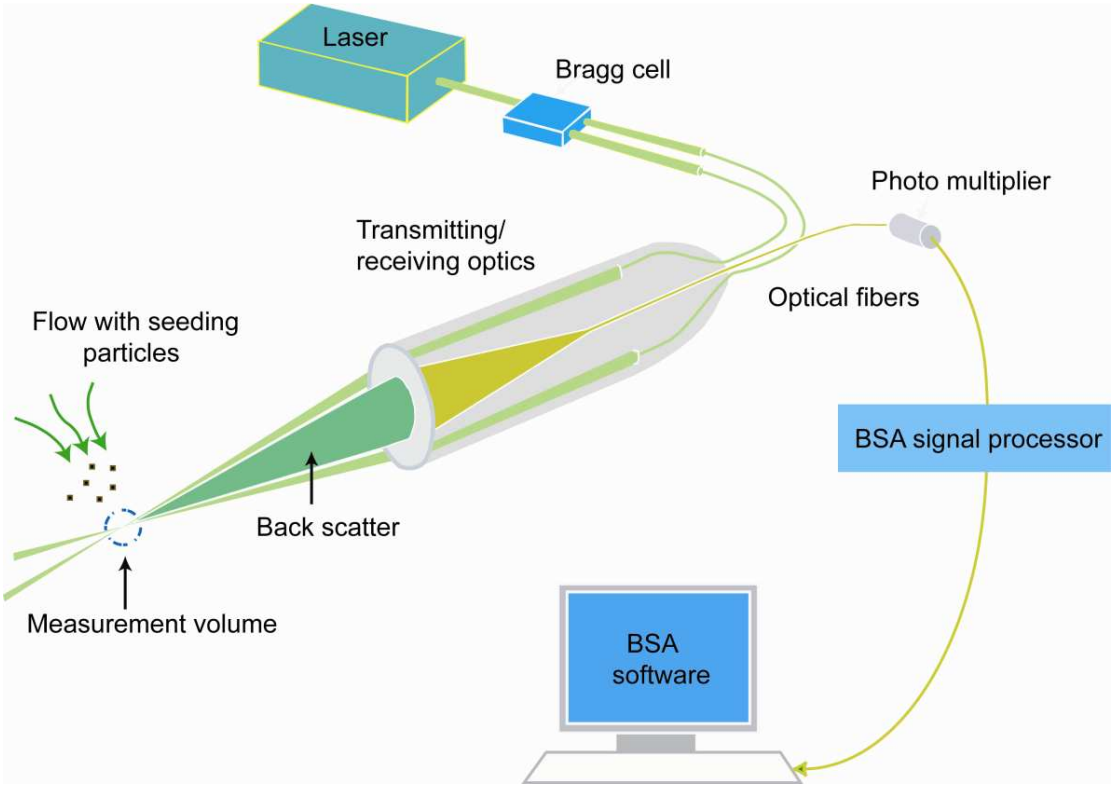

Figure 2-11 LDA system, 2D presentation

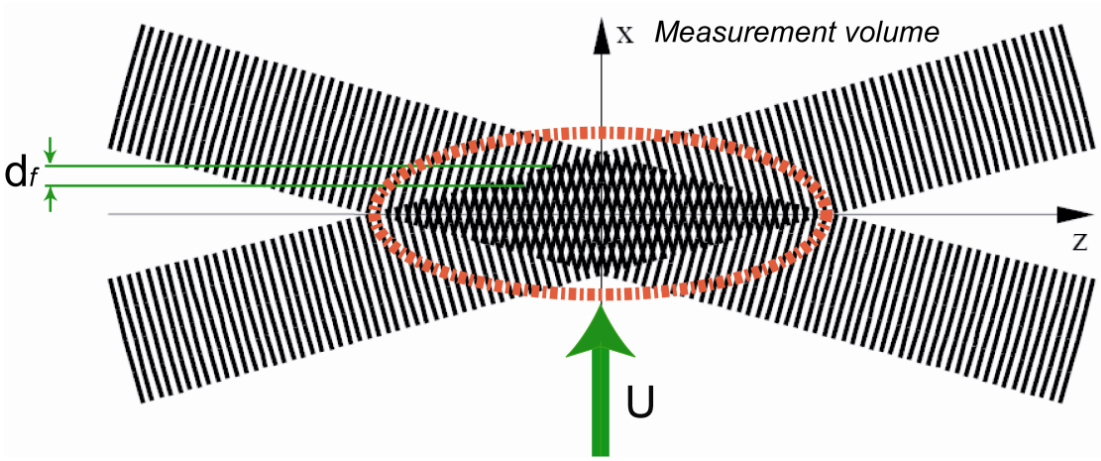

Figure 2-12 Fringes

To detect this frequency, the back scattered light is captured by the transmitting receiving optics or the fiber flow. A photo multiplier converts the light intensity fluctuations to fluctuation in a voltage signal. The BSA signal processor is then used to determine the frequency of the signal and therefore the velocity of the flow. The processing results are handled by the BSA flow software.

❖ Description of the used LDA system

The system is a DANTEC flowlite 2D integrated laser-optics unit. This is a dual beam single component system. It consists of a probe, fiber-optic cable, an optics unit and FVA [Flow Velocity Analyzer] enhanced signal processor [Figure 2-11]. An interface card installed the computer allows the FVA to be controlled and read from the computer. Nominal optical characteristics of the system are presented in Table 2-3,

Laser power	
diode pumped solid state laser	20mW / 488nm
diode pumped frequency double	30mW / 532nm
Probe	27mm
Focal length	100mm
Probe Volume	
Diameter	0.046 mm
Probe volume length	0.62mm
Fringe spacing	3.26µm
Gaussian beam diameter at sending lens	1.35mm [NV]
Beam separation at sending lens	15mm [NV]

Table 2-3 System optical configuration

BSA Flow Software is used to control the LDA system from the lab computer, and to collect the measurements made [Figure 2-13]. BSA Flow Software also enables to control 2-axis traverse.

The Flowlite probe is mounted on a 3-axis traverse gear made from a milling machine base. Being so heavy the traverse gear provides a stable means of precisely positioning the measurement volume at any point in the test section. The probe mount also allows the probe to be rotated about its axis by 150° degrees, and to change the component of the velocity being measured. The probe can thus be used to measure either horizontal or vertical velocity component, and is controlled by a LabView program.

❖ Seeding particles

The LDA is completely dependent on the availability of adequate particle seeding in the flow, which meant a good choice for the seeding system and particle must be done [(155), (156) & (157)].

In fact, LDA does not measure the velocity of the flow, but the velocity of particles suspended in the flow. In this respect these seeding particles can be considered to be the actual velocity probes. The particles must be small enough to track the flow accurately, yet large enough to scatter sufficient light for the photo-detector to be able to detect the Doppler frequency.

In general the motion of a particle suspended in a fluid is affected by,

- o Particle shape
- o Particle size
- o Relative density of particle and fluid
- o Concentration of particles in the fluid
- o Body forces.

Ideally, the particles should also be neutrally buoyant in the fluid that is they should have approximately the same density as the fluid itself, but in many experiments this is a secondary consideration (158).

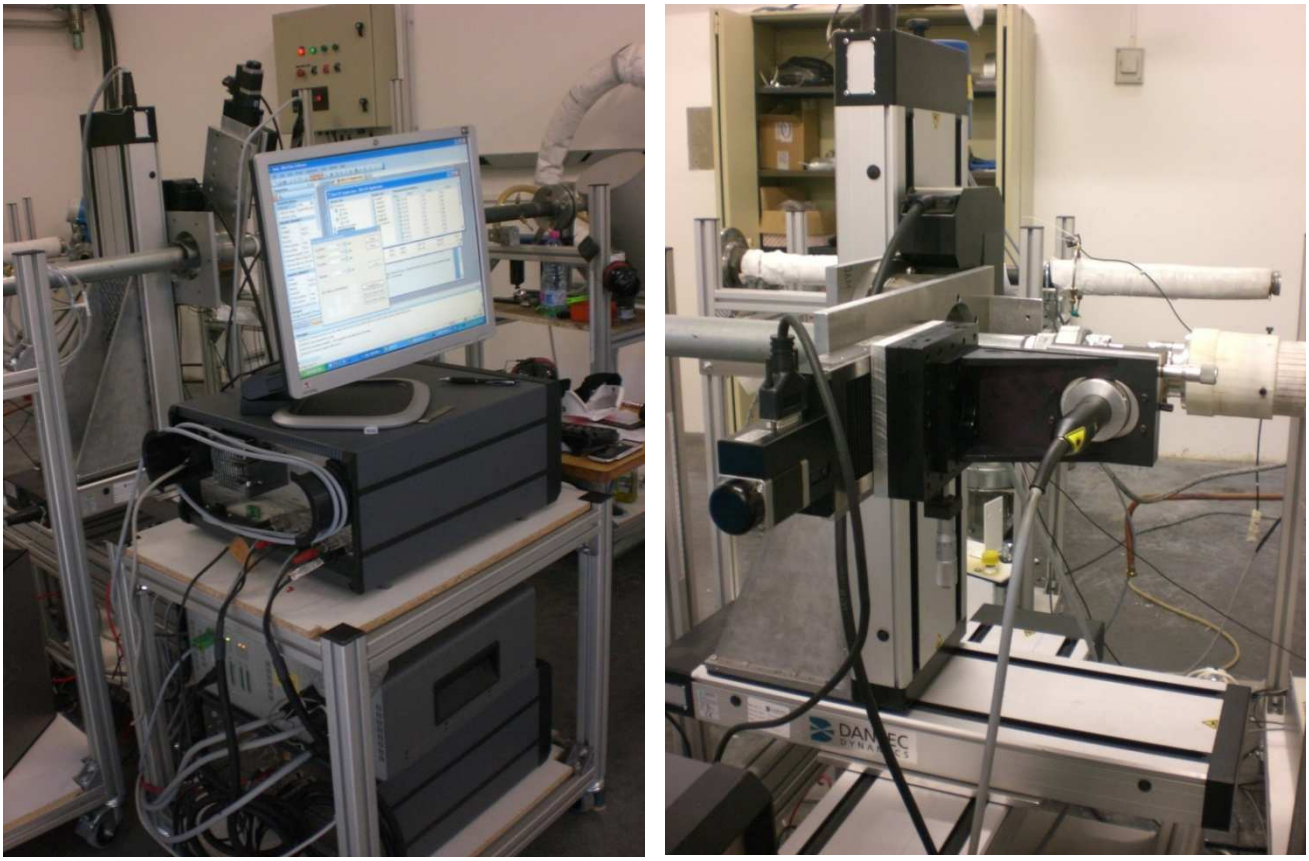

Figure 2-13 overall view of the 3 axes traverser [to the right]. BSA flow software [to the left]

Durst et al, 1981 (159) state the following desired properties of seeding particles. Particles whose motion is used to represent that of a fluid should be:

- Able to follow the flow.
- Good light scatterers.
- Conveniently generated
- Cheap
- Non-toxic, non-corrosive, non-abrasive
- Non-volatile, or slow to evaporate, chemically inactive and clean

Figure 2-14 Atomizer used to generate oil droplets

For this work, and after testing different seeding particles, olive oil was finally chosen, and the oil droplet obtained had a diameter of approximately 1µm. The seeder chosen is a commercially available high pressure atomizer to generate droplet of oil [Figure 2-14].

The optical access was a small plat window of glass, with 10mm in large and 50mm in length. It was designed and mounted on the duct for allowing optical access [Figure 2-15].

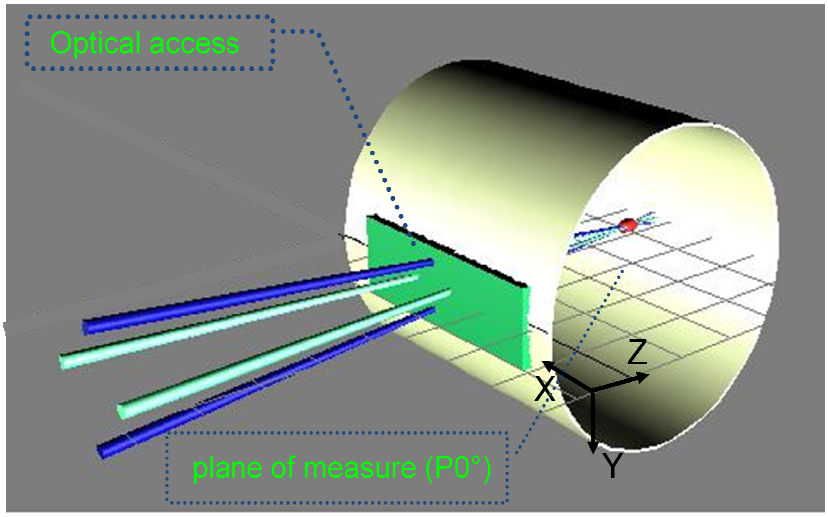

Figure 2-15 Optical access window, and plane of measurement

Window fouling was one of the problems encountered in the measurements [Figure 2-16]. Excessive window fouling has often been found to be to the excessive concentration of oil seeding particles. This is a repeating problem and measure must be stopped every 20 minutes [less time spent at high flow rates] for cleaning the window. Moreover, measuring close to surface was not possible. The first measured point was at 2 mm from the window, and the last point measure at 2 to 3 mm far from the outer surface of the duct. This limitation is due to the quantity of reflection of light and boundary layer at the walls.

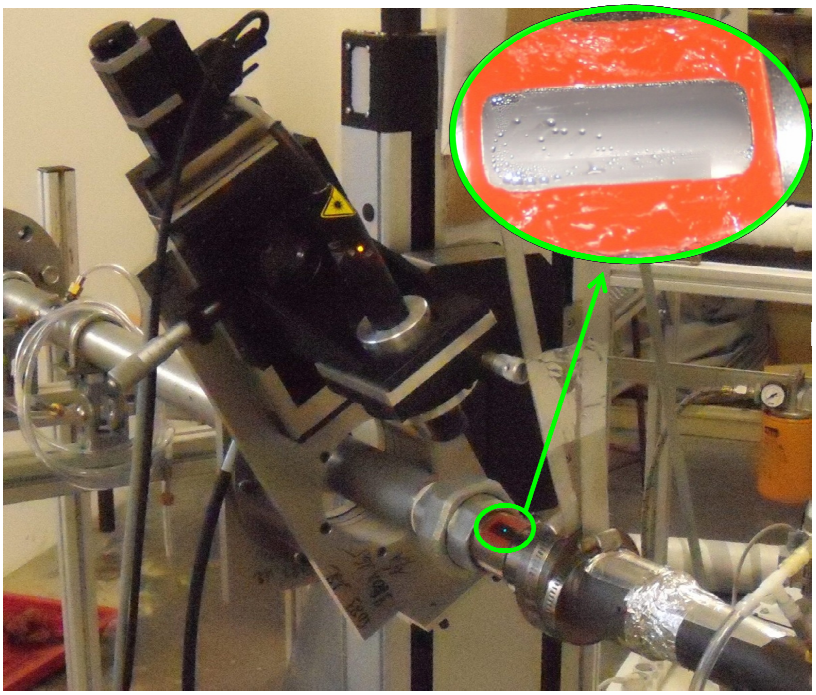

Figure 2-16 windows fouling encountered in the measurements

2.4 Results uncertainty analysis

This section treats the question of how reliable the results of the presented experiments are. Due to non ideal measurement conditions typically encountered during compressor performance testing, it is imperative to define measurement uncertainties to the presented experiments. Very limited information is available in the public domain describing turbocharger compressor field test measurement uncertainties.

Before proceeding let us define certain terms carefully.

Error in a measurement is usually defined as the difference between its true value and the measured value. This definition is not helpful in situation where true value is not known. Then in most situations we cannot talk confidently about what error in a measurement is, we can only talk about what it *might be* (160).

By Uncertainty we mean *a possible value that an error may have*. This definition attributed by by Kline & McClintock, 1953 (161) to Sir George Bidell Airy, 1879.

By multiple sample experiments we mean experiments in which uncertainties are evaluated by repetition, and by single sample experiments we mean experiments in which uncertainties are not found by repetition.

Uncertainty can be categorized in two ways according to GUM [Guide to the Expression of Uncertainty in Measurement in 1993 [Kirkup, 2007 (162)]]. *Type A* and *Type B* uncertainty.

Type A uncertainties are evaluated by the statistical analysis of the series of measurements [case of multiple sample experiments], and *Type B* uncertainties are evaluated by mean other than the statistical analysis of a series of measurements [case of single sample experiments]. In type B uncertainties, we must use previous measurement data, calibration certificates, manufacturers' specifications, data tables and like for both the best estimate of the input quantity and the uncertainty.

Experiments affected in this work are single-sample experiments, so in this section we will be treating *Type B* uncertainty. Estimation of uncertainty of single-sample experiments was first described by Kline & McClintock, 1953 (161) and his work still forms the basis of this branch of art.

2.4.1 Sources of uncertainties in the measurement

The uncertainty attributed to a measurement is an estimate of the possible residual error in the measurement after all proposed corrections have been made (160). Sources of errors can be *fixed* or *random* depending whether the introduced errors are steady or change during the time of one complete experiment. Errors themselves are called *bias* or *precision* errors, and precision error is presumed to behave randomly, with zero mean.

Temperature, T pressure, P rotational speed,N and mass flow rate,Q are the four measurements needed to determine the performance map of the compressor. In this section source of errors of each of the measured parameters are described.

- Temperature uncertainties:

Kline & McClintock (161) showed five major sources of uncertainties in temperature and pressure measurements.

1. Location errors: incorrect position of the sensor in the air stream. Higher location errors occur if measurements are taken close to elbow and other flow obstructions [ex. just downstream of an axial guide vane]. Also in the discharge side of the compressor, at the volute exit, significant temperature gradients can be produced [Brun & Kurz, 2001 (163)]

2. Installation errors: wall conduction heat transfer to and from the sensor due to inadequate insulation
3. Calibration errors: instrument drift, nonlinearities, reference temperature errors
4. Device errors: inherent accuracy limitation of the sensor
5. Acquisition: amplifier, noise, read, and analog-digital conversion errors.

The first three factors were minimized in these experiments [proper location of sensor, isolation, calibration]. Factors 4 and 5 *are measuring system errors* and these are fixed and variable errors introduced by each component of the measuring system, usually given by the manufacturer.

Kline & McClintock, 1953 (161) presented typical values of the above five errors for different temperature sensors encountered at field tests of gas turbine driven compressor. To obtain temperature uncertainty, the individual uncertainties have to be added using the root sum square method [RSS]. VDI 2045, 1993 (163) assumes a tolerance of ±1℃ for thermocouples.

- Pressure uncertainties
  1. Location errors: incorrect position of the pressure sensor in the air stream. This error will depend largely on the flow at the measuring location.
  2. Installation errors: piping vibration transmission to the pressure pick-up due to in adequate damping.
  3. Calibration errors: instrument drift, nonlinearities, hysteresis, and reference pressure errors
  4. Device errors: inherent accuracy limitation of the sensor device
  5. Acquisition errors: amplifier, noise, read, and analog-digital conversion errors.

The first three factors were minimized in these experiments [proper location of sensor, isolation, calibration]. Factors 4 and 5 *are measuring system errors* and these are fixed and variable errors introduced by each component of the measuring system, usually given by the manufacturer.

- Flow measurement uncertainties

  The flow measurement uncertainty is affected by

  1. Installation: All meter types should follow required upstream length / flow conditioning specifications. If the flow profile is not fully-developed or not flow conditioned, this produces bias error in the flow measurement.
  2. Range of the flow measurement: Proline t- mass65 has a higher uncertainty on the low end range than at higher flow range.
  3. Pulsation in the flow field: pulsation adversely affects most types of meters and will add to the uncertainty in the test measurement. However, as most flow measurement instruments provide a low frequency output response, it is often difficult to determine pulsation magnitudes and frequencies [Burn & Nored, 2008 (164)].

The first factor was minimized by properly installing the flow meter. Factor 3 has an effect on values very near to the surge line, however, the surge line corresponds to the last stable points for each rotational speed. Hence, there is no pulsation in the flow field and this error can be neglected. Factor 2 is given by the manufacturer and was included in the uncertainty calculation.

- Rotational speed uncertainties
  Rotational speed uncertainties can be affected by, installation errors [due to non proper location of the sensor in the casing], and calibration errors.

2.4.2 Uncertainty in single measurement

In this section the term δY_i refers to the uncertainty in a measurement Yi .

To calculate the uncertainty of calculated results, the uncertainties in the measured parameters have to be known, i.e. Q,T_{1s}, T_{2s},N, P_{atm}, p_{1s} and p_{2s}. In this work, manufacturers specifications were used to obtain the uncertainty in the measured results.

As shown in Table 2-1, the manufacturer's specification gives upper and lower limits of errors [$e_+ and\ e_-$].This specification must be converted into an equivalent standard deviation σ. If we are given no information regarding which values lying between the limits e_+ and e_- are likely to be more probable, we have little alternative but to assume value between those limits to be equally probable. As a consequence, the probability distribution representing the variability of values to be rectangular [Kirkup, 2007 (162)].

Standard deviation of rectangular distribution is given by

$$s_d = \frac{e}{\sqrt{3}} \qquad 2\text{-}17$$

For Type B uncertainties, standard deviation is taken to be the standard uncertainty, δ

Hence,

$$\delta = s_d = \frac{e}{\sqrt{3}} \qquad 2\text{-}18$$

2.4.3 Uncertainty in the results

The result G of an experiment is assumed to be calculated from a set of measurements and is presented by:

$$G = G(Y_1, Y_2, Y_3, \dots, Y_i) \qquad 2\text{-}19$$

The effect of the uncertainty in a single measurement on the calculated result, if only that one measurement were in error would be

$$\delta G_{Yi} = \left\{\frac{\partial G}{\partial Y_i}\delta Y_i\right\} \qquad 2\text{-}20$$

The partial derivative of G with respect to Yi is the sensitivity coefficient for result G with respect to the measurement Yi [Moffat, 1988].

When several independent variables are used in the function G, the individual terms are combined by a root-sum-square method [RSS].

$$\delta G = \sqrt{\sum_{i=1}^{n}\left(\frac{\partial G}{\partial Y_i}\delta Y_i\right)^2} \qquad 2\text{-}21$$

This is the basic equation of uncertainty analysis. Each term represents the contribution made by uncertainty in one variable,δY_i to the overall uncertainty in the result, δG.

❖ Calculating the uncertainty of each calculated parameter

The parameters that are measured during centrifugal compressor field tests are:

1. Inlet mass flow rate, Q
2. Compressor rotational speed, N
3. Inlet and outlet static temperature, T_{1s} and T_{2s}
4. Inlet and outlet static pressure, p_{1s} and p_{2s}
5. Atmospheric pressure, P_{atm}

When substituting equations 2-1 to 2-15 into equation *2-21*, the uncertainty of each of the calculated parameters is obtained,

o Inlet static pressure

Inlet static pressure can be presented by,

$$P_{1s} = f(p_{1s}, P_{atm})$$

$$\delta P_{1s} = \sqrt{\left(\frac{\partial P_{1s}}{\partial p_{1s}}\delta p_{1s}\right)^2 + \left(\frac{\partial P_{1s}}{\partial P_{atm}}\delta P_{atm}\right)^2} \qquad 2\text{-}22$$

$$\delta P_{1s} = \sqrt{(\delta p_{1s})^2 + (\delta P_{atm})^2}$$

o Outlet static pressure

$$P_{2s} = f(\mathrm{p}_{2s}, P_{atm})$$

$$\delta P_{2s} = \sqrt{(\delta p_{2s})^2 + (\delta P_{atm})^2} \qquad 2\text{-}23$$

o Inlet absolute velocity

Taking into consideration only the measured values which have significant uncertainty, inlet absolute velocity can be presented by,

$$C_1 = f(T_{1s}, Q, P_{1s})$$

$$\delta C_1 = \sqrt{\left(\frac{\partial C_1}{\partial T_{1s}}\delta T_{1s}\right)^2 + \left(\frac{\partial C_1}{\partial Q}\delta Q\right)^2 + \left(\frac{\partial C_1}{\partial P_{1s}}\delta P_{1s}\right)^2} \qquad 2\text{-}24$$

$$\delta C_1 = \frac{R}{A_1}\sqrt{\left(\frac{Q}{P_{1s}}\delta T_{1s}\right)^2 + \left(\frac{T_{1s}}{P_{1s}}\delta Q\right)^2 + \left(\frac{QT_{1s}}{P_{1s}^2}\delta P_{1s}\right)^2}$$

Note that flow area is not included in the measured values, since it has negligible error in the diameter.

o Absolute outlet velocity

$$C_2 = f(T_{2s}, Q, P_{2s})$$

$$\delta C_2 = \frac{R}{A_2}\sqrt{\left(\frac{\partial C_2}{\partial T_{2s}}\delta T_{1s}\right)^2 + \left(\frac{\partial C_2}{\partial Q}\delta Q\right)^2 + \left(\frac{\partial C_2}{\partial P_{2s}}\delta P_{2s}\right)^2}$$

$$\delta C_2 = \frac{R}{A_2}\sqrt{\left(\frac{Q}{P_{2s}}\delta T_{2s}\right)^2 + \left(\frac{T_{2s}}{P_{2s}}\delta Q\right)^2 + \left(\frac{QT_{2s}}{P_{2s}^2}\delta P_{2s}\right)^2} \quad 2\text{-}25$$

- Inlet total temperature

Perfect gas assumption, Cp is constant, Total outlet temperature can be presented by,

$$T_{1t} = f(T_{1s}, C_1)$$

$$\delta T_{1t} = \sqrt{\left(\frac{\partial T_{1t}}{\partial T_{1s}}\delta T_{1s}\right)^2 + \left(\frac{\partial T_{1t}}{\partial C_1}\delta C_1\right)^2} \quad 2\text{-}26$$

$$\delta T_{1t} = \sqrt{(\delta T_{1s})^2 + \left(\frac{V_1}{Cp}\delta C_1\right)^2}$$

- Outlet total temperature

$$T_{2t} = f(T_{2s}, C_2)$$

$$\delta T_{2t} = \sqrt{\left(\frac{\partial T_{2t}}{\partial T_{2s}}\delta T_{2s}\right)^2 + \left(\frac{\partial T_{2t}}{\partial V_2}\delta C_2\right)^2} \quad 2\text{-}27$$

$$\delta T_{2t} = \sqrt{(\delta T_{2s})^2 + \left(\frac{V_2}{Cp}\delta C_2\right)^2}$$

- Inlet total pressure

$$P_{1t} = f(\mathrm{T_{1t}}, \mathrm{T_{1s}}, P_{1s})$$

$$\delta P_{1t} = \sqrt{\left(\frac{\partial P_{1t}}{\partial T_{1t}}\delta T_{1t}\right)^2 + \left(\frac{\partial P_{1t}}{\partial T_{1s}}\delta T_{1s}\right)^2 + \left(\frac{\partial P_{1t}}{\partial P_{1s}}P_{1s}\right)^2} \quad 2\text{-}28$$

$$\delta P_{1t} = \sqrt{\left(\frac{kP_{1s}\,(\mathrm{T_{1t}})^{k-1}}{(\mathrm{T_{1s}})^k}\delta T_{1t}\right)^2 + \left(\frac{kP_{1s}\,(\mathrm{T_{1t}})^{k}}{(\mathrm{T_{1s}})^{k+1}}\delta T_{1s}\right)^2 + \left(\left(\frac{\mathrm{T_{1t}}}{\mathrm{T_{1s}}}\right)^k \delta P_{1s}\right)^2}$$

- Outlet total pressure

$$P_{2t} = f(\mathrm{T_{2t}}, \mathrm{T_{2s}}, P_{2s})$$

$$\delta P_{2t} = \sqrt{\left(\frac{\partial P_{2t}}{\partial T_{2t}}\delta T_{2t}\right)^2 + \left(\frac{\partial P_{2t}}{\partial T_{2s}}\delta T_{2s}\right)^2 + \left(\frac{\partial P_{2t}}{\partial P_{2s}}P_{2s}\right)^2} \quad 2\text{-}29$$

$$\delta P_{2t} = \sqrt{\left(\frac{kP_{2s}\,(\mathrm{T_{2t}})^{k-1}}{(\mathrm{T_{2s}})^k}\delta T_{2t}\right)^2 + \left(\frac{kP_{2s}\,(\mathrm{T_{2t}})^{k}}{(\mathrm{T_{2s}})^{k+1}}\delta T_{2s}\right)^2 + \left(\left(\frac{\mathrm{T_{2t}}}{\mathrm{T_{2s}}}\right)^k \delta P_{2s}\right)^2}$$

- Outlet isentropic temperature

Considering that the specific heat ratio γ does not change with temperature, then k is constant and exit isentropic temperature can be written as,

$$T_{2i} = f\left(\mathrm{T_{1t}}, P_{1t,} P_{2t}\right)$$

$$\delta T_{2i} = \sqrt{\left(\frac{\partial T_{2i}}{\partial T_{1i}}\delta T_{1i}\right)^2 + \left(\frac{\partial T_{2i}}{\partial P_{1t}}\delta P_{1t}\right)^2 + \left(\frac{\partial T_{2i}}{\partial P_{2t}}\delta P_{2t}\right)^2} \qquad 2\text{-}30$$

$$\delta T_{2i} = \sqrt{\left(\left(\frac{\mathrm{P_{2t}}}{\mathrm{P_{1t}}}\right)^{(1/k)}\delta T_{1t}\right)^2 + \left(\frac{\mathrm{T_{1t}}(\mathrm{P_{2t}})^{(1/k)}}{k(\mathrm{P_{1t}})^{(k+1/\mathrm{k})}}\delta P_{1t}\right)^2 + \left(\frac{\mathrm{T_{1t}}(\mathrm{P_{2t}})^{(1-k/k)}}{k(\mathrm{P_{1t}})^{(1/\mathrm{k})}}\delta P_{2t}\right)^2}$$

- Isentropic total to total efficiency

$$\eta_{tt} = f(\mathrm{T_{2t}}, \mathrm{T_{1t}}, T_{2i})$$

$$\delta\eta_{tt} = \sqrt{\left(\frac{\partial \eta_{tt}}{\partial T_{1t}}\delta T_{1t}\right)^2 + \left(\frac{\partial \eta_{tt}}{\partial T_{2t}}\delta T_{2t}\right)^2 + \left(\frac{\partial \eta_{tt}}{\partial T_{2t}}\delta T_{2i}\right)^2} \qquad 2\text{-}31$$

$$\delta\eta_{tt} = \sqrt{\left(\frac{(T_{1t}-T_{2i})}{(T_{2t}-T_{1t})^2}\delta T_{1t}\right)^2 + \left(\frac{2T_{2i}T_{2t}+T_{1t}}{(T_{1t})^3}\delta T_{2t}\right)^2 + \left(\frac{1}{(T_{2t}-T_{1t})}\delta T_{2i}\right)^2}$$

- Total pressure ratio

$$TPR = f(\mathrm{P_{2t}}, \mathrm{P_{1t}})$$

$$\delta TPR = \sqrt{\left(\frac{\partial P_r}{\partial P_{1t}}\delta P_{1t}\right)^2 + \left(\frac{\partial P_r}{\partial P_{2t}}\delta P_{2t}\right)^2} \qquad 2\text{-}32$$

$$\delta TPR = \sqrt{\left(\frac{P_{2t}}{(P_{1t})^2}\delta P_{1t}\right)^2 + \left(\frac{1}{P_{1t}}\delta P_{2t}\right)^2}$$

- Corrected rotational speed

$$N_c = f(\mathrm{N}, \mathrm{T_{1t}})$$

$$\delta N_c = \sqrt{\left(\frac{\partial N_c}{\partial N}\delta N\right)^2 + \left(\frac{\partial N_c}{\partial T_{1t}}\delta T_{1t}\right)^2} \qquad 2\text{-}33$$

$$\delta N_c = \sqrt{\left(\sqrt{\frac{T_{1t}}{T_0}}\delta N\right)^2 + \left(\frac{N}{2\sqrt{T_0 T_{1t}}}\delta T_{1t}\right)^2}$$

- Corrected mass flow rate

$$Q_c = f(Q, \mathrm{T_{1t}}, \mathrm{P_{1t}}) \qquad 2\text{-}34$$

$$\delta Q_c = \sqrt{\left(\frac{\partial Q_c}{\partial Q}\delta Q\right)^2 + \left(\frac{\partial Q_c}{\partial T_{1t}}\delta T_{1t}\right)^2 + \left(\frac{\partial Q_c}{\partial P_{1t}}\delta P_{1t}\right)^2}$$

$$\delta Q_c = \sqrt{\left(\sqrt{\frac{T_{1t}}{T_0}}\frac{P_0}{P_{1t}}\delta Q\right)^2 + \left(\frac{QP_0}{2P_{1t}\sqrt{T_0 T_{1t}}}\delta T_{1t}\right)^2 + \left(\sqrt{\frac{T_{1t}}{T_0}}\frac{QP_0}{{P_{1t}}^2}\delta P_{1t}\right)^2}$$

2.4.4 Procedure of calculating uncertainty experimental results

The compressor performance test uncertainties are predicted by evaluating equations, 2-22 to 2-34 with assumed measurement uncertainties as suggested in Table 2-1. See Figure 2-17.

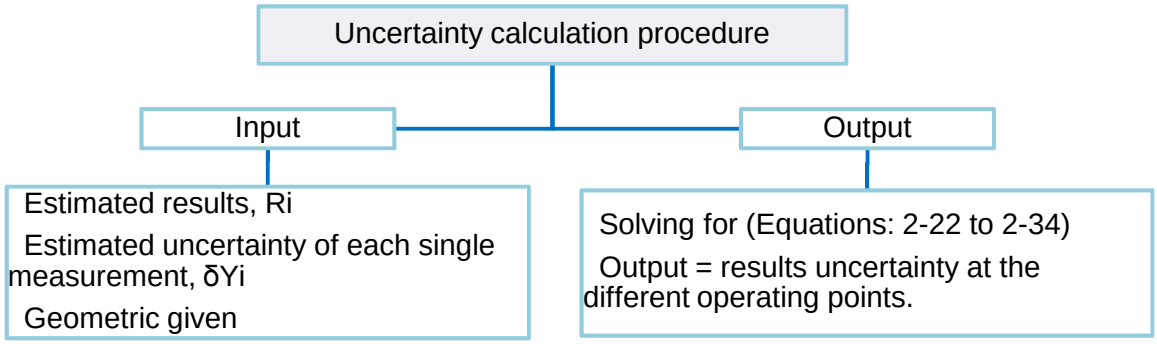

Figure 2-17 Calculation procedure for uncertainty calculations

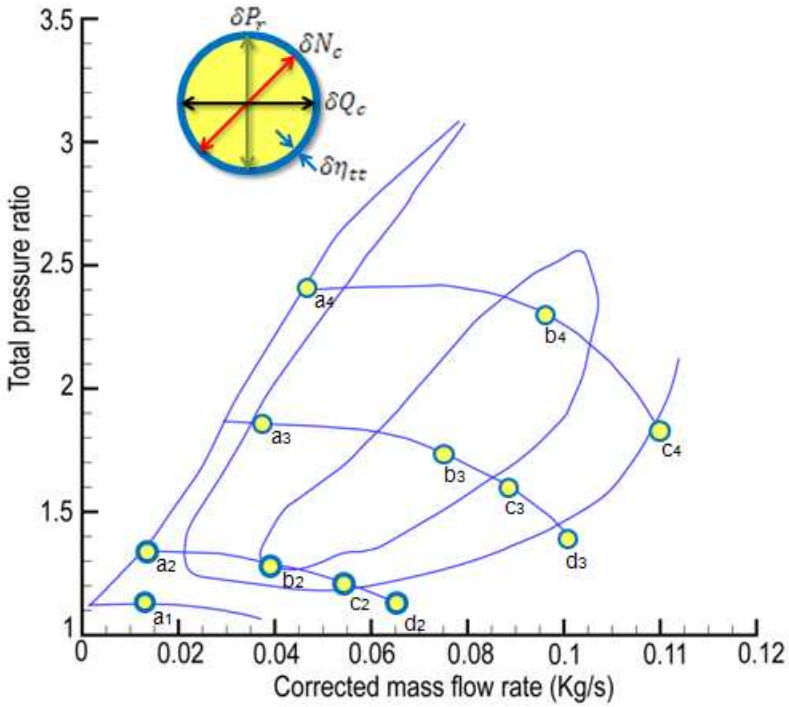

Figure 2-18 Uncertainty analysis at different operating points

Example: Test conditions:

Uncertainty analysis of different compressor functioning points was done. The different points $[a_1, a_2, a_3, a_4, b_2, b_3, b_4, c_2, c_3, c_4, d_2, \text{and } d_3]$ are located at four different rotational speeds $N_c = 60, 95, 145 \text{ \& } 180\text{K rpm}$ [Figure 2-18]. Points are chosen to show the effect of pressure ratio, mass flow rate and rotational speed on results uncertainty.

Measured values are substituted to obtain compressor performance characteristics using equations [2-1 till 2-15]. Using equations [2-22 till 2-34] and substituting for measured uncertainties of Table 2-1, one can obtain result uncertainty at the different functioning points.

Measurement uncertainty of the different functioning points is presented bellow.

$$\begin{Bmatrix} F.Point \\ a_1 \end{Bmatrix} \quad \begin{Bmatrix} Q_c\ (kg/s) \\ 0.0126 \end{Bmatrix} \begin{Bmatrix} TPR \\ 1.109 \end{Bmatrix} \begin{Bmatrix} \eta_{tt} \\ 0.518 \end{Bmatrix}$$

$$\begin{Bmatrix} \delta Q_c\ (\%) \\ 1.293 \end{Bmatrix} \begin{Bmatrix} \delta TPR\ [\%] \\ 1.359 \end{Bmatrix} \begin{Bmatrix} \delta \eta_{tt}[\%] \\ 15.323 \end{Bmatrix} \begin{Bmatrix} \delta N_c[\%] \\ 0.201 \end{Bmatrix}$$

$$\begin{Bmatrix} F.Point \\ a_2 \\ b_2 \\ c_2 \\ d_2 \end{Bmatrix} \quad \begin{Bmatrix} Q_c\ (kg/s) \\ 0.0144 \\ 0.0394 \\ 0.0549 \\ 0.0653 \end{Bmatrix} \begin{Bmatrix} TPR \\ 1.3710 \\ 1.2928 \\ 1.1978 \\ 1.1152 \end{Bmatrix} \begin{Bmatrix} \eta_{tt} \\ 0.5359 \\ 0.7082 \\ 0.6379 \\ 0.4564 \end{Bmatrix}$$

$$\begin{Bmatrix} \delta Q_c\ (\%) \\ 1.2933 \\ 1.2929 \\ 1.2919 \\ 1.2910 \end{Bmatrix} \begin{Bmatrix} \delta TPR\ [\%] \\ 1.296 \\ 1.329 \\ 1.342 \\ 1.349 \end{Bmatrix} \begin{Bmatrix} \delta \eta_{tt}[\%] \\ 5.094 \\ 6.370 \\ 8.945 \\ 14.463 \end{Bmatrix} \begin{Bmatrix} \delta N_c[\%] \\ 0.114 \\ 0.120 \\ 0.122 \\ 0.123 \end{Bmatrix}$$

$$\begin{Bmatrix} F.Point \\ a_3 \\ b_3 \\ c_3 \\ d_3 \end{Bmatrix} \quad \begin{Bmatrix} Q_c\ (kg/s) \\ 0.0385 \\ 0.0761 \\ 0.0887 \\ 0.1014 \end{Bmatrix} \begin{Bmatrix} TPR \\ 1.8826 \\ 1.7512 \\ 1.5948 \\ 1.3927 \end{Bmatrix} \begin{Bmatrix} \eta_{tt} \\ 0.6144 \\ 0.7197 \\ 0.6931 \\ 0.5691 \end{Bmatrix}$$

$$\begin{Bmatrix} \delta Q_c\ (\%) \\ 2.739 \\ 3.022 \\ 3.562 \\ 4.868 \end{Bmatrix} \begin{Bmatrix} \delta TPR\ [\%] \\ 1.241 \\ 1.267 \\ 1.280 \\ 1.293 \end{Bmatrix} \begin{Bmatrix} \delta \eta_{tt}[\%] \\ 2.739 \\ 3.022 \\ 3.562 \\ 4.86 \end{Bmatrix} \begin{Bmatrix} \delta N_c[\%] \\ 0.077 \\ 0.078 \\ 0.079 \\ 0.078 \end{Bmatrix}$$

$$\begin{Bmatrix} F.Point \\ a_4 \\ b_4 \\ c_4 \end{Bmatrix} \quad \begin{Bmatrix} Q_c\ (kg/s) \\ 0.0461 \\ 0.0966 \\ 0.1200 \end{Bmatrix} \begin{Bmatrix} TPR \\ 2.3966 \\ 2.3385 \\ 1.8317 \end{Bmatrix} \begin{Bmatrix} \eta_{tt} \\ 0.5712 \\ 0.7055 \\ 0.6221 \end{Bmatrix}$$

$$\begin{Bmatrix} \delta Q_c\ (\%) \\ 1.293 \\ 1.287 \\ 1.285 \end{Bmatrix} \begin{Bmatrix} \delta TPR\ [\%] \\ 1.186 \\ 1.206 \\ 1.231 \end{Bmatrix} \begin{Bmatrix} \delta \eta_{tt}[\%] \\ 2.261 \\ 2.156 \\ 2.80 \end{Bmatrix} \begin{Bmatrix} \delta N_c[\%] \\ 0.063 \\ 0.063 \\ 0.063 \end{Bmatrix}$$

As it can be seen, the pressure ratio, corrected mass flow rate, and corrected rotational speeds uncertainties, don't respectively exceed 1.36%, 1.3%, and 0.2% of their estimated values.

Efficiency uncertainty is seen to be increasing with pressure ratio decrease, as can be shown in Figure 2-19. The very high uncertainty at low pressure ratios [$\delta\eta_{tt}\ (a_1) = 15.3\%$ at $P_r\ (a_1) = 1.1$] makes it not precise to present efficiency results in this zone of the compressor map.

The small uncertainties at high pressure ratio can be explained by the fact that the larger the temperature or pressure inlet outlet difference, the smaller the relative influence on the individual measurement errors on the total uncertainties.

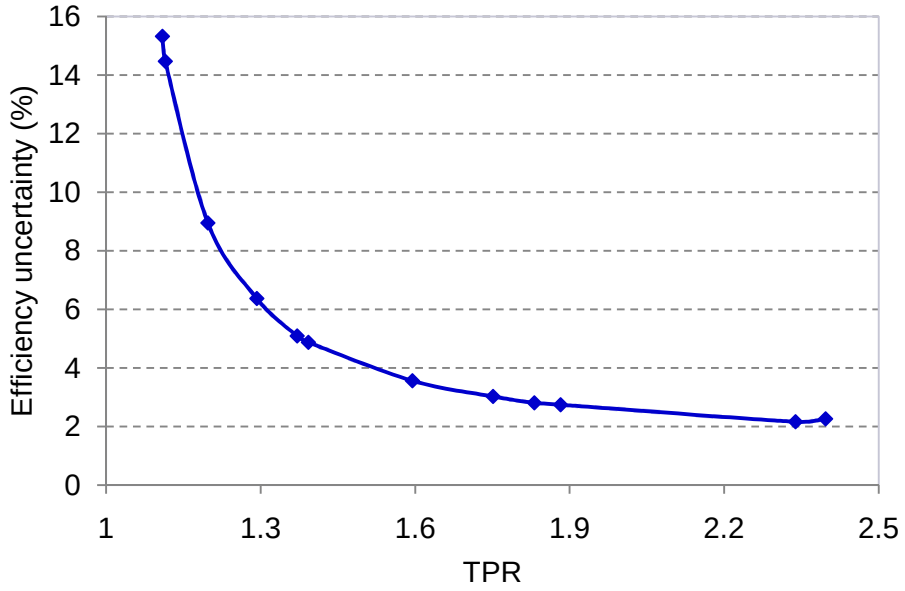

Figure 2-19 Efficiency uncertainty versus mass flow rate

2.4.5 Individual measurement uncertainties effect on the overall uncertainty

In this part we hope to provide a guide line as to which uncertainty most significantly effects the overall performance parameter uncertainties. In other words, to study the effect of individual measurement uncertainties on the overall compressor performance uncertainties.

Error, %	δP_{1s}	δP_{2s}
0.01	3.0221	3.01944
0.1	3.0222	3.02221
1	3.0243	3.28606
2	3.0308	3.98023
3	3.0566	4.92433
4	3.0566	6.00153

Table 2-4 Isentropic efficiency uncertainty [%], at different pressure sensor uncertainties

The operating point b_3 as presented in Figure 2-18 is used as a basis for the bellow studies.

Table 2-4 and Table 2-5 show a quantitative comparison of the individual measurement uncertainties effect on the compressor isentropic efficiency uncertainty. For these studies only one measurement uncertainty parameter was varied while all others were left at the values described in Table 2-1.

Table 2-4 shows that the influence of the outlet pressure uncertainties on the total isentropic efficiency uncertainty is higher than the inlet pressure uncertainties. Table 2-5 shows that the inlet temperature uncertainty has a stronger influence on the isentropic efficiency total uncertainty than the outlet temperature uncertainty.

Error, K	δT_{1s}	δT_{2s}
0.25	1.844	2.511
0.5	2.132	2.621
1	3.02	3.02
2	5.235	4.255
3	7.602	5.753
4	10.023	7.354

Table 2-5 Isentropic efficiency uncertainty [%] at different temperature sensor uncertainties

Overall efficiency uncertainty was tested at 4 different operating points $a_1, b_2, b_3, and b_4$ [Figure 2-18], and different inlet temperature uncertainties. As shown in Figure 2-20, at low pressure ratios, efficiency uncertainties can reach 50% of the estimated value for an inlet temperature sensor error of 4K. This is unacceptably high.

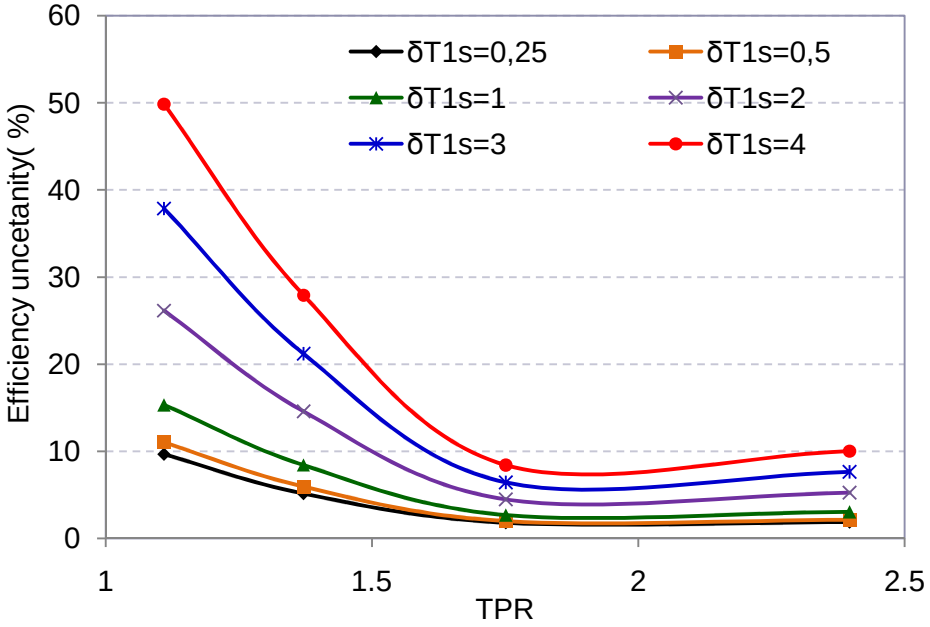

Figure 2-20 Effect of different inlet temperature sensor uncertainties on total efficiency uncertainty

In this section, uncertainty analysis has been done to the experimental results. The complete procedure to calculate overall compressor package performance measurement has been explained.

A number of parametric studies describing uncertainty at different operating points of the compressor map have been done. It was concluded that results uncertainties are high at low pressure ratio zone and very small at high pressure ratios.

Moreover, the effect on the overall performance uncertainty of different individual measurement uncertainties has been studied. This study serves to limit the overall compressor package performance measurement uncertainty.

Other than describing uncertainties in reported experimental results, uncertainty analysis can serve as a diagnostic tool during the phase of test bench conception, in which the choice of the different sensors can be done based on the demanded degree of performance uncertainties.

3 Chapter 3: Tested Compressor Characteristics

Two main parts are presented in this section:

- *compressor geometric and aerodynamic characteristics,*
- *compressor instability analysis*

Compressor geometric characteristics will serve to analyze the effect of different prewhirl types on compressor performance in chapter IV.

Instability analysis is very interesting to introduce and better understand the results obtained when using different mechanisms to improve compressor stable functioning [chapter IV].

Chapitre 3: Caractéristique de compresseur testé

Ce chapitre est composé de 2 parties :

- *caractéristiques géométriques et aérodynamiques du compresseur étudié*
- *analyse des instabilités de ce compresseur*

Les caractéristiques géométriques serviront à analyser l'effet de différents pré-rotateurs testés au chapitre 4.

L'analyse des instabilités est importante pour comprendre et analyser les résultats obtenus lors de l'utilisation de différents mécanismes permettant d'améliorer la stabilité de fonctionnement du compresseur

3.1 Geometric and aerodynamic analysis parameters of the tested compressor

The compressor is a part of a BorgWarner variable geometry turbocharger. It employs a back swept impeller and 12 radial blades at exit: six of them are short splitters. The diffuser is vane-less with radial parallel plates. The geometric and aerodynamic parameters are listed in Table 3-1 [See Figure 3-1 and Figure 3-2 for more clarity].

Impeller exit diameter	$\mathbf{D_2}$	46 mm
Impeller tip width	$\boldsymbol{b}$	2.55 mm
Impeller tip to hub ratio	$\mathbf{D_{1s}/D_{1h}}$	2.8 mm
Impeller inlet angle	$\boldsymbol{\beta_{1m}}$	51.6°
Exit blade angle	$\beta_{2m} = \frac{\beta_{2t} + \beta_{2h}}{2}$	40.7 °
Number of blades	$\boldsymbol{Z}$	12 [6 splitters]
Diffuser area distribution	$\boldsymbol{a * b}$	const
Diffuser radius ratio	$\boldsymbol{D_3/D_2}$	1.17
Circumferential Mach number	$\boldsymbol{Mu} = \frac{\boldsymbol{U_2}}{\boldsymbol{a_{01}}}$	1.08 at N=150K rpm
Volute exit diameter	$\boldsymbol{D_v}$	30 mm

Table 3-1 geometric and aerodynamic parameters of tested compressor

The impeller inlet flow area is defined in equation 3-1

$$S_1 = \frac{\pi \cdot \left(D_{1s}^2 - D_{1h}^2\right)}{4} = 3.65\ 10^{-4}\ [m^2] \qquad 3\text{-}1$$

$$S_d = \pi D_2 b = 3.68\ 10^{-4}\ [m^2] \qquad 3\text{-}2$$

Diffuser inlet flow area is defined in equation 3-2

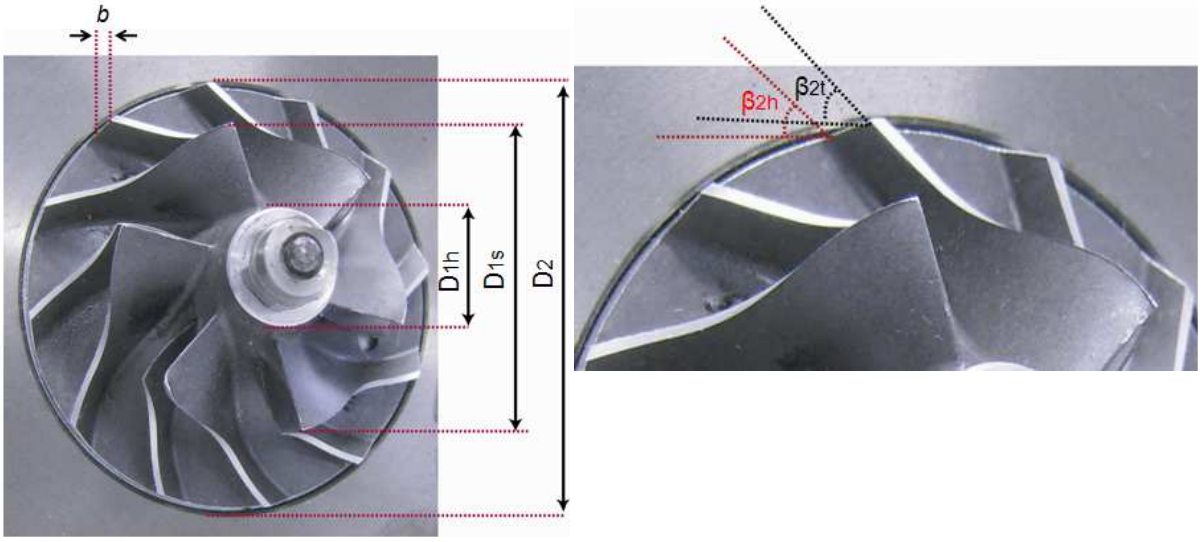

Figure 3-1 Impeller geometric parameters

Figure 3-2 Diffuser geometric characteristics

❖ Blade leading edge angle distribution

Blade angle distribution at different radii was measured, to analyze the incidence angle at different radii from hub to tip. Figure 3-3 shows the blade leading edge angle distribution for the tested compressor. Suction side [SS], pressure side [PS], and average blade angle at different radii, are presented.

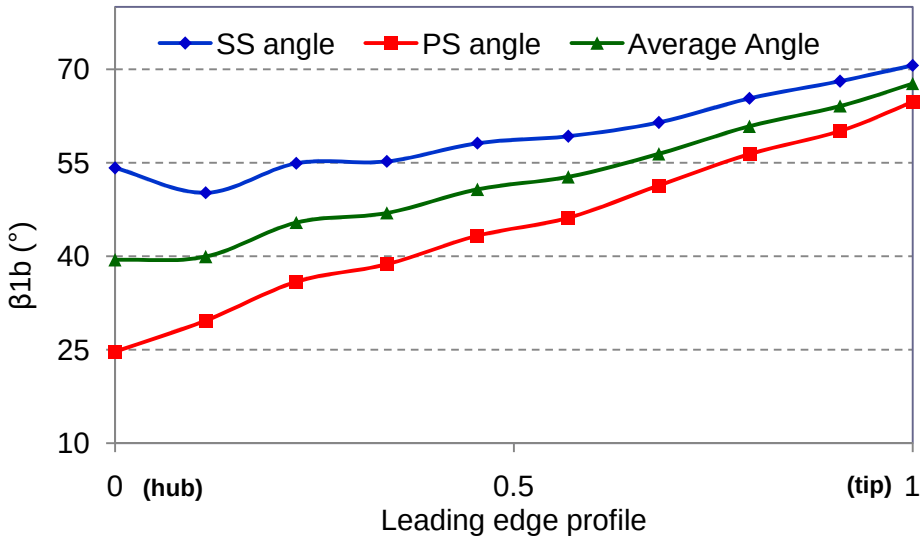

Figure 3-3 leading edge blade angle

3.2 Tested turbocharger compressor basic map characteristics

To study the effects of the different mechanisms to suppress compressor instabilities, we need to analyse tested compressor stability.

Figure 3-4 shows the base compressor characteristics, in which the compressor entry was a straight tube. Total pressure ratio in function of corrected mass flow rate at eight corrected rotational speeds, respectively: Nc=90, 100, 120,140,155,170,185 and 195Krpm. Lines of constant total to total efficiency [lines in green] in the pressure graph corresponds to 0.6, and 0.7 respectively, and the pointed line [in red] is the surge line.

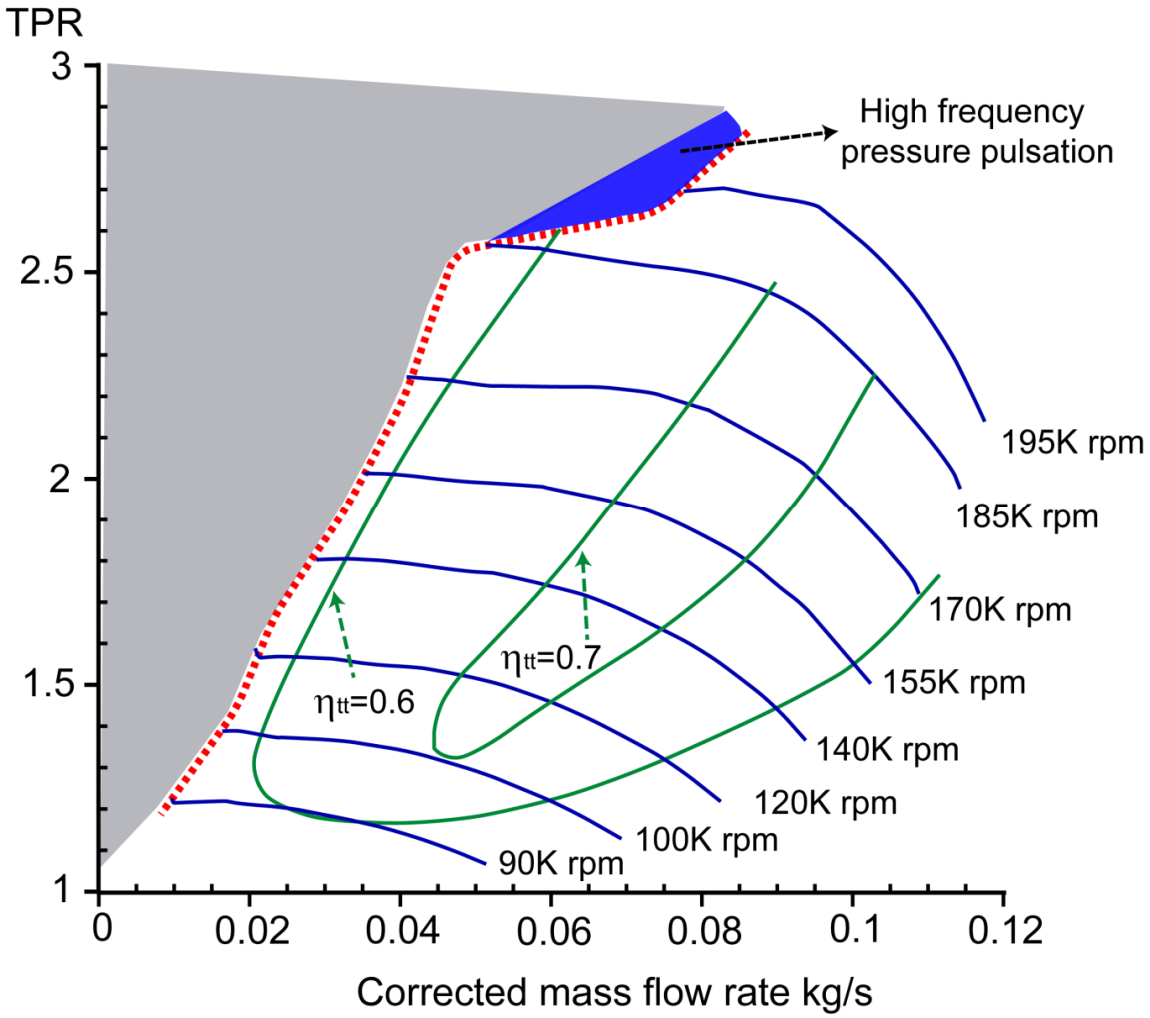

Figure 3-4 Basic compressor characteristics

The clear areas in the compressor map are regions of stable flow. The lightly highlighted area [in gray] is a zone of unstable functioning. The highlighted area [blue area] is a zone of high frequency pressure pulsation [around 70Hz]. This precedes the strong pressure fluctuation of surge point at high speed lines. When compressor operating in this zone, strong vibration and hard noise prevented us to reduce more the flow rate, and to go search for surge at high speeds [more than 185K rpm]. This, to not damage the compressor.

Since the goal of the current work is to shift the surge [dotted] line to low flow rates, then one have to understand what are the compressor components which trigger stage stall at the different map zones [low, mean and high speeds]. Hence, delaying stall onset, using different techniques [this will be detailed in chapter IV]

3.3 Impeller inducer incidence analysis

Figure 3-5 shows the compressor efficiency in function of impeller inducer tip incidence angle, and relative inlet Mach number. The incidence angle is defined as equation 3-3, and calculated using leading edge angle distribution [Figure 3-3] and relative flow angle at each measured point [equation 3-4].

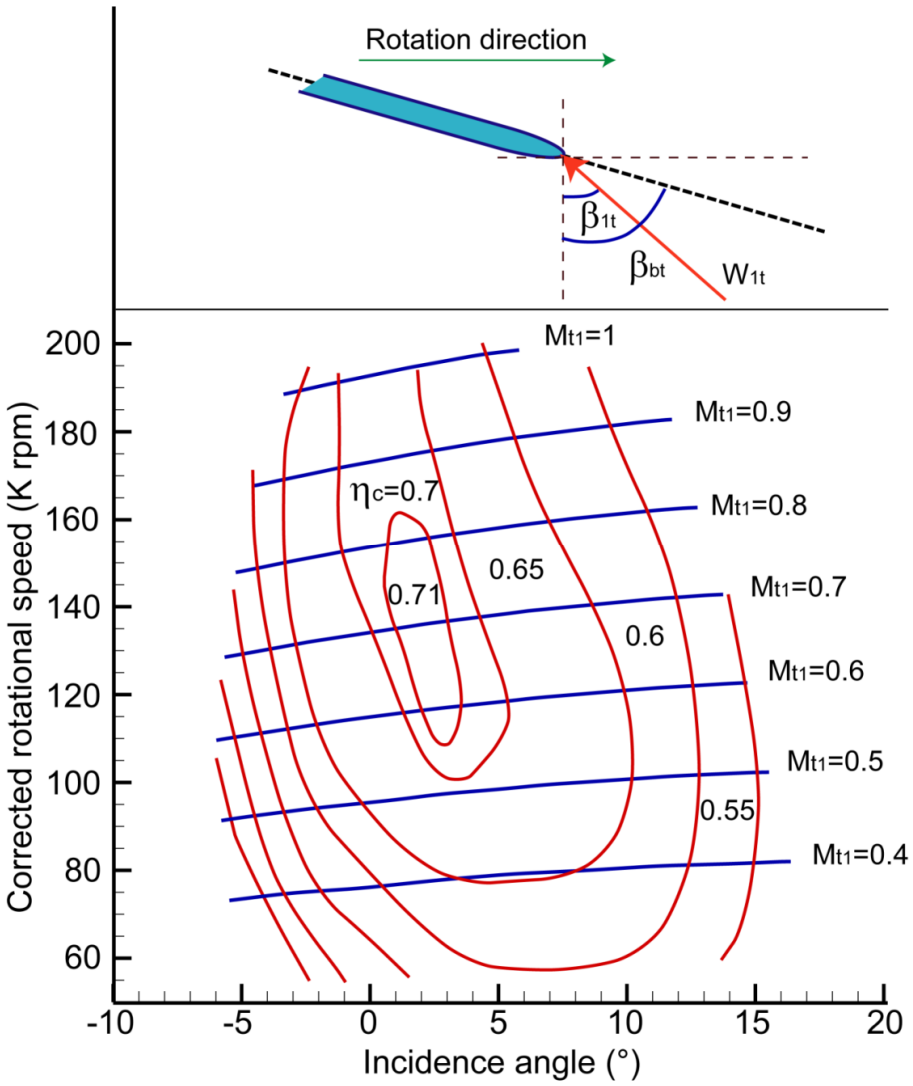

Figure 3-5 Compressor isentropic efficiency against inducer incidence angle

As it can be seen, compressor optimum efficiency is obtained for incidence angle between 0° and 5°.

$$i_t = \beta_{bt} - \beta_{1t} \quad \text{3-3}$$

$$\beta_{1t} = atan\left(\frac{C_1}{U_1}\right) \quad \text{3-4}$$

The blade is almost designed as a number of radially stacked sections. Each individual blade section operates over a range of incidence angles for which the loss incurred in the flow around the blade section is relatively small. If the blade section is forced to operate at incidence angles outside the loss-low range, the losses generally rise very rapidly and the blade section may stall [Steinke et al, 1967 (118)]. Good efficiency for the complete blade is realized when all the individual blade sections are operated in the low-loss incidence range.

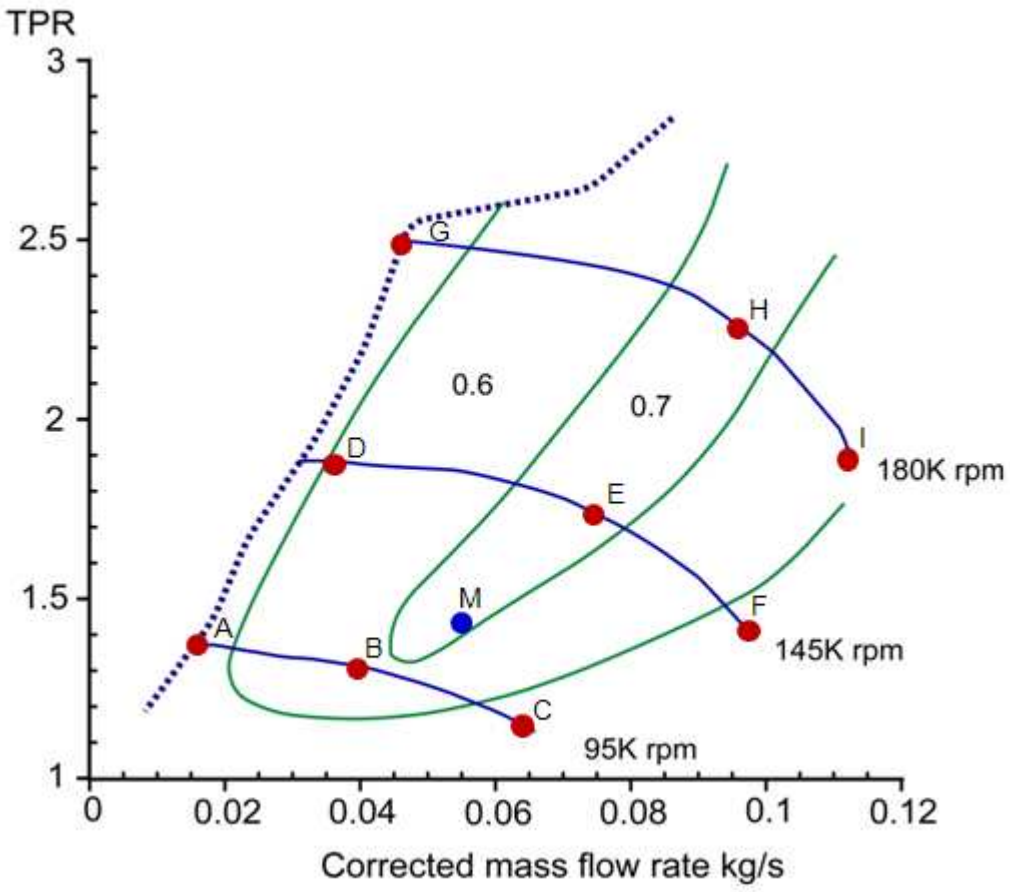

Figure 3-6 the nine different operating points

To study the incidence angle at different impeller eye radii, nine different operating points were chosen, as shown in Figure 3-6. The different operating points are $\mathrm{A, B, C, D, E, F, G, H, I and\ M}$, and are chosen so that they can be classified into:

- Three different mass flow rate zones: Low middle and high flow rates
- Three different rotational speed zones: $N = 95$, 145 and 180 $K\ rpm$
- Three different pressure ratio zones: Low, middle and high pressure ratio capacities.

The point on blue [M] is the point of maximum efficiency [Figure 3-6].

To study the incidence distribution at the different radii [from hub to tip of the impeller leading edge] and different operating points, a simple computer model was done.

- Model inputs: leading edge geometry angle distribution, temperature, pressure [at compressor inlet] and the rotational speed at the different operating points.
- Model output: angle of incidence at the different radii.

Results are shown in Figure 3-7. Incidence losses increase at low and high flow rates, and are in the range of [-10°, +6°] at middle flow rate s. The tip incidence angle at maximum efficiency [point M] is in the range of [+2°, -6°, from hub to tip]. The tip incidence angle for the maximum compressor total to total efficiency point is around -6°.

For points A, D, and G, blade sections near the hub side operate at incidence angles outside the loss-low range, and losses drops in the tip side sections. However, for points C, F and I, blade sections near the tip side operate at incidence angles outside the loss-low range, and losses drops in the hub side sections. It's worth mentioning that, incidence losses are less at high flow rates, than those of low flow rates.

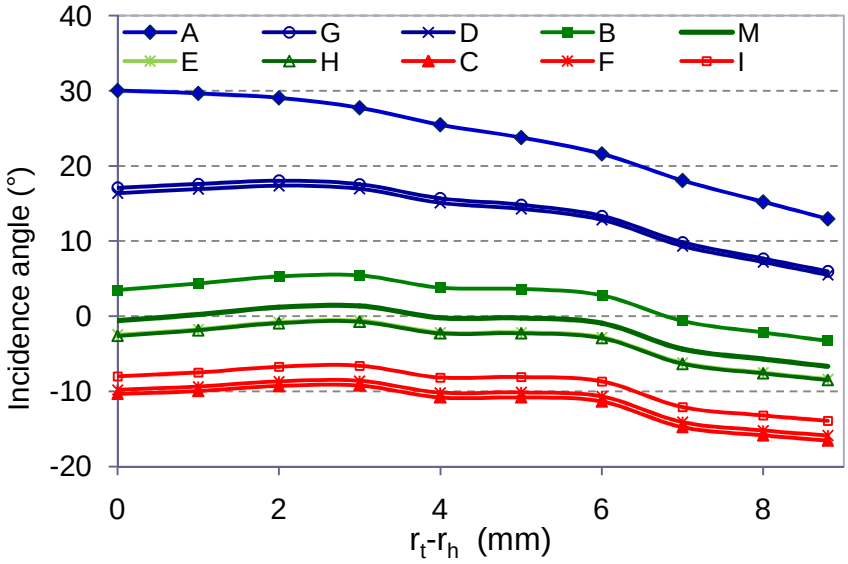

Figure 3-7 Incidence angle at all radii from hub to tip at the different operating points

3.4 Compressor instability analysis

In this section, the relative importance of each compressor stage element, which leads eventually to stage stalls, and consequently compressor surge, is diagnosed.

This study is necessary to understand the causes of stage stall at different compressor rotational speeds [low, mean and high]. For this goal, proper static pressure measurement at inlet, and outlet of each component was done. Careful attention was paid to this instrumentation, so that the necessary level of coverage and accuracy were obtained [Figure 3-8 and Figure 3-9]. For this configuration pressure transducers were positioned along the shroud line.

Figure 3-8 Pressure transducers installation

As it was previously mentioned [section 1.4.1], compressor stage can operate in unstable conditions during a long period of time without a stage stall, and with no significant noise or pressure fluctuations. However, if the component stall becomes stronger, or another component comes also to stall then a stage stall will result. If flow rate reduces, stage stall can provoke a system surge (81).

Since the overall static pressure is the sum of the static pressure increase in each of the compressor components, and stall can be regarded as the cessation of a continued rise in static pressure recovery in the diffuser or impeller (71). Then the static pressure increase in diffuser and impeller indicates when stall exists in each of these elements, and which triggers first stall.

Static pressure increase in the rotor, diffuser, and volute at different rotational speeds were tested in the turbocharger test facility. Study was done at four rotational speeds, these are 90,130,160, and 190K rpm. The choice of these speed lines was to analyze stall in the different elements at low, middle, and high speeds.

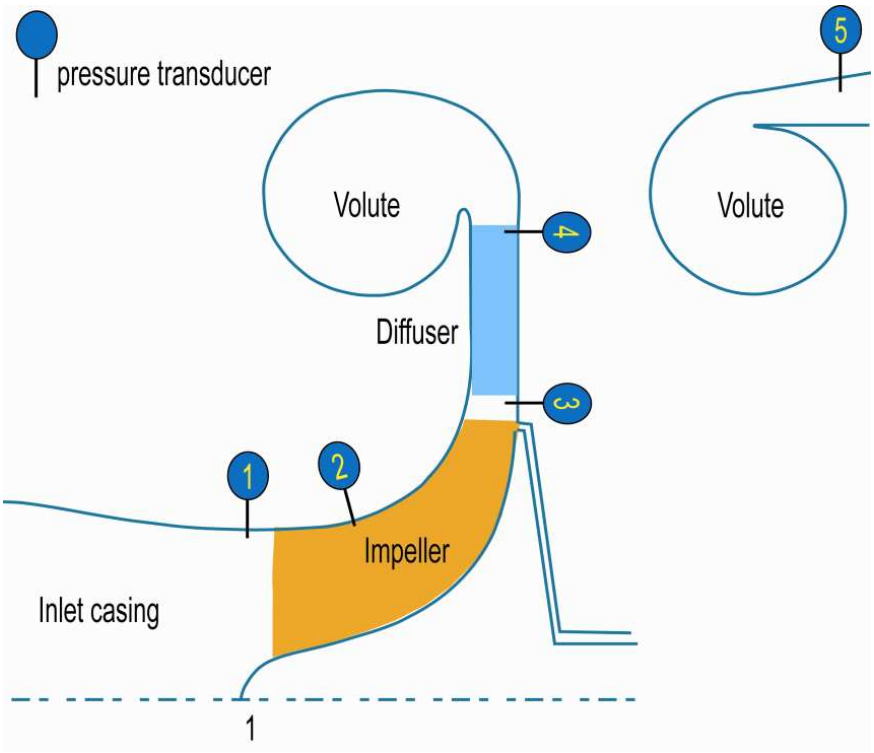

Figure 3-9 2D presentation of pressure transducers at different compressor stations

❖ Results and analysis

The static pressure difference in the impeller and the diffuser along the four rotational speeds, are presented in Figure 3-10 and Figure 3-11 respectively. The cessation in static pressure increase in the impeller at high rotational speeds [Figure 3-10] and that of the diffuser at low speeds [Figure 3-11] indicates these components stall at the corresponding rotational speeds.

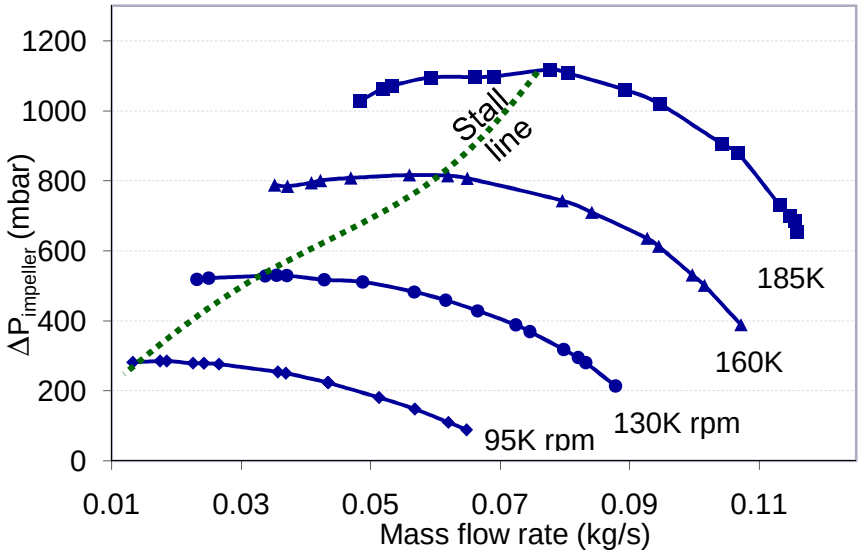

Figure 3-10 Impeller static pressure increase

As can be seen in Figure 3-11, at high rotational speeds and middle mass flow rate, pressure increase in the diffuser cesses to increase when reducing flow rate. This is probably due to a rotating stall occurring in the diffuser. This dynamic stall disappears when flow rate is reduced [pressure difference continues to increase in the diffuser at lower flow rate].

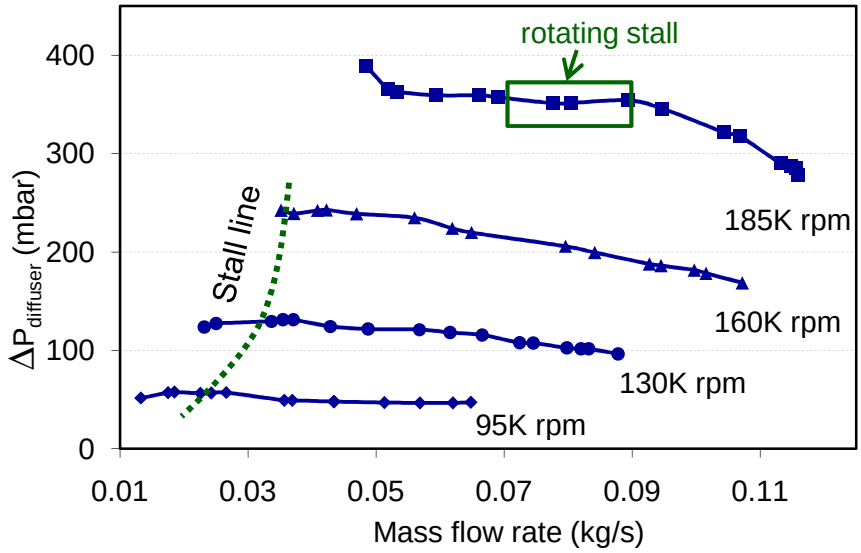

Figure 3-11 Diffuser static pressure increase

Another presentation of the diffuser and impeller stall lines as a function of rotational speeds and mass flow rate is shown in Figure 3-12. As it can be seen, diffuser stall precedes impeller stall at low rotational speeds. At 140K rpm, impeller and diffuser stall at the same mass flow rate, and at high rotational speed, impeller stall precedes that of the diffuser.

These results do not agree with the conclusion of Kammer et al,1985 (80) who considered that, the diffuser causes stage stall at high speeds and impeller stall at low speeds.

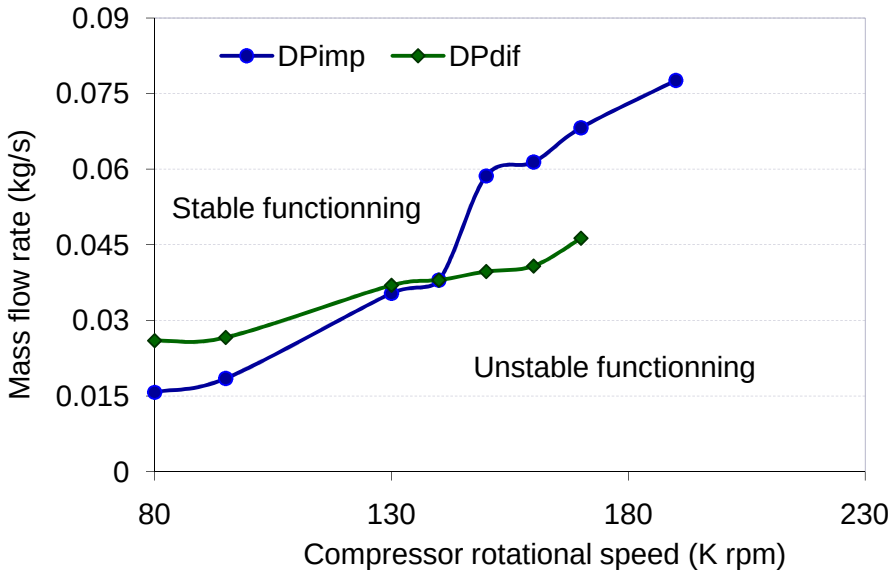

Figure 3-12 Diffuser static pressure increase

The surge is almost caused by a stage stall [De jager, 1995 (81)], and stage stall occurs when a single compressor component stalls or a when two components stall at once. Thus at low rotational speeds, the combination of rotor and diffuser stall probably causes the stage stall. However, at very high rotational speeds, a very hard impeller stall may be the cause of stage stall and hence, system surge.

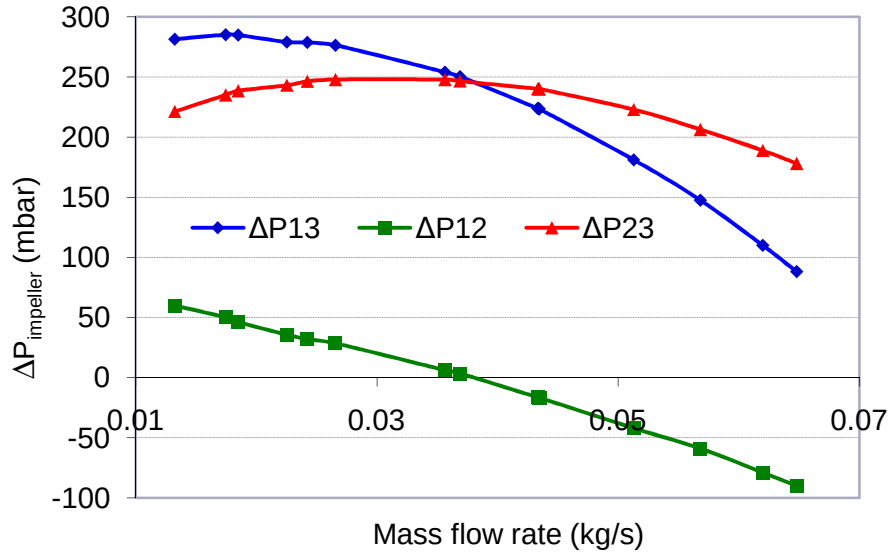

Figure 3-13 Static pressure rise in the inducer and the radial part of the impeller, at 95K rpm

To determine if the inducer or the radial part of the impeller triggers impeller instabilities, a pressure transducer was introduced at the inlet of the second row blades [splitters]. This transducer is presented as P2 in Figure 3-9. The pressure increase in the inducer [ΔP12], in the radial portion of the impeller [ΔP23] and the overall impeller static pressure increase [ΔP13], at 95K rpm is presented in Figure 3-13. As it can be seen, flow separation occurs in the radial part of the impeller. However, in the inducer part static pressure continues to increase from negative values [depression] at high flow rates to positive at low flow rates.

The same conclusion is obtained at 185K rpm [Figure 3-14]. Moreover, same results are obtained at the other different rotational speeds [160, and 130K rpm]. Hence, one can conclude that the pressure drop in the impeller comes probably from the radial part and not from the inducer part.

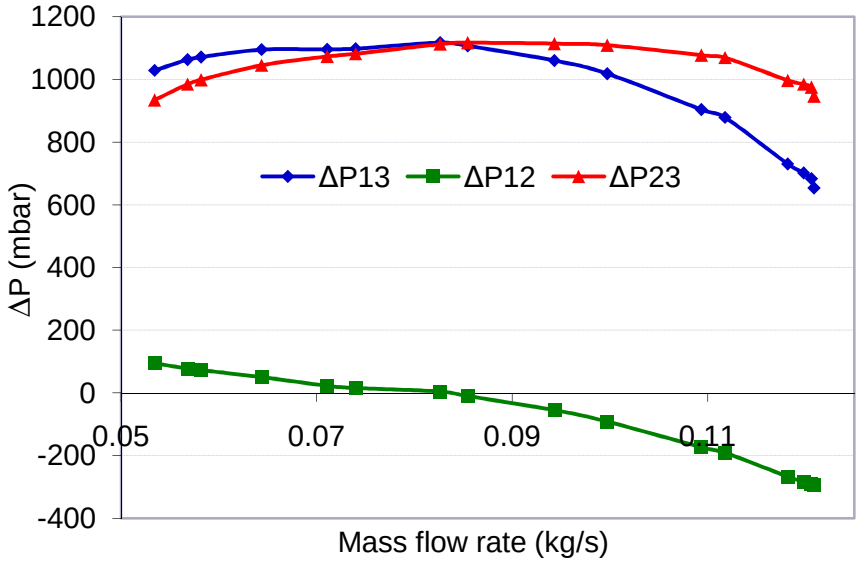

Figure 3-14 Static pressure rise in the inducer and the radial part of the impeller, at 185K rpm

However, although the static pressure increase in the inducer part can indicates a healthy inducer [good diffusion], but it can also indicates a high inlet recirculation. In fact, we are still not able to answer this question. A study of the static pressure evolution along the impeller [high response pressure transducers at many points through the inducer and the impeller radial part] is needed to this end. This will be done in the near future.

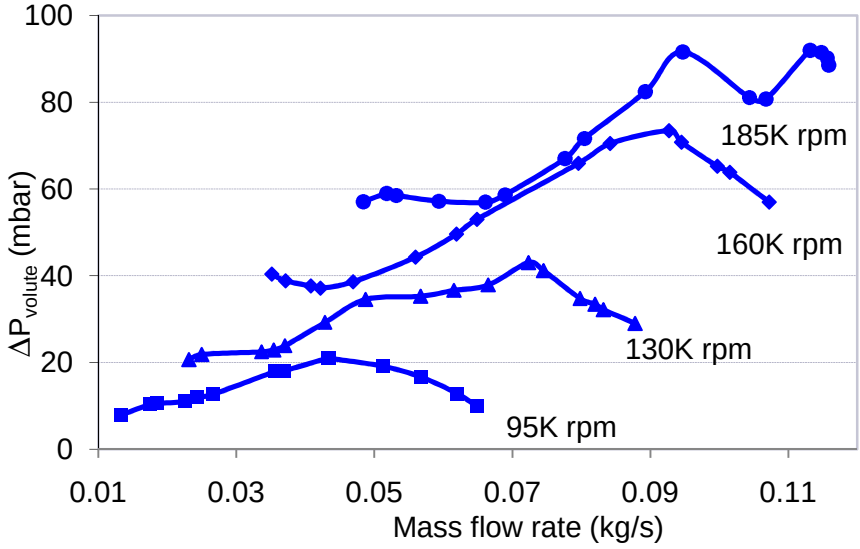

Figure 3-15 Static pressure rise along the volute

The last component of the compressor to be studied is the volute. The volute non uniform pressure distribution, acts back on the diffuser and the impeller [Sorokes,et al, 1998 (60)]. To study the effect of the pressure distribution of the volute, the diffuser and the impeller, static pressure rise through the volute was measured.

Figure 3-15 shows the pressure rise along the volute, as it can be seen the pressure rise cessed to increase at very high flow rates. Hence, compressor continues to function stably at these flow rates. This is probably due to a blockage at the tongue of the volute, which increases the volute circumferential pressure. This non uniform distribution acts back on the impeller and the diffuser. However, we're not yet able to explain the 'hole' in the pressure increase curve, at 185K rpm and high flow rates.

Instantaneous pressure measuring at the volute, diffuser and impeller exit was also measured. Results are presented in Figure 3-16 Instantaneous pressure distribution at impeller, diffuser, and volute exits, at 200K rpm. [To the right stable functioning, to the left a near surge point]

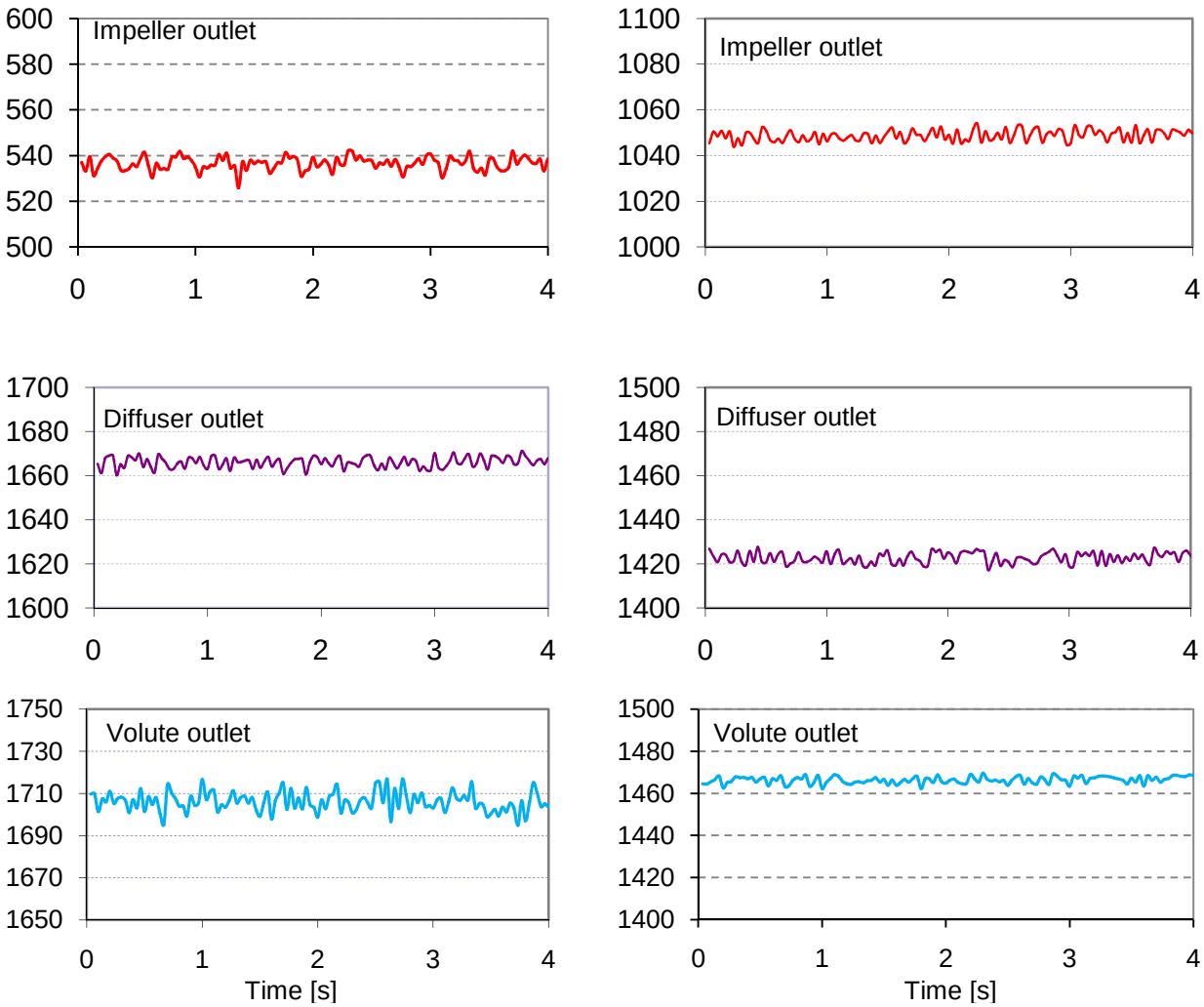

Figure 3-16 Instantaneous pressure distribution at impeller, diffuser, and volute exits, at 200K rpm. [To the right stable functioning, to the left a near surge point]

3.4.1 Conclusion

In this section, compressor geometric and aerodynamic characteristics were presented, impeller incidence analysis was done, and compressor instability analysis was investigated.

Pressure increase through the impeller and diffuser, and instantaneous pressure distribution analysis through the three components, drive us to the following conclusions:

- At low rotational speeds, diffuser stall triggers compressor stage stall, and consequently system surge.

- At high rotational speeds, impeller triggers stage stall. Static pressure measured at the inducer exit, shows that, pressure still increases in the inducer, however, decreases in the radial impeller part. These results do not give an indication of good diffusion in the inducer part, some more sophisticated measures have to be done to study flow separation in the impeller, and indicate which part of the impeller triggers stall. This work will be done in the near future.

Moreover, while the impeller causes the stage stall at high speeds, volute instabilities probably originate these instabilities, acting back on the impeller or the diffuser. This was shown when static pressure rise and instantaneous pressure measures were done along the volute.

The volute is probably not creating a stage stall, but its back affect on the impeller and the diffuser significantly influences compressor instabilities.

4 Chapter 4: Delaying compressor instabilities

This chapter is divided into five sections. It deals with delaying stall in each compressor component [inducer, radial impeller, diffuser, and volute].

In the first section, the effect of imparting swirl [counter and positive] at impeller inducer on compressor performance and surge margin was studied. A theoretical study was conducted to find out the most favorable prewhirl type to the tested impeller. Then four different swirl generators were tested. Local velocity measures downstream of the different tested swirl generators were done. Finally a new swirl generator [NS] was proposed and tested. The new system was based on experimental results [local and global], and theoretical study.

Section two refers to delaying impeller instabilities. The conventional MWE [Map width enhancement] system was tested. Holes were used as a connecting apparatus between the outer pipe and main inducer inlet. Two different configurations were tested, their effect on compressor performance and surge line was studied. The effect of extending the inlet pipe length was also investigated.

In the third section, delaying instabilities in the diffuser was studied. Two different techniques were investigated. These are pinched and J-grooves. The latter is conventionally used for pomp applications. Different configurations of the two techniques, and their effect on compressor performance and surge line were studied.

In section four, the volute tongue was retracted and rounded to study the effect of separation around the tongue, and pressure distribution in the volute on compressor performance and surge line.

In last section, the synergy effect between delaying inducer and diffuser instabilities was studied. The NS was used to impart swirl at impeller inlet, accompanied with a pinched diffuser.

Chapitre 4: Caractéristique de compresseur testé

Ce chapitre est composé de 5 paragraphes. Ils traitent de la possibilité de repousser le décrochement dans chaque partie du compresseur (entrée de la roue, partie radiale de la roue, diffuseur et volute).

Dans la première section, un tourbillon dans le sens de rotation de la roue ou contre-rotatif est généré à l'entrée de la roue et son effet sur les performances du compresseur et sur la limite de pompage est étudié. Une étude théorique a été conduite afin de déterminer la pré-rotation la plus favorable pour le compresseur testé. Puis 4 types de pré-rotateur ont été testés. Des mesures locales de vitesse en aval de ces mécanismes ont été effectuées. Finalement, un nouveau mécanisme (NS) de pré-rotation a été conçu, réalisé et testé. Il est basé sur les résultats expérimentaux (locaux et globaux) et sur l'analyse théorique.

La deuxième section traite de la possibilité de repousser les instabilités dans la roue. Le système conventionnel MWE a été testé. Des trous furent utilisés comme canaux de circulation entre la tubulure de retour et l'entrée principale de la roue. Deux configurations différentes furent testées et leurs influences sur les champs de fonctionnement et les lignes de pompages sont présentées. L'effet de l'extension du tube de retour est aussi analysé.

Dans la troisième section, la possibilité de repousser les instabilités dans le diffuseur est étudiée. Deux techniques différentes sont analysées : le pincement et les sillons radiaux. Cette dernière technique est utilisée habituellement pour les pompes. Plusieurs configurations des 2 techniques ont été testées.

Dans la section 4, le bec de volute a été raccourci et arrondi pour étudier son effet sur la séparation de l'écoulement et sur la distribution de pression dans la volute. Les conséquences sur le champ de fonctionnement et sur la ligne de pompage sont présentées.

Finalement, dans la dernière section, l'effet de synergie entre la réduction simultanée des instabilités en entrée de roue et dans le diffuseur a été étudié. Le système NS a été utilisé ainsi que le pincement dans le diffuseur.

4.1 Delaying inducer instabilities

Imposing prewhirl at inducer inlet reduces incidence angle, hence incidence losses, and delay inducer stall. In this section, different pre rotation mechanisms have been tested; their effect on compressor performance and surge line was studied.

The section begins with a theoretical study of the effect of the different prewhirl types on incidence angle at impeller inlet. Presentation of the different tested mechanisms and the pressure losses through them is investigated in the second part of the section, finally the effect of tested mechanisms on the overall compressor performance and surge line improvement is investigated in the last part. Moreover, LDA measurements were done to understand global results obtained from overall performance study.

4.1.1 Theoretical analysis

This subsection deals with the following points:

1. What is the effect of different types of prewhirl on the impeller incidence angle, and what type of prewhirl is the most convenient for the tested compressor.
2. Is it possible to create zero incidence angles at impeller leading edge, and what are the characteristics of the Ideal prewhirl generator, which can produce the zero incidences with zero losses at all operating points.

The different operating points chosen for this study are presented in chapter III [Figure 3-5]. These different operating points are $A, B, C, D, E, F, G, H, I and\ M$.

- ❖ Prewhirl types effect on the impeller incidence angle

The study and the use of inlet guide vanes to give desired radial distributions of velocity diagrams at the rotor inlet and/or rotor inlet relative Mach number has been investigated by Steinke et al, 1967 (118) and Whitfield et al, 1975 (107). This work is bases on their study.

The effect of possible prewhirl types on compressor performance, particularly any effect on the impeller incidence losses has been studied in this section. The analysis was based on the radial equilibrium approach. This approach is detailed by Dixon, 1998 (165).

This study is concerned with the effects of changing guide vane turning or guide vane outlet flow direction on the inlet flow condition to a succeeding rotor row. Thus, computations were carried out only at an axial station between the guide vane and the rotor. All velocities and angles presented are those associated with the velocity diagram at this station.

$$tan\alpha = \left(\frac{r^{2n} tan^2 \alpha_t}{1 + 2tan^2 \alpha_t \left[\frac{(1+n)}{2n} (1 - r^{2n}) \right]} \right)^{1/2} \qquad 4\text{-}1$$

For a specified prewhirl angle at the shroud α_t , equation 4-1 enables the prewhirl angle at all radii to be calculated (107).

A Matlab code was done to calculate the incidence angle at the impeller eye, when imparting the different swirl types. The four prewhirl types were investigated, on 3 near surge points [A, D and G] at three different rotational speeds, N=95, 145 and 180K rpm.

Basic inputs to the computer program are:

- o Mass flow rate,
- o Rotational speed,
- o Inlet static pressure
- o Inlet static temperature

- Blade angle distribution with radius at the leading edge
- A radial distribution of tangential velocity, which has the general form:

$$C_{\alpha=}Kr^{n} \qquad 4\text{-}2$$

The radial tangential velocity distributions are identified as follows:

- Forced vortex: n=1
- Free vortex: n=-1
- Constant swirl: n=0
- Quadratic: n=2

For more clarity, Figure 4-1 shows the different tested prewhirl types.

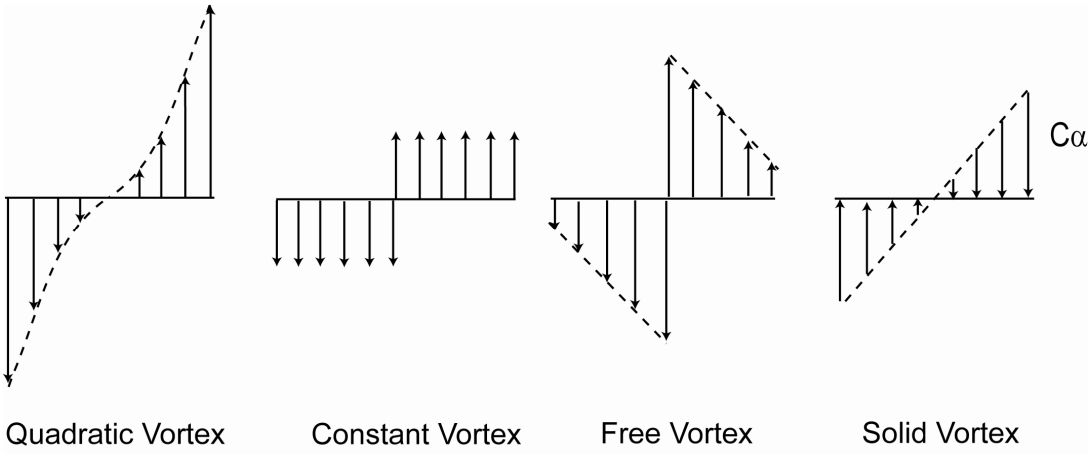

Figure 4-1 studied prewhirl types

Figure 4-2 shows the effect of the different prewhirl types on inducer incidence angle, at points A, D and G.

For point A, it can be seen that free vortex prewhirl yields the most favorable inducer incidence variation with radius. While constant prewhirl yields the most undesirable inducer characteristics.

For point D, effect of prewhirl types on inducer incidence angle, at point D [mean speed] shows that constant prewhirl yields the most favorable inducer incidence variation with radius. The free vortex prewhirl yields the most undesirable inducer characteristics.

Finally, for point G [high speeds], constant prewhirl yields the most favorable inducer incidence variation with radius. The solid vortex prewhirl yields the most undesirable inducer characteristics.

It can be concluded that, constant prewhirl distribution was advantageous at mean and high speeds [at near surge points], however free vortex shows a minimum incidence angles at low speed point. Thus a favorable prewhirl type depends on the compressor functioning point.

This preliminary study shows that, a simple plate vanes yielding a constant whirl with radial, is interesting for minimizing incidence losses [increasing stage efficiency] for near surge points at mean and high speeds.

Note that, the full benefits of inducer prewhirl can only be achieved if the initial compressor design was performed with a view to accommodating the prewhirl type (107).

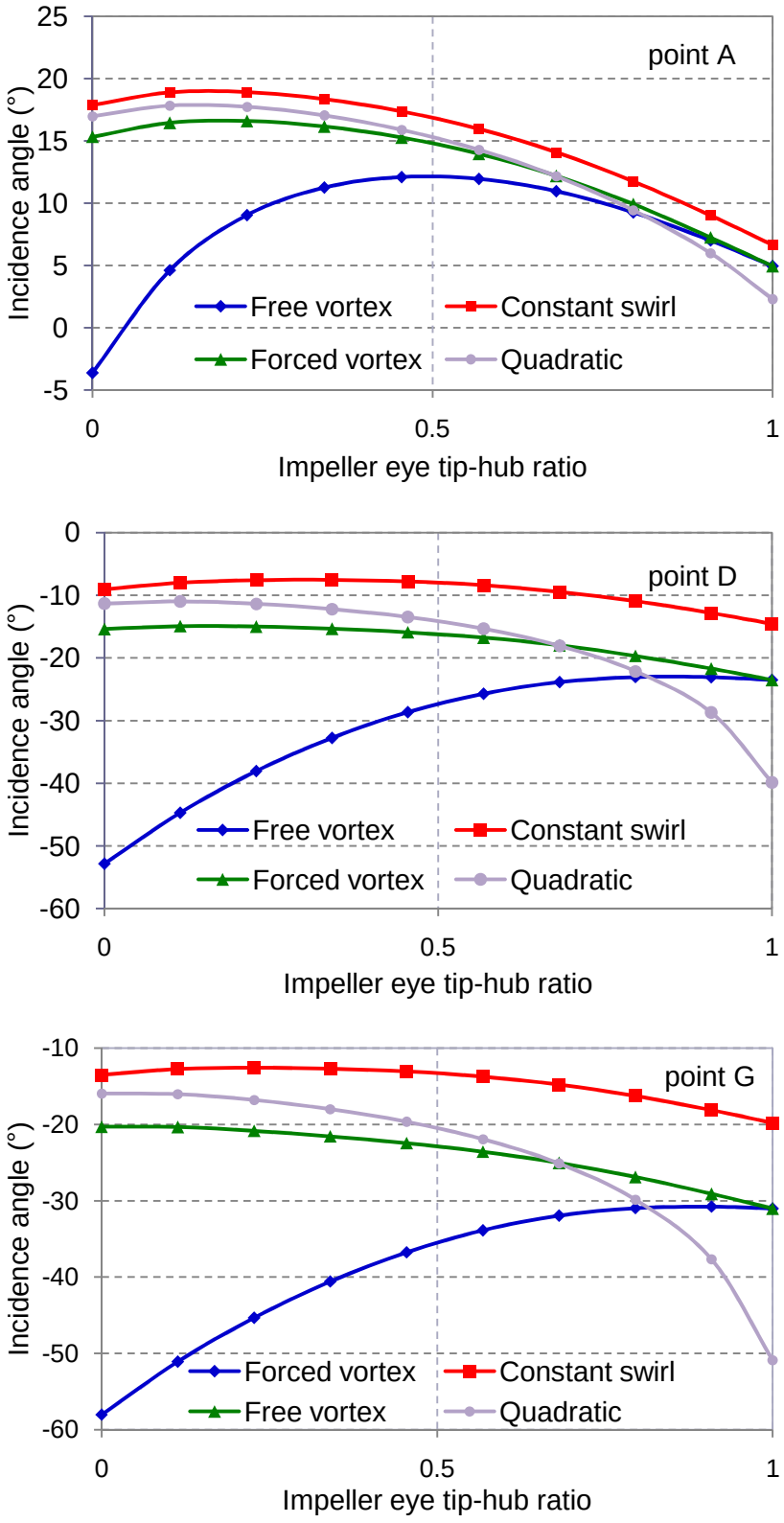

Figure 4-2 Inducer incidence variation for three types of prewhirl

❖ Ideal guide vane

After investigating the effect of different prewhirl types on compressor inducer incidence angles, we'll try - in this section - to find out the characteristics of the ideal guide vane system, and how a guide vane can produce an ideal velocity distribution at the impeller leading edge.

An ideal variable guide vane system, is a prewhirl generator which,

1. produces zero pressure losses.
2. produces a zero incidence angle at all radii [from inducer hub to tip], at all operating points
3. simple, easy to manufacture, and low-priced

To produce a zero pressure losses, the guide vane has to have excellent surface quality, minimum guide vane thickness, minimum area obstruction, and produces no separation.

To produce zero incidence at all radii, and all operating points, the ideal stabilization system has to produce a specific velocity distribution [from hub to tip] for each compressor operating point.

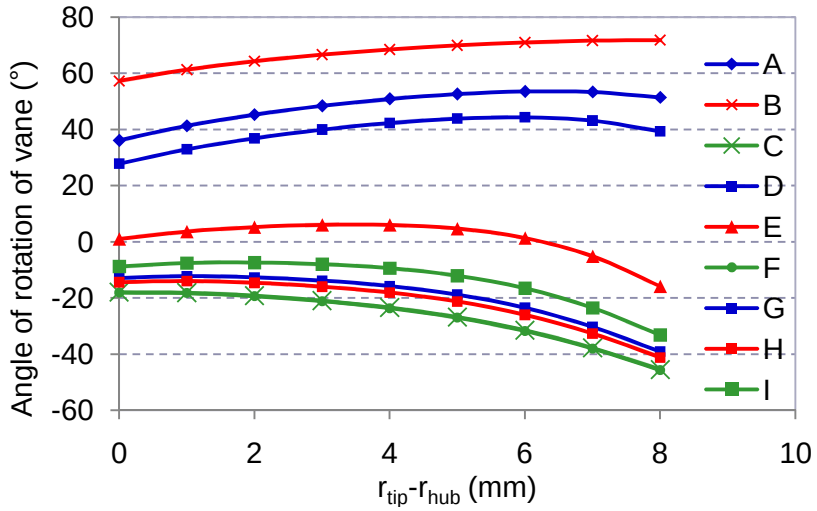

Figure 4-3 Ideal vane angle over the leading edge at 9 different functioning points

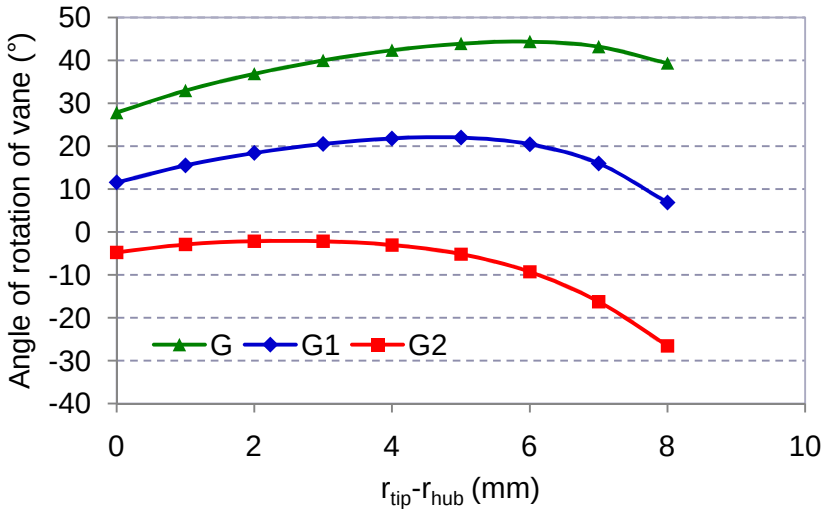

Figure 4-4 Ideal guide vane at constant mean flow rate and 3 different rotational speeds

Here is an example of the nine different operating points [figure 3-5] on the compressor map. For these nine operating points, the ideal guide vane is that which has ideal vane angle variation with radius, thus producing zero incidence angles at each operating point.

Figure 4-3, shows the ideal vane angle distribution at the 9 points. At each point, different vane shape is needed. Ideal tangential velocity distribution at constant mass mean flow rate is presented in Figure 4-4, and that at a constant speed of 180K rpm presented in Figure 4-5. As it can be seen, important variations is needed, to produce a zero incidence at the different points.

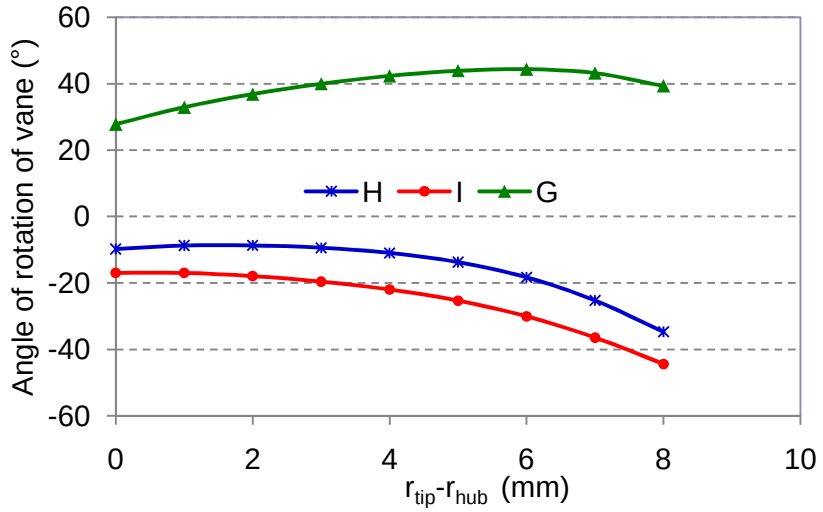

Figure 4-5 Ideal guide vane at 3 operating points of constant rotational speed

However, some interesting results are obtained at high flow rate points. The curves of points C, F and I are nearly superimposed.

The ideal angle distribution at 7 high flow rate points [flow rate ranges from of 0.09 and 0.11 kg/s and speeds from 93 to 180K rpm] is presented in Figure 4-6. Results show that it is possible to design a guide vane system which produces minimum incidence losses at high flow rates.

We can produce an ideal angle distribution at high flow rates if a guide vane is designed with a vane angle θ Increaseing in a parabolic relation from -17.79 at the hub to –46 at tip, with the parabolic equation: $\theta[r] = -0.002r^4 + 0.009r^3 - 0.359r^2 + 0.088r - 17.79$

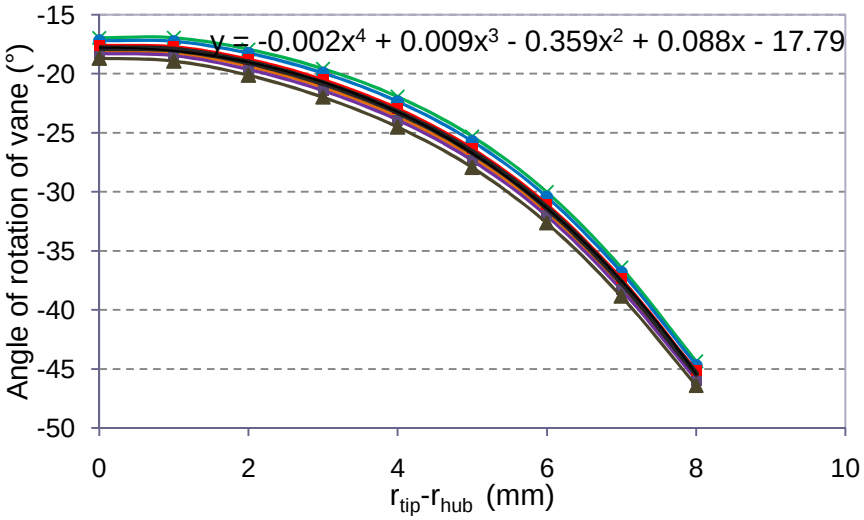

Figure 4-6 Ideal angle distribution at different high flow rate operating points

Theoretical study has been carried out to determine the most favorable prewhirl type at different points of near surge functioning. It was shown that, while constant prewhirl was the most satisfactory type at high speeds, free vortex was more favorable at low speeds. The prewhirl type which produces a satisfactory incidence variation with radius depends on compressor operating point.

What is the ideal guide vane system [which produces zero incidences at all impeller eye radii, all operating points, and creates zero pressure losses]. This question was answered in this section. Ideal vane angle distribution for the tested compressor, at different functioning points was calculated. As predicted, different vane angle distributions are needed to produce ideal velocity distribution at different operating points. However, some interesting results were obtained at high flow rates, where a specific vane profile can significantly reduce incidence losses, for the tested compressor.

To obtain an ideal flow angle distribution along the leading edge- at each operating point- a complicated vane system is needed, where each vane is divided into sub-vanes, and each sub-vane is commanded separately to obtain the needed profile for each operating point.

4.1.2 Presentation of tested swirl generators

Four different compressor inlet swirl generators have been experimentally tested in this work. These are:

- Variable axial guide vane system [AGVs]
- Variable one blade radial guide vane system [one blade RGVs]
- Flexible guide vane system [FGVs]
- Proposed new swirl generator, we called New System [NS]

The four tested systems are presented bellow,

❖ Variable axial guide vane system [AGVs]

The variable AGVs system is a 9 flat plate vane system [Figure 4-7]. It was designed by CNAM [Conservatoire National des Arts et Métiers] with cylindrical section passage and no center body. The inlet guide vanes are pivotally mounted within the guide vane housing, and setting angles varied from -90° to +90° by means of an external linkage. A graduation system has been mounted to the system to fix the different setting angles.

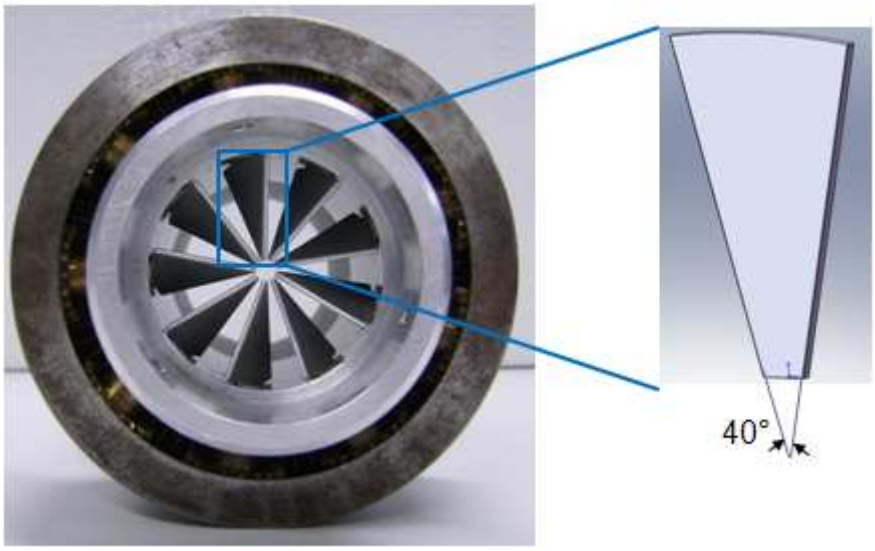

Figure 4-7 Tested variable axial guide vane system [AGVs] to the left, and vane design to the right.

❖ Variable one blade radial guide vane system [one blade RGVs]

The radial variable geometry used in this experiment is a one plate vane system, designed by CNAM, with setting angles varying from -90° to + 90° by means of an external linkage [Figure 4-8]. To better explain the mechanism, a 2D illustration shows the effect of a positive setting angle in the flow passing through the one-RGV, in the same figure. The system was installed at a distance of $2R_1$ from the impeller inlet.

Figure 4-8 Tested one blade radial guide vane system [RGVs]

❖ Flexible guide vane system [FGVs]

The flexible guide vane system is composed of 4 stationary flexible guide vanes, including fixed area connected to the support section [Figure 4-9]. It was installed at a set distance $1.8R_1$ from the Impeller leading edge.

Figure 4-9 Tested flexible guide vane system [FGVs]

Vanes produce flow vectoring in the direction of rotation of the rotor [positive swirl], and deform under the effect of flow velocity. It is worth noting that the tested FGVs is currently applied for a passenger car engine.

❖ New swirl generator [NS]

The new swirl generator was fabricated at the Ecole Centrale de Nantes, a flexible and variable geometry system [Figure 4-10]. NS will be used to denote 'New Swirl Generator' for the rest of the work. Details of fabrication will be presentation in section [4.1.4.4].

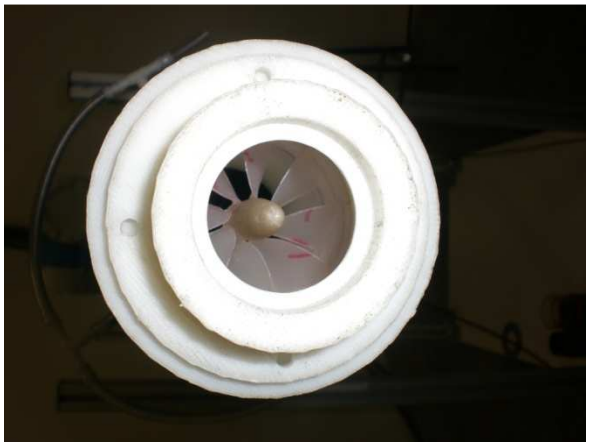

Figure 4-10 tested NS system [a forward view]

After presenting the different tested pre rotation mechanisms, the coming section deals with pressure losses through these systems.

4.1.3 Pressure losses through the different systems

The methodology to obtain the pressure loss caused by the different swirl generators was similar to that used by Galindo et al, 2006 (28). It was adapted here to the different swirl generator systems. It is based on two experiments.

The first one consists in measuring the pressure drop through a line formed only by the swirl generator inlet and outlet ducts but without the swirl generator [total pressure drop between points A and B without the swirl generator [Figure 4-11]]. This pressure loss is ΔP_{AB}. Its purpose is to determine the total pressure loss between the two points at the inlet and outlet of the system.

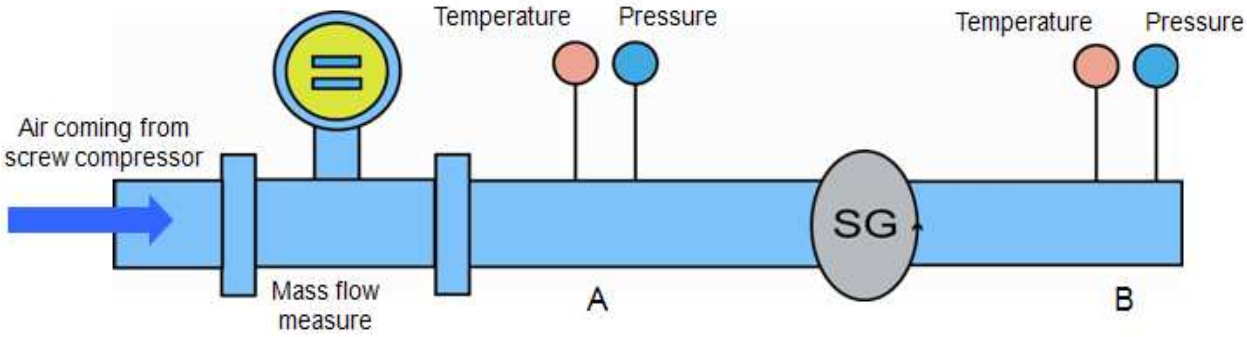

Figure 4-11 Schematic of pressure loss test bench

In the second experiment, the swirl generator is mounted and the pressure loss coefficient of the whole set-up is determined, the result is ΔP_{sum} . The difference between both total pressure losses yields the total pressure loss of the swirl generatorΔP_{SG}. Equation, 4-3

$$\Delta P_{SG} = \Delta P_{sum} - \Delta P_{AB} \quad 4\text{-}3$$

The same procedure was repeated for the different tested swirl generators [FGVs, AGVs, One blade RGVs, and the New swirl generator [NS]].

The operative variable measured and the corresponding transducers are presented in chapter II.

❖ Pressure losses through the AGVs

AGV pressure loss test bench is shown in Figure 4-12, points A and B and a zoom on the AGVs are also shown in the same figure. To calculate the position angle of the AGVs a graduation system was done, the system is shown in the zoom of Figure 4-12. The position angle uncertainty is about ±1°.

Mass flow rate has been varied from 0 kg/s to about 0.12 kg/s. In Figure 4-13, the variation of AGVs shows that the pressure drop is more significant and steeper for large setting angles and it increases with the mass flow rate. Values of negative AGVs angles coincide with the positive angles presented in due to the symmetric design of the AGVs.

Figure 4-12 AGVs pressure loss test bench

For θ [vane angle] values of 30°, 45° and 60° and at the lowest air mass flow rates [below 0.02 kg/s], the pressure drop in the AGVs is very low [Figure 4-13], therefore the uncertainties in the calculation are very high. Significant pressure losses through the system at high setting angles and high flow rates can be explained by the big area reduction and separation losses.

Coppinger & Swain, 2000 (117) have studied a similar AGVs [industrial application] and concluded that the AGVs performs more as a throttle than an efficient swirl generator, and this is due to,

- Low swirl induction for high pressure losses
- At high setting angles, the AGVs permits an axial jet to pass into the impeller as a core flow within an outer swirling flow, due to the significant leakage area at the center
- At intermediate angles, a clearance area at the outer edge of the blade, results in a pressure loss increase and distorted boundary layer growth at the outer flow region.

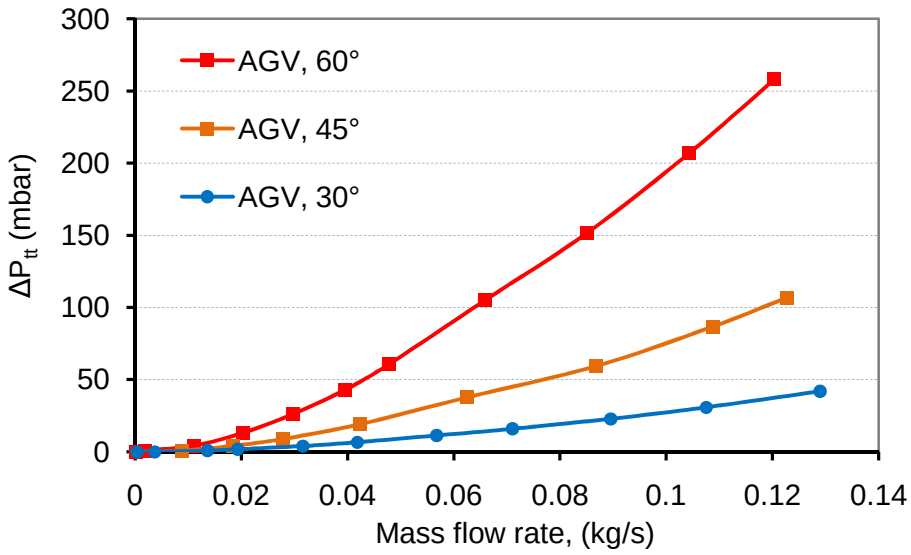

Figure 4-13 Pressure losses through the AGVs, at different setting angles

❖ Pressure losses through the one blade RGVs

One blade RGVs pressure loss test bench is shown in Figure 4-14. Points A and B and a zoom on the RGVs are also shown in the same figure. To calculate the position angle of the RGVs a graduation system was done, the system is shown in the zoom of the same figure. The position angle uncertainty is about ±1°.

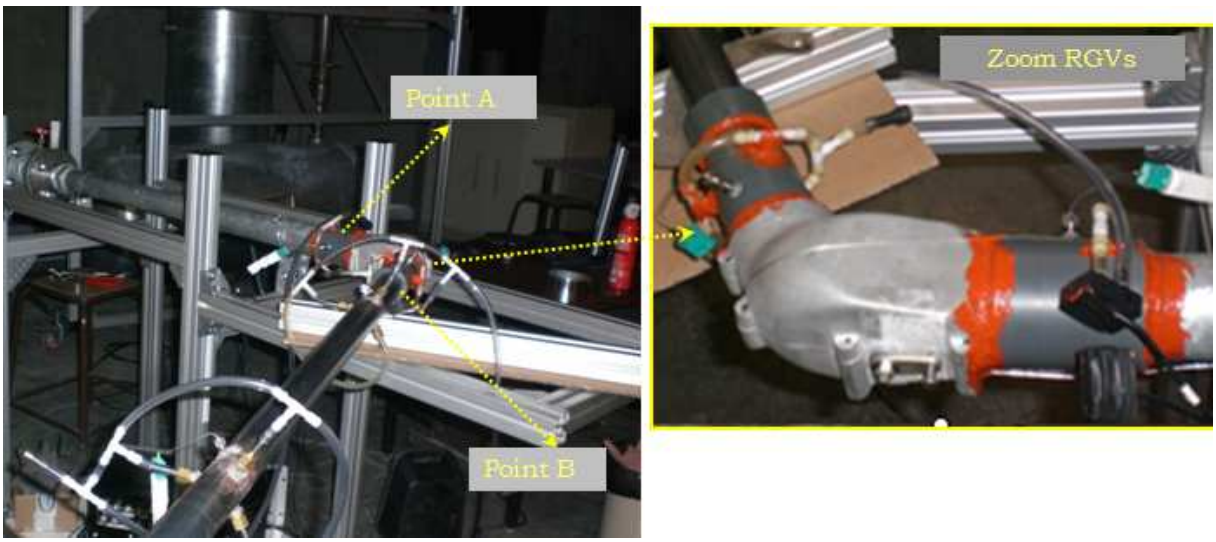

Figure 4-14 One blade RGV pressure loss test bench

Mass flow rate has been varied from 0 kg/s to about 0.11 kg/s. Figure 4-15 and Figure 4-16 present pressure losses through the RGV positive and negative configurations. Results show that the pressure drop is more significant and steeper for large values of the angle θ and it

increases with the mass flow rate. As may be also observed, values of negative RGVs angles do not coincide with the positive due to the non-symmetric design of the RGVs. With negative angles having higher losses than positive angles.

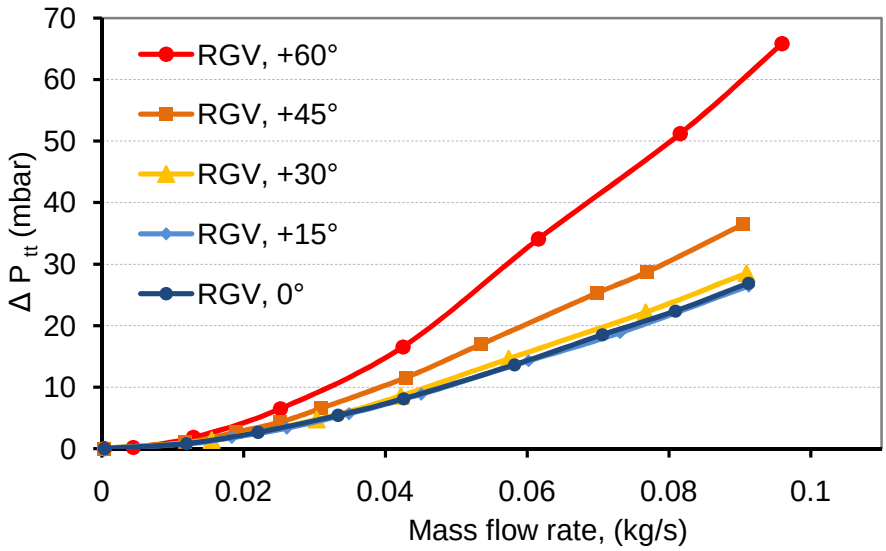

Figure 4-15 Pressure losses through the one blade RGVs for positive setting angles

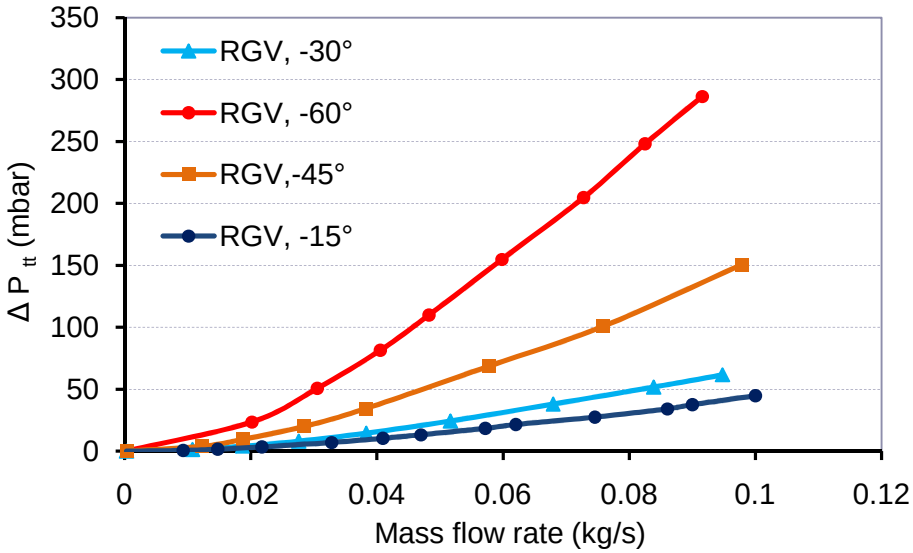

Figure 4-16 Pressure losses through the one blade RGVs for negative setting angles

❖ FGVs pressure losses

Pressure losses through the FGVs are negligible as it can be seen in Figure 4-17. The system slight reduce of the passage area, together with the good surface quality can explain these very low losses.

❖ Pressure losses through the NS system

Losses through the NS system are presented in Figure 4-18. Different vane positions were tested [a vane position corresponds to the angle with respect to the vertical of the fixed area of the new system]. Results show that, the pressure losses through the system are similar to those through the AGVs. In fact, although the separation losses are eliminated with the new

system, but the surface quality of the tested prototype was not good, this can explain in great part these losses. Surface quality and some more details will be improved in the new version of the NS system.

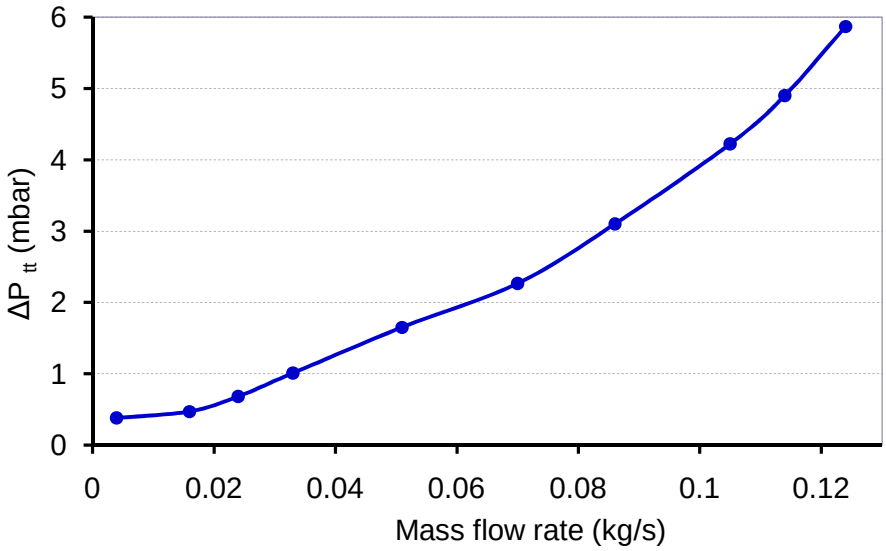

Figure 4-17 Total pressure loss through the FGVs

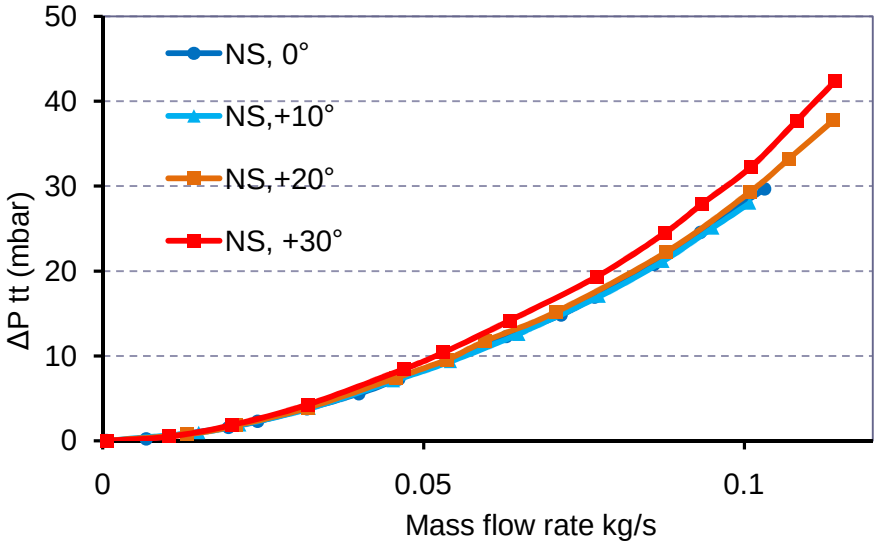

Figure 4-18 Pressure losses through the proposed swirl generator [NS]

4.1.4 Effect on the overall compressor performance and surge line, of the different pre rotation mechanisms

After studying pressure loss through the different tested mechanisms, the overall compressor performance and its new surge line when installing the four systems at its inlet is studied in this section. Moreover, local flow measurements were done to explain and better understand obtained results.

4.1.4.1 Effect of variable Axial Guide Vanes system [AGVs] on overall compressor performance and surge line

The influence of the AGV setting angles on the compressor characteristics compared to base data has been investigated. In order to better understand the obtained results, velocity triangles at compressor inlet were reconstructed using LDA measurements.

The initial test was performed with zero pre rotation by setting the plate vanes axially. Compared to basic characteristics, the pressure and efficiency lines of the two maps were superimposed. However, the surge line was shifted to low flow rates at high speeds. This slight shift may be due to change of the system impedance [B factor, equation 1-64], by changing the volume at compressor inlet.

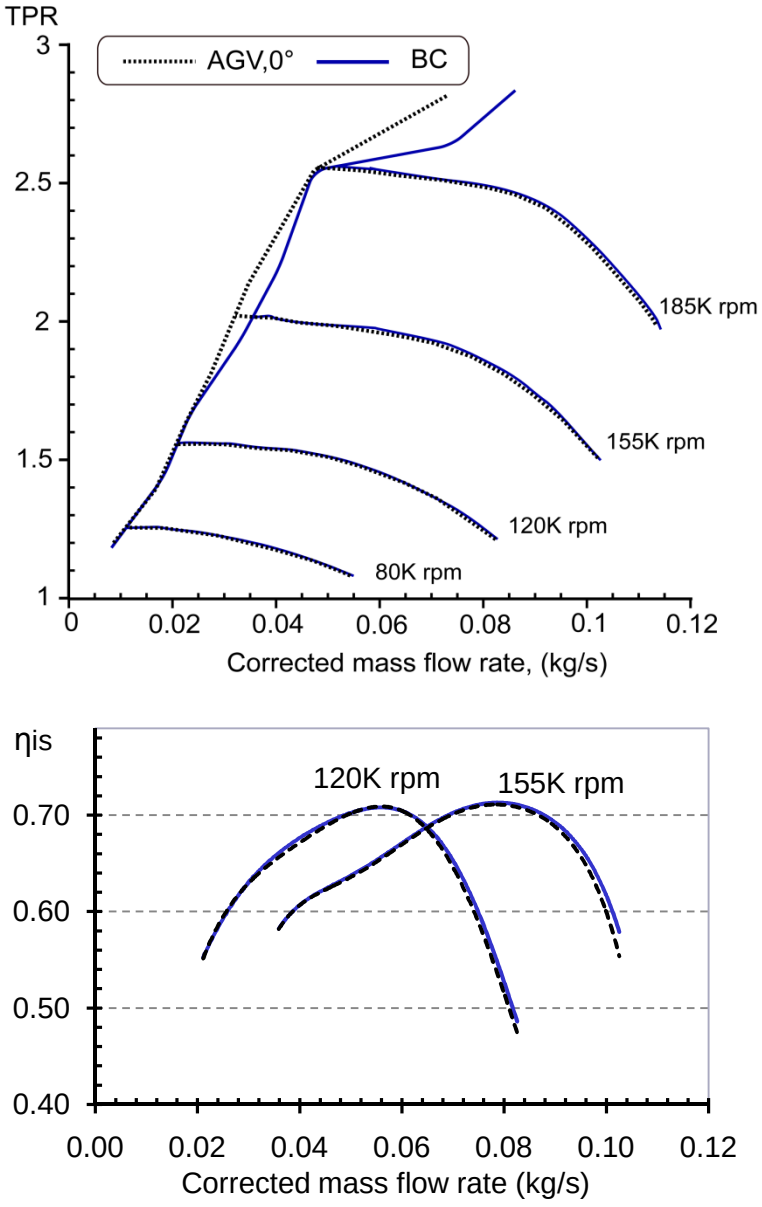

Figure 4-19 Basic characteristics compared to AGV, 0°

It's worth noting that, due to the major influence of heat transfer from the turbine on the compressor efficiency [Cormerais, et al., 2006], the comparison was not done with the

efficiency supplied by the manufacturer [for all the tested mechanisms] because of the higher temperature at the turbine inlet used by the manufacturer, 873K.

Tests were conducted at different rotational speeds and AGV, and setting angles, θ =0°,+30°, +60°,-30° and -60°.

❖ Effect of positive swirl imposed by the AGV system

In order to indicate the effect of positive swirl on the compressor map widening. Figure 4-20 presents the pressure ratio as function of corrected mass flow rate, for the AGV setting angles θ =0°, +30° and +60°, and rotational speeds Nc=80,12 0,155, and 185K rpm

Figure 4-20 [bottom] presents the total to total isentropic efficiency as function of corrected mass flow rate and AGV angles for each of the two corrected rotational speeds corresponding to 120K rpm and 170K rpm.

Results obtained from the positive configuration, can be resumed by the following 3 points,

1. Pressure ratio drop all over the flow range when imparting positive swirl, compared to compressor basic characteristics, with bigger pressure drop at high AGVs setting angles [at 0.06 kg/s corrected mass flow rate and Nc=150K rpm, the pressure ratio loss for 30° and 60° AGV setting angles, are respec tively 3 % and 34% less than that of zero angle case].
2. Surge line slight improvement at low rotational speeds, and better improvement at high rotational speeds, with bigger θ values producing better results [at TPR=2.8, the surge line improvement for 30° and 60° AGV setting angles are respectively 33.4% [18,4%] and 44% [29%] less than that of basic characteristic [zero angle case]], and lower θ values producing non significant shift, particularly at low speeds.
3. Efficiency drops at middle and high flow rates, with higher drops at big AGV setting angles. However, a slight increase at low flow rates was obtained.

These results can be partly explained by,

1. In addition to the influence of pressure losses through the AGVs which become bigger at high AGV setting angles, pressure drop when imparting positive swirl is due to decreasing compressor work input, by increasing the tangential velocity at impeller inlet [Euler equation]. Note that, the exit velocity triangle is considered constant and independently of the inlet swirl flow [This is not strictly true, since flow in the impeller exit is affected by inlet conditions. However, when imparting positive swirl, the change in exit tangential velocity is considered negligible with respect to inlet term].
2. For the tested compressor, impeller causes compressor stall at high rotational speeds. Incidence angle reduction when imparting positive swirl with respect to the axial configuration, has improved impeller flow by changing inducer flow characteristics with respect to basic configuration. This point is to be developed by reconstructing the velocity triangle at impeller inlet [LDA section].
3. Efficiency drop at high flow rate is due to friction losses caused by the AGV system, and incidence losses at the impeller eye. The slight increase at low flow rates is due to lower incidence angles, hence less incidence losses.

Finally it worth noting that, for θ =+30° and θ=+60°, no noise change or low frequency vibrations were observed during the experiment, which may be caused by wakes downstream the AGVs [Watson, 1982]. Hence, it is necessary to prove the non existence of wakes downstream of the AGV system, this point is investigated in the coming section, where flow downstream of the AGVs, is analysed.

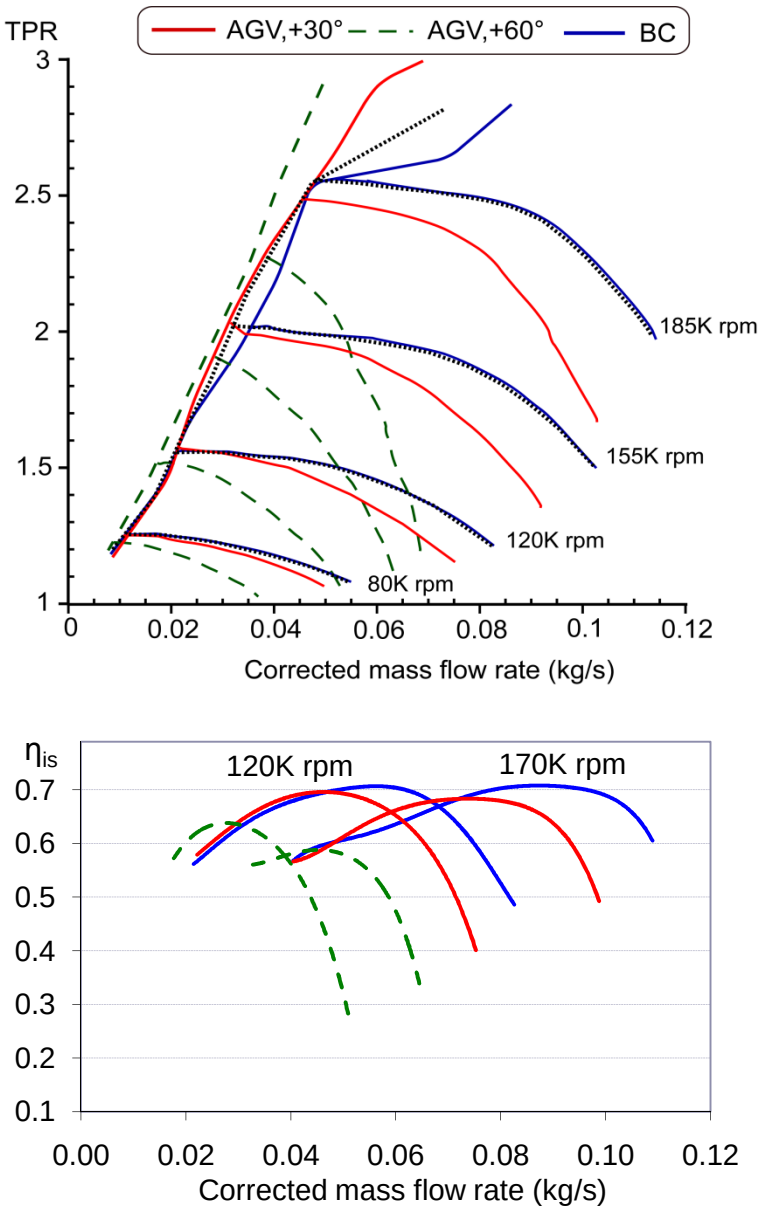

Figure 4-20 Different AGVs positive setting angles compared to basic characteristics

❖ Effect of counter swirl imparted by the AGVs

In order to indicate the effect of negative swirl on the compressor performance and map widening, Figure 4-21 presents the pressure ratio and isentropic efficiency as function of corrected mass flow rate, for the AGV setting angles θ = -30° and -60°. Maps are compared to basic characteristics in the same figure. The dotted line in the pressure ratio map, corresponds to AGV, 0°.

Figure 4-21 [bottom] presents the total to total isentropic efficiency as function of corrected mass flow rate and AGV angles at two non dimensional rotational speeds corresponding to 120 and 170K rpm.

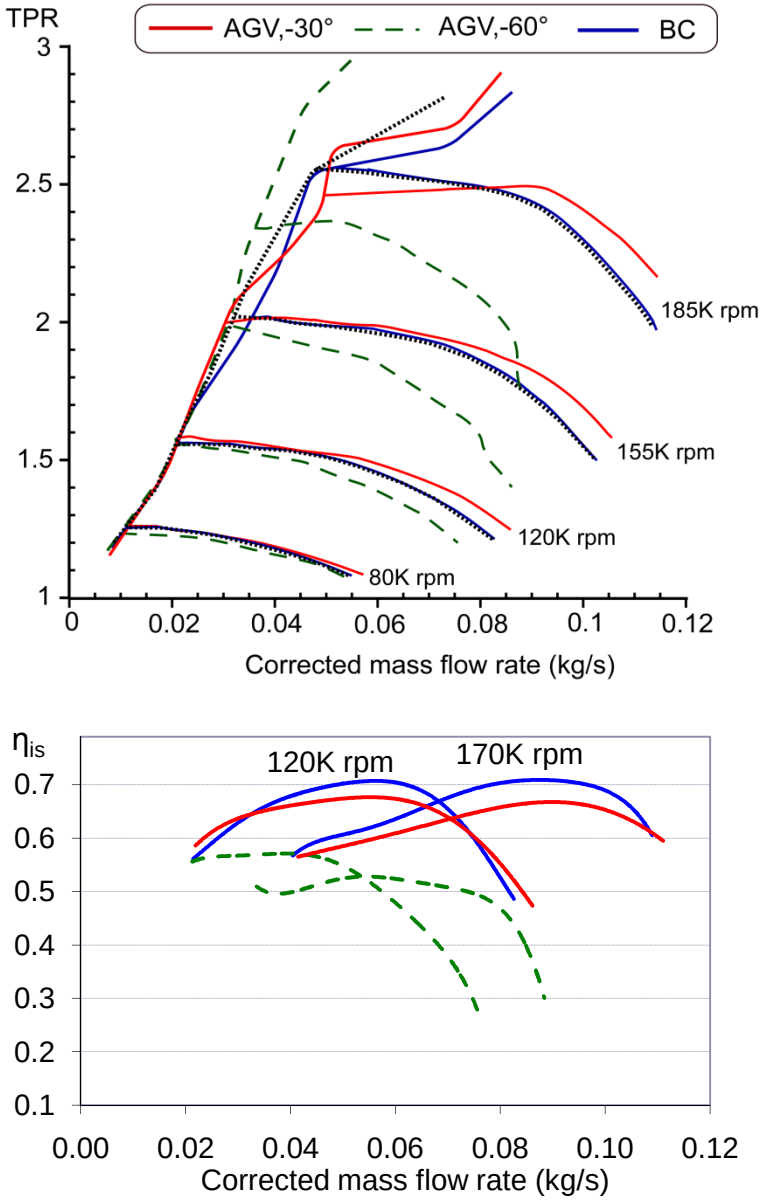

Figure 4-21 Different AGVs negative setting angles compared to basic characteristics

Results obtained from negative AGV configuration, can be resumed by the following points,

1. Pressure ratio increases at middle and high flow rates with respect to that of basic characteristics for setting angles θ =-30°. However, pressure ratio drops at -60° setting angle [at 0.06 kg/s corrected mass flow rate, and Nc=150K rpm, the pressure increase for -30° AGV setting angles is +0,6%, and drops for θ =-60° by 5,5 % less than that of Zero angle case].
2. Surge line slight improvement at low rotational speeds, and better improvement at high rotational speeds. With bigger angles having better results [at TPR=2.8, the surge line improvement for -30° and -60° AGV settin g angles are respectively 5.7% [-9,3%] and 45% [30%] less than that of basic characteristic case [zero angle case]].
3. Efficiency drops at the overall flow range, with higher drops at big AGV setting angles.

These results can be partly explained by,

1. Pressure increase when imparting negative swirl is due to increasing compressor work input [Euler equation]. The pressure loss at big AGV negative angles can be explained by pressure losses through the AGV system and incidence losses. To completely understand the effect of swirl imparted by the AGVs on pressure at high angles, there is necessity to reconstruct the compressor map after subtracting the pressure losses through the AGV system.
2. The surge line slight shift at AGV, -30°, and big shift at -60°, particularly at high speeds, can come from the increase in relative velocity, although the incidence angle increase with respect to the basic configuration. With relative velocity increase, the flow can better overcome the resistive pressure downstream of the compressor, so that the fluid in the impeller becomes more stable and the stall phenomenon is delayed. However, this point is to be clarified by conducting local studies downstream of the AGVs.
3. Imparting negative swirl increases relative velocity at impeller inlet. With the velocity increase in the impeller friction losses increases, hence efficiency drops. Moreover, counter swirl increases incidence angle, hence higher incidence losses.

Results obtained when imposing negative and positive swirl, were partly explained above [points 1,2, and 3]. We use 'partly' for the following reasons:

- Pressure ratio curves should be reconstructed without pressure losses through the AGV system, so that we can obtain the swirl influence on the compressor pressure ratio and efficiency. Thus, being able to better differentiate between the effect of pressure losses through the system and that of incidence losses produced by the AGVs, on the compression ratio curves.
- Flow analysis downstream of the AGVs has to be done to better understand the flow structure downstream of the system, and its effect on incidence losses, thus compressor efficiency. These measurements will also help us understand why surge line improvement was better at high speeds for AGV, -60° than that of +60°, and why positive configuration shows better surge line improvement at low speeds compared to negative configuration.

❖ Reconstructing the compressor maps and isentropic efficiency by subtracting the influence of pressure losses through the AGVs

If pressure loss through the AGV system [section 4.1.3] is subtracted from values pressure measured downstream of the AGVs, then we can obtain the absolute pressure just upstream the impeller inlet. Thus, isentropic efficiency and compression ratio will be calculated without the effect of the pressure losses in the different tested systems.

For better understanding, in Figure 4-22 there is a diagram that shows how the thermodynamic process from point 1 to point 2 changes when the pressure loss value is eliminated. The thermodynamic process from 1' to 2 is closer to the isentropic evolution, because the calculated point 1' has lower pressure than the measured point 1, but point 2 does not change [Galindo et al, 2006 (28)]. Points 1, 1' and 2 are shown in Figure 4-22[to the right]

In the same way, pressure losses through the different tested swirl generators [AGVs, RGVs, FGVs, and NS], was added to the overall pressure ratio obtained with the swirl generators. This to study the effect of the swirl imparted by these systems on compressor performance, considering zero pressure losses through the systems.

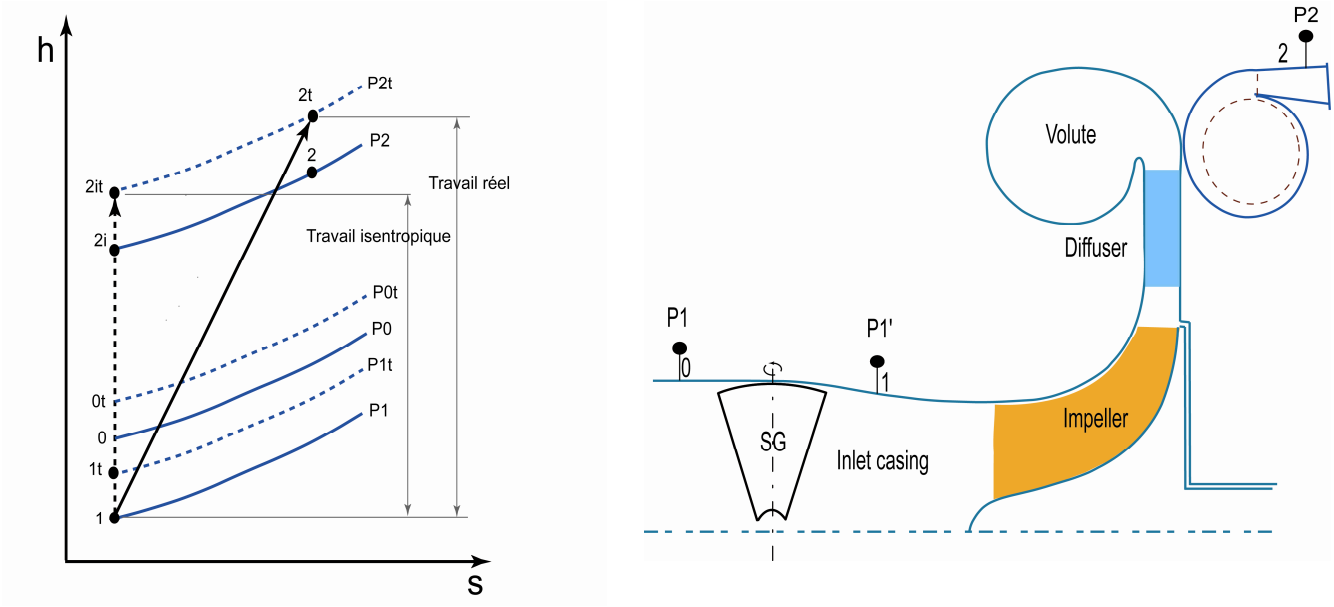

Figure 4-22 Thermodynamic process with pre rotation system pressure losses [to the left], compressor with a swirl generator mounted at inducer inlet [to the right]

Compressor maps and efficiency curves are reconstructed without pressure losses through the system, and results should be coherent with the swirl influence on the velocity vectors at the compressor inducer.

Some interesting results were obtained when reconstructing pressure and efficiency curves after subtracting pressure losses through the AGVs. The effect of positive and counter swirl produced by the system on the compressor performance is presented in Figure 4-23 and Figure 4-24.

Effect of positive swirl imposed by the AGVs:

1. With pressure loss through the AGV added to total pressure, the reconstructed pressure ratio increases with respect to non constructed maps, but still less than that of standard characteristics at almost all rotational speeds. This is due to decrease in work input [Euler equation].
2. Very slight surge line shift compared to non constructed results, due to the non significant pressure losses through the AGV at low flows.
3. Efficiency slightly increase compared to that of non constructed. Hence, we conclude that efficiency losses at high flow rates come not from losses through the system, but incidence losses at the impeller inlet.

Effect of counter swirl imposed by the AGVs:

1. Increase in pressure ratio at almost all rotational speeds compared to basic characteristics, except at high flow rate and RGV, -60° [4.2% and 2.5% increase compared to basic characteristics, at 0,06Kg/s and 150K rpm for setting angle AGV, -60° and -30° respectively]. This increase is due to the increase in work input [Euler equation]. Note that, losses through the AGV system largely influence the compression ratio capability at high flow rates. This was not the case with positive setting angles where choke line shifts to low flow rates.
2. Very slight surge line shift compared to non constructed results, due to low AGV losses at low flow rates.

3. Adding the pressure loss through the AGV, efficiency still less than those of basic characteristics at almost all the flow range, with higher drop at higher setting angles. Except a slight improvement at AGV,-30°. This drop will be well understood after reconstructing velocity triangles at impeller inlet using LDA measurement [LDA section].

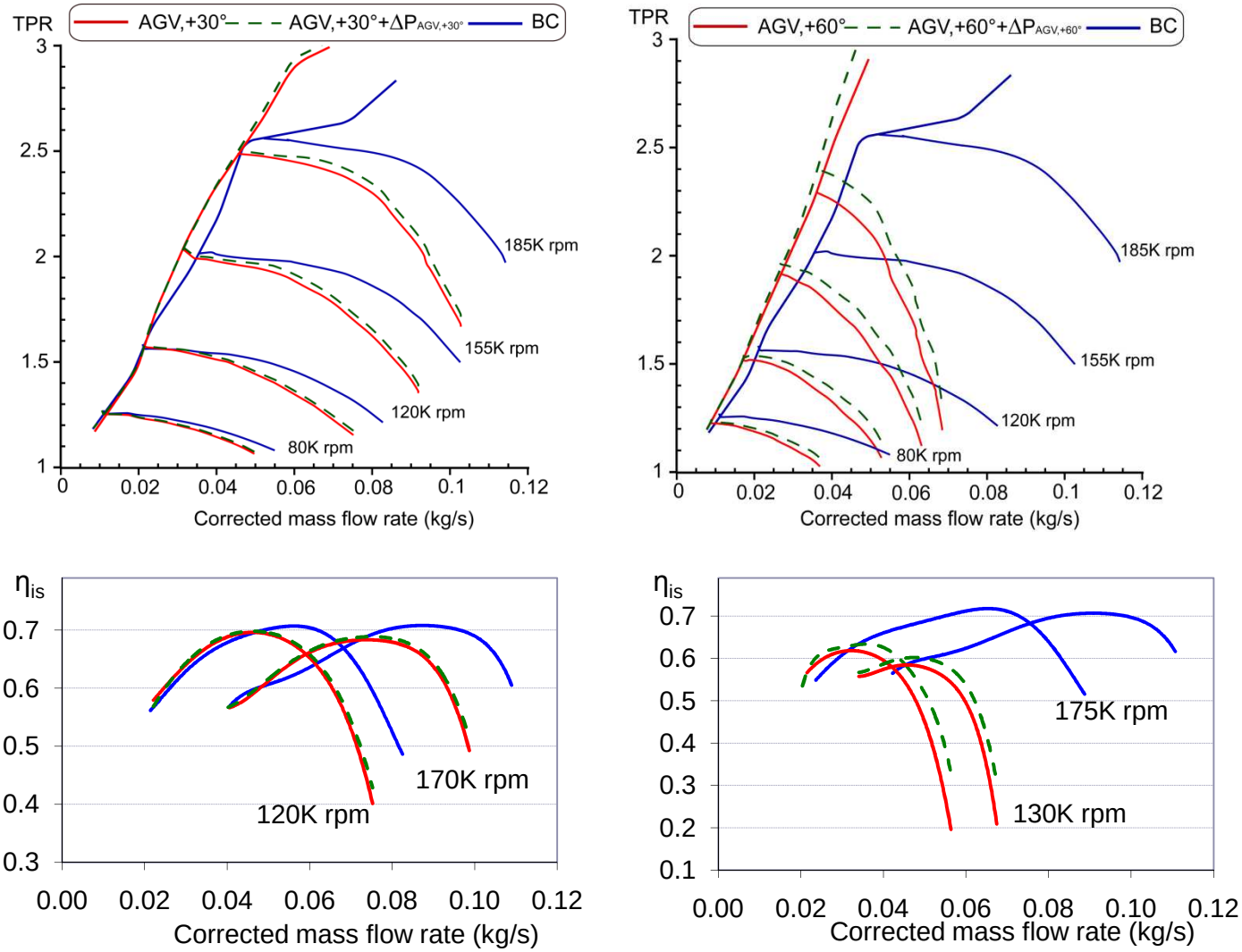

Figure 4-23 Reconstructed pressure and efficiency curves after subtracting pressure losses through the AGVs, for setting angles, θ =+30°,+60°

Reconstructing compressor maps and efficiency curves after subtracting pressure losses, clarified some points concerning compression ratio. However, we still need to better understand the cause of efficiency loss and surge line shift. LDA measurement was conducted to this end.

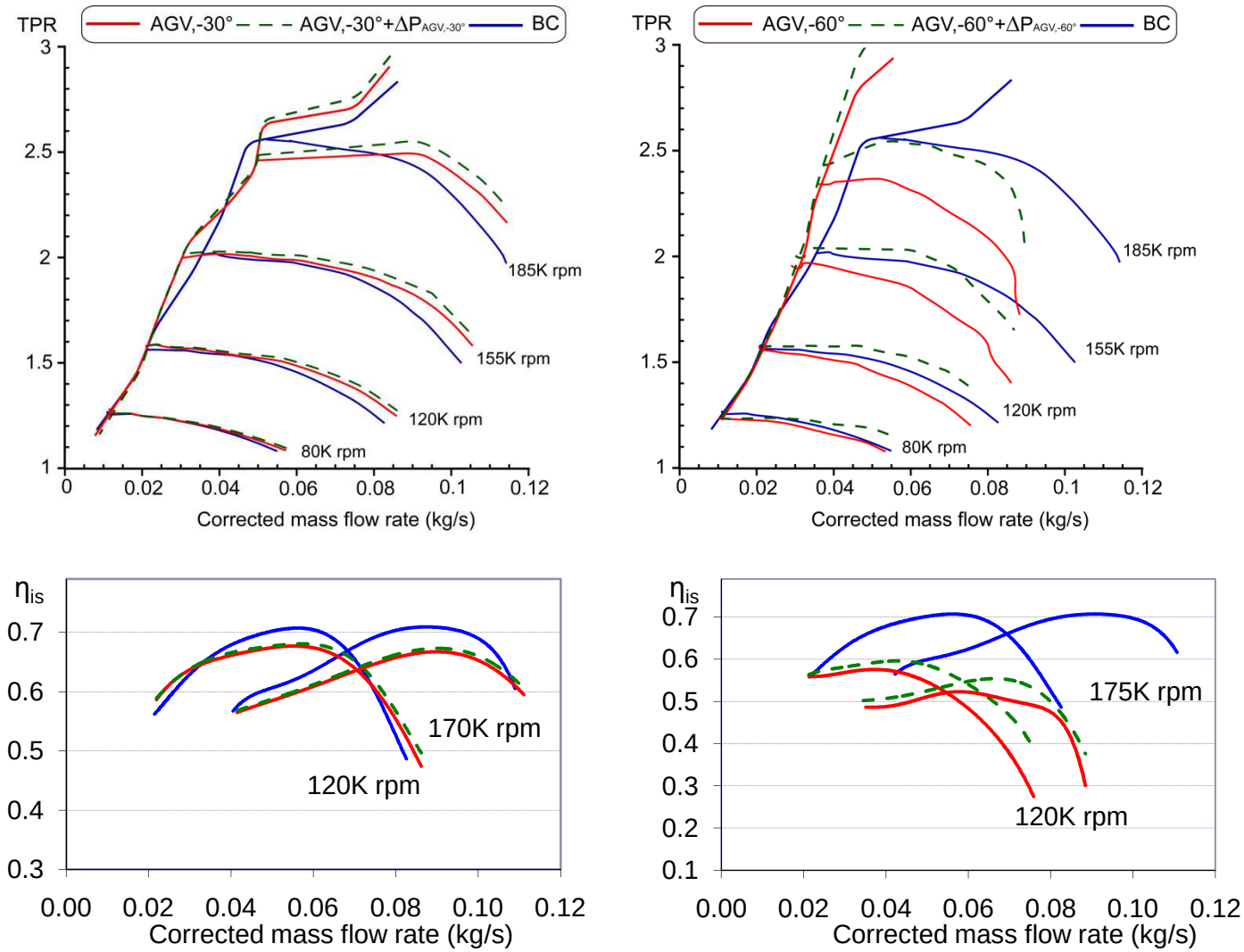

Figure 4-24 Reconstructed pressure and efficiency curves after subtracting pressure losses through the AGVs, for setting angles, θ =-30°,-60°

❖ Using LDA measurements to understand obtained results

After studying the influence of different setting angles on overall compressor performance and surge line, LDA measurement was conducted at the compressor inlet to bring about a better understanding of the AGV influence in the flow fields at the compressor inlet [Figure 4-25].

LDA measurements have been performed for two operation conditions close to the surge line of the compressor map,

a. for a mass flow rate of about 0.013kg/s [corresponds to 80K rpm, and a pressure ratio of 1.25 bar, near surge point],
b. for a mass flow rate of about 0.02kg/s [corresponds to 120K rpm, and pressure ratio of 1.6 bar, near surge point],

The effect of the AGV emplacement upstream of the compressor inlet, wake downstream of the guide vanes, and prewhirl type imposed by the system are investigated in this section. Note that measures were done without taking in effect the impeller.

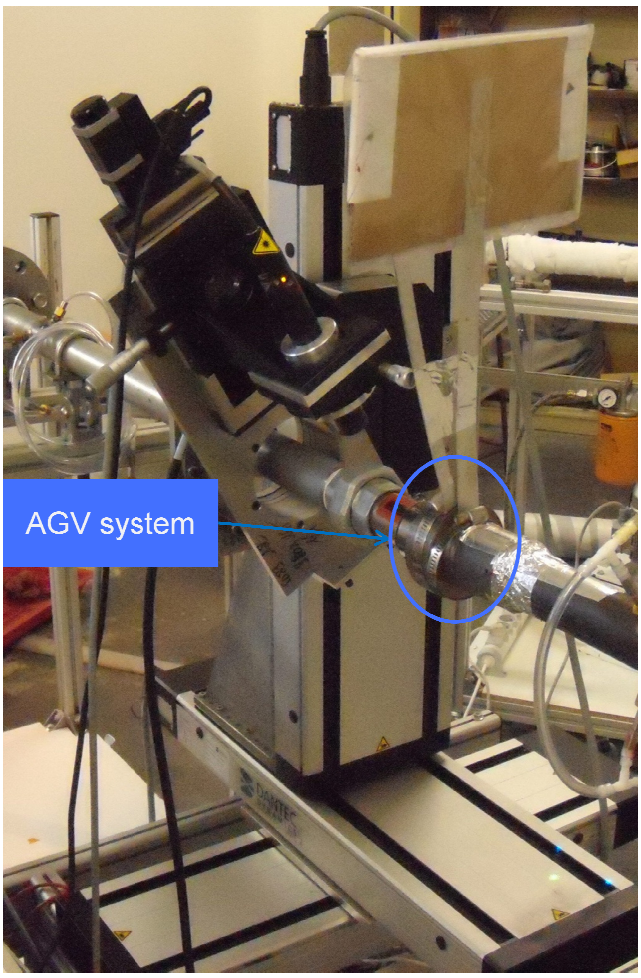

Figure 4-25 LDA measurement downstream of the AGVs

❖ Effect of AGV emplacement with respect to impeller inlet, on angle of flow rotation.

Test was conducted at low mass flow rate of 0.013kg/s [near surge point at 80K rpm]. Vanes were positioned at the positive setting angles of 15°, 30°, 45° and 60° . Axial and vertical velocity components are measured at 18 points along the diameter direction [Figure 4-26] and five points X0, X5, X10, X15, X20 and X25 along the flow direction [X direction], for a total of 90 points of measure for each vane setting angle. Where X0 is at 25mm distance downstream the AGV system and X5 is the second point of measurement at 5mm from the first point X0, and so on [Figure 4-27].

The first step in the experiment was to measure the velocity and angle of flow rotation downstream of the AGVs. Figure 4-28 shows the axial velocity component as a function of diameter localization at different distances downstream the AGVs corresponding to X0, X5, X10, X15, X20 and X25, for the AGVs settings angles of 15°,30°,45° and 60° respectively.

Figure 4-28 a, and b show that the flow was not perturbed at vane setting angles of θ= 15° and 30°, the velocity is maximum at the most part of the diameter and it drops down at the pipe walls due to the boundary layer. For θ= 45 an axial jet takes place at the center, the maximum velocity of the jet decreases as we proceed in the X direction downstream of the AGVs. The jet form at the center is probably due to the significant leakage area existed at the center of the inlet ducting for AGVs setting angles around 45°, this leakage facilitate the flow to pass through the center [Figure 4-28 c]. For vane setting angles θ= 15°, 30° and 45° the velocity profile being non uniform over the diameter may come from the fact that the cross

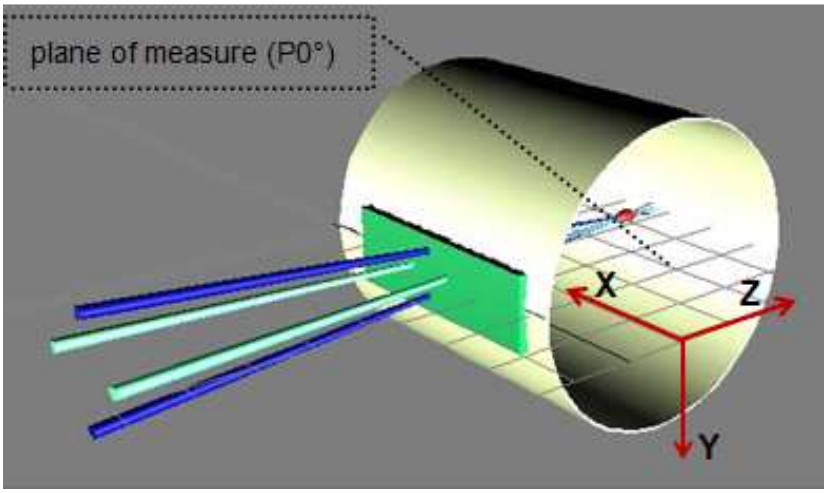

Figure 4-26 Measure point in the plane measurement P0°

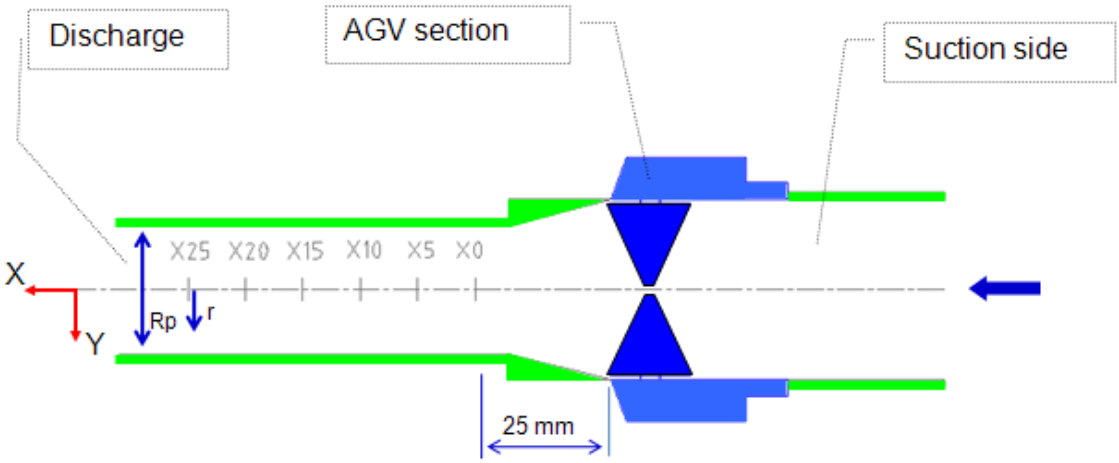

Figure 4-27 AGV test section

section of the tube is not circular. The addition of the transparent plate window could have varies the cross section.

For θ= 60°, the flow non symmetry with respect to center is fairly clear. Velocity profiles for X15 and X20 are fairly smooth. Those for X0, X5 and X10 on the other hand, change to a greater degree over the diameter. Moreover, Figure 4-28 shows that, two core flows take place with different velocities around the center, as we proceed axially in the Z-axis toward the pipe walls difference in velocities becomes lower. The non symmetric flow with respect to the center of the pipe is may be a result of geometric imperfection in the AGV system assembly.

Figure 4-29 a, b, c and d show the angle of rotation of the flow as a function of diameter localization at different distances corresponding to X0, X5, X10, X15, X20 and X25 downstream the AGVs for the AGVs settings angles of 15°,30°,45° and 60° respectively.

The angle of rotation of flow, β is defined as the ratio of V_y and V_x [equation 4-4]

$$\beta = arctan\left(\frac{V_y}{V_x}\right) \qquad 4\text{-}4$$

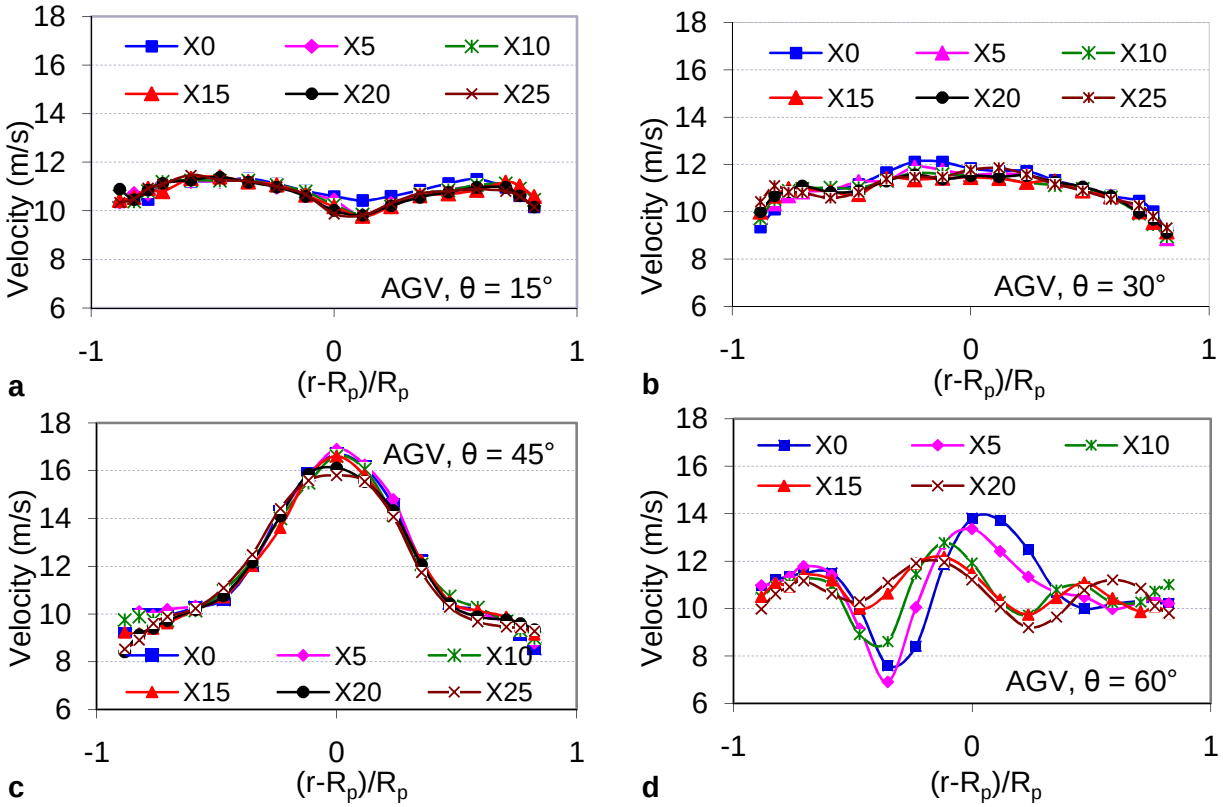

Figure 4-28 Effect of AGV setting angle in the axial velocity, downstream of the AGV system.

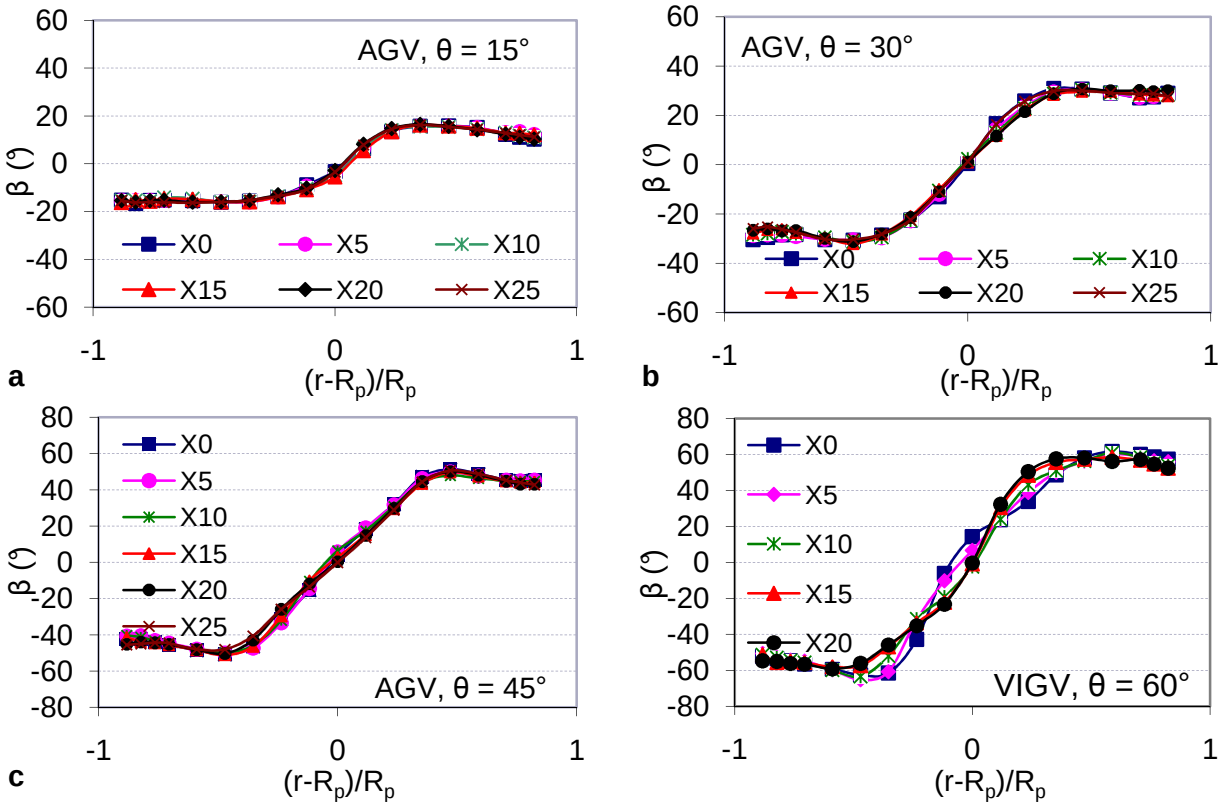

Figure 4-29 Flow angle of rotation β, downstream different AGV setting angles

Figure 4-29 a, b and c show that for AGV setting angles, θ= 15°, 30° and 45° the angle of rotation of flow doesn't change along the distance between X0 and X25, while we observe a change around the center at θ= 60, this change can be explained by the axial velocity profile around the center of the pipe for AGV, θ= 60° [Figure 4-29 d]. The maximum and minimum angle of rotation of flow is at a circle of radius 0.35Rp from the center of the pipe, for the AGV setting angles, θ= 15° and 30° [Figure 4-29 a, and b], and at a circ le of radius 0.47Rp for θ= 30° and 60° [Figure 4-29 c, and d]. The angle of rotation of flow begins with zero at the center of the pipe and increases to surpass the AGVs setting angles and then it stabilizes as we proceed axially along the Z-axes toward the pipe walls. The boundary layer at the pipe walls is probably the cause for not having the maximum angle of rotation of flow at the pipe boundaries.

Now to study the wake downstream of the AGVs, Figure 4-30 shows the LDA measurements of the axial velocity distribution, for the AGV setting angle θ=30°, at different plane measurements P0°, P10°, P20°, P30° and P40° [where P10° is the plane of measure, rotated along the X axes, by an angle 10° with respect to t he plane of measure P0°, see Figure 4-26] at Distance X0 from the AGV are shown in Figure 4-27, and indicate that the wake disappears at distance X0 downstream the AGV. This may be due to the low flow rate and the distance between the AGV and the point X0. Tests at high flow rates have to be done, to confirm or not the existence of wake at these flow rates [mid and high flow on the compressor map]. However, it is still difficult to conduct high flow rate LDA measurement, before solving the problem of excessive window quick fouling at high flows.

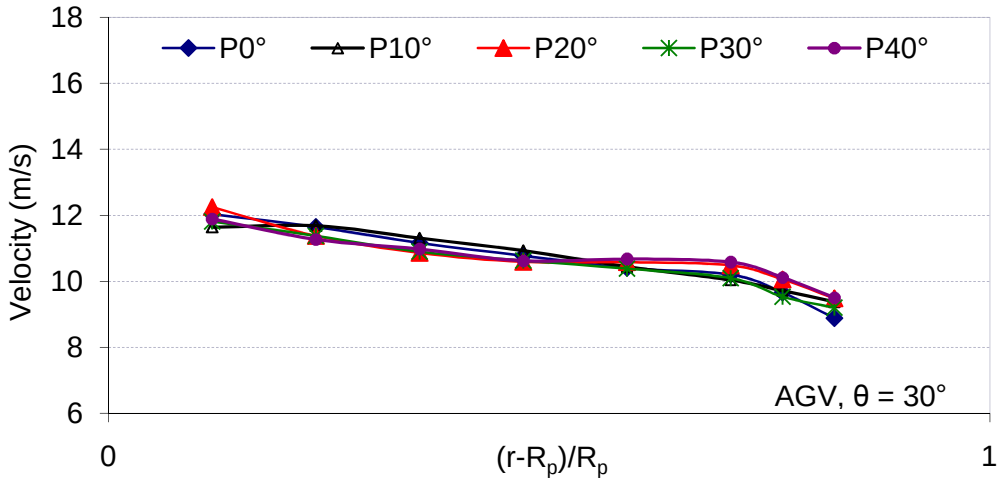

Figure 4-30 Axial velocity distribution for different planes of measurement, at AGV setting angle θ=30°, and distance X0 downstream of the AGV

❖ Prewhirl type

LDA measurements of the tangential velocity distribution, at different plane measurements P0°, P60°, and P120 [measures were done over the en tire diameter], and mass flow rate of 0.02, is presented in Figure 4-31. Measures were done at Distance X0 from the AGV. Figure shows that the tangential velocity distribution, C_α for setting angles θ=+60°.

As it can be seen, the tested AGV system yields a nearly forced vortex prewhirl, with the dashed line representing the tangential velocity distribution [$C_\alpha = kr$ with k=1.21 for the tested flow rate]. From the theoretical study [section 4.1.1]., this prewhirl is not appropriate for high flow rate operating points.

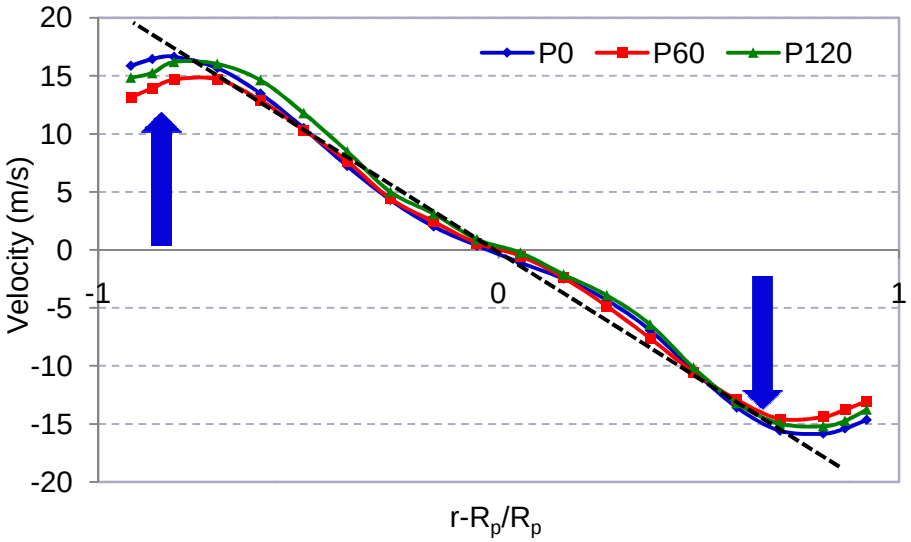

Figure 4-31 Tangential velocity distribution produced downstream the AGV at setting angle, +60°

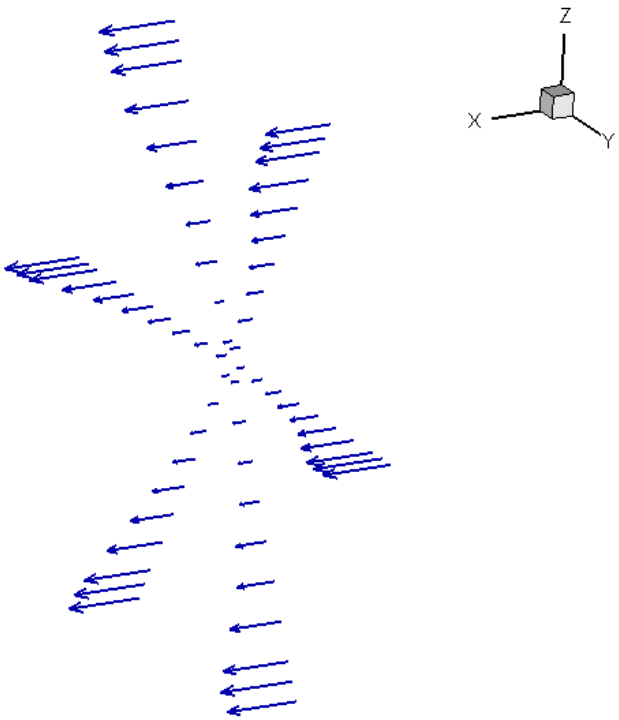

Figure 4-32 Axial velocity distribution at three different diameters and setting angle θ=+60°

Axial distribution for AGV, +60°is presented in Figure 4-32. As it can be seen, velocity is high at boundaries and low at center, this is due to a big area restriction at center of the AGVs, for high setting angles.

❖ Reconstruction of velocity triangle at compressor inlet

In order to better explain the modifications of the line that limits the surge region with negative and positive swirl, the velocity triangles at the inducer inlet have been reconstructed.

The air flow pattern predicted by the LDA measurement at the AGV outlet has been used to obtain the variables necessary for drawing the velocity triangles at the inducer tip inlet.

According to the LDA measurements, the air mass flow distribution is different at the impeller entry section for each position of the AGV, and the flow passing in the impeller is concentrated at the periphery of the inlet section.

The tip linear velocity of the rotor U_{1t} together with C_1 [axial velocity] and $C_{\alpha t}$ define the vectors of the velocity triangle at impeller tip. Hence W_{1t} can be calculated and the value of the approach angle is obtained from equation 4-5,

$$tan\beta = \frac{U_{1t} - C_{\alpha t}}{W_{1t}} \qquad 4\text{-}5$$

The reconstruction of the velocity triangles has been performed for ±60° AGV vane apertures but only for the point that limit surge region and at the inducer tip. The incidence angle and the relative velocity are presented in Figure 4-33, and compared with the corresponding values in the axial inlet configuration. The incidence angle is defined by equation 4-6 applied at the impeller tip.

$$i = \beta_b - \beta \qquad 4\text{-}6$$

As it can be seen, relative velocity and incidence angle are higher for the -60°, AGV compared to axial configuration, and lower in the case of AGV, +60°.

At near surge point of 120K rpm, surge line was not improved when imposing negative swirl [AGV, -60°] compared to basic characteristics. This was not the case when imparting positive prewhirl of AGV, +60°. We can conclude that this is probably due to higher incidence losses when imparting negative swirl.

However, at high rotational speeds, negative configuration shows better surge line shift compared to positive one. Hence we can conclude that, at high speeds, the increase in relative velocity was more advantageous in surge line improvement, than the decrease in incidence losses when imparting positive swirl [the same conclusion was obtained by Galindo et al (28)]. This was not the case at low speeds, where incidence angle was more important.

On the other hand, high relative velocity produced when imposing negative swirl increases impeller losses, hence drops efficiency. Lower relative velocities when imposing positive swirl, reduces impeller losses and hence increases efficiency at the tested point [0.02 kg/s and 120K rpm].

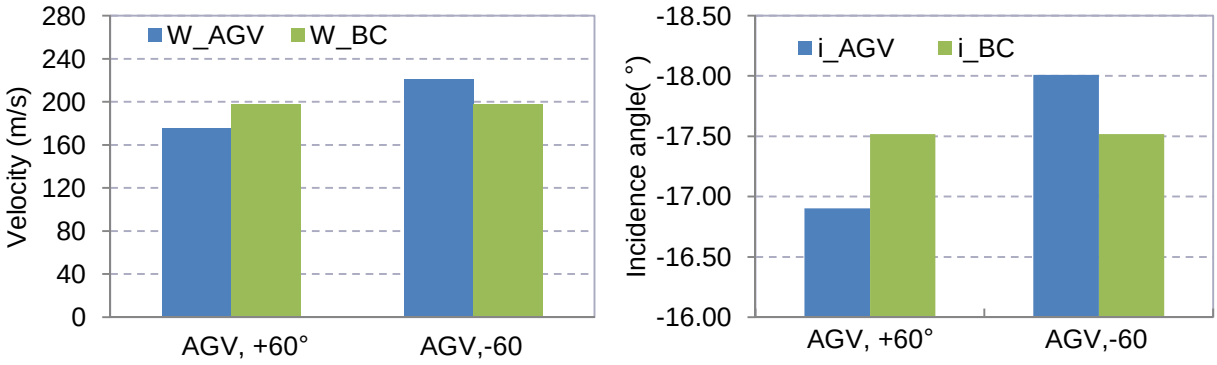

Figure 4-33 Incidence angle [i] and relative velocity [W1] calculated for point of the surge limit at N=120K rpm, line with negative and positive AGV vanes angle

From this study, it can be concluded that the AGV improves surge margin particularly at high speeds [190K rpm]. Positive swirl imposed by the AGV, improves surge line at almost all speeds, and negative swirl improves surge line at high speeds, with a better improvement than positive configuration at AGV, -60° and high pressure ratios [TPR=2.8]. Moreover, negative configuration was advantageous in increasing pressure ratio at almost all flow range. However, efficiency was dropped within all flow rates.

In general angles of incidence are lower with positive configuration, and higher relative velocities are obtained in the case of negative AGV angles. For the tested AGV system, the effect of the incidence angle was more important for shifting the surge-limit line at low speeds [where the diffuser is responsible of compressor stage stall]. However, relative velocity was more advantageous in surge line shift at high speeds, where the impeller triggers stage stall. Indeed, the flow can better overcome the resistive pressure downstream of the compressor when W1 is large, so that the fluid in the impeller becomes more stable and the stall phenomenon is delayed (28). The previous conclusion is especially evident in the case of AGV, ±60° vane aperture.

The increase in relative velocity when imposing negative swirl, causes efficiency drop compared to axial configuration, due to increase in impeller friction losses. This was not the case when imparting positive swirl. However, the efficiency drop at high flow rate can be explained by incidence losses, this may be due to the non favorable prewhirl type [forced prewhirl] at high speeds.

4.1.4.2 Effect of one blade radial guide vane system [RGVs] on overall compressor performance, and surge line

The influence of the RGV setting angles on the compressor characteristics compared to base data was investigated in this section. Different RGV setting angles were tested and results were compared to basic compressor characteristics.

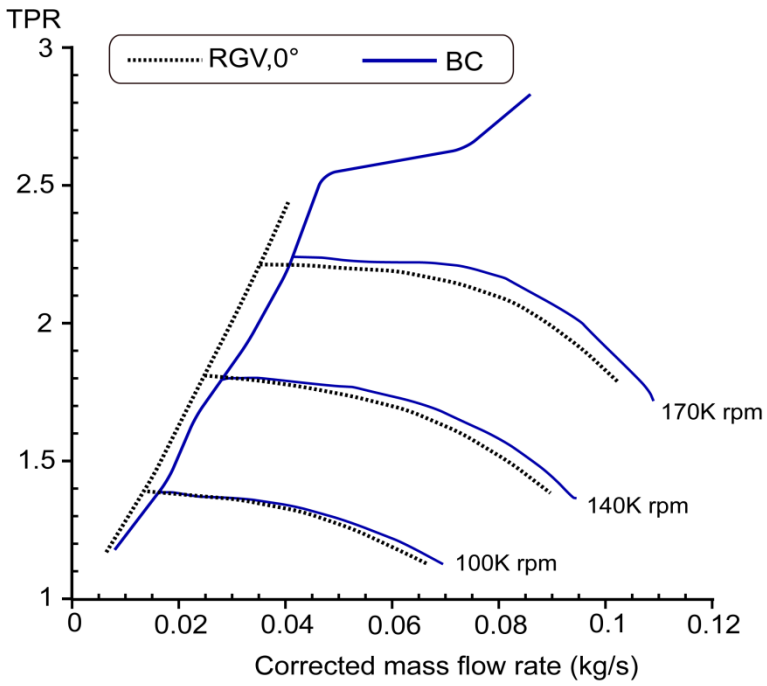

Figure 4-34 RGV, θ=0° compared to basic characteristics [BC]

The initial test was performed with zero setting RGV angle, and results are presented in Figure 4-34. As it can be seen, surge line and compressor map shifts to low flow rates. This shift is greatly due to changing system response due to change in system impedance, by changing the inlet ducting volume [bigger volume, for the RGVs due to RGV bigger radius, compared to straight inlet pipe]. However, we need to make sure if any kind of positive swirl is produced by the RGV, 0°. Since positive swirl can also explain part of this shift. The pressure losses are probably due to losses through the system.

In order to better understand the obtained global results, velocity triangles at compressor inlet were reconstructed using LDA measurements.

- Effect of prewhirl imposed by the RGV system, on compressor performance and surge line

In order to indicate the effect of positive swirl on the compressor map widening. Figure 4-35 [to the top] presents the pressure ratio as function of corrected mass flow rate, for the RGV setting angles θ=0°, +30° and +60°.

Figure 4-35 [in the bottom] presents the isentropic efficiency as function of corrected mass flow rate and RGV setting angles of θ= +30° and +60°, for each of the three non dimensional rotational speeds corresponding to 100, 140 and 170K rpm.

Obtained results can be resumed by the following 3 points,

1. Pressure ratio drop all over the flow range when imposing positive swirl, compared to compressor basic characteristics [at 0.06 kg/s corrected mass flow rate, and Nc=150K rpm, the pressure ratio loss for 30° and 60° AGV setting angles are respectively 2.6 % and 10.5% less than that of zero angle case]. With bigger pressure drop at high RGVs setting angles.
2. Surge line was not improved at low rotational speeds, and RGV ,θ=+30° compared to zero configuration. However, better improvement was obtained at high rotational speeds and RGV ,θ=+60° [at TPR=2.8, the surge line improvement for 30° and 60° AGV setting angles are respectively 33.4% and 44% less than that of basic characteristics]
3. Efficiency drops at middle and high flow rates, with higher drops at big RGV setting angles. However, a slight increase at low flow rates was obtained.

These results can partly be explained by,

1. Pressure drop when imparting Positive swirl is due to decreasing compressor work input [Euler equation]. In addition to the influence of pressure losses through the RGVs [which become bigger at high RGV setting angles].
2. In general, positive swirl decreases incidence losses with respect to basic configuration, this decrease delays impeller inlet instability. However, this point has to be clarified by reconstructing velocity triangle at compressor inlet.
3. Efficiency drop at high flow rate can be explained by friction losses caused by the RGV system, and incidence losses at the impeller eye. The slight increase at low flow rates is due to lower incidence losses.

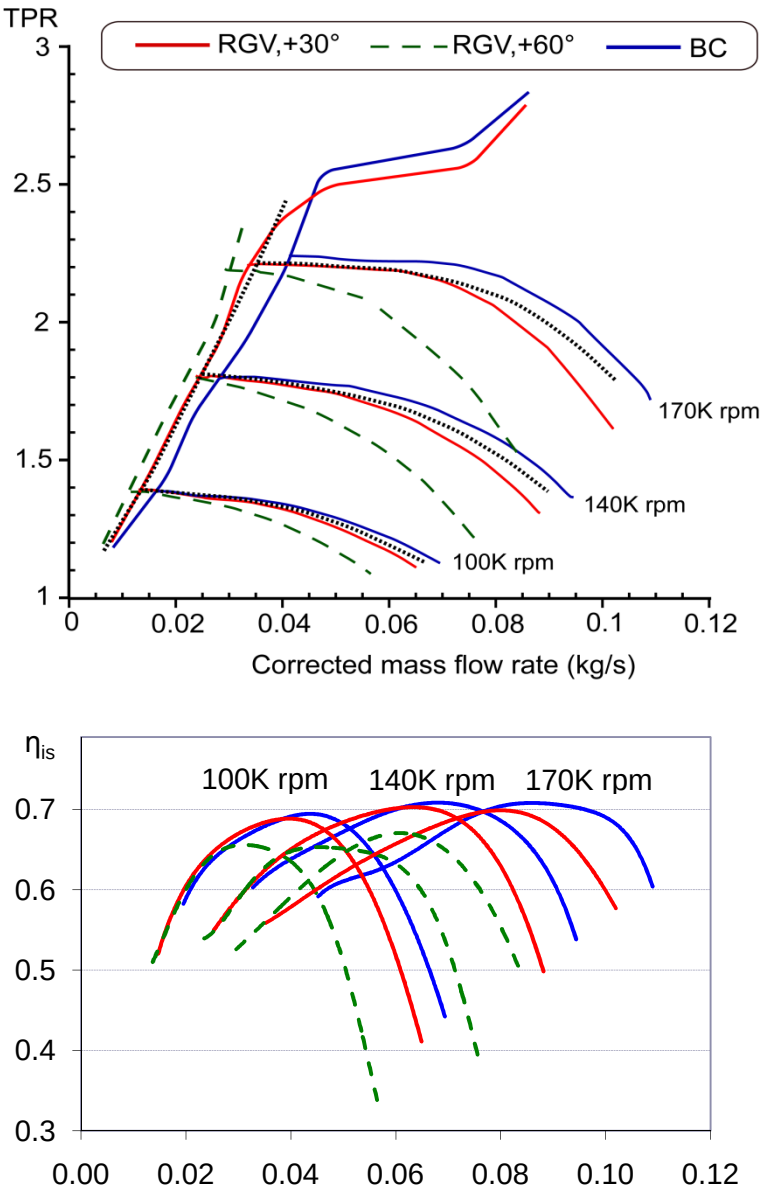

Figure 4-35 RGV compared to basic characteristics

In order to indicate the effect of negative swirl on the compressor performance and map widening. Figure 4-36 presents the pressure ratio as function of corrected mass flow rate, for the RGV setting angles θ=0°,-30° and -60° compared to basic characteristics .

Figure 4-36 [to the bottom] presents the isentropic efficiency as function of corrected mass flow rate and RGV setting angles θ=-30° and -60°, at two non dimensional rotational speeds corresponding to 120K rpm and 170K rpm.

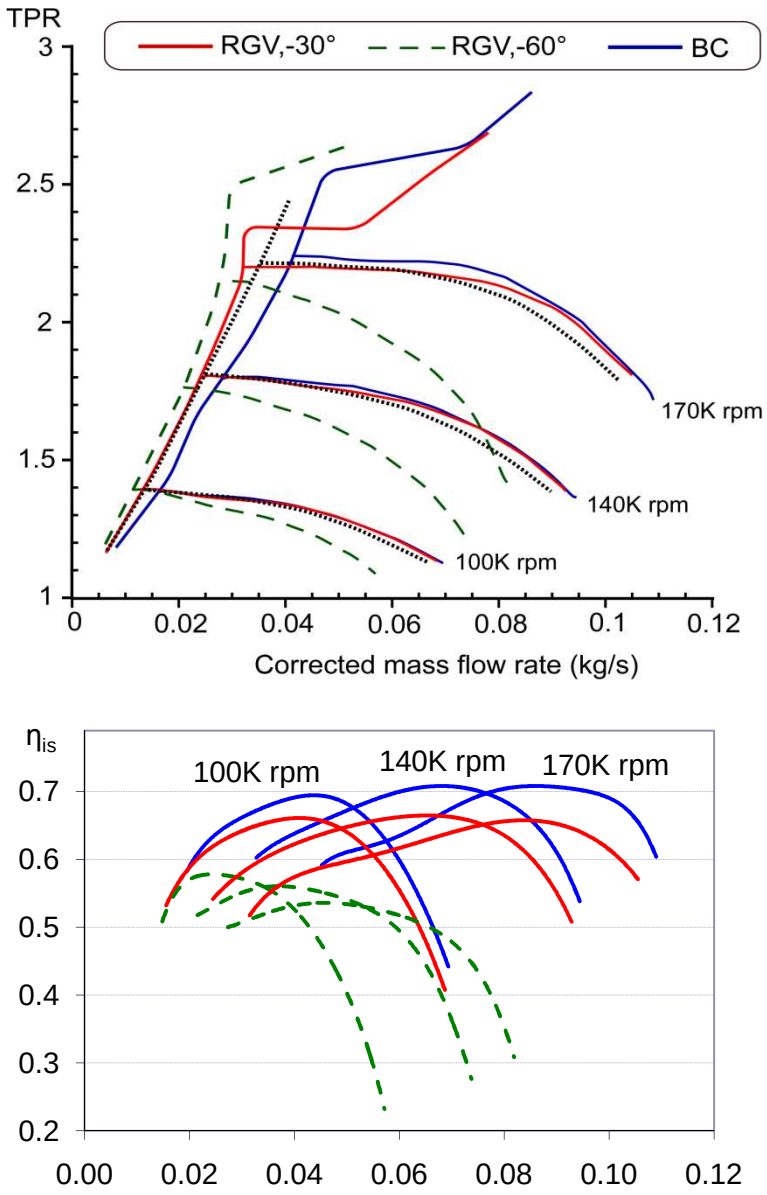

Figure 4-36 RGV negative setting angles compared to BC

Results can be resumed by the following 3 points,

1. Pressure ratio stays almost constant at middle and high flow rates with respect to that of basic characteristics, for RGV, -30°. However, p ressure ratio drops at -60° setting angle [at 0.06 kg/s corrected mass flow rate, and Nc=150K rpm, the pressure ratio loss for -30° and -60° RGV setting angles are respe ctively 0.7% and 13.15% less than that of Zero angle case].
2. Surge line was not improved at low rotational speeds, and RGV ,θ=-30° compared to zero configuration. However, better improvement was obtained at high rotational speeds and RGV ,θ=-60° [at TPR=2.5, the surge line improvement for - 30° and -60° AGV setting angles are respectively 5.7% and 45% less than that of zero angle case]. Note that surge line improvement was slightly greater when imparting negative swirl than that of positive swirl.

3. Efficiency drops at the overall flow range, with higher drops at big RGV setting angles.

These results can be partly explained by,

1. Pressure increase when imparting counter swirl is due to increasing compressor work input [Euler equation]. The pressure loss at big RGV negative angles can be explained by pressure losses through the RGV system. Hence, there is necessity to reconstruct the compressor map after subtracting the pressure losses through the AGV system, to better clarify its effect on compressor compression ability.
2. The slight surge line improvement can be explained by flow non uniformity produced by the RGVs. This point is to be treated in the LDA section
3. Imparting negative swirl increases relative velocity at impeller inlet. With the velocity increase in the impeller, friction losses increases, and efficiency drops. In addition to the incidence angle increase, which produces incidence losses.

The effect of the swirl [positive and counter] imparted by the RGV system without system losses. This can be concluded by reconstructing compressor characteristics after subtracting losses through the RGVs

❖ Reconstructing the compressor maps and isentropic efficiency by subtracting the influence of pressure losses through the RGVs

Some interesting results were obtained when reconstructing pressure and efficiency curves after subtracting pressure losses through the RGVs. Effects of positive and negative prewhirl produced by the system on the compressor performance are presented in Figure 4-37 and Figure 4-38.

Effect of positive swirl imposed by the RGVs

1. With pressure loss through the RGV added to total pressure, the reconstructed pressure ratio increases with respect to non constructed map [2.6% increase at 0.06Kg/s and 150K rpm for setting angle AGV, +60°], but still less than that of standard characteristics at almost all rotational speeds. This decrease is due to decrease in work input [Euler equation].
2. Very slight surge line shift compared to non constructed results, because the influence of pressure losses is not very significant at these low air mass flows.
3. Efficiency slightly increase compared to non constructed. Hence, efficiency losses at high flow rates come not from losses through the system, but incidence losses at the impeller inlet.

Effect of negative swirl imparted by the RGVs:

1. Increase in pressure ratio at almost all rotational speeds compared to basic characteristics [at 0.06Kg/s and 150K rpm, pressure ratio increases by 14% with respect to non constructed pressure ratio], instead at high flow rate and RGV, -60°. This increase is due to the increase in work input [Euler equation]. Note that, losses through the RGV system largely influence the compression ratio capability. This was not the case with positive setting angles [positive angles produce more losses than positive angles].

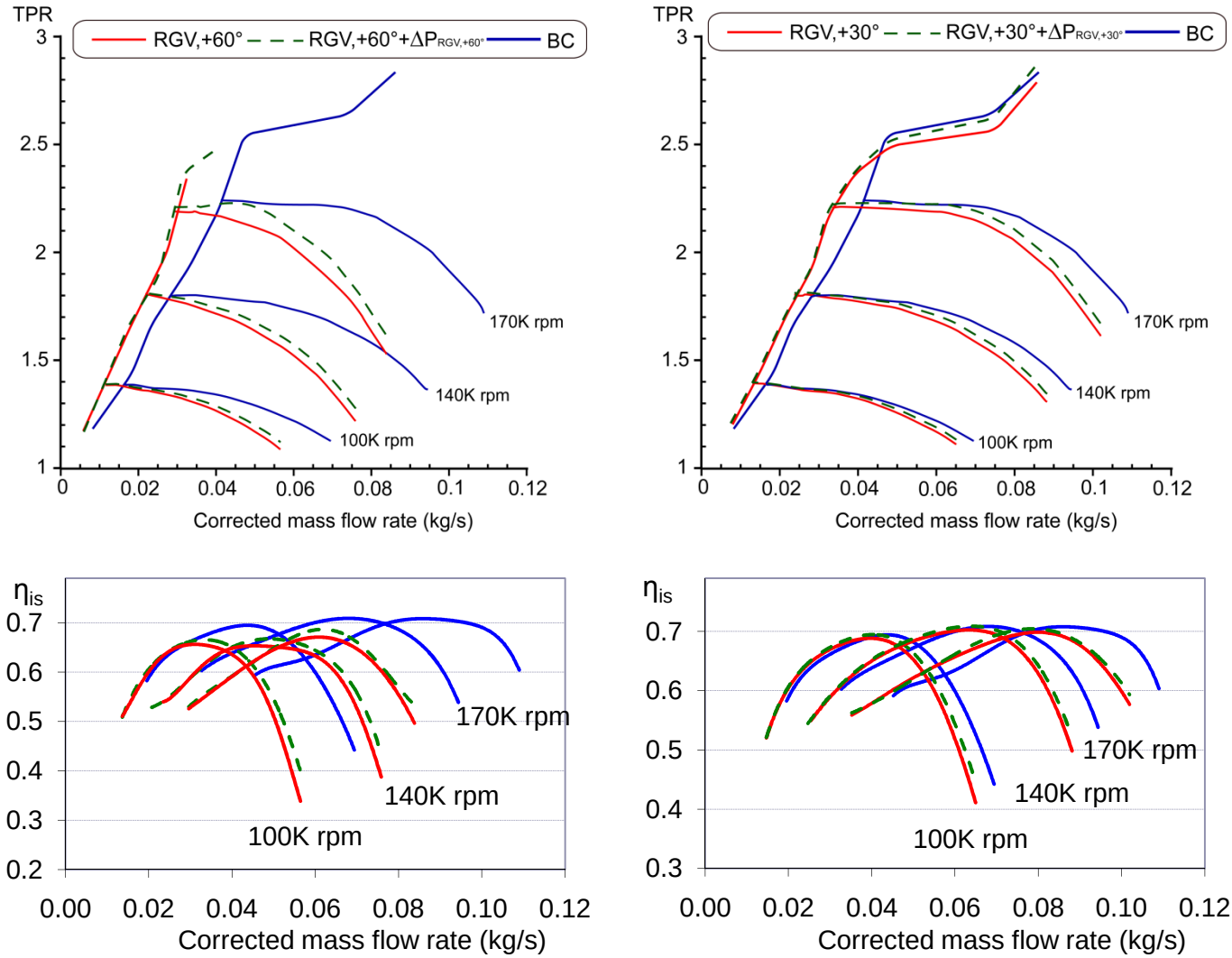

Figure 4-37 Reconstructed pressure and efficiency curves after subtracting pressure losses through the RGVs, for setting angles, θ =+30°,+60°

2. Very slight surge line shift compared to non constructed results, because the influence of pressure losses is not very significant at these low air mass flows.
3. Adding the pressure loss through the RGV, efficiency still less than those of basic characteristics at almost all the flow range, with higher drop at higher setting angles. This drop will be explained with LDA measurement [LDA section]

❖ Using LDA measurements to understand measured behavior

After studying the influence of different RGV setting angles on overall compressor performance and surge line, LDA measurement was conducted at the compressor inlet to bring about a better understanding of the RGV influence in the flow fields at the compressor inlet [Figure 4-39].

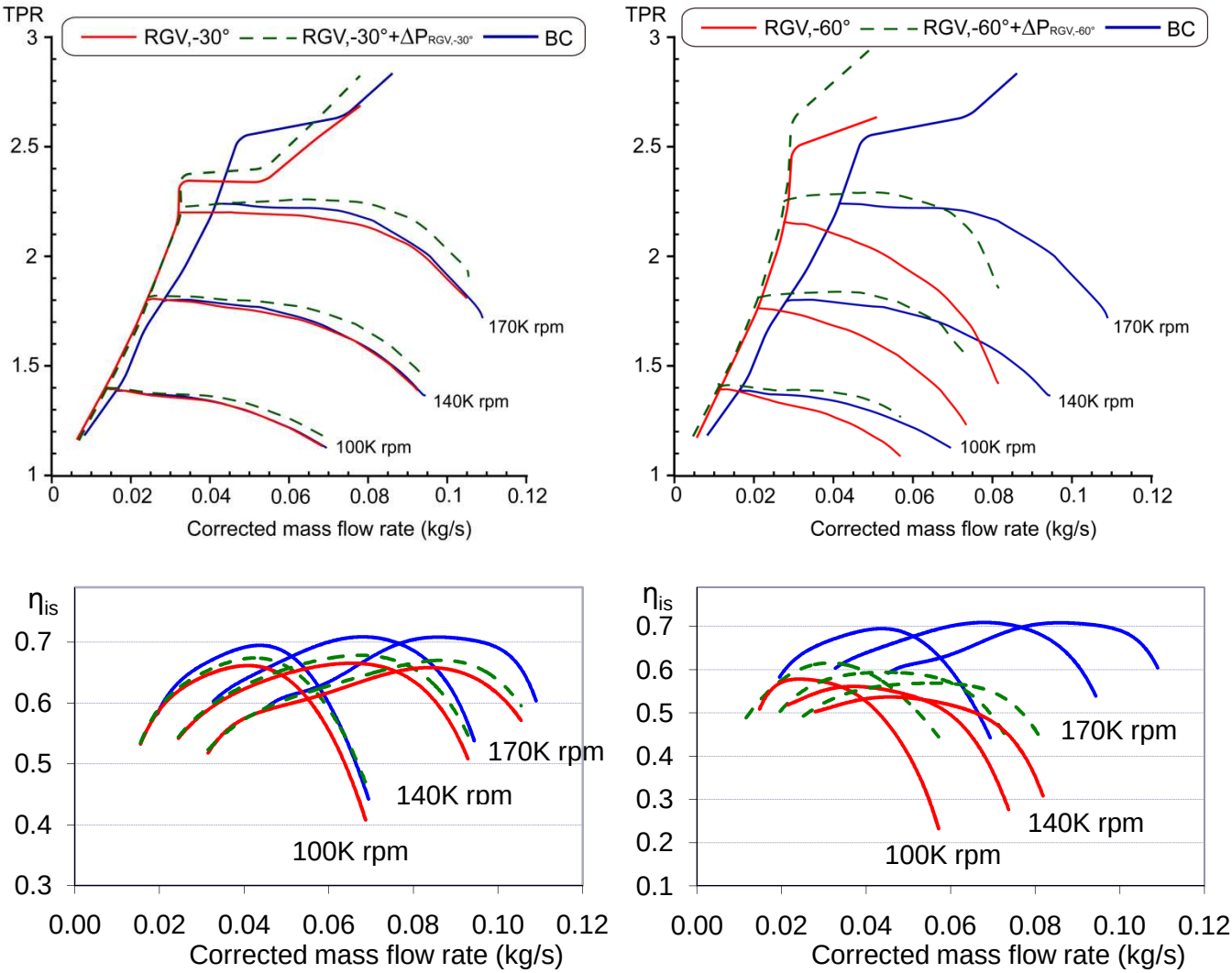

Figure 4-38 Reconstructed pressure and efficiency curves after subtracting pressure losses through the RGVs, for setting angles, θ =-30°,-60°,

LDA measurements have been performed for one operation condition close to the surge line of the compressor map for a mass flow rate of about 0.0258kg/s [corresponds to 120K rpm near surge point, and a pressure ratio of 1.6 bar].

The prewhirl type imposed by the RGV system, and a reconstruction of the inlet velocity triangle are investigated in this section. Note that measures were done without taking in effect the impeller.

Vanes were positioned at the positive setting angles of 30°, and 60° and negative angles of -30° and -60°. Axial and vertical velocity componen ts are measured at 19 points along the diameter direction [Z direction], and at different plane measurements P0°, P60°, and P120° [where P60° is the plane of measure, rotated with a n angle 60° with respect to the plane of measure P0° shown in Figure 4-26] for a total of 57 points of measure for each vane setting angle.

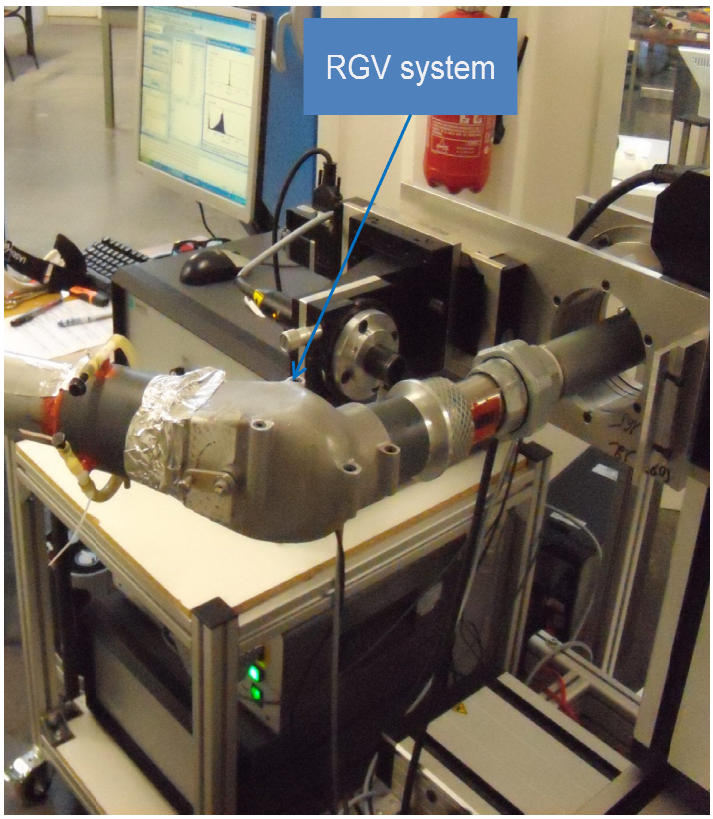

Figure 4-39 LDA measurement downstream of the RGVs

The first step in the experiment was to measure the axial and vertical velocity downstream of the RGVs. Figure 4-40 shows the axial velocity component as a function of RGV setting angles of -30°,- 60°, 0°, +30° and +60° r espectively.

For the axial velocity distribution, Figure 4-40 shows that the axial flow was not perturbed at vane setting angles of θ= -30°,+30° and 0°. The velocity is maximum at the mos t part of the diameter and it drops down at the pipe walls due to the boundary layer, with more uniform flow for θ= 0°.

For θ=-60° an d +60°, flow is non uniform over the diameter, axia l velocity is greater at the outer wall of the elbow, this comes from the elbow which forces the flow to go from vertical to horizontal, so the flow has the tendency to leave the inside wall of the elbow and accelerate in the outer side wall. This flow non uniformity can cause a non uniformity in the flow field inside the impeller.

The tangential velocity distribution downstream of the RGV system as shown in Figure 4-41, indicates a solid body vortex produced by positive and negative setting angles. For θ=-60° and -30°, tangential velocity in the outer wall is much higher than that in the inside wall, this was not the case for setting angles θ=+60°and +30°.

Due to assembly non symmetry, tangential velocity downstream of the setting angles θ=-60°and - 30° setting angles are bigger that those produced b y θ=+60°and +30°.

Since in the partial load region, the radial flow distribution influences considerably the performance of the impeller [Kassens & Rautenberg, 1998 (166)], the non uniform radial distribution when imparting counter swirl, with the high incidence losses causes high efficiency losses at low flow rates.

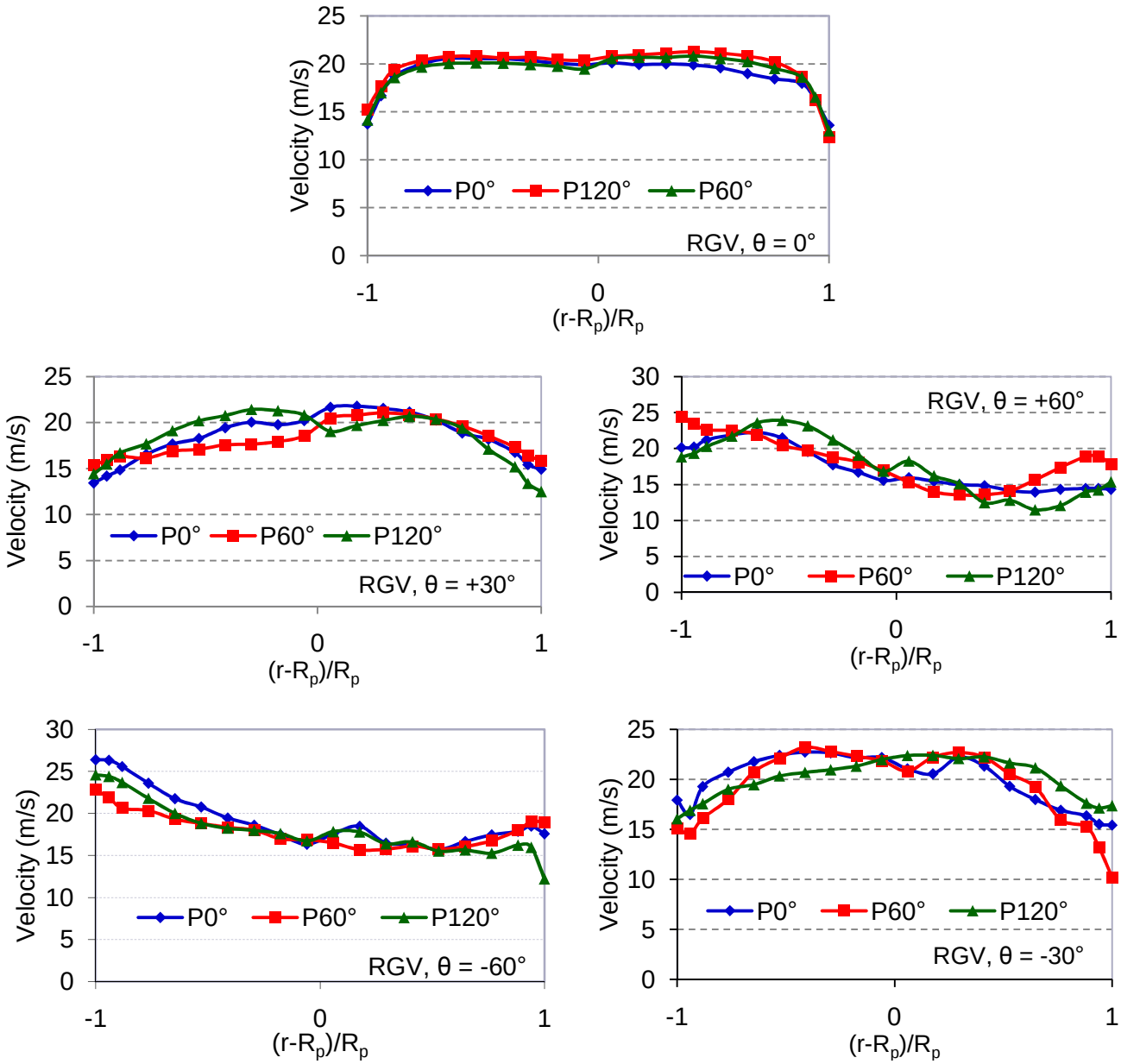

Figure 4-40 Effect of RGV setting angle in the axial velocity, downstream of the RGV system.

At RGV, θ=0° the tangential velocity component in very small , hence for the case of RGV, θ=0° the surge line shift compared to basic configur ation [straight inlet], is due to changing system impedance and not to any prewhirl imposed by the system at zero setting angle [no local contribution to system surge line shift].

As it can be seen from Figure 4-41, the tangential velocity distribution when imposing positive and negative swirl in non uniform over the inlet section. Velocity in the outside wall is greater for the two configurations compared to that of the outside wall. This non uniformity leads non uniform flow at the impeller eye, and non uniformity in the impeller, hence impeller losses increase.

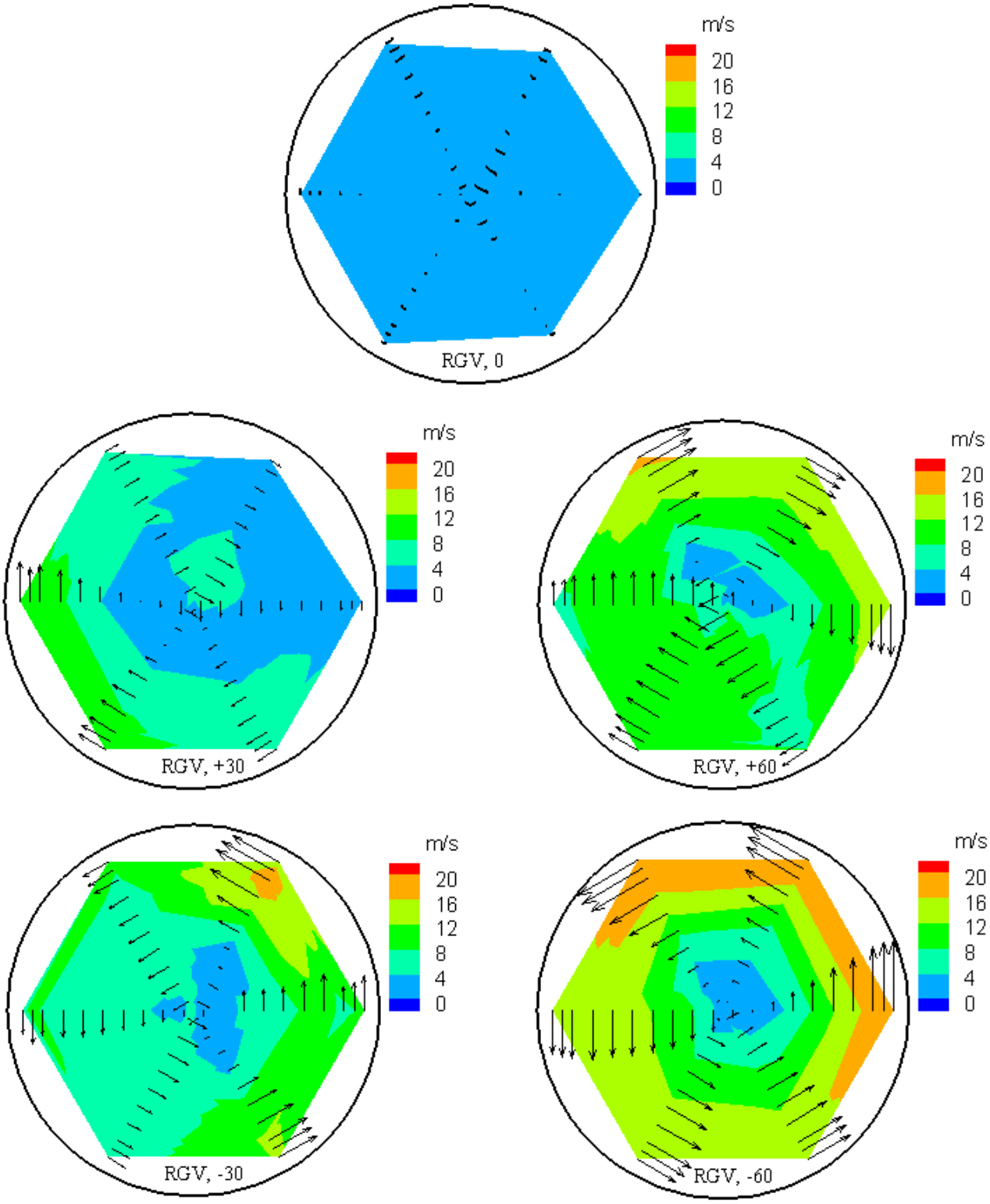

Figure 4-41 Tangential velocity distribution downstream of the RGVs

❖ Reconstruction of velocity triangle at compressor inlet

In order to better explain the modifications to the surge line when imposing negative and positive swirl, the velocity triangles at the inducer inlet were reconstructed.

The air flow pattern predicted by the LDA measurement at the RGV outlet was used to obtain the variables necessary for drawing the velocity triangles at the inducer tip inlet.

According to the LDA measurements, the air mass flow distribution is different at the impeller entry section for each position of the RGV vanes and the flow passing in the impeller is concentrated at the periphery of the inlet section.

The tip linear velocity of the rotor U_{1t} together with C_1 [axial velocity] and $C_{\alpha t}$ define the vectors of the velocity triangle at impeller tip. Hence W_{1t} can be calculated and the value of the approach angle is obtained from equation 4-7,

$$tan\beta = \frac{U_{1t} - C_{\alpha t}}{W_{1t}} \qquad 4\text{-}7$$

The reconstruction of the velocity triangles has been performed for RGV, ±60°vane apertures but only for the points that limit surge region and at the inducer tip. The incidence angle and the relative velocity are presented in Figure 4-42 and compared with the corresponding values in the basic configuration.

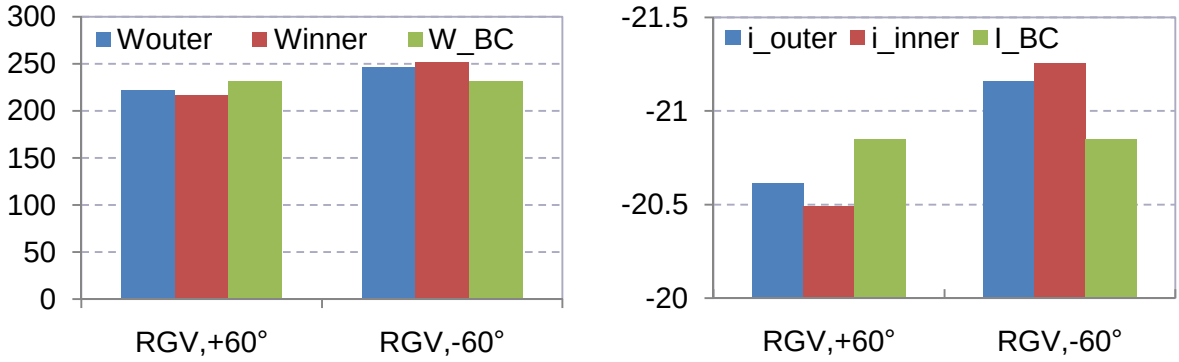

Figure 4-42 Incidence angle [i] and relative velocity [W1] calculated for point of the surge limit at N=140K rpm, line with negative and positive RGV vanes angle.

LDA measurements, confirms negative swirl increases relative velocity and incidence losses compared to positive swirl [Figure 4-42]. Moreover, the difference between inside and outside wall relative velocity and incidence angle, can be clearly seen in the same figure.

Compared to AGVs, the RGV system improves less the surge line. Surge line was improved at high speeds, and high RGV setting angles. No improvement was obtained for RGV, 30° setting angle. After LDA analysis, the non uniform flow produced by the RGVs system at inducer inlet compared to that of the AGVs, can explain the smaller surge line shift obtained when using the RGVs.

If this system is to be chosen, the negative swirl produced with the RGV device allows obtaining higher compression ratios than the positive swirl, so that the negative configuration of the device is recommended in spite of its lower isentropic efficiency compared to positive swirl. Moreover, The RGV configuration, with a 90° compressor inlet, allows solving the packaging problem when installed in automotive engine.

With the positive swirl the incidence angle [i] is much more reduced than negative swirl, and some improvements in surge margin have also been presented. Nevertheless, the combination of excellent relative velocities [W1] and incidence angles [i] lower than with axial inlet configuration makes the negative configuration the optimum.

4.1.4.3 Effect of prewhirl imparted by the flexible guide vane system [FGVs], on overall compressor performance and surge line

The effect of the positive swirl imparted by the FGVs on compressor characteristics is studied in this section. The tested FGVs is already installed in a turbocharged engine.

❖ Results and discussions

Figure 4-43 shows the pressure ratio as function of corrected mass flow rate for the FGVs compared to that of basic characteristics [straight inlet], at the four corrected rotational speeds Nc=80, 120, 155 and 185K rpm.

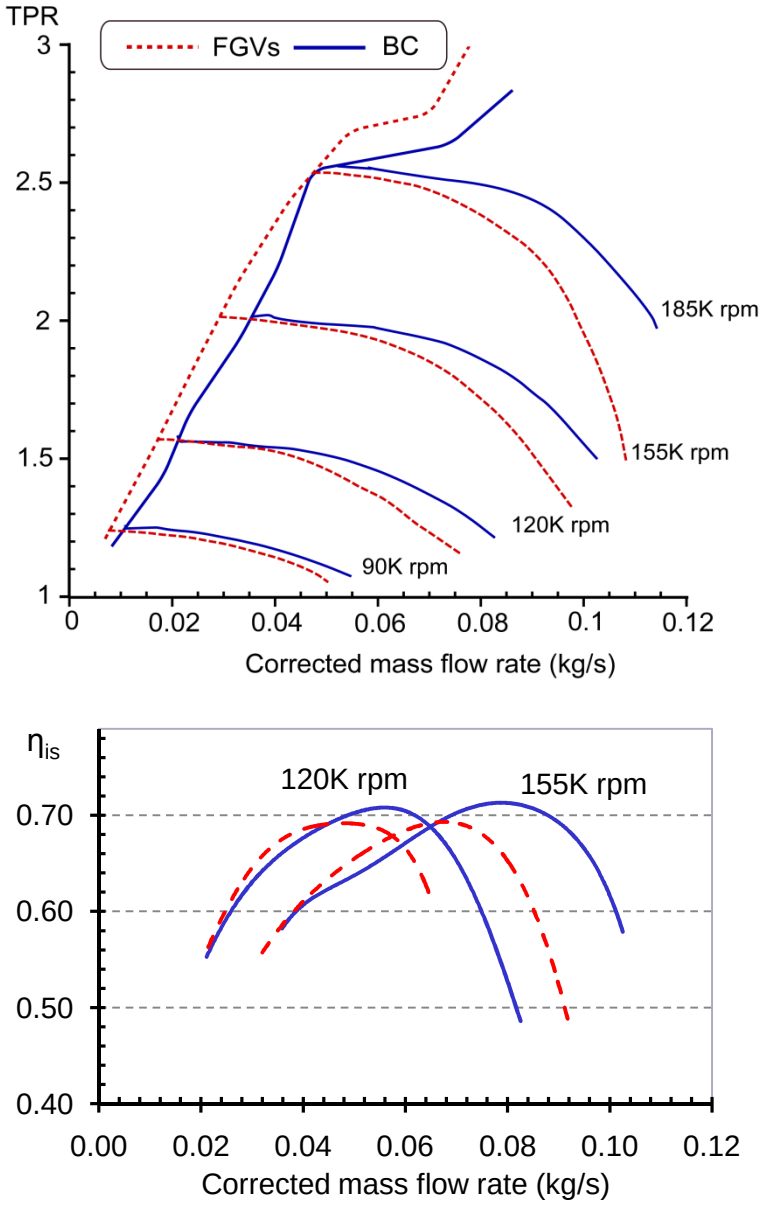

Figure 4-43 FGVs compared to BC

The volume of the inlet ducting was slightly changed when installing the FGVs, compared to the straight inlet tube [FGVs has a slight bigger diameter, than the straight in let pipe]. It can be seen that the line of surge moves to low flow rates and the pressure ratio drops at the four rotational speeds with a bigger drop at high flow rates, and high rotational speeds.

The isentropic efficiency as a function of corrected mass flow rate for the two non dimensional rotational speeds Nc=120, and 155K rpm is presented in Figure 4-43. The efficiency increased at low flow rates, while it drops at high flow rate and high rotational speed. This drop is probably due to the incidence losses created by the FGVs at the compressor entry, taking in consideration that pressure losses through the system were small.

While the flexible system was designed to produce zero swirl at high flows [deforms to axial position under the effect of flow velocity], this was not the case when installed to the tested turbocharger. Indeed the maximum flow rate was not sufficient to deform the FGV vanes. A bigger turbocharger [higher mass flow], can force the tested FGV to produce zero angle at high flows.

Since the FGV vanes do not deform at high flow rates. The FGV system still produces prewhirl at high flow rates [acts as a nearly fixed vane system], which explain the pressure losses due to Euler equation, and confirms efficiency drop at these flow rates to be caused by incidence losses.

LDA measurements were not done to find out the type of prewhirl type, imposed by the FGVs.

The FGVs was not advantageous for the tested turbocharger, although it slightly shifts compressor map to the left, and slightly increases efficiency at low flow rates. However, this was accompanied with high losses at high flow rates. Even if the FGV vanes deform at lower flow rates, the gain obtained from the prewhirl imposed by the system, is not worth.

4.1.4.4 New swirl generator to delay inducer instabilities

In this section, design and manufacturing of a new swirl generator [NS] is studied, and its effect on compressor performance and surge line is presented.

- Design and manufacturing of the New swirl generator system [NSs]

The NSs was manufactured at the Ecole Centrale de Nantes, its design was based on: one dimensional analysis, results obtained from the last tested pre rotation mechanisms [FGV, AGV], and the work of Wimmer et al, 2004 (123).

The NSs was designed to,

1. Produce high swirl angles with minimum associated pressure losses,
2. Produce different prewhirl types. This can be done, by being able to change vanes and replace by new vane forms [easily changeable vanes],
3. Suppress the angle of attack at the inlet of the swirl generator,
4. Produce uniform flow at the center of the impeller inlet

The device has flexible guide vanes including a fixed area and a deformable area, where the deformable area is connected with a support section. The fixed area of the guide vanes is connected with a circular adjusting section. The deformable section is fixedly arranged in inlet casing. The fixed area is adjustable and is controllable by a control device [manual for this prototype]. Moreover, a centerpiece [center body] was added to the system to improve center flow.

Minimum pressure losses:

To minimize pressure losses through the NS system, one has to minimize friction and separation losses. To suppress separation losses, the system was designed so that zero angle of attack is obtained at vane inlet [fixed area section].

To minimize friction losses one have to ensure smooth surface [good surface quality], and minimum area reduction for a given setting angle, thus producing high swirl angles for small NS vane angle. This was done using one dimensional analysis [radius of the NS vanes, and the center body radius were optimized to obtain high swirl angles for small NS vane angles]. Note that, the NS vane tip radius is limited by different factors including space and material cost [big radius, thus more material and more space], and that of center body by a uniform flow at impeller center and minimum diameter by its ability to support the movable vanes.

Analysis was based on velocity triangle relation between the vane exit [position 1] to that at the eye of the impeller [position 2], by applying the conservation of mass and the conservation of angular momentum equations [Figure 4-44]:

$$\rho_{1'} C_{1'} A_{1'} = \rho_1 C_1 A_1 \qquad 4\text{-}8$$

$$r_{1'} C_{\theta 1'} = r_1 C_{\theta 1} \qquad 4\text{-}9$$

In addition, to the various isentropic relations relating total and static pressures and total and static temperatures, together with the equation of state, are used to complete the solution.

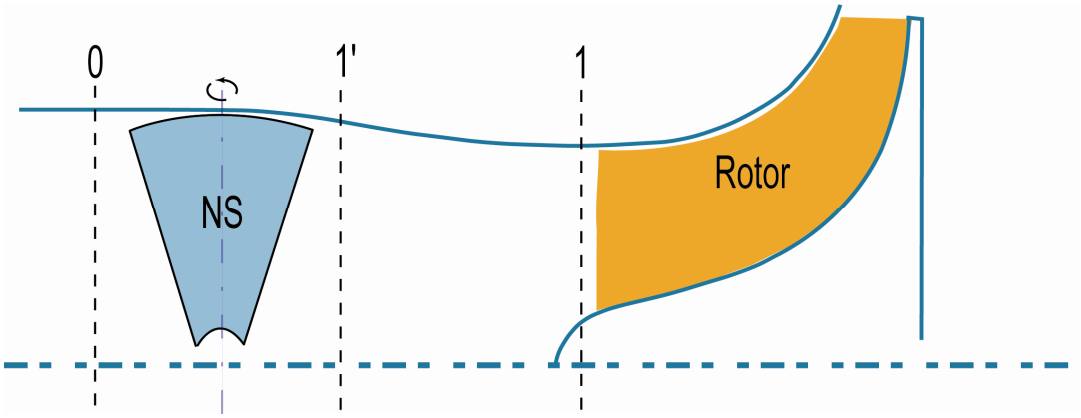

Figure 4-44 New system guide vane

Best results were obtained, when vane tip to impeller tip radius ratio equals 1.6. Angles at impeller eye with respect to vane angle for this radius ratio are presented in Figure 4-45.

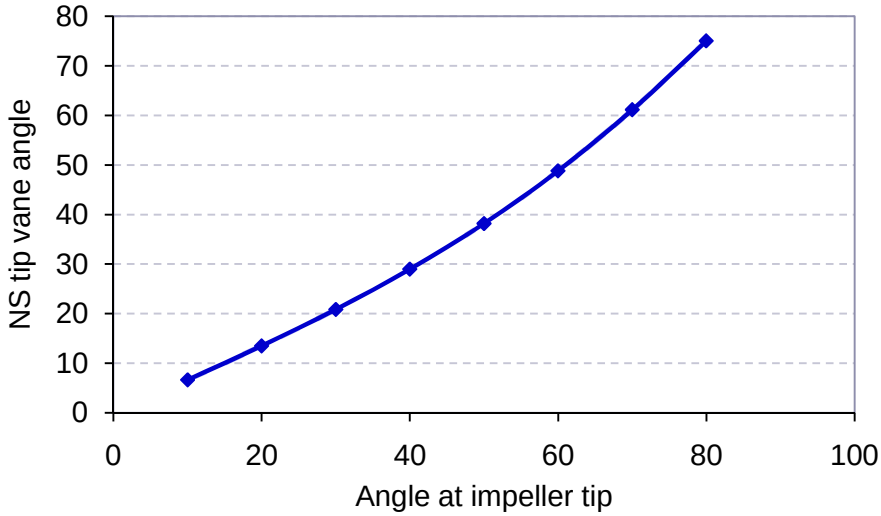

Figure 4-45 Absolute velocity angle at impeller eye as a function of vane angle

Changeable vanes:

Eight plate vanes were used for this system. Vane number was calculated so that, swirl is imposed to all stream lines passing through the NS section [which was not the case of the FGVs, where the 4 vanes were not sufficient to impose swirl to all passing flow, hence four core flows in the center of the recirculating flow could be obtained]. The maximum vane number was also limited by area reduction hence, pressure losses.

Vanes are changeable and easily manufactured, the leading edge is fixed to the center body and the cylindrical section and the trailing edge just fixed to the cylindrical section. The type of fixation to the cylindrical section and the form of the vane controls the produced prewhirl type [Figure 4-46].

Deformable and thin mater was used to manufacture NS vanes, the ability to easy cut and form vanes important in choosing the material. Moreover, vane thickness has not to increase losses through the system.

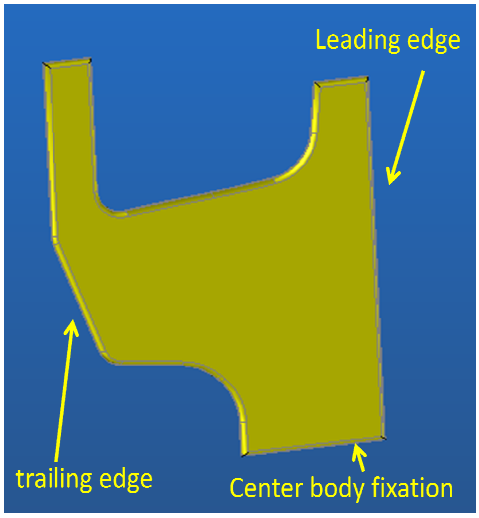

Figure 4-46 NS vane form [free vortex configuration]

Center body:

With center body all flow passes through the NS vanes, all flow stream lines were pre rotated, and no core flow was produced at the center. Center body was formed so that pressure losses were minimized. In addition to a sharp edge form, to minimize wake production, a careful attention was done to surface quality.

Finally, the NS was easily manufactured and not expensive, however its aerodynamic performance is impaired by a number of features:

- Cylinder surface quality was not good, and that encourages more pressure losses.
- Vane fixation need to be more precisely manufactured.

❖ Effect of NS system on compressor performance and surge line.

The effect on the compressor performance and surge line of the proposed new system compared to basic characteristics is presented in Figure 4-47. For this test the form of vanes which encourage a free vortex were used.

Figure 4-47 shows the compression ratio in function of mass flow rate at 90,120,155, and 185K rpm rotational speeds. As it can be seen, pressure ratio increases with negative NS configuration [NS,-30°], and decreases with that of positive configuration, and this can be explained by Euler equation.

Figure 4-47 shows, the total to total efficiency in function mass flow rate, at three corrected rotational speeds corresponding to 120,155, and 185K rpm.

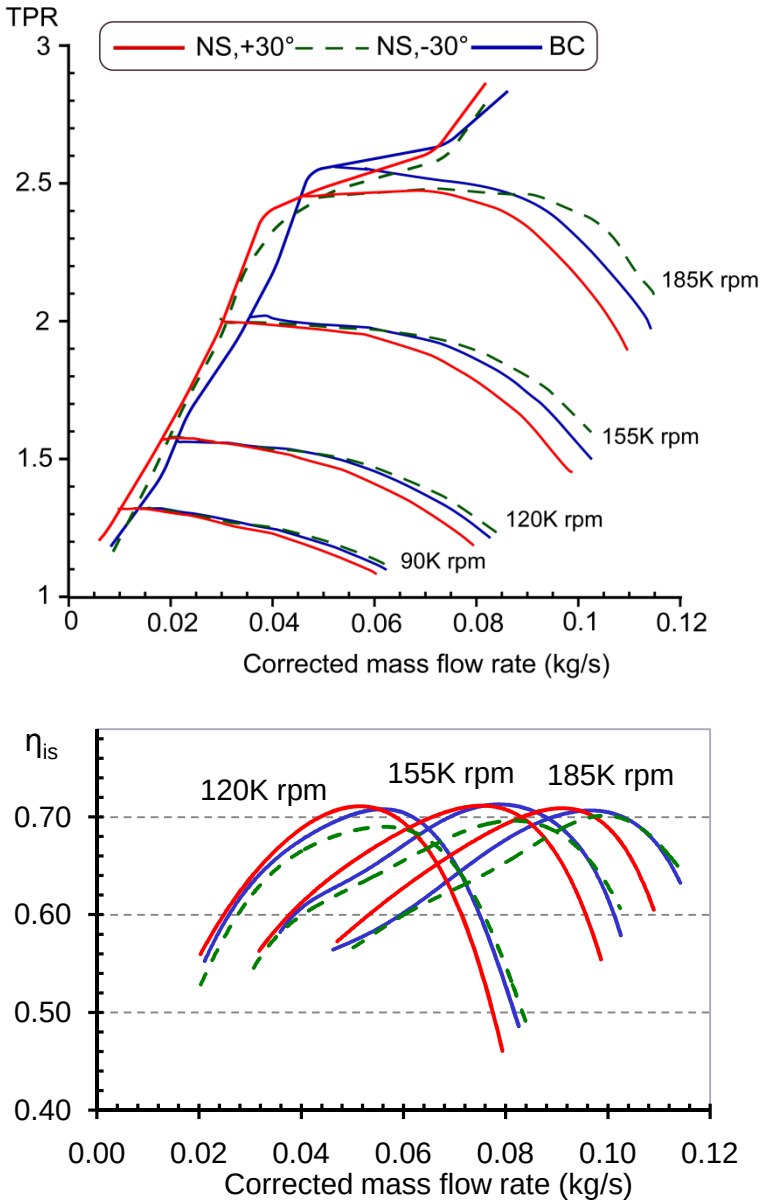

Figure 4-47 New system [NS] compared to basic characteristics

Some interesting results were obtained: First the efficiency increase at middle and low flow rates when imparting positive swirl, this increase [particularly at high speeds] needs local measurement to understand the prewhirl type produced by the NSs, so that incidence losses were minimized.

When imposing positive swirl [NS, +30°], good surge line improvement was obtained at low speeds compared to basic characteristics, Moreover, a slight surge line shift was obtained at middle speed. With negative swirl [NS, -30°], surge line shift was similar to that of the positive configuration, except at low speeds where no surge line shift was obtained.

❖ Reconstructing compressor maps and isentropic efficiency by subtracting the influence of pressure losses through the AGVs

To study the effect of pressure losses through the NSs on the pressure ratio and isentropic efficiency, compressor maps using the reconstructed pressure upstream of the compressor inducer are presented [Figure 4-48].

Due to relatively low pressure losses through the NS system, the reconstructed compression ratio and efficiency curves were almost similar. Taking in consideration the low pressure losses through the NS, one can conclude that the pressure losses and efficiency losses at high flow rates are due to incidence losses at impeller inlet.

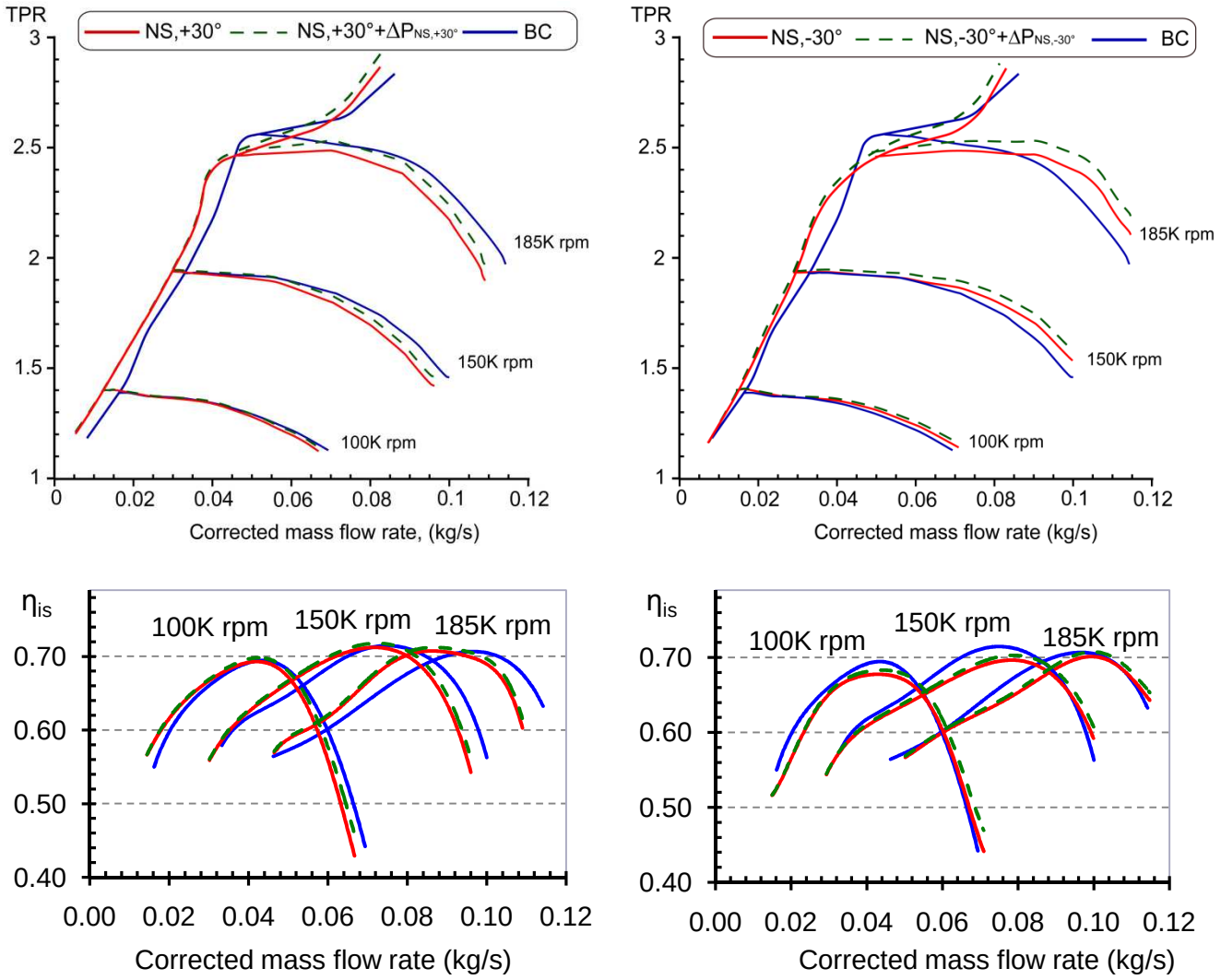

Figure 4-48 Reconstructed pressure and efficiency curves after subtracting pressure losses through the NS, for setting angles, θ =-30°,+30°

After studying the influence of NS positive and negative configuration on overall compressor performance and surge line, LDA measurement was conducted at the compressor inlet to bring about a better understanding of the NS influence in the flow fields at the compressor inlet.

Tests were done at 0.028Kg/s [corresponds to a near surge point of 100K rpm]. Only measures at plane P0° were done [11 measure points]. Tests were done several times to confirm results.

As it can be seen in Figure 4-49, tangential velocity distribution is nearly that of a free vortex [high velocities at the center and zero at the walls]. In the axial velocity distribution, we can see that, center velocity is smaller than boundary velocities [downstream of NS vanes]. This is due to center body.

At low speeds, free vortex produces the minimum incidence losses [theoretical study, section 4.1.1]. This can explain the surge line shift at low speeds, due to imparting free vortex positive prewhirl.

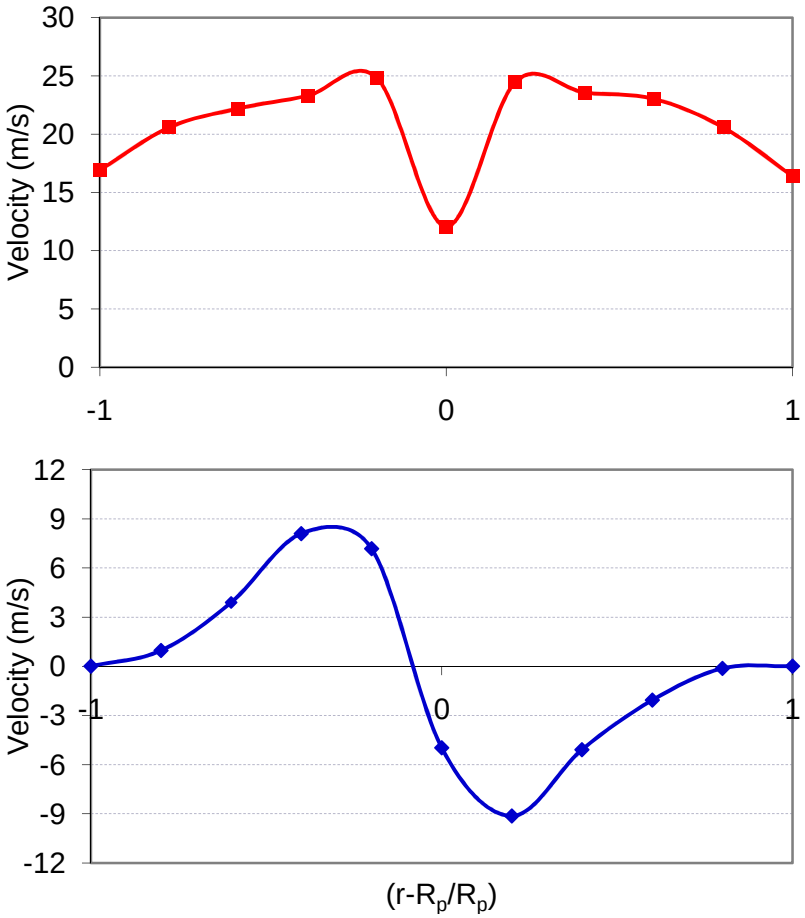

Figure 4-49 Axial velocity downstream of the NS [to the top], and tangential velocity [bottom]

LDA measurements were not done at higher flow rates due to excessive fouling problem. However, it would be interesting to find out if a free vortex is also obtained at high flow rates.

With slight surge line improvement at low and middle flow rates, the free vortex NS configuration produces not significant surge line improvement compared to basic characteristics. However, some interesting results were obtained, where efficiency was increased at middle and low flow rates at almost all speeds. This increase is probably due to more uniform flow at impeller inlet, with center body improving center flow upstream he impeller.

It'll be interesting to find out the effect of solid vortex NS configuration on compressor performance and surge line. We believe that, some significant increase in surge line will be obtained [relatively near to those of AGVs], while conserving or increasing efficiency at low and middle flows, when imposing positive swirl. Indeed, we had begun this test, and unfortunately not being able to continue due to unforeseen technical problems.

4.1.5 Conclusion

Four different pre rotation mechanisms were tested in this section, an AGVs, a RGVs, a FGVs and a new swirl generator designed and fabricated at the Ecole Centrale de Nantes. The New system has the advantage to produce 2 different prewhirl types, a free and a fixed vortex. In addition to producing high swirl angles for relatively low pressure losses.

Positive swirl produced by the different systems was advantageous in improving surge line and slightly increasing efficiency at low flow rates. AGVs produced the greatest improvement compared to other systems, this can be explained by the uniform tangential velocity distribution produced by the system compared to the RGVs, which makes just slight surge line shift compared to RGV,0° [probably due to a no n uniform flow distribution produced by the RGVs]. However, the surge line shift when using AGVs was accompanied with high pressure and efficiency losses.

We can conclude that the local contribution of imposing swirl at impeller inlet, to surge line shift was not significant. Except at high speeds and high setting angles [case of AGVs]. Indeed, it is known that imparting swirl at high speed impellers is not significantly efficient in improving impeller instabilities. However, is very efficient for moderate speed impellers

4.2 Delaying impeller instabilities

Flow-recirculation is a form of casing treatment which increases flow range by suppressing the onset of compressor stall [delaying impeller stall]. The tested flow-recirculation system, is Fischer's MWE system with holes replacing slots or grooves. These holes are designed to re-energize impeller low energy regions by flow from high energy regions [Magdougal et al, 1982 (140)].

As discussed in literature review section, much work has been carried out to optimize bleed slots [or grooves] locations, percentage of open area, their depth and width. The significance of the length of the inner tubular wall [L] has been also investigated [Figure 4-49]. Extending the length of the inner tubular wall with respect to conventional MWE tubular wall length [In conventional MWE structure, L/Di do not exceed 0.5 [Nikpour, 2007 (143)]], was proportional to significant surge line improvements.

Whereas much work has been previously carried out to study the apparatus communicating between the annular flow passage and the impeller wheel, an apparatus with multiple holes has not been previously considered. In this section experiments have been inducted to study the effect of different configurations of an MWE structure with plurality of holes on the performance and stable functioning of a turbocharger centrifugal compressor. The effect of extending the length of the inner tubular wall has also been investigated.

Two different MWE configurations were studied, MWE1 and MWE2. A brief explanation of the conception of the two systems is presented, and their effect on compressor performance and surge line is investigated.

4.2.1 MWE1 System

A preliminary internal map width enhancer was designed, this system was purely based on the literature (93) [Figure 4-50], it has been developed at the Ecole Centrale de Nantes. It consists of plurality of holes that connects the annular chamber [formed between the wall forming the compressor inlet and the wall defining the compressor inducer] to the main flow channel.

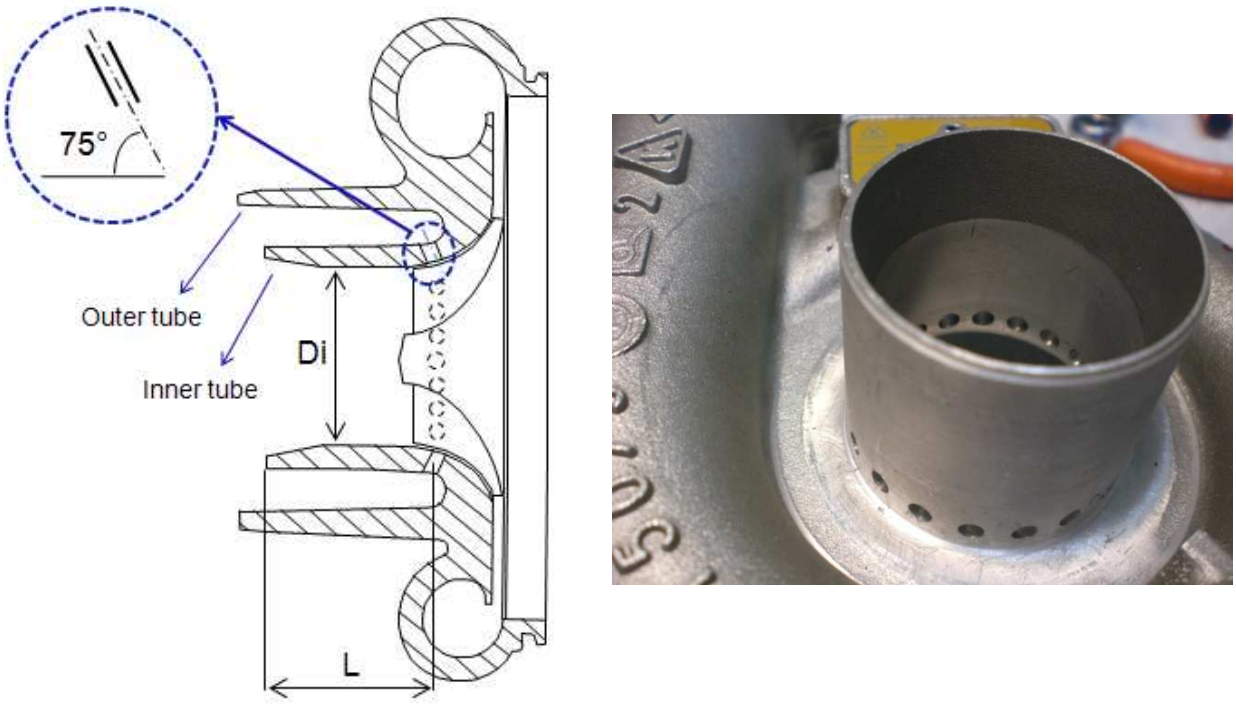

Figure 4-50 Tested MWE1 system, with a 2D schematic to the left

The total area of holes is 20.3% of the inducer annular area, and are arranged in an angle of 75° with the horizontal (93). The holes point location is at 31% along the meridional length from the leading edge just upstream of the point of minimum pressure [Figure 4-50].

The number of holes is arranged so that it is not equal to, a multiple of, or a factor of impeller blades number. If the number of the holes is a multiple of or a factor of the number of blades, then vibratory excitation can be induced (93). In the arrangement shown in Figure 4-50, the number of holes is 19 [Figure 4-59], and blade number is 12.

The system was fixed to the compressor in the following way: the inner tube [annular chamber] - has the same diameter of the inducer inlet- is connected to the inducer inlet, and the outer tube is fixed to the compressor volute, by a support system fabricated at the Ecole Centrale de Nantes. The support system was designed so that no leakage will exist between the connection with the volute and the main inner tube [Figure 4-51].

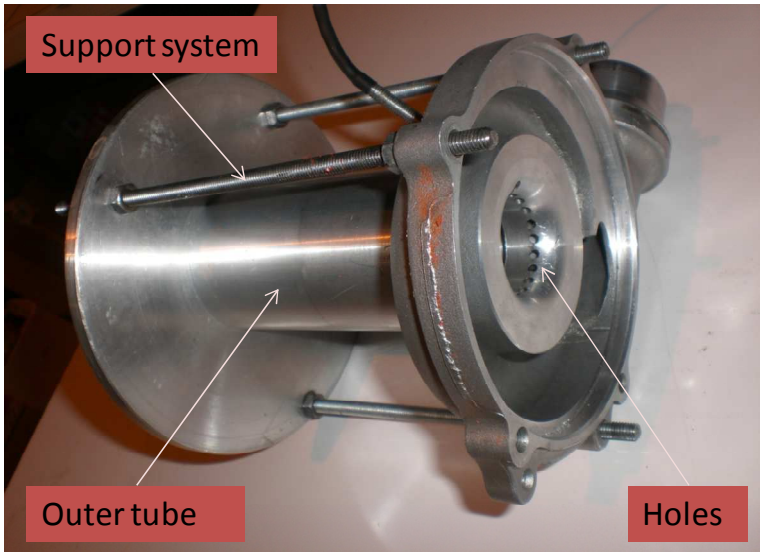

Figure 4-51 MWE1 Support system

❖ Results and discussion

In this section, the system's effect on the compressor, and surge and choke line improvements is discussed.

Different inner tube lengths were tested and their effect on the compressor stable functioning, and performance is presented in APPENDIX D. The tests were conducted on the turbocharger test facility configuration 2.

Three different inner tube lengths were tested, L/Di=0.3, 0.6 and 0.93 respectively. Where, L is the length of the annular passage through which air will flow at surge and Di is the inlet diameter [Figure 4-50].

Results showed that the shape of pressure ratio versus the mass flow characteristics is very similar in the three cases. The increase in L to Di ratio from 0.3 to 0.93 has not positively influenced the surge line for this particular design, the surge line has moved to high flow rates at high rotational speeds.

Results can be resumed by,

1. A shift of surge line to high flow rates, at middle and high rotational speeds,
2. Pressure ratio increase at middle flow rates, this increase becomes big at higher rotational speed [At mass flow rate equal to 0.078Kg/s and corrected rotational speed

of 190K rpm, the pressure ratio has increased by 8% at the three different pipe lengths]

3. Efficiency decreases at low flow rate and remains nearly constant at high flow rates.

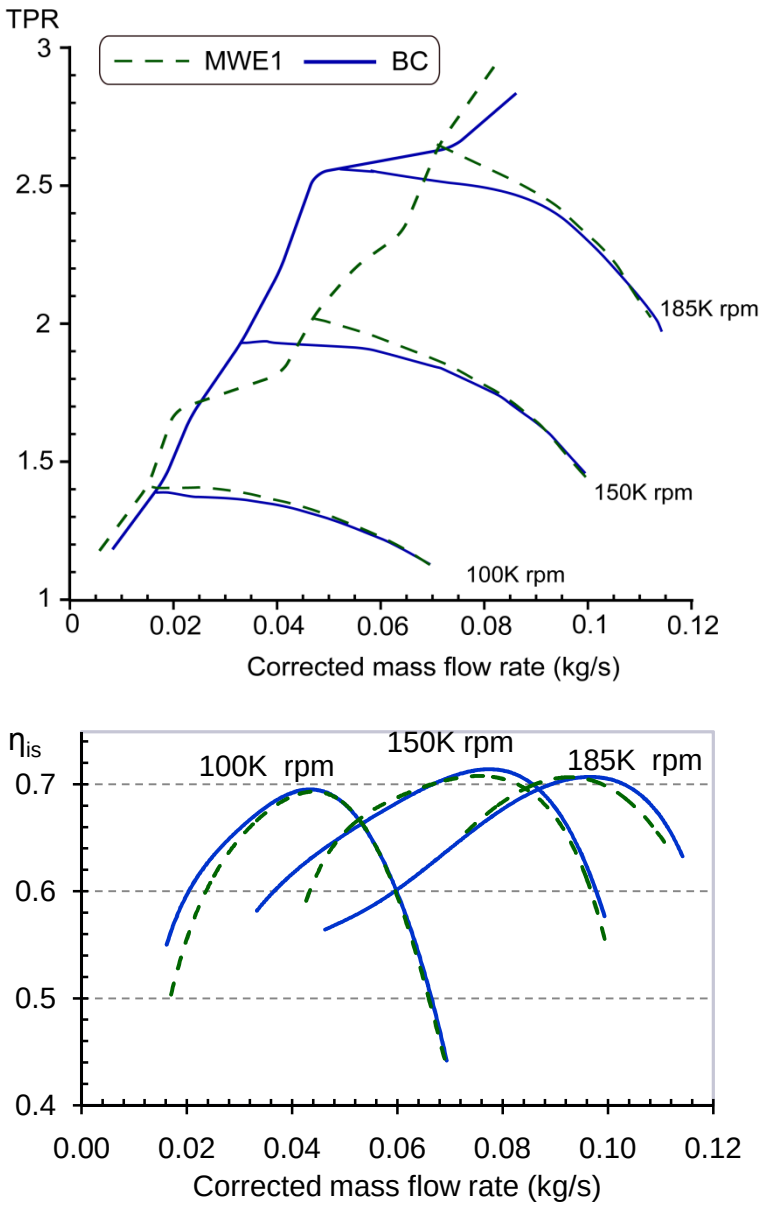

Figure 4-52 MWE1 system compared to basic characteristics

Figure 4-52 shows the basic compressor characteristics obtained in the test facility configuration 1, compared to MWE1 system with L/Di=0.3. Total pressure ratio and isentropic efficiency in function of corrected mass flow rate at three corrected rotational speeds, respectively: N=100, 150 and 185K rpm, are presented.

As it can be seen, the results obtained in configuration 1 are similar to those obtained at test facility configuration 2. To explain these results, we will treat each point separately and try to understand the effect of the MWE1 configuration on the compressor characteristics and stability. In the absence of CFD analysis and complex local flow studies, results will be explained by testing of different MWE configurations.

A. Low flow rate efficiency decrease

At low flow rates, efficiency decrease is probably due to increasing temperature at compressor inlet due to air recirculation [temperature of the recirculated air increase after being compressed in the inducer].

At high flow rates, the very slight efficiency decrease can be explained by increase in impeller losses at high flow rates, due to velocity increase [MWE flow adds to the main flow to increase impeller low rate, hence its velocity].

B. Pressure ratio increase at middle and low flow rates

The pressure ratio increase at middle and low flow rates when using the MWE1 system can be explained in two different ways.

1. An increase in the work input. This increase can be explained by either an increase in the tangential component of the compressor outlet, compressor inlet [negative swirl] , or the two terms at the same time [Euler equation, 4-10].

$$W_{Input} = U_2 C_{\alpha 2} - U_1 C_{\alpha 1} \qquad 4\text{-}10$$

2. A healthier impeller. This is due to a better diffusion when installing the MWE1 system compared to basic characteristics.

For point 1, the hole structure cannot encourage any negative pre-rotation at the impeller inlet, hence no increase in the impeller inlet tangential component [$C_{\alpha 1}$]. However, an increase in the impeller outlet tangential component [$C_{\alpha 2}$] is possible if the diffusion in the impeller is better.

The MWE1 probably improves impeller diffusion, and hence work input increase compared to basic characteristics was due to increasing diffuser inlet tangential component. Now the question is why surge line shifts to high flow rates, with a healthier impeller.

C. Surge line shift to high flow rates

Surge line shift to high flow rates at high rotational speeds, can be interpreted in the following ways,

1. Holes- apparatus communicating between the annular flow passage and the impeller wheel, has encouraged a negative pre-rotation at inducer inlet, hence stall incidence angle occurs at higher flow rates.
2. Stall shifts to the diffuser at high rotational speeds, due to good impeller diffusion, hence the diffuser causes the compressor stall.
3. Instabilities in the volutes provokes compressor stall at high speeds,
4. Non uniform flow at the compressor inlet due to mixing between the recirculating flow and the main flow, and this can cause a strong inducer stall.

These points are developed bellow,

Point 1: MWE1 encourages negative pre rotation at impeller inlet

If the tested MWE1 configuration imposes negative pre-rotation at impeller inlet, this can explain the surge line shift to high flow rates, since negative pre-rotation triggers inducer stall at higher flow rates, due to high incidence losses.

However, as mentioned before, the hole apparatus cannot encourage any negative pre-rotation at the impeller inlet, due to the thickness of the inlet compressor inlet tube [3mm] and the angle 90° of holes with the tangential directio n.

Point 2: Holes have improved impeller diffusion,

Improved impeller diffusion can be seen in the healthy form of the pressure line. The good impeller diffusion decreases velocity in the diffuser, hence the angle at the inlet of the diffuser which triggers a diffuser stall at higher flow rates. Then shifting diffuser stall at high rotational speed can explain the early surge.

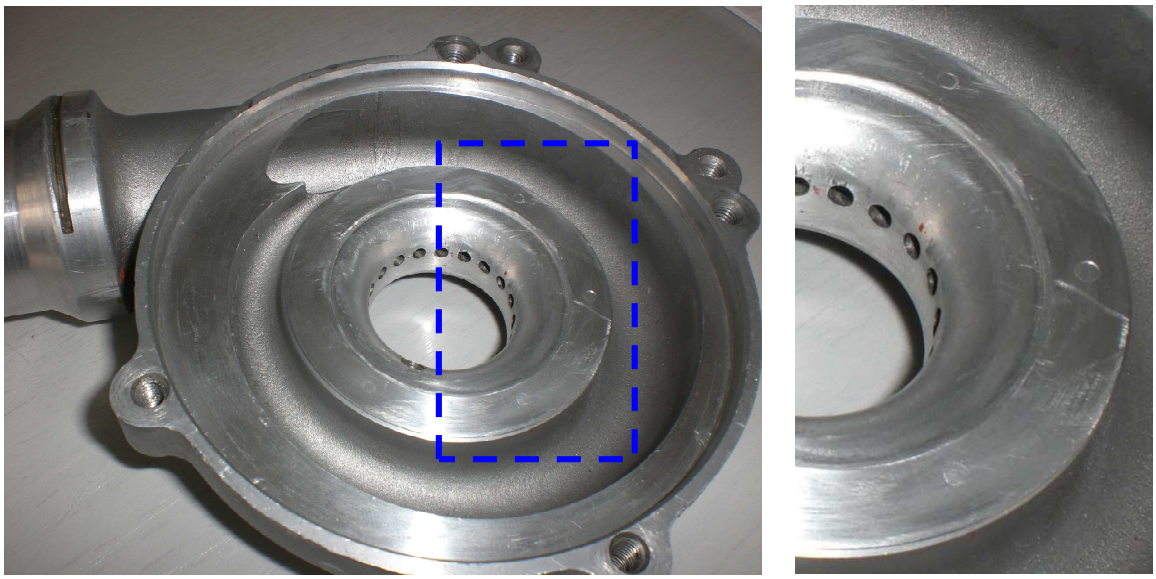

Figure 4-53 MWE1 system accompanied to a pinched diffuser [a zoom to the pinched zone to the left]

To verify this hypothesis, a new test was done with a pinched diffuser accompanied the MWE1 system. The goal of this test was to increase diffuser inlet angle, and see if the diffuser was responsible of surge.

The tested pinched MWE1 is shown in Figure 4-53. A pinch was introduced at the shroud side of the diffuser, so that the diffuser area was decreased by 20%.

Instabilities suppress in the diffuser, was obtained by increasing radial velocity in the vaneless diffuser by mounting pinches in its shroud side. As it can be seen from Figure 4-54, the pinched MWE1 system has improved surge line at low rotational speeds [diffuser is responsible of compressor stall at low rotational speeds [chapter III]]. However, very slight surge line improvement was obtained at high rotational speeds. Hence we can conclude that the diffuser does not cause surge line shift at high rotational speeds.

Figure 4-54, shows the isentropic efficiency when mounting pinches on the MWE1 system compared to basic characteristics and standard MWE1. As it can be seen, efficiency drops at almost all the flow range, with greater drop at high flow rates. This can be explained by friction losses increase in the diffuser, due to velocity increase. Moreover, efficiency drop at low flow rates comes probably from flow recirculation which increases inlet temperature.

Point 3: Early surge can be explained by volute instabilities,

Volute circumferential pressure distribution propagates upstream and imposes periodic outlet conditions on the impeller [Van den Braembussche, 2006 (61)]. Moreover, Fischer, 1988 (93) observed that the volute tongue sets up a circumferential disturbance that gives to a non uniform pressure field in the inducer, which can cause premature stalling, eventually leading to surge. This strong interaction between the impeller and the volute is still not very well understood.

Some changes to flow conditions in the volute was done by slight increasing the diffuser area [11% increase], so that the diffuser velocity decreases hence radial velocity in the volute decreases. This changes the pressure distribution in the volute, and hence the effect of the volute on the impeller.

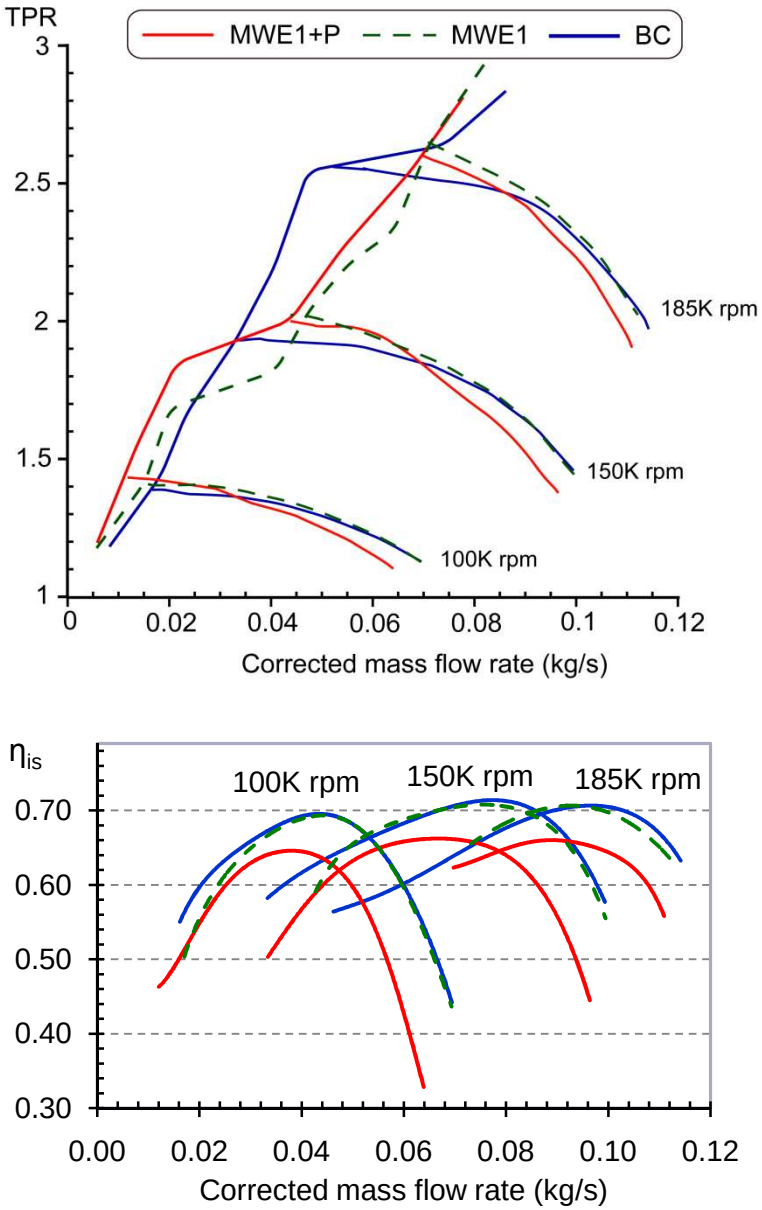

Figure 4-54 MWE1 with pinched diffuser compared to standard MWE1

Figure 4-55 shows the effect of this slight increase in diffuser area on compressor performance and surge line. It can be seen that a very slight improvement in surge line was observed, however, compression ratio ability increases all over the flow range.

The slight surge line improvement can be explained by unloading volute [changing circumferential pressure distribution], and reducing angle at the volute tongue, which delay volute instabilities.

The increase in diffuser area, reduces radial velocity, hence increases volute diffusion. This increases pressure recovery in the volute, and increases compressor compression ability.

Since there is often an efficiency loss arising from the inability of the volute to convert the kinetic energy associated with radial velocity. Reduction of radial velocity, increases volute efficiency.

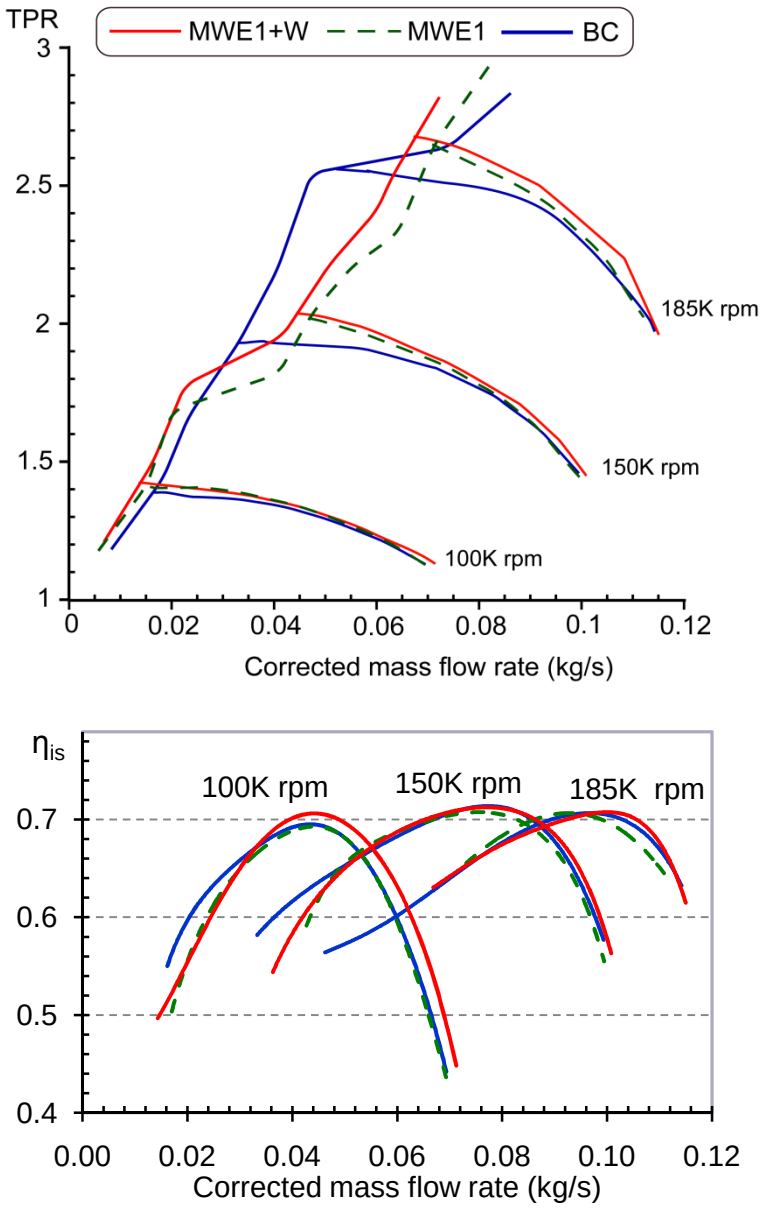

Figure 4-55 MWE+WI compared to standard MWE

Point 4: very strong inducer stall

Using standard MWE1 case, the reverse flow coming out of the MWE holes is remixing with the main flow inlet and therefore causing a disturbance to this flow. This disturbance can cause a strong inducer stall and enter the stage in a strong stall which triggers compressor stall.

A simple method to suppress this disturbance is to increase the inlet pipe length. The long pipe helps to move the recirculating flow further upstream and therefore the impeller inlet is more uniform.

Figure 4-56 Tested Super-MWE system

For this goal, a long inlet pipe was mounted in the MWE1 system, so that L/Di equals 32,3. Braham, [2004] called the new system, a super MWE1 system [we will use this nomination for the rest of this work]. Inner pipe length extension and the complete support system [fabricated at the Ecole Centrale de Nantes] is shown in Figure 4-56.

	TPR=2.5	TPR=2
MWE1+L / BC	37 %	30 %
MWE1+L / MWE1	57 %	46.7 %

Table 4-1 surge line improvement using MWE1+L compared to BC and standard MWE1

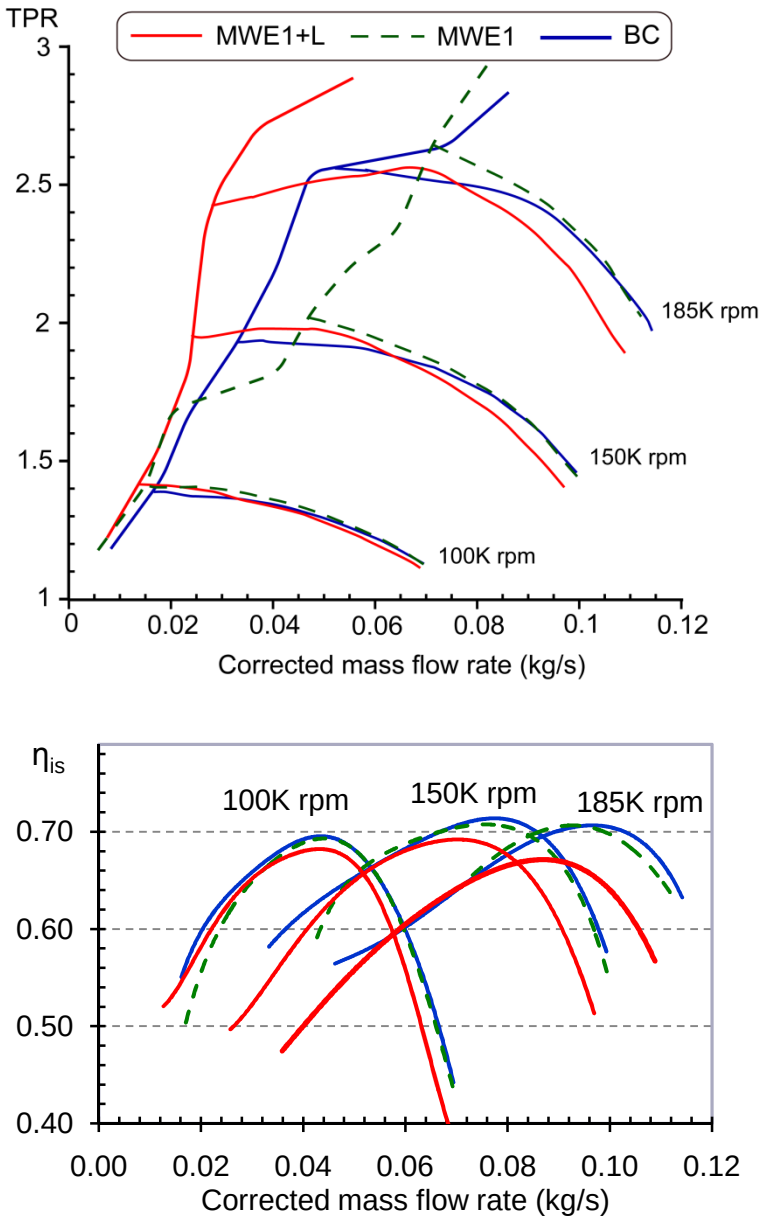

Figure 4-57 Super MWE1 system compared to standard MWE1

As it can be seen in Figure 4-57, increasing the inlet pipe length results in proportional improvements in surge margin, with a great increase at high rotational speeds. A 37% improvement in surge line is obtained at TPR=2.5 compared to compressor basic characteristics [Table 4-1].

The surge line improvement can be explained by the more uniform flow at the impeller inlet. This is due to moving the recirculating flow further upstream of the impeller. This improvement is very interesting since, while eliminating the hypothesis of diffuser stall at high speeds, and good impeller diffusion compared to the basic characteristics. One can conclude from the preceding results that the inducer stall can explain compressor stall at high speeds, and this stall is caused by flow disturbance due to mixing of MWE flow and main flow.

An infinite pipe length would provide ultimate improvement, hence isolating the MWE from the main compressor inlet. However, practically we cannot operate the compressor with the slots or holes completely opened.

Finally, the MWE+L causes a decrease in efficiency accompanied with pressure drop at high flow rates. This may be due to increase in flow velocity, hence friction losses, when more flow enters the impeller through the holes.

4.2.2 MWE2 System

The tested hole apparatus in system MWE1, did not support flow in the direction of rotor rotation at low flow rates. However, the surge line improvement obtained by Nikpour, 2004 (112), and Hunziker et al, 2001 (141), was explained by the positive pre-rotation imposed by the bleed slots at the compressor inlet which lowers the relative tip Mach number in the impeller entrance, and helps in unloading the impeller, hence shifting surge line to low flow rates.

Then it is interesting to study a new MWE configuration, with holes encouraging flow rotation at impeller inlet, in the direction of rotor rotation. The new configuration is presented and tested in this section.

The new configuration was based on the following points,

- The static pressure distribution at the casing, for the two flow rates, one near surge and one near choke, at a constant speed line [Figure 4-58]. We used Matlab to program the one dimensional model, where the program output is the static pressure along the shroud casing. More details of one dimensional model are presented in Appendix B.
- The results of MWE1, in addition to the angle with the vertical used in MWE1, an angle with the tangent was added to produce a negative swirl when mixing with the air entering the compressor. Moreover, a maximum number of holes was done so that the MWE2 was similar to a bleed slot system with vanes to produce swirl to the recirculating fluid.

The holes were positioned at 40% from the leading edge along the meridional length. The position was chosen so that in operating near surge the pressure difference between downstream holes and the bypass inlet forces some part of the fluid entering the impeller to recirculate.

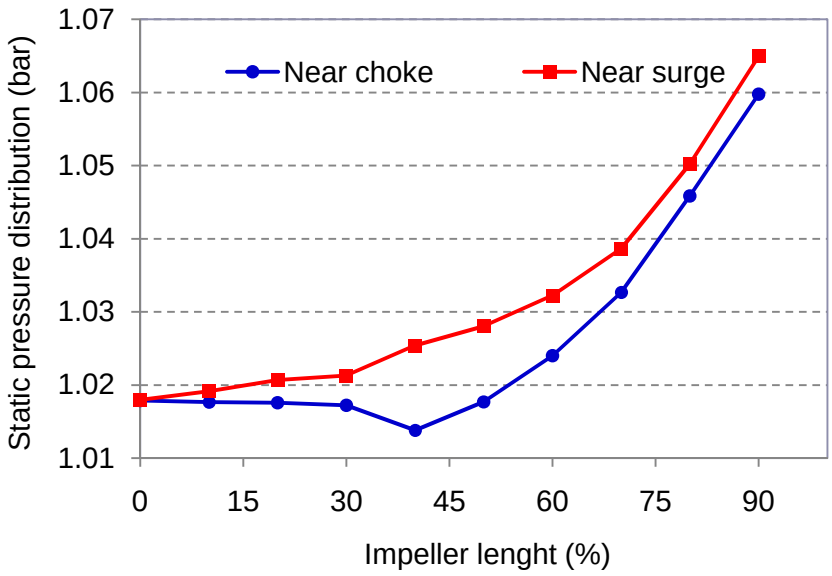

Figure 4-58 Static pressure distribution along the casing

On the other hand, at the near choke operating points with inducer negative incidence the pressure difference between the downstream hole and the bypass is negative and fluid is sucked into the impeller, bypassing the inducer inlet.

Between these two operating points an operating condition exists at which no pressure difference between the downstream holes and the bypass inlet occurs, under these conditions, there will be no flow through the map width enhancer system and no improvement in surge line will appear.

The design process is completed by the choice of three variables, namely the diameter if the holes, the angle with the vertical [perpendicular to the axis of the compressor in the radial direction], the angle with the tangent [tangent to the rotor], and the number of holes.

As mentioned before, the idea was to maximize the number of holes while maintaining a reasonable distance between them. 30 holes were done with 2mm diameter. The number of holes is arranged so that it is not equal to, a multiple of or a factor of the number of impeller blades. The overall holes area was about 14.3% of the annular inlet area. The tested MWE2 is presented in Figure 4-60.

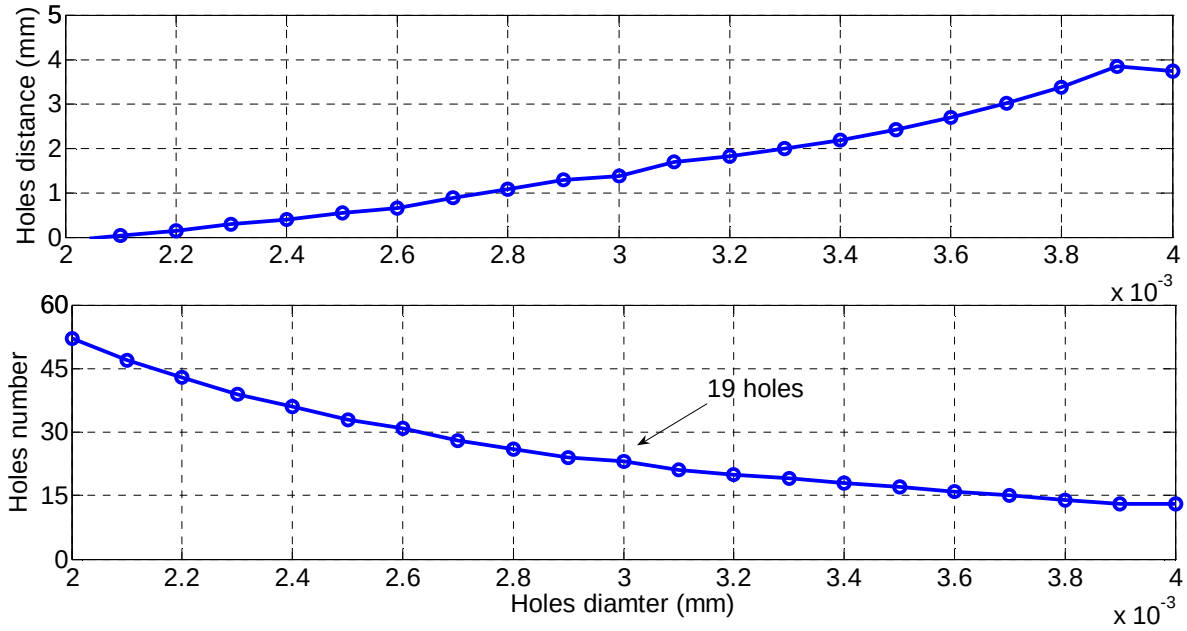

Figure 4-59 Number of holes and distance between them for different hole diameters, for a total hole surface of 20.3% of annular inlet, case of MWE1

❖ Results and discussions

The New MWE configuration was designed to support flow in the direction of rotor rotation at low flow rates, which lowers the relative tip Mach number in the impeller entrance, thus delaying impeller stall [[Nikpour, 2004 (112)] and [Hunziker et al, 2001 (141)]].

Effect on compressor performance and surge line of the MWE2 compared to the MWE1 configuration is presented in Figure 4-61. As it can be seen, the two maps [MWE1 and MWE2] are nearly superimposed in terms of compression ratio capability and isentropic efficiency.

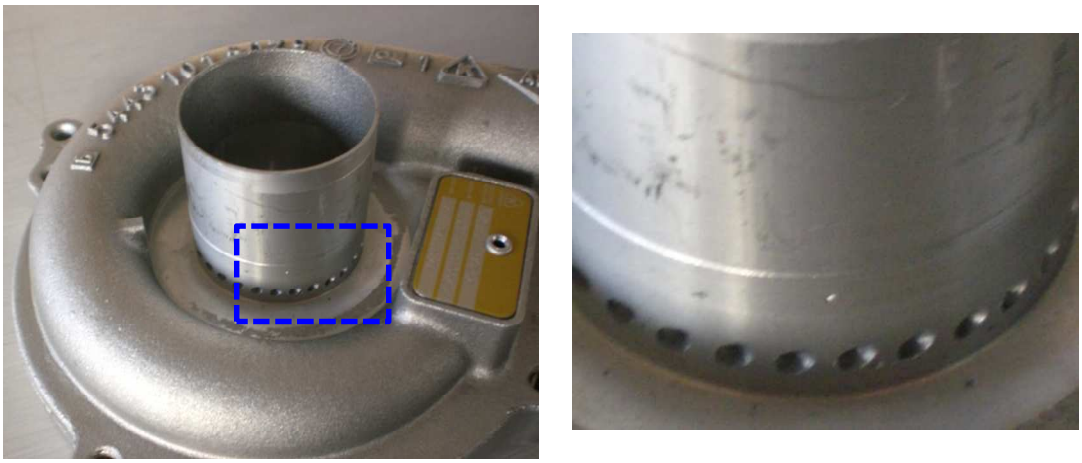

Figure 4-60 the tested MWE2 system [to the left], with a zoom on the holes [to the right]

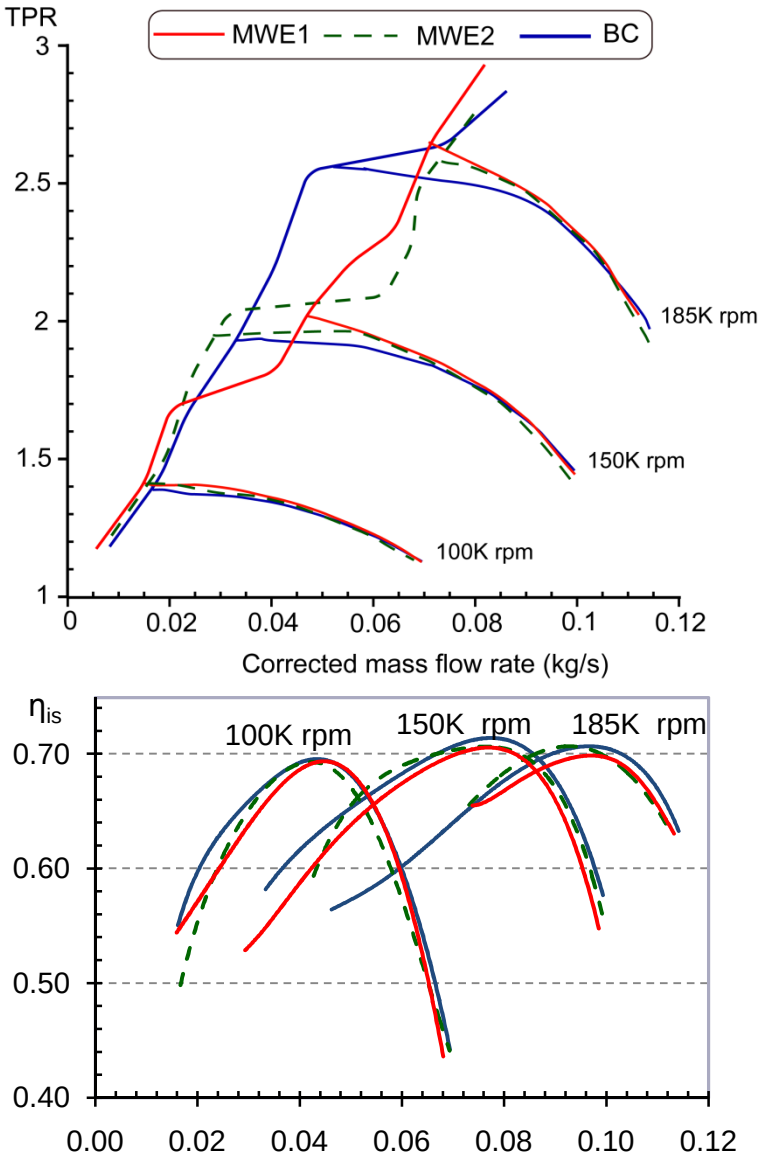

Figure 4-61 MWE2 compared to MWE1

On the other hand, the surge line shifts to low flow rates compared to MWE1 configuration, at middle rotational speeds. However, the MWE1 was more advantageous at high rotational speeds. One can conclude that the flow rotation in the direction of rotor rotation, imposed by the MWE2 configuration has not positively influenced impeller instabilities at high rotational speeds.

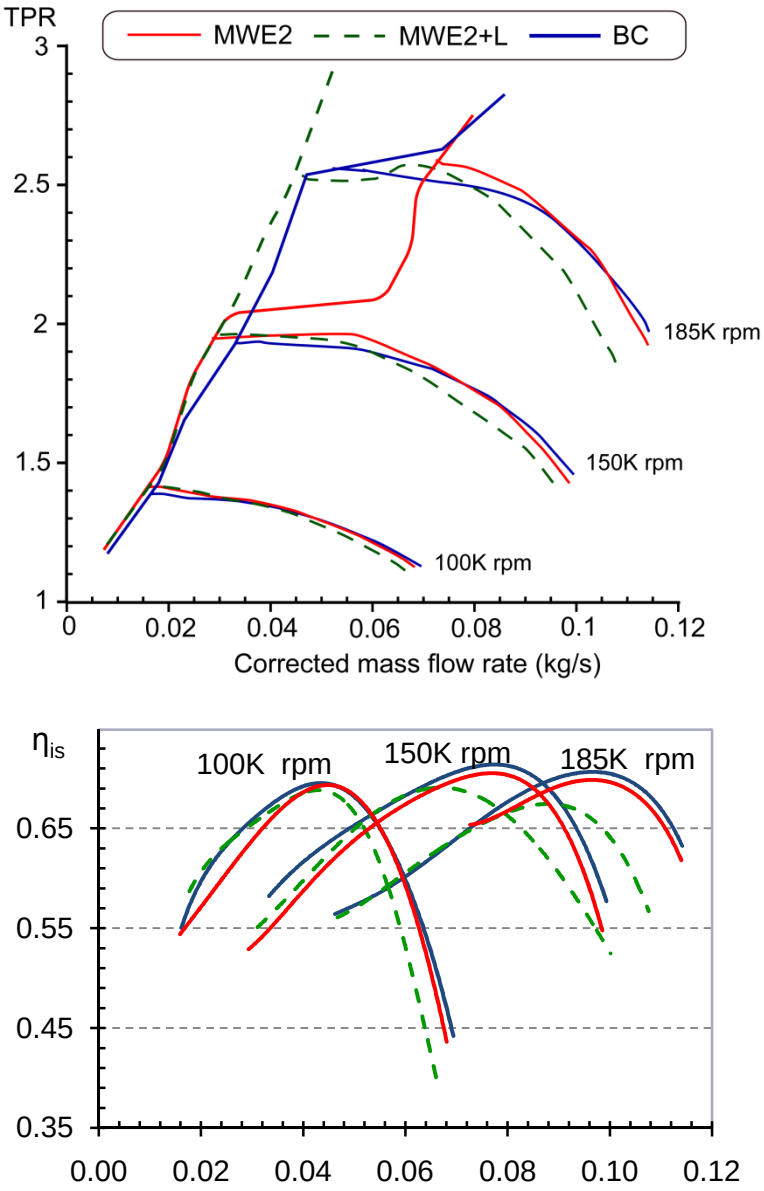

Figure 4-62 MWE2 system compared to MWE2+L

Experiment was conducted with increasing the pipe length of the MWE2 configuration, and results show a significant improvement with respect to standard MWE2. This increase is significant at high rotational speeds [40% surge line shift to low flow rates compared to basic characteristics].

The surge line shift to low flow rate, is probably due to a more uniform flow at compressor inlet, due to delaying impeller stall, when extending the inner pipe length.

As it can be seen from the isentropic efficiency curves, efficiency and pressure ratio drops at high flow rates, while it remains nearly constant at low flow rates compared to basic characteristics. This can be explained by the more uniform flow at impeller inlet.

Efficiency results are quiet interesting, since, if a kind of variable geometry system can be designed so that the holes are open at low flow rates and closed for high flow rates. Then we'll be able to improve surge margin without scarifying compressor efficiency.

4.2.3 Conclusion

Applying casing treatment to turbocharger compressor was studied in this work, different MWE configurations were tested, with holes as connecting apparatus between the inner and outer tubular. Two series of holes were tested:

MWE1 configuration: 19 holes, with 3mm diameter each (an overall holes area of 20.3% inducer inlet area), holes having angle 75 degree with the axial direction.

MWE2 configuration: 30 holes, with 2 mm each (overall holes area of 14.3% inducer inlet area). Holes having an angle 45 degrees with the tangential direction (tangent to rotor rotation) and angle 30 degrees with the radial direction.

The two configuration increase compressor pressure ratio capability, this is probably due to a better diffusion in the radial portion of the impeller. Efficiency was nearly conserved at high flow rates and drops at low flow rates due to flow recirculation (temperature increase of the recirculated flow at low flow rates).

Surge line was not improved at high speeds, in the either cases (MWE1 and MWE2 standard configurations). This was probably due to a strong inducer stall caused by flow disturbance due to mixing between the main flow and the MWE flow. Increasing pipe length helped to displace flow disturbance further upstream of the impeller inlet, thus having a more uniform flow at compressor inlet. This improves significantly surge line particularly at high rotational speeds, with higher shift obtained when using MWE1 configuration (up to 47% in the MWE1 case, and 40% in the MWE2 case, with respect to basic characteristics, at high pressure ratio). The more surge line shift when using MWE1 configuration is probably due to bigger total holes area (20.3% of inducer annular area) compared to MWE2 configuration (14.3% of inducer annular area).

In addition to the surge line shift obtained when increasing the pipe length, efficiency was nearly conserved at low flow rates. Even if at high flow rates, pressure and isentropic efficiency drops, this result is very interesting in case we can use a variable geometry MWE system, so that holes open at low flow rates and closed for high flow rates (with holes closed, compressor characteristics does not changes with respect basic characteristics). Then we're be able to improve surge margin without scarifying compressor efficiency.

It will be interesting to test the super MWE configurations to inlets having one or more bends (inner and outer tubular which have axis which curves away from the axis of the impeller). In addition to a variable geometry system to close and open holes when necessary.

Further work is needed to find the best practical ways of exploiting the improvements observed.

4.3 Delaying diffuser instabilities

Approaching diffuser stall, the radial velocity is much smaller than tangential velocity. Increasing stall critical angle can be done by either decreasing tangential component or increasing the radial one or the two at the same time.

This section is organized as follows: increasing radial velocity component in the diffuser using pinches and its effect on compressor overall performance and surge line, is given in

the first part. In the second part, the effect on the compressor performance of decreasing the tangential component using radial shallow grooves mounted in the diffuser casing wall, is studied.

4.3.1 Effect of pinched diffuser on compressor surge line and performance

Even though a vast amount of literature is available on vaneless diffusers in centrifugal compressors, there is a lack of information about the effect of the pinch on the turbocharger centrifugal compressor performance.

This research has two main objectives.

1. To study the effect of suppressing vaneless diffuser instabilities on surge line, pressure and isentropic efficiency of the turbocharger centrifugal compressor. Instabilities suppress, was obtained by increasing radial velocity in the vaneless diffuser by mounting pinches in its shroud side.
2. To establish the most creditable basis for a practical variable geometry device.

Case	$\left({}^{b_p}/_{b}\right) * 100$	pinch
1	100	BC
2	57	P1
3	76.5	P2
4	87.5	P3

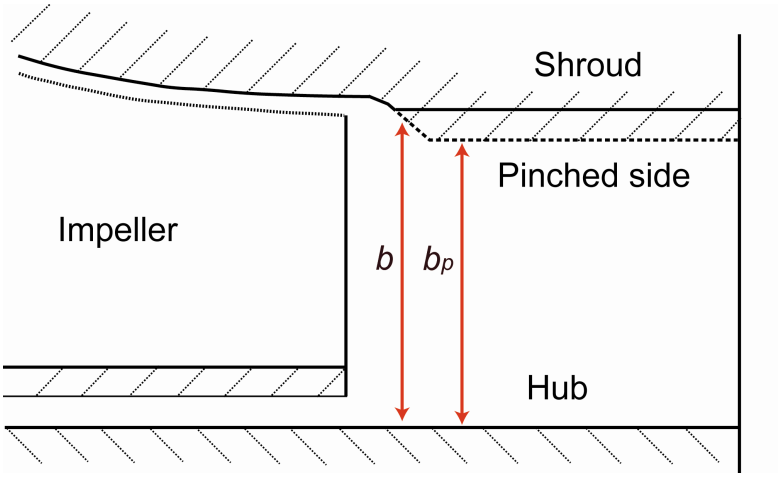

Table 4-2 Different pinch constructions

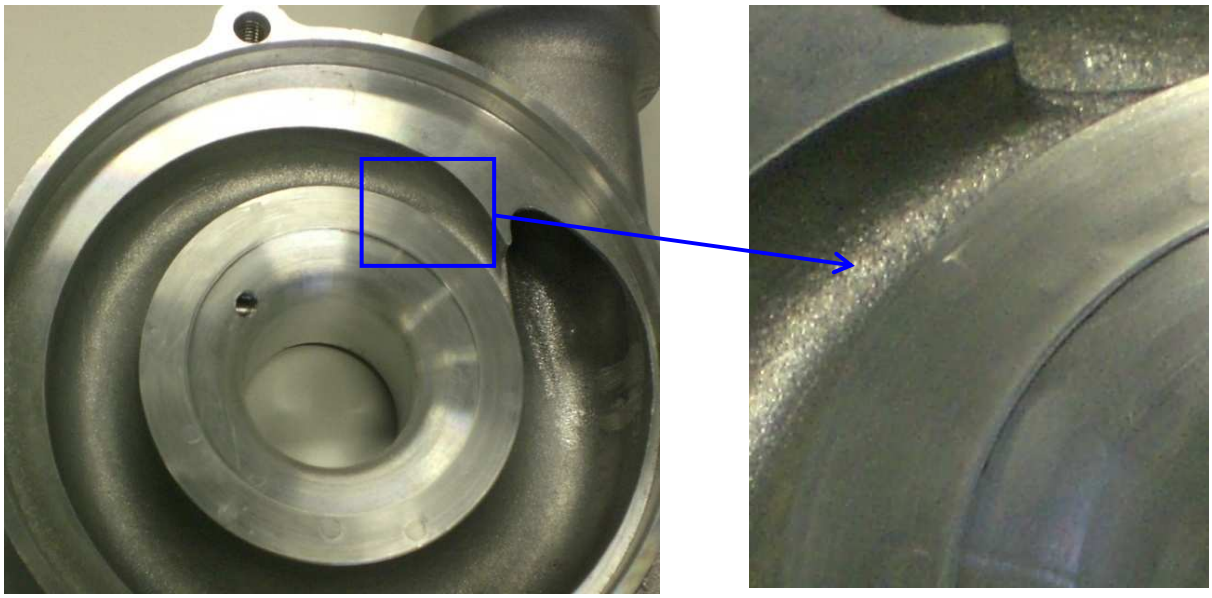

Figure 4-63 tested Pinched configuration. P3 to the left and zoom to the right

Three different vaneless diffusers geometries were investigated by introducing pinches at the shroud side of the diffuser, to simulate a variable geometry diffuser which could be achieved through a system that will be proposed later. Table shows the geometry of the three tested configurations, together with a 2D scheme to clarify. [P3] tested configuration is presented in Figure 4-63.

❖ Result presentation

As it can be seen from Figure 4-64, shrouded pinches have moved surge line to low flow rates, with small pinches having the smallest effect and highly pinched diffuser having the greatest improvement. On the other hand, this surge line shift is accompanied by a total pressure drop which increases with pinch increase.

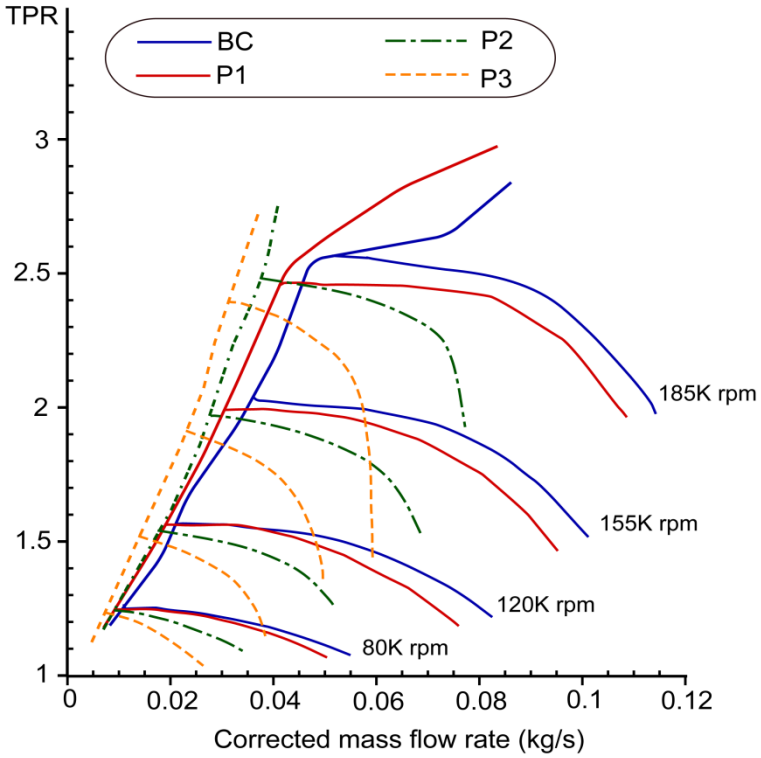

Figure 4-64 Compressor total pressure ratio, using three different configurations compared to basic characteristics

Table 4-3, represents a quantitative comparison between improvements obtained when using a pinched diffuser compared to compressor basic characteristics at two different pressure ratios. As it can be seen, a 30% increase in surge line can be obtained using [P1] at TPR=2.

Pinched diffuser	P1	P2	P3
Surge line displacement [%] , TPR =2	30	17.4	11.4
Surge line displacement[%], TPR =2.5	28.2	17.3	8.6

Table 4-3 Surge line improvement for each of the pinch configurations compared to the compressor basic characteristics at TPR=2 and TPR=2.5.

Table 4-4 shows another way to look at the improvement obtained when using pinched diffuser. The total stable pressure increase for a corrected mass flow rate of 0.03 kg/s and

0.02 kg/s respectively. About 0.5 bar total stable pressure increase was obtained when mounting the [P1] configuration.

Pinched diffuser	P1	P2	P3
TPR increase [bar], at 0.03kg/s	0.48	0.22	0.13
TPR increase [bar], at 0.02kg/s	0.25	0.1	0.09

Table 4-4 Total stable pressure increase when using pinched diffuser compared to the compressor basic characteristics at TPR=2 and TPR=2.5

As it can be seen from Figure 4-65, using pinches has dropped the compressor isentropic efficiency at high flow rates. However, for pinched diffuser configurations [P2] and [P3], isentropic efficiency almost matches the efficiency of the baseline configuration at near surge line zone. A quantitative study is presented in Table 4-5.

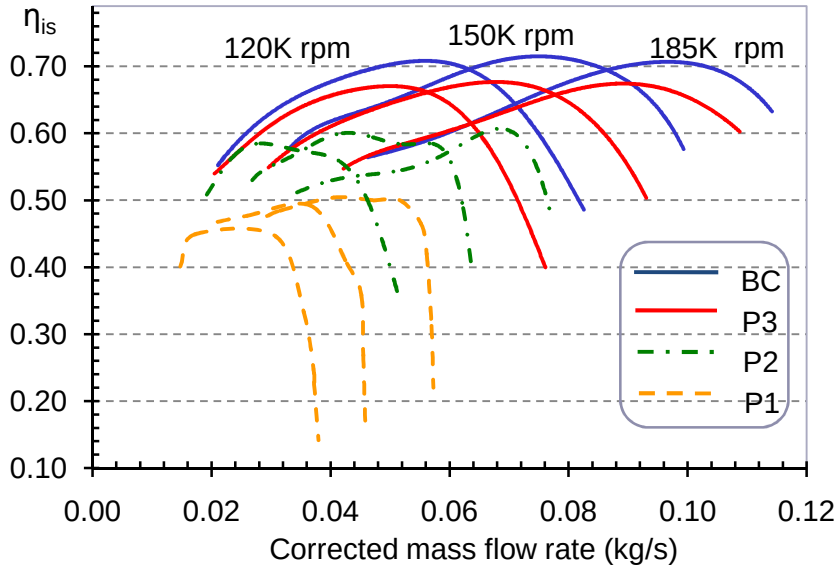

Figure 4-65 Compressor isentropic efficiency when using the three configurations compared to basic characteristics

Pinched diffuser	P1	P2	P3
η_{is} decrease at S1	15.9	3.2	1.4
η_{is} decrease at S2	13.6	2.24	0.5
η_{is} decrease at S3	10.5	2.1	0

Table 4-5 Total to total isentropic efficiency at three pinch configurations, at three near surge points: S1, S2, and S3

Where,

S1 is the surge point at N=120K rpm [Qc=0.0219 kg/s]

S2 is the surge point at N=150 K rpm [Qc=0.033 kg/s]

S3 is the surge point at N=185 K rpm [Q_c=0.046 kg/s]

❖ Result analysis

The surge line move to low flow rate, can be interpreted in the following way,

- Suppressing instabilities in the diffuser due to increasing the radial velocity and consequently the flow angle at the diffuser inlet, hence decreasing the critical flow angle.
- Since a stage stall is a collective stall of different components, then suppressing the diffuser instabilities, may delay the stage stall and hence the system surge.
- More impeller uniform flow, due to improving impeller diffuser interaction.

On the other hand, the pressure losses due to pinch mounting can be explained by the two following points

- Increase in friction losses due to increase in the diffuser radial velocity, due to reduction in flow area.
- Losses due to dissipation of radial component of velocity in the volute.

The increase, in surge margin and total pressure stable functioning at low flow rates was accompanied by a high pressure drop at high flow rates. The pressure drop is caused by frictional losses increase due to increasing velocity, and radial energy losses in the volute.

We focused on the effect of applying the different configurations on the compressor performance and surge line in the near surge line zone. Hence, future industrial application can be to apply a variable geometry diffuser, where diffuser area can be reduced in real time near the surge line hoping to move surge to low flow rates,

To illustrate the effect of introducing variable geometry to the vaneless diffuser, different diffuser area reductions have been studied in this section. It has been showed that varying diffuser area can significantly move surge line to low flow rates. If a variable geometry diffuser can be machined so that it can decrease the diffuser area at near surge in real time, a great increase in surge operating range can be obtained.

In addition to increasing surge line, the introduction of a variable component, for reasonable values of diffuser area decrease[$b_p / b < 0.7$], can at least match the efficiency of the baseline configuration in this region.

Whitfield and Sutton [1989], concluded that a greatest modification of compressor performance can be obtained if the hub side of the diffuser is modified. It will be interesting to study the effect of hub modifications. Unfortunately, this type of modifications is difficult to be done and was not tested due to machining constraints and complexity.

4.3.2 Effect of diffuser J-grooves on compressor surge line and performance

Most of the studies done on shallow grooves agreed that the groove reverse flow rate critically evaluates the effectiveness of the grooves, since it is responsible of increasing diffuser inlet flow angle, due to the following effects [Gao et al, 2009 (90)]

1. Flow in the grooves losses all its angular momentum
2. Most of the groove flow re-enters into the main flow at the groove starting segment and thus increases the radial velocity near diffuser walls.

The groove reversed flow can be calculated using radial pressure gradient equations after substituting for the wall shearing stress. Reverse flow is expressed by Gao et al, 2009 (90) as,

$$m_G = 2.87 \frac{\vartheta^{\frac{-1}{7}} \bar{C}_\alpha^{\frac{8}{7}} d^{\frac{12}{7}} w^{\frac{12}{7}} n}{(2d+w)^{\frac{5}{7}} R^{\frac{4}{7}}} \quad 4\text{-}11$$

Where, $\bar{C}_\alpha$ denotes the average value over the groove section, and ϑ air kinematic viscosity. According to equation 4-11, the effectiveness of reverse flow in J-grooves is greatly determined by the following geometrical parameters:

- Width of the groove, w
- Length of the groove, l
- Depth of the groove, d
- And number of grooves, n

Based on equation 4-11, a combination between the different geometrical parameters, named F, to be the governing relation between groove parameters to control stall was proposed by Gao et al (90). The author also included the influence of the upstream impeller to make this parameter more meaningful, and therefore the impeller exit radius was used in equation 4-12.

$$F = \left(\frac{d}{R_2}\right)^{\frac{12}{7}} \left(\frac{w}{R_2}\right)^{\frac{12}{7}} \frac{n}{\left(\frac{2d}{R_2} + \frac{w}{R_2}\right)^{\frac{3}{7}} \left(\frac{l}{R_2}\right)^2} \quad 4\text{-}12$$

4.3.2.1 Tested groove configurations

Two configurations have been tested to study the effect on compressor performance and surge margin of J-grooves mounted in the diffuser casing wall [shroud side]. Geometrical characteristics of tested J grooves are shown in Table 4-6.

Tested grooves geometrical characteristics are based on the afore mentioned discussions, and are as follows,

Grooves length, l was chosen to have the diffuser length. This decision was based on the work of Kurokawa et al, 2000 (167), who studied the effect on suppressing rotating stall of different groove lengths, and he concluded that only the longest groove totally suppress rotating stall even at zero flow rate.

Case	Groove geometry parameter	Groove
1	n=12; w=3; d=0.3; l=11	GR1
2	n=6; w=3; d=0.3; l=11	GR2

Table 4-6 Different groove constructions

For parameters w, d and n. Dimensioning was based on the work of Gao et al, who concluded that no matter how d, w, and n vary as long as the value of F is not changed the effect of grooves would be approximately the same. Moreover, they added that, the greater the value of F, the smaller the critical flow rate is hence greater the stable margin of the diffuser. Figure 4-66 shows the two tested grooves GR1 and GR2.

Figure 4-66 tested J grooves configurations. GR1 to the left and GR2 to the right

For this study, we chose to study two different values of F [big and small value]. Limited by manufacturing constraints, w and d were not changed, and the value of n was varied to change the value of F [Figure 4-67].

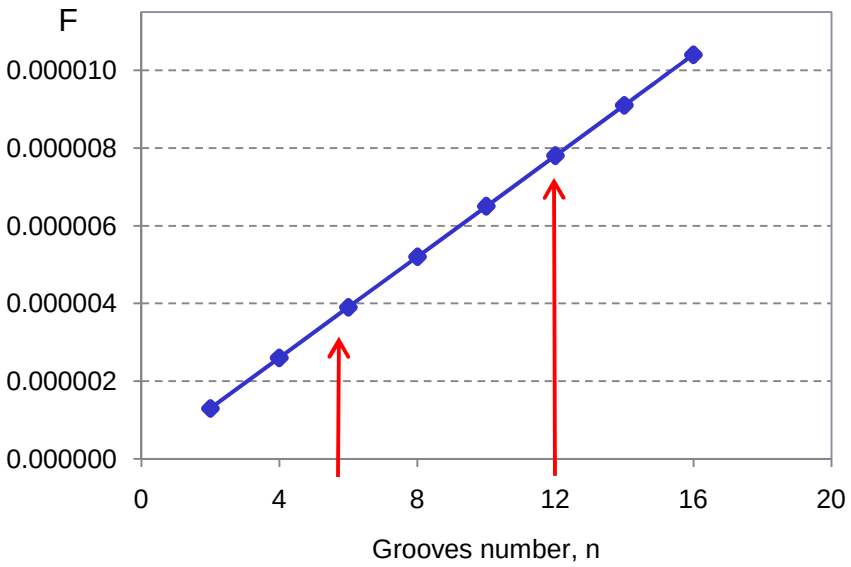

Figure 4-67 High and low values of F were chosen

❖ Results and discussions: GR1 configuration

Figure 4-68 shows the effect on the compressor performance and surge line of GR1 configuration. As it can be seen, the surge and choke lines move to low flow rates. Surge line shift can be explained by increase in diffuser operating range. This stability increase, delay the compressor stage stall.

The choke line move to low flow rate, can be explained by the high increase in the radial component at diffuser exit and choke may exist at the volute tongue due to high angle of attack which causes flow separation in the exit cone and downstream the tongue.

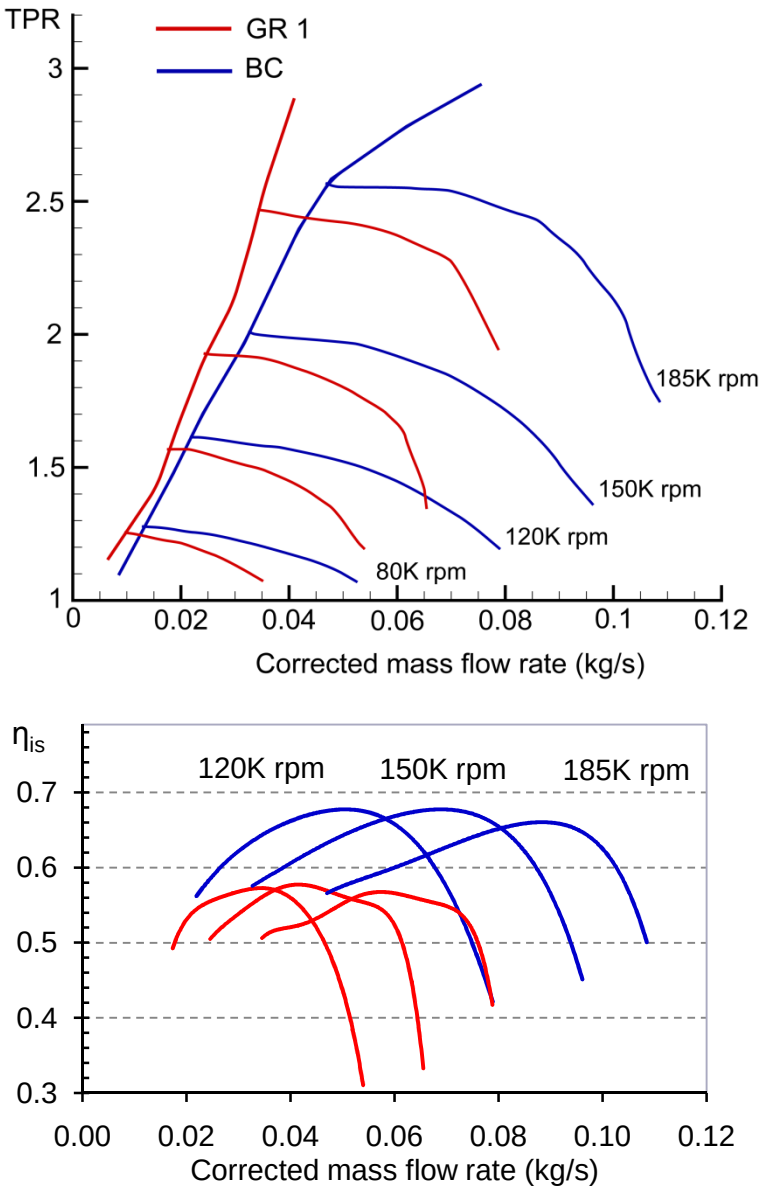

Figure 4-68 Effect on compressor performance and surge line of GR1 configuration

The surge line move to low flow rate was due to increasing diffuser stability by increasing radial velocity and consequently inlet diffuser angle.

The surge line move toward low flow rate is accompanied by high total pressure loss. This pressure loss can be explained by the following factors.

1. Increase in diffuser skin losses due to increase in surface area
2. Loss in the volute of the kinetic energy associated with the radial component at the Increase in the radial component in the volute,

Big F values were advantageous in delaying diffuser instabilities. However, the surge line shift was accompanied by efficiency decrease, and total pressure drop.

❖ Results and discussions: GR2 configuration

Interesting results were obtained when using GR2 configuration. At high flow rates and almost all speeds, pressure and efficiency increases accompanied by surge margin slight increase [Figure 4-69].

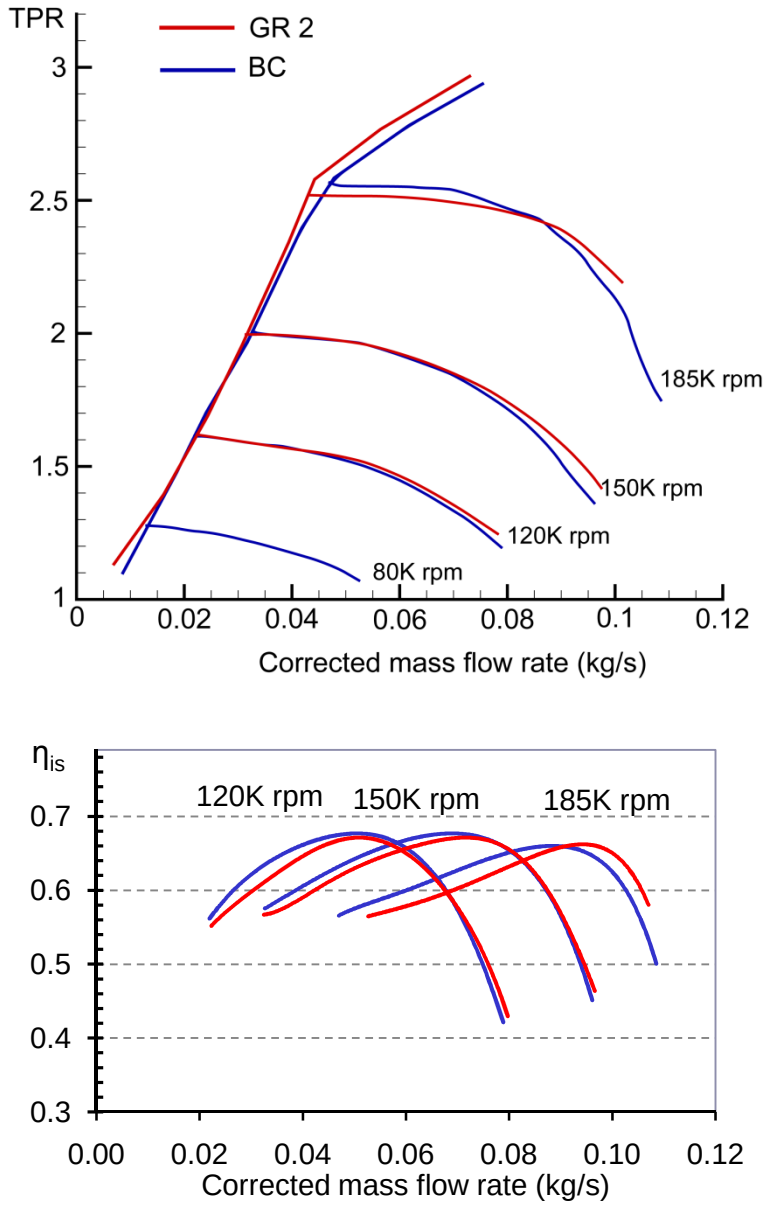

Figure 4-69 Effect on compressor performance and surge line of grooved system, GR2

The slight diffuser area increase was probably advantageous in improving impeller diffuser interaction. Hence, more uniform flow in the impeller and the diffuser. This can explain the slight efficiency and pressure increase at high flow rates.

The slight surge line shift is probably due to tarden diffuser instabilities, due to radial velocity increase in the diffuser. However, this increase was lesser than that obtained for high F values [GR1 configuration].

4.3.3 Synergy effect of pinched diffuser and grooves: GRP configuration

The idea behind the GRP configuration is to add two different techniques to increase radial velocity. GRP configuration is presented in Figure 4-70 and its geometrical characteristics in Table 4-7.

Groove geometry parameter	Pinch geometry	Configuration
n=6; w=3; d=0,3; l=9,5	$b_p / b = 0.85$	Pinched shroud + grooves [GRP]

Table 4-7 configuration geometry

Figure 4-70 Tested Grooves on pinched diffuser [GRP]

❖ Results and discussion

As it can be seen from Figure 4-71, results obtained are similar to those obtained when using GR2 configuration, with much higher efficiency, pressure ratio increase at high flow rates, and more efficiency and pressure losses at low flow rates, compared to the same configuration.

Efficiency increase at high flow rate is quite interesting. However, unfortunately we still have no exact explanation of this increase. It's highly possible that the GRP configuration improves impeller diffuser interaction, hence more uniform flow in these two components.

Different pinched, and grooves diffuser configurations are tested in this section. While these techniques are used in industrial compressor to suppress diffuser instabilities by increasing radial velocity in the diffuser at low flow rates, there is still a lack of information about their effect on turbocharger compressor.

While pinches were efficient in delaying diffuser instabilities. It creates high pressure and efficiency losses, due to friction losses increase in the diffuser. Reasonable area reduction is advantageous in improving impeller diffuser interaction.

Grooves are probably advantageous in delaying diffuser instabilities, hence shifting surge line to low flow rates. However, grooves number and dimensioning affect on compressor performance varies from surge line increase [high F values] to slight surge line shift but efficiency and pressure ratio increase at high flow rates [for small F values]. This efficiency increase is probably due to impeller diffuser interaction.

Further investigations are needed to better understand the obtained results.

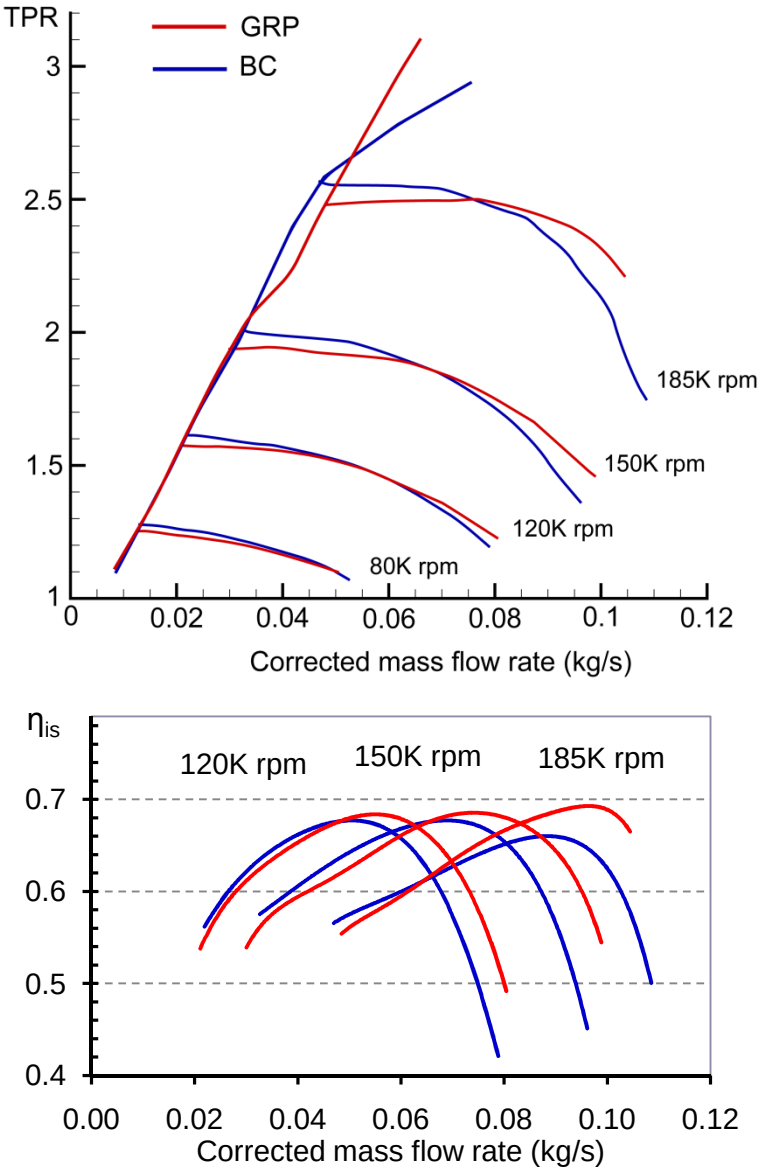

Figure 4-71 Effect on compressor performance and surge line of grooves mounted on a shrouded pinch diffuser, GRP

4.4 Delaying volute instabilities

The effect of the tongue shape on the overall characteristics of the compressor is experimentally investigated in this section. The tongue was retracted and rounded, as presented in Table 4-8.

	$\frac{t}{D_3}$	α_{tg}
TG1	0.085	27°
TG2	0.125	44°

Table 4-8 New volute tongue

Where t is the clearance between diffuser and the tongue and D_3 is the diffuser diameter. α_{tg} is the tongue angle with respect to the tangential [Figure 4-72].

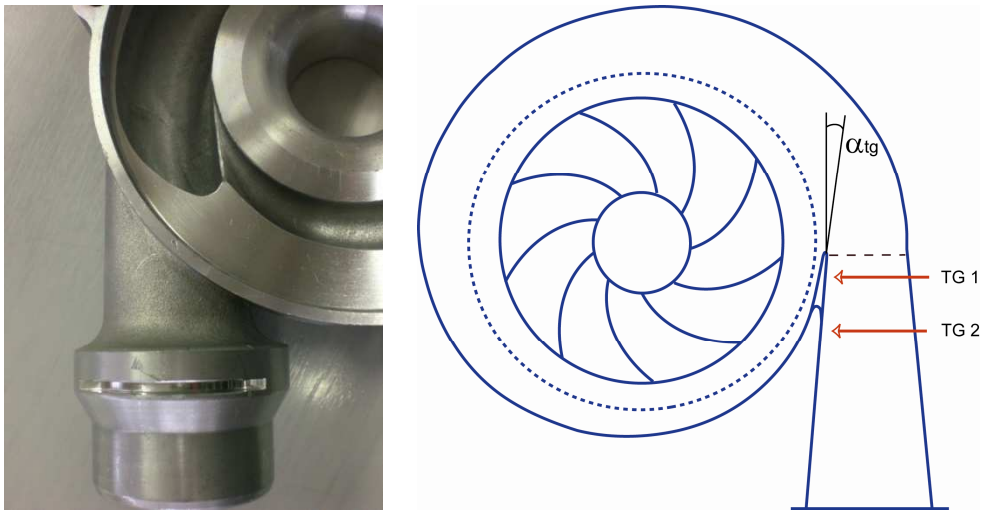

Figure 4-72 Tongue shape TG2 compared to basic tongue shape TG 1 a] tested volute b] 2D presentation

❖ Results and discussion

Results obtained when retracting and rounding volute tongue can be resumed in the following 3 points,

1. Compression ratio slightly increases both at low and high flow rate while retracting and rounding the tongue, this increase becomes higher at high rotational speeds. A similar head increase was reported by Dong et al,1997 (69) when retracting a tongue of a pump volute.
2. The isentropic efficiency increases at middle flow rates.
3. Unless a very slight increase in the surge line at high rotational speed, surge line has not been affected by tongue retraction. Its worth noting that, Lipski [1979] experiments on pump volute, showed that the pump efficiency at the design point was also increased by shortening of the tongue, which indicates the volute or the tongue were also mismatches.

Results can be explained in the following way,

1. Compression ratio increase can come from a more uniform pressure distribution in the tongue, a more uniform static pressure around the circumferential which creates a more uniform flow in the impeller or the diffuser. This same explanation can proof the stage efficiency increase
2. As discussed in chapter III, blockage at the tongue of the volute was believed to increase the circumferential pressure along the volute, the non uniformity may lead impeller or diffuser to operate unstably, or can amplify impeller or diffuser instabilities. However, it is not the volute that directly controls stall. This explanation is confirmed in this section. The volute tongue changes have not influenced the surge line.

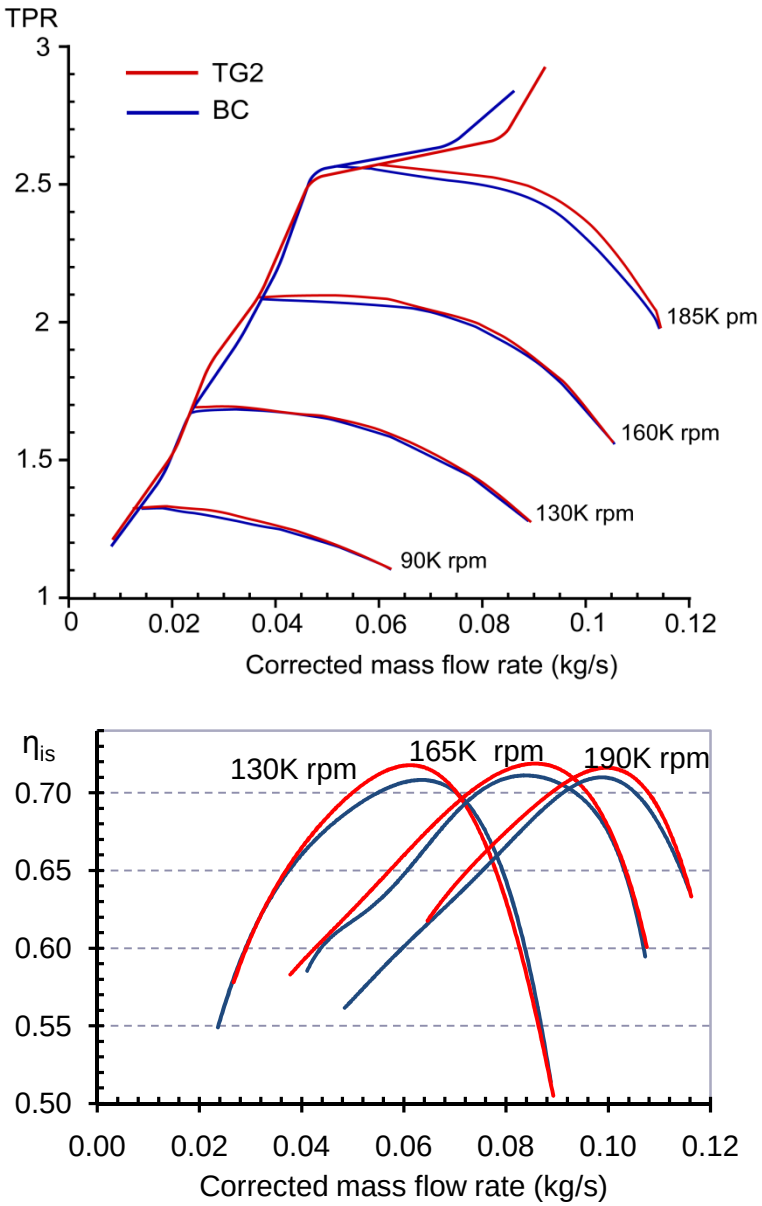

Figure 4-73 Compression ratio and isentropic efficiency with and without modified tongue

This study was necessary to better understand the affect of the volute circumferential pressure distribution on compressor surge line and performance. Retracting and rounding tongue has improved compressor efficiency at almost all flow rates.

Moreover, results indicates that the volute or the tongue were also mismatches. This is a very interesting point, since 1D analysis is always used to design compressor volute, this simple approach is probably not sufficient to find out the optimum volute for a given compressor.

4.5 Synergy effect of variable geometry in the diffuser and at the compressor inlet.

Further improvements should be possible if delaying instabilities at the impeller inlet [using a pre rotation system] accompanied with delaying diffuser instabilities, using a small pinched.

❖ Results and discussions

In order to suppress instabilities at the impeller and tarden surge occurrence, the new system was used. On the other hand, the shrouded pinched diffuser [P3] was used to delay diffuser instabilities.

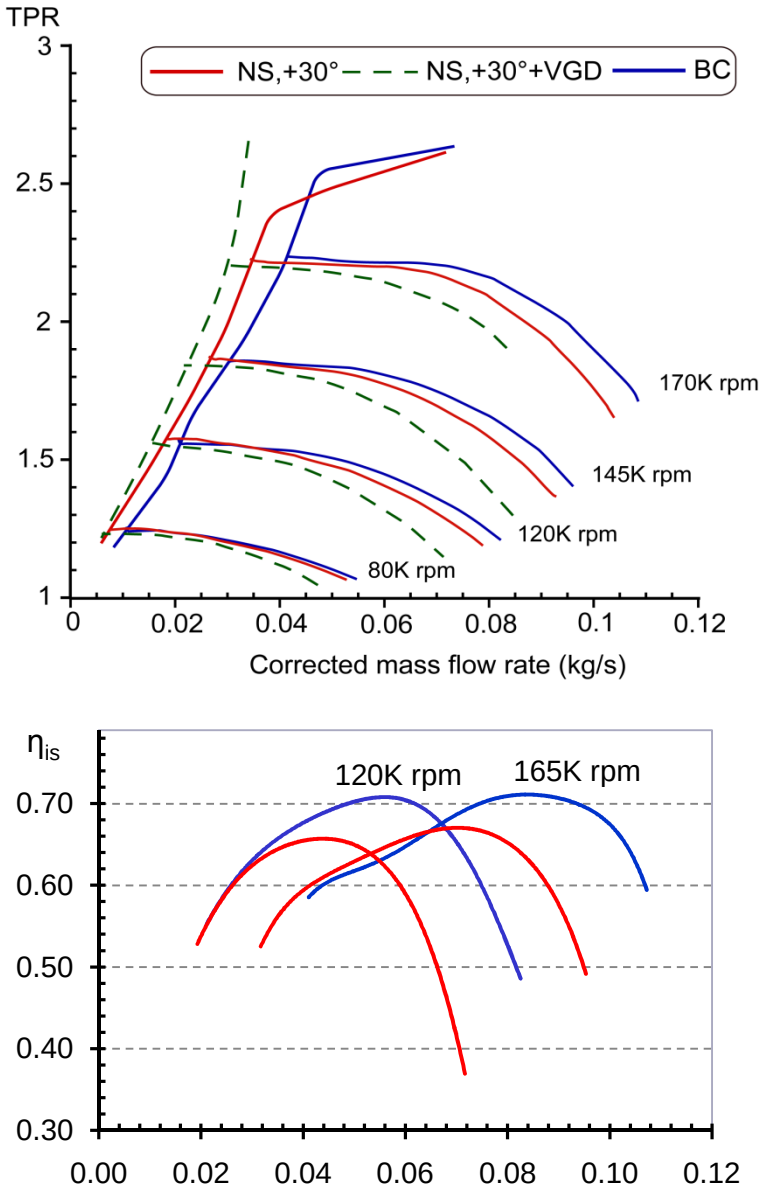

Figure 4-74 Effect of synergy between a variable geometry at inlet and the diffuser on the compressor compression ratio

As it can be seen from Figure 4-74, a wide operating was obtained when incorporating both a variable geometry at the impeller inlet and in the diffuser. We found that delaying instabilities in the impeller and diffuser have marked effects on surge limits: At TPR=2.7 the surge line improvement NS+VGD is 54.4% less than that of basic characteristic case. Another way to look at surge line improvement is the 36.5% stable pressure increase at 0.035Kg/s flow rate.

As it can be seen, the surge line was improved much more than it was possible when using a pre-rotation system alone, while conserving little pressure drop at near surge.

The improvement in surge line was accompanied by a slight increase in efficiency at near surge points. As it can be seen in Figure 4-74, efficiency increase can be noticed at 165K rpm at low flow rates, near the surge line.

If we minimize pressure losses through the NS to zero, the effect of the synergy between the zero pressure loss NS system and the VDG are shown in Figure 4-75. The new maps are reconstructed by subtracting the influence of the pressure losses in the NS system. Due to low losses through the NS system, the two maps are nearly superimposed.

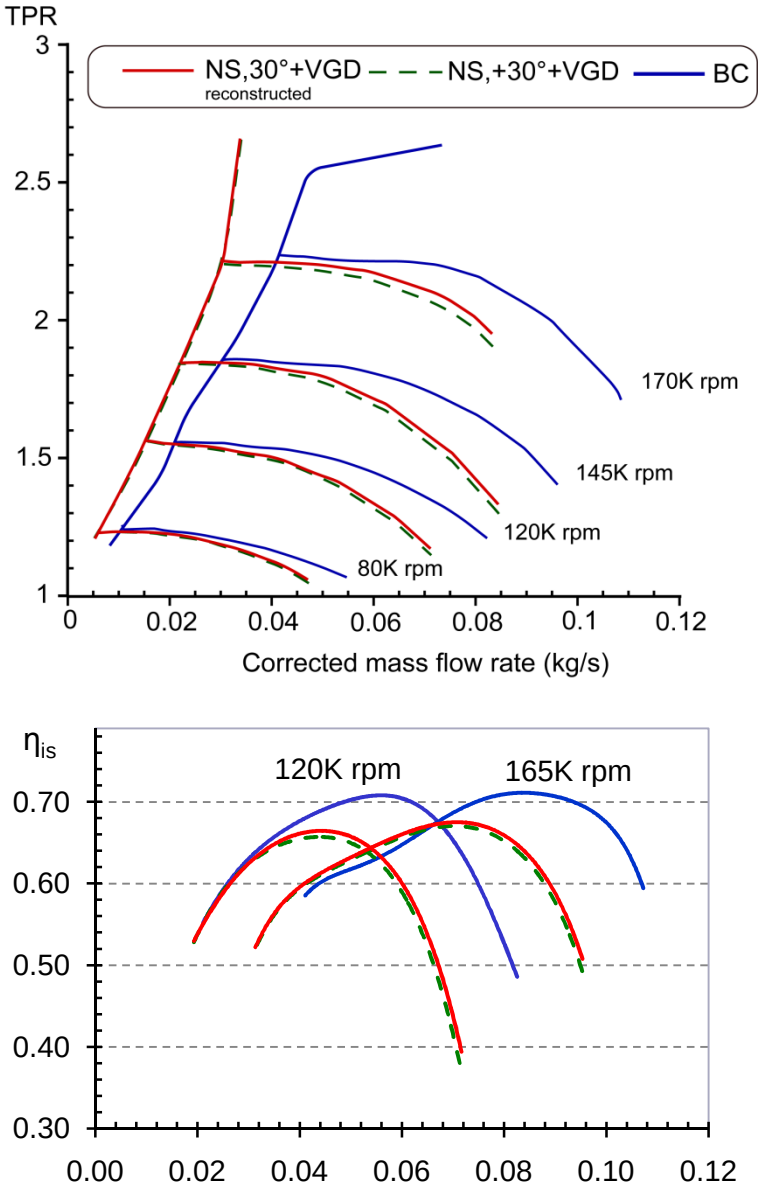

Figure 4-75 Reconstructing synergy effect maps after subtracting pressure losses through the NS

Very interesting results were obtained when coupling a pinched diffuser with a prewhirl generator. A big shift in surge margin was obtained while conserving efficiency at low flow rates.

Knowing that the NS prewhirl generate a free vortex prewhirl, it is worth trying the RGVs and AGVs with the pinched diffuser to see the effect of the other prewhirl types coupled to pinched diffuser.

Conclusions and perspectives

A theoretical and experimental study has been carried out to study the effect on a turbocharger compressor performance and surge line, of different existing techniques to increase compressor surge margin. The specific objective of these techniques, being to suppress the onset of compressor surge and extend the stable operating range to reduced flow rates.

Local contribution of surge onset has been studied and different techniques to suppress instabilities at inducer, impeller, diffuser and volute was investigated.

First, compressor stability analysis was done, to find out the compressor component which triggers stage stall, at different compressor rotational speeds. It was found that - for the tested compressor - the diffuser triggers stall at low speeds, and impeller at higher speeds. Moreover, the volute blocks at very high flow rates, and probably causing impeller or diffuser instabilities.

Then after, different existing techniques to suppress compressor inducer, impeller, diffuser, and volute instabilities were tested. These are detailed bellow,

- *Suppressing inducer instabilities*

To suppress inducer instabilities, variable axial guide system [AGVs], one blade radial guide vane system [RGVs], and flexible guide vane system [FGVs] were tested. The effect of the positive and counter swirl, obtained by the different systems on compressor performance and surge line improvement was investigated.

It was obtained that, the effect of the different prewhirl produced by the tested mechanisms, was limited by a slight increase of surge line at middle speeds, and better improvement at higher speeds. Moreover, a slight efficiency increase was obtained at low flow rates when imparting positive prewhirl. However, the benefits of the different systems still not convincing compared to total cost and complexity that will add to the turbocharger unit.

Local flow analysis, using LDA measurements, was performed to analyze the results obtained of the different swirl mechanisms, on overall compressor performance and surge line. Moreover, local studies served to study the prewhirl type produced by the different tested mechanisms. It was obtained that the AGVs and the RGVs produce a ‘near’ forced vortex at inducer inlet. The AGVs produces more uniform velocity distribution compared to RGVs.

Moreover, a theoretical study was done to study the effect of different prewhirl types on incidence angle at inducer inlet. Results showed that free swirl was favorable at low compressor speeds, and fixed swirl the most suitable for higher speeds.

The second step, was concentrated on the development of a variable geometry guide vane system, which produces high swirl angles for low pressure losses. The new system has the particularity to produce fixed and free vortex prewhirl, by an easy change of vanes. System conception was based on the results obtained from the tested mechanisms [AGVs and FGVs], LDA results, and theoretical analysis.

Some good results were obtained, when imparting free swirl using the new system [NS]. This was a good surge line improvement at low speeds. Indeed, free swirl produces minimum incidence losses for low speeds operation.

Coming steps in suppressing inducer instabilities will be to:

1. Develop a new system capable to producing a constant prewhirl, and study its effect on compressor high rotational speeds.
2. Improve the NS system [surface quality], and study the effect of its fixed prewhirl on compressor performance and surge line.
3. Extend the proposed swirl system [NS] application to turbochargers of different applications. Particularly, impellers where favorable prewhirl types is suitable to that of system outlet [free vortex and fixed vortex].
4. Test the effect of the NS on engine performance.

❖ *Suppressing impeller instabilities*

To suppress impeller instabilities, map width enhancement system [first developed by Fishcer,[1988]], was tested. Holes were used to replace slots [usually used]. Two different configurations, with different holes dimensions, were developed for use in turbocharger. Holes dimensions, emplacement and angles are based on literature, for the two configurations. The hole emplacement of the second configuration [MWE2], was based on static pressure distribution along the shroud [one dimensional model].

Results obtained show that, the tested compressor is susceptible to casing treatment and the tested configurations tend to affect its performance at almost all flow range.

After testing the two configurations, it was concluded that. The tested systems were advantageous in increasing compressor compression ratio capability. However, surge line shifts to high flow rates at high rotational speeds.

The second step, was to study the effect of extending the MWE inlet tube length, and the effect of adding pinches or increasing diffuser width, on the compressor performance. Some interesting results were obtained.

Significant surge line shift was obtained, when extending the inner length tube for the first MWE configuration [MWE1], together coupled with a slightly increasing diffuser width. This improvement is probably due to a combination of suppressing inlet disturbance, and improving impeller diffuser interaction. With the former having more effect, since good improvement was also obtained when extending the inner tube of the MWE2 configuration, where the diffuser width was not changed.

The advantageous of the MWE system, is that it is simple, and poses no durability issue. Moreover, it is very cost effective, since it involves very slight changes to the installation.

Further work to be done:

1. Make CFD analysis together with experimental study, to optimize holes dimensioning and emplacements.
2. Study the possibility to have a variable geometry Super-MWE configuration [extended inlet MWE length] to overcome the adverse affects of the casing treatment, at high flow rates.
3. Engine testing of the two configurations [MWE1 and MWE2], and the new Super-MWE system.

❖ *Suppressing diffuser instabilities*

To suppress diffuser instabilities, two different techniques were tested. These are different configurations of pinches and grooves. Pinches increase radial velocity in the diffuser, hence increasing inlet diffuser angle and delaying diffuser instabilities. Grooves, used in pumps to suppress diffuser instabilities while reducing diffuse inlet radial velocity.

Pinched diffuser was advantageous is shifting surge line to low flow rates. However, this improvement was accompanied by high losses due to increasing diffuser velocity, hence increasing friction losses.

Two grooves configurations were tested. Their effect on compressor surge line was similar to that of pinches. However, some interesting results were obtained, with increasing the pressure ratio at high flow rates.

The effect of changing diffuser area was more significant on shifting surge line, at high rotational speeds, than when imparting prewhirl at inducer inlet. This is probably due to improving impeller diffuser interaction, and suppressing impeller instabilities [radial part impeller].

Future work to be done:

1. Design of a fully variable diffuser, during compressor operation. It is possible that the fully variable diffuser design will be less costly and more readily operated than variable swirl generator.
2. Study its affect on engine performance when located on an engine.

❖ *Suppressing volute instabilities*

To suppress volute “blockage” around volute tongue, the volute tongue was shortened and rounded, to suppress separation around it. Tongue changes slightly increases efficiency and compression ratio.

It is probable that, the standard volute used for this stage is not the optimum. Further work will be to study different possibilities to improve volute performance, these can be:

1. tongue geometry modifications
2. circumferential geometry changes
3. The possibility to design a variable geometry volute.

❖ Suppressing two instabilities at same time [synergy]

The synergy effect between suppressing inlet and diffuser instabilities was tested. The NS coupled to a pinched diffuser was studied. Surge line significantly increases at almost all rotational speeds, with higher increase at high speeds, while, conserving efficiency at near surge points. Coming steps will be to test the effect of the synergy between diffuser and inducer, on engine performance.

Conclusions et perspectives

Une étude expérimentale et théorique a été effectuée, pour étudier les effets sur un compresseur centrifuge de suralimentation automobile, de différentes techniques existantes chargées d'augmenter la marge au pompage. L'objectif spécifique de ces techniques étaient de supprimer l'apparition du pompage et d'étendre la plage de fonctionnement stable vers les bas débits.

La contribution des phénomènes locaux sur l'apparition du pompage a été étudiée et différentes techniques de suppression des instabilités dans la roue, le diffuseur et la volute, ont été testées.

Tout d'abord, une analyse de la stabilité du compresseur a été présentée, afin de trouver quel composant du compresseur déclenche le décrochement d'étage pour différentes vitesses de rotation. Il a été trouvé que - pour le compresseur testé – le diffuseur déclenche le décrochement aux basses vitesses, et que c'est la roue aux hautes vitesses. De plus, la volute est responsable de chocs aux très hauts débits et est probablement la cause d'instabilités dans la roue et dans le diffuseur.

Puis ensuite, différentes techniques existantes de suppression ont été testées, notamment au niveau de l'entrée de la roue, dans la roue, dans le diffuseur et dans la volute. Elles sont décrites ci-dessous :

Suppression des instabilités en entrée de roue

Pour supprimer les instabilités en entrée de roue, un système axial de pré-aubage flexible (FGVs), un système de pré-aubage radial à une aube (RVGs), et un système axial de pré-aubage orientable, ont été testés. L'effet sur les performances du compresseur et sur les lignes de pompage des pré-rotations positives (dans le sens de rotation de la roue) ou contra-rotatives obtenues par les différents systèmes a été étudié.

Il a été obtenu que l'effet des différentes pré-rotations produit par les mécanismes testés était limité à une légère amélioration de la ligne de pompage aux vitesses de rotation moyennes et une amélioration plus importante aux hautes vitesses de rotation. De plus, une légère augmentation du rendement a été obtenue aux bas débits pour des pré-rotations positives. Cependant, le bénéfice obtenu avec les différents systèmes est limité par rapport au coût et à la complexité ajoutés au turbocompresseur.

Une analyse locale de l'écoulement en utilisant des mesures LDA a été effectuée pour analyser les résultats obtenus avec les différents mécanismes de pré-rotation. De plus, l'étude locale a permis de caractériser le type de pré-rotation obtenu avec les différents types de pré-rotateur. Ainsi, il a été obtenu que les systèmes AGVs et RGVs produisaient des vortex forcés à l'entrée de roue. Le système AGVs produit une distribution de vitesse plus uniforme que le RGVs.

De plus, une étude théorique a été faite sur le compresseur testé pour étudier l'influence de différents types de pré-rotations sur l'angle d'incidence en entrée de roue. Les résultats indiquent qu'un vortex libre est favorable aux basses vitesses de rotation, et qu'un vortex fixe est adapté aux hautes vitesses de rotation.

La seconde étape a consisté au développement d'un pré-rotateur axial à géométrie variable qui produit une rotation importante pour une perte de charge faible. Le nouveau système a la particularité de produire des vortex libres ou forcés en changeant les aubages. La

conception de ce système est basée sur les résultats obtenus avec les mécanismes testés (AGVs et FGVs), sur les résultats de mesure LDA et sur l'analyse théorique.

Des bons résultats furent obtenus en induisant un vortex libre avec le nouveau système (NS). En particulier, une bonne amélioration de la ligne de pompage a été obtenue à basse vitesse de rotation. Le vortex libre induit des pertes d'incidence minimum pour les basses vitesses de rotation.

Les perspectives dans la suppression des instabilités en entrée de roue sont les suivantes :

1. Développer un nouveau système capable de produire un vortex constant et étudier son effet à haute vitesses de rotation.
2. Améliorer le système (NS) (qualité de surface) et étudier l'effet pour un vortex fixe sur les performances du compresseur et sur la ligne de pompage.
3. Etendre le système (NS) à d'autres turbocompresseurs, en particulier, pour des roues adaptées au type de vortex produit (libre et forcé)
4. Tester l'effet du système (NS) sur le fonctionnement d'un moteur à combustion interne

Suppression des instabilités dans la roue

Pour supprimer les instabilités de roue, un système de recirculation dans le carter (MWE) proposé initialement par Fischer [1988] a été testé. Des trous ont été utilisés à la place des canaux (habituellement utilisés). Deux configurations, avec des dimensions de trous différentes, ont été réalisées pour le turbocompresseur testé. Les dimensions des trous, leurs emplacements et angles ont été choisis à partir de l'étude bibliographique. L'emplacement des trous pour la seconde configuration (MWE2) a été choisi à partir d'un calcul 1D de la distribution de pression statique le long de la veine.

Les résultats obtenus montrent que le compresseur testé réagit à ce type de traitement et que les configurations testées modifient ses performances à tous les débits.

Après avoir testé les 2 configurations, il a été conclu que les 2 systèmes étaient avantageux en augmentant les capacités de compression. Cependant la ligne de pompage est décalée vers les hauts débits pour fortes vitesses de rotation.

Un décalage important de la ligne de pompage a été obtenu en allongeant le tube d'entrée pour le premier système de recirculation dans le carter (MWE1), couplé à un diffuseur de largeur légèrement augmenté. Cette amélioration est sans doute due à l'amélioration des interactions roue-diffuseur et à la suppression des perturbations à l'entrée de la roue. Ce dernier semble avoir l'effet le plus important, puisque une bonne amélioration a été obtenue avec le système MWE2, où le diffuseur n'a pas changé.

L'avantage du système MWE est qu'il est simple et ne pose pas de problème de fragilité. De plus il est bon marché car il entraîne peu de modification sur le système de suralimentation.

Les travaux sur ce système doivent être réalisés ultérieurement :

1. entreprendre une analyse expérimentale et par CFD pour optimiser la dimension des trous et leur emplacement.
2. étudier la possibilité de concevoir un système MWE à géométrie variable pour contrer les effets du système à haut débit
3. tester ces systèmes sur des moteurs à combustion interne

Suppression des instabilités dans le diffuseur

Pour supprimer les instabilités dans le diffuseur, deux techniques ont été testées : différents sillons et pincements. Les pincements augmentent la vitesse radiale dans le diffuseur et ainsi augmente l'angle d'entrée dans le diffuseur et repoussent les instabilités. Les sillons sont utilisés dans les pompes pour supprimer les instabilités de diffusion en réduisant la vitesse circonférentielle.

Les diffuseurs à pincement ont déplacé la ligne de pompage vers les bas débits. Cependant, cette amélioration est accompagnée par des fortes pertes dues à l'augmentation de la vitesse dans le diffuseur, et ainsi à l'augmentation des pertes par frottement.

Deux configurations de sillons ont été testées. Leurs effets sur la ligne de pompage sont similaires à celles du pincement. Cependant, certains résultats intéressants furent obtenus avec une augmentation du taux de compression à hautes vitesse de rotation.

L'effet lié au changement de la surface de passage du diffuseur a été plus important sur le déplacement de la ligne de pompage à hautes vitesses de rotation que celui obtenu avec une pré-rotation à l'entrée de roue. Ceci est probablement du à l'amélioration de l'interaction roue-diffuseur et à la suppression des instabilités de roue dans la partie radiale.

Les perspectives dans ce domaine sont liées

1. à l'élaboration d'un diffuseur à géométrie variable, modifiable pendant le fonctionnement du compresseur. Il est possible qu'un diffuseur à géométrie variable soit moins onéreux et plus facilement utilisable qu'un générateur de tourbillon variable.
2. aux tests de ce système sur moteur à combustion interne

Suppression des instabilités dans la volute

Pour supprimer le blocage autour le bec de volute, celle-ci a été raccourcie et arrondie afin de diminuer la séparation de l'écoulement. Ces modifications ont légèrement augmenté le rendement et le taux de compression.

Il est probable de la volute utilisée pour ce compresseur n'est pas l'optimum. Des travaux supplémentaires pourraient être d'étudier plusieurs possibilités d'amélioration des performances de la volute :

1. modification de la géométrie du bec de la volute
2. changement de la géométrie sur toute la circonférence
3. volute à géométrie variable

Suppression de plusieurs instabilités en même temps (effet de synergie)

L'effet de synergie lié à la suppression des instabilités en entrée roue et dans le diffuseur a été étudié. Le système NS couplé à un diffuseur à pincement à été testé. La sensibilité au pompage a été améliorée à presque toutes les vitesses de rotation, avec une amélioration plus importante à haute vitesse, tout en conservant le rendement près du pompage.

La prochaine étude sera de tester l'incidence de la synergie créée entre l'entrée roue et le diffuseur, sur les performances d'un moteur.

APPENDIXES

A. Some Thermodynamics and Fluid Mechanics Relations

Corrected mass flow and rotational speeds

In this section various non dimensional quantities related to compressor are presented.

Flow rate coefficient:

$$Qc = Q\frac{\sqrt{T_{01}}}{\sqrt{T_{ref}}}\frac{P_{ref}}{P_{01}} \quad \text{A-1}$$

Corrected rotational speed:

$$Nc = N\frac{\sqrt{T_{ref}}}{\sqrt{T_{01}}} \quad \text{A-2}$$

Where T_{01} and P_{01} are total temperature and pressure at compressor inlet, and T_{ref} and P_{ref} are given values, equals 288 K and 1 bar respectively.

Calculating conditions at compressor inlet

Considering a straight converging inlet duct at the compressor entry with no inlet guide vanes, then the absolute velocity, C_0 at station 0-0 is axial [Figure 1-7]. Given the temperature and pressure at compressor section 0-0, then for a given mass flow rate, the Mach number M_0 at this section is calculated from equation (A-3) (derived from the continuity equation and isentropic relations between static and stagnation thermodynamic parameters (Dixon, 1998) after substituting for total temperature and pressure from equations (A-6) and (A-7)

$$\frac{\dot{m}\sqrt{\frac{\bar{R}T_{0t}}{\gamma}}}{P_{0t}A_0} = M_0\left(1+\frac{\gamma-1}{2}{M_0}^2\right)^{\frac{-1(\gamma+1)}{2(\gamma-1)}} \quad \text{A-3}$$

Where

$$M_0 = \frac{C_0}{a_0} \quad \text{A-4}$$

And

$$a_0 = \sqrt{\gamma\bar{R}T_0} \quad \text{A-5}$$

Total conditions at station 0-0 can be calculated from the temperature

$$T_{0t} = T_0\left(1+\frac{\gamma-1}{2}{M_0}^2\right) \quad \text{A-6}$$

Total pressure

$$P_{0t} = P_0\left(1 + \frac{\gamma - 1}{2} {M_0}^2\right)^{\frac{\gamma}{\gamma-1}} \quad \text{A-7}$$

Total density

$$\rho_{0t} = \frac{P_{0t}}{\bar{R}T_{0t}} \quad \text{A-8}$$

Absolute velocity C_{1s} can be calculated from (A-3) applied to section A_1 using total temperature and pressure at station 0-0.

Supposing absolute velocity C1 is axial at station 1, we can calculate, isentropic temperature, density and pressure at 1i using equations

Static temperature, pressure at point $1i$ can be calculated from the isentropic relations between static and stagnation thermodynamic parameters (equations (7), (8), and (9)).

$$T_{0t} = T_{1i}\left(1 + \frac{\gamma - 1}{2} {M_1}^2\right) \quad \text{A-9}$$

$$P_{0t} = P_1\left(1 + \frac{\gamma - 1}{2} {M_1}^2\right)^{\frac{\gamma}{\gamma-1}} \quad \text{A-10}$$

$$\rho_{1i} = \frac{P_1}{RT_{1i}} \quad \text{A-11}$$

To calculate for conditions at point 1, we introduce friction coefficient factor in the inlet convergent.

$$\delta = \frac{2\Delta H_{01}}{C_{1i}^2 - C_0^2} \quad \text{A-12}$$

$$\Delta H_{1t} = \frac{1}{2}\left(C_{1i}^2 - C_1^2\right) \quad \text{A-13}$$

Where ΔH_{01} represents the losses in the inlet convergent (between 0 &1).

$$T_1 = T_{1i} - \frac{1}{2}\Delta H_{1t} \quad \text{A-14}$$

B. Static Pressure Distribution along the Compressor Casing

A one dimensional model using Matlab was done to calculate the static pressure distribution along the casing. The model is presented in Table B-1. it is based on the work of (Watson, 1982).

Model entry is:

- Blade angle at different locations [cuts] along the axes,
- Number of impeller blades at each cut,
- Inlet static pressure and temperature,
- Mass flow rate
- And compressor rotational speed.

Flow in the impeller is assumed steady and gas as perfect.

Model output is:

- Pressure side static pressure at the different cuts along the compressor axes,

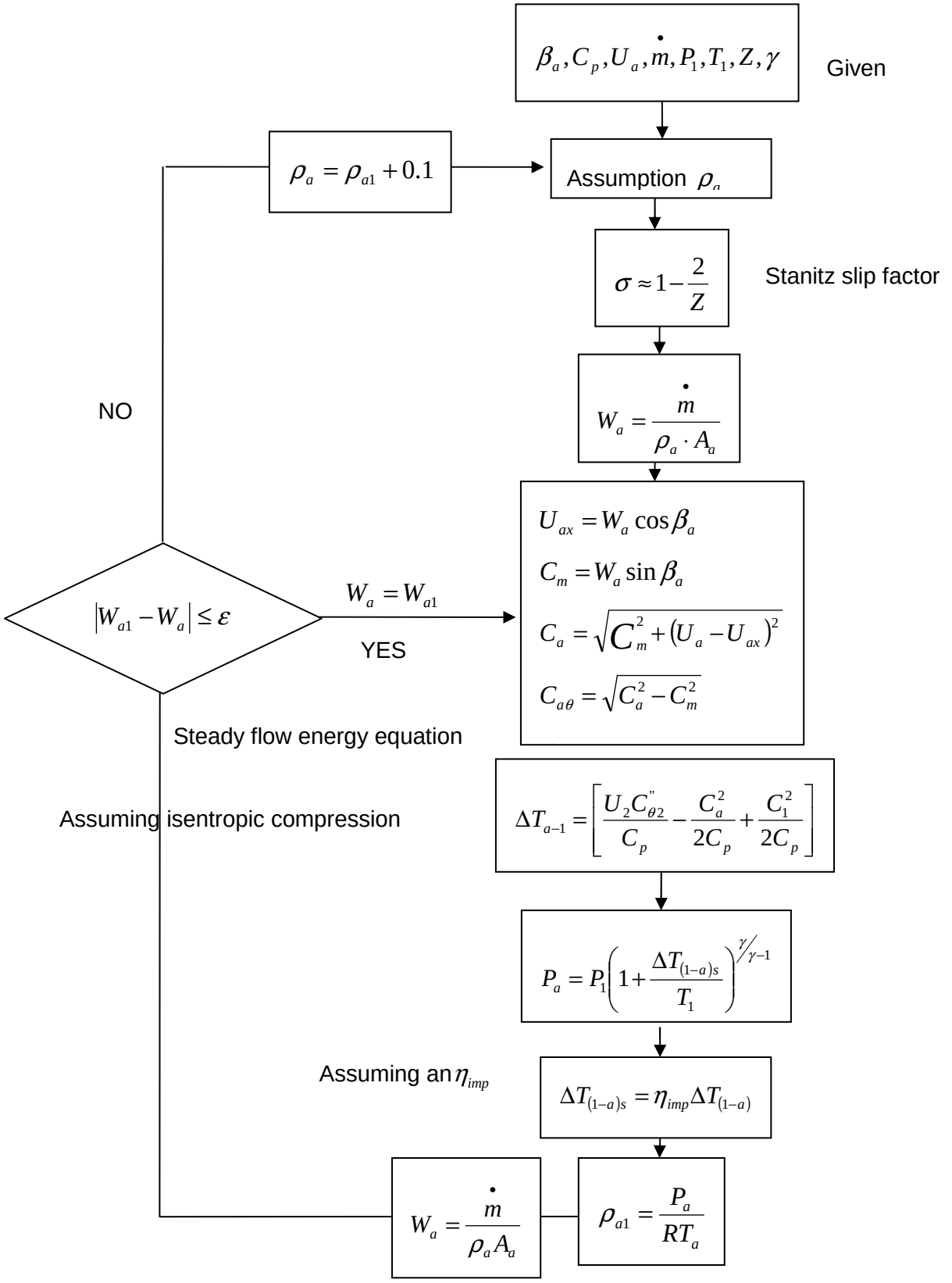

Table B-1 Static pressure distribution model

C. Why Tests were Repeated Several times

A very careful attention has to be given to tests conducted. In this annex some results will be presented to show how small details can have a great effects on results and how verification is very important at the beginning of each test.

- Damaged inducer

Figure C-1 and C-2 show the effect of damaged rotor inlet on compressor performance compared to proper impeller inducer.

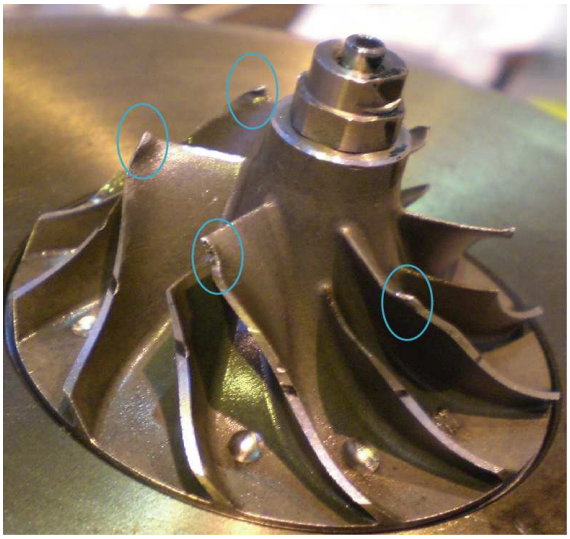

Figure C- 1 Damaged impeller

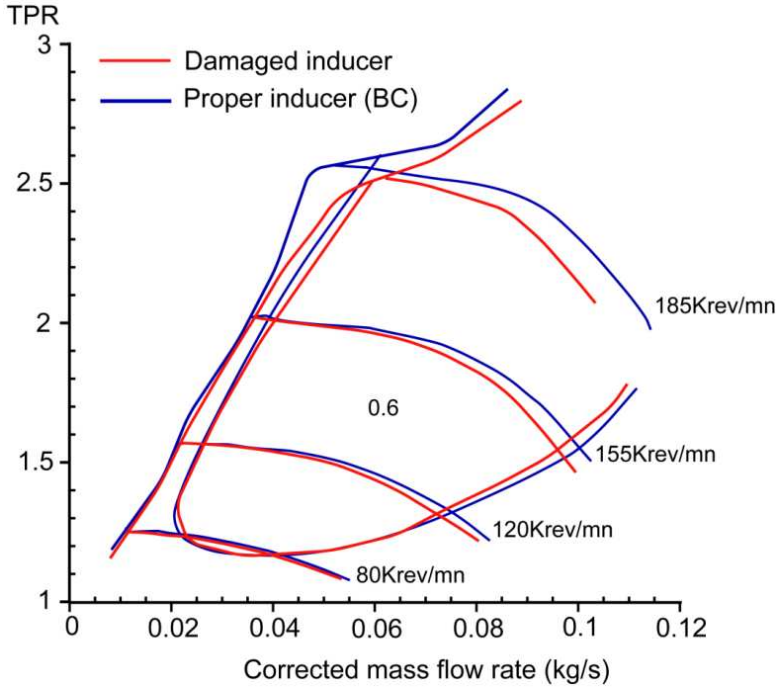

Figure C-2 Damaged compared to proper inducer inlet

The effect of the damaged impeller inducer inlet compared to basic characteristics is presented in Figure C-2 and the effect on efficiency at 120 and 150K rpm is presented in Figure C-3. As expected, impeller tip damages at inducer inlet have dropped pressure ratio and efficiency at high flow rates.

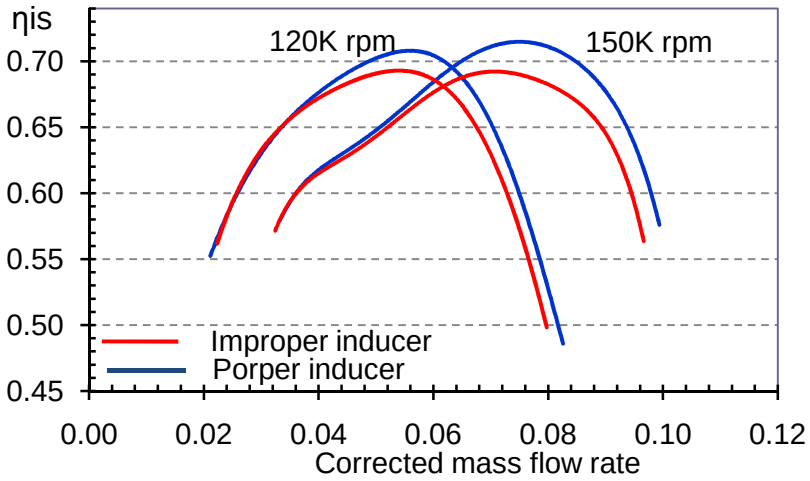

Figure C-3 Efficiency losses with an improper inducer impeller compared to basic characteristics

❖ Connection at compressor inlet

What is the effect of improper connection between compressor casing and inlet tube on the compressor performance. The results of a 1mm diameter difference between the inlet tube and the compressor inlet casing is presented in Figure C-4 and Figure C-5. Results confirm how important is to verify even very small details before doing the experiment.

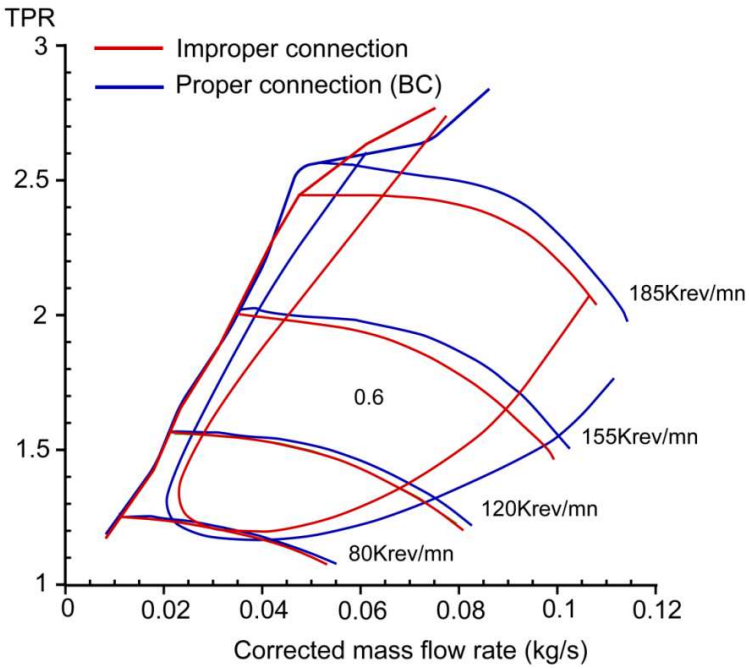

Figure C-4 Proper versus improper connection between inlet tube and compressor casing

The results show that an improper connection produces pressure and efficiency losses. These losses become big at high flow rates. Pressure losses can be explained by the non uniform flow produced at impeller inlet because of the bad connection.

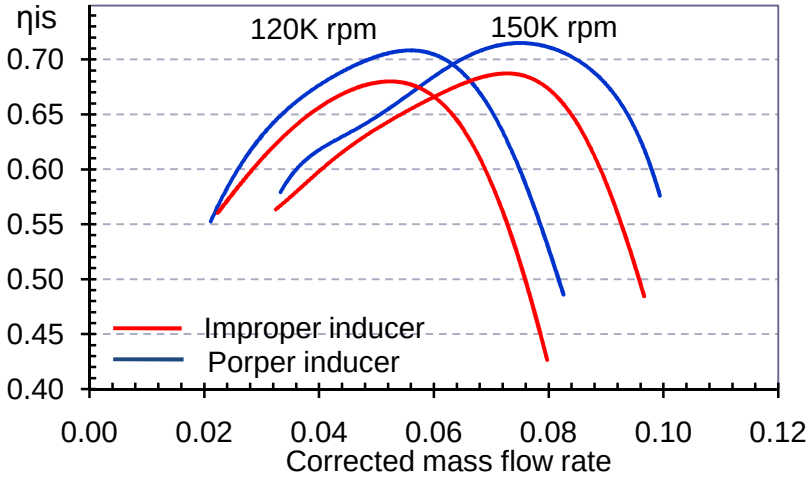

Figure C-5 Efficiency losses caused by improper connection at compressor inlet

❖ Compressor damages during tests

After presenting the results of the experimental analysis done on the tested turbocharger centrifugal compressor, it's worth to mention some of the damages the experimental study causes and how steps from building a test bench to realizing tests were difficult. Beginning with the error of sudden complete close of the compressor exit valve [Figures C-8], to a sudden system violent surge [Figure C-10] and finally, damages caused by non filtered air at the compressor inlet are shown in Figure C-11.

Figure C-8 Closing to 7% the electric vane at compressor exit at TPR=2bar

Figure C-9 The rest of the flexible guide vanes system !

Figure C-10 damaged impeller leading edge due to non filtered air at the compressor inlet

❖ Manufacturing processes

Finally, some of the system machining at the university workshop are shown. Example, the machining of one of the MWE systems is presented in Figure C-11.

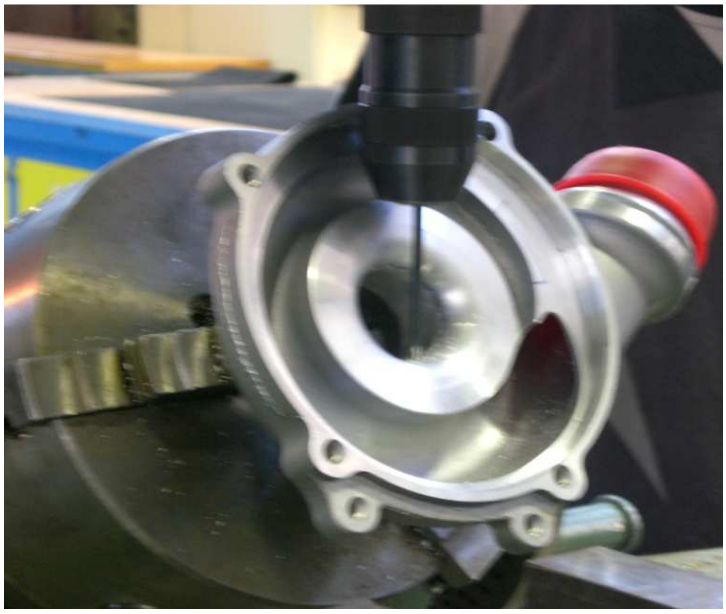

Figure C-11 MWE system manufacturing

D. Why Tests were Repeated Several times

The MWE1 system was tested at the turbocharger test bench, configuration 2 . Results were presented at the ASME turbo expo [Mohtar et al, 2009 (168)].

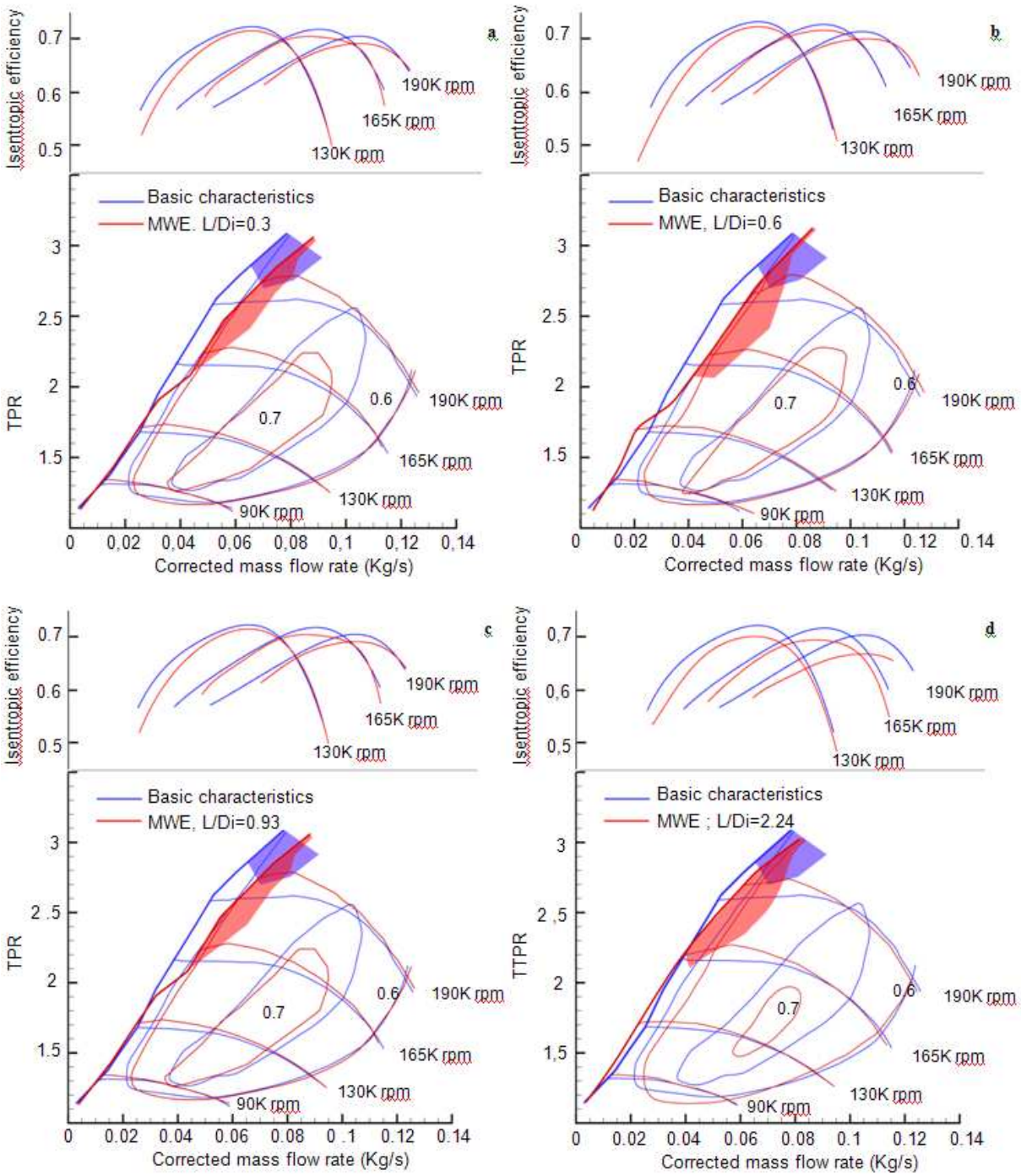

Figure D- 1 MWE system with different L/Di lengths

Figures D-1 a. b and c show the effect of the MWE1 structure - with different inner tubular lengths - on the compressor performance and surge line. As it can be seen, the shape of pressure ratio versus the mass flow characteristics is very similar in the three cases. The increase in L to Di ratio from 0.3 to 0.93 has not influenced the surge line for this particular design. The surge line has moved to high flow rates at high rotational speeds, and no shift was obtained at low speeds.

Bibliography

1. **Heywood, J B.** *Internal combustion engine fundamentals.* New York : McGraw Hill, 1988.

2. *Design and development of e-turbo for SUV and light truck applications.* **Balis, C, Middlemass, C and Shahed, S M.** Newport, RI : Garret Engine Boosting systems, 2003. Diesel engine emission reduction conference.

3. **Baines, N C.** *Fundamentals of turbocharging.* s.l. : Concepts ETI, Inc, 2005.

4. The Frame convention of the United Nation. [Online] 1992. http://www.unfccc.de/resource/convkp.html.

5. Kyoto Protocol. [Online] http://www.unfccc.de/resource/convkp. html..

6. *United Nations climate change conference.* Copenhagen, Denmark : s.n., 2009.

7. *Turbocharger compressor developments for passenger car gasoline engine applications.* **Chen, H and Connor, W.** s.l. : IMecH, 2002. Seventh international conference on turbocharging and turbochargers. pp. 13-18.

8. **Matsumoto, K, Jinnai, Y and Tojo, M.** *Development of compact and high performance turbocharger for 1,050℃ exhaust gases.* s.l. : Mitsubishi heavy industries. Ltd Tedchnical review Vol. 45. No.3, 2008.

9. *Turbocharging the AD465 gasoline engine.* **Zhang, P, Zong, L J and Wang, Y.** s.l. : Journal of Marine Science, 2008.

10. *Downsizing of Gasoline Engine: an efficient way to reduce CO2 Emissions: an efficient way to reduce CO2 Emissions.* **Leduc, P, Dubar, B and Ranini, A.** s.l. : Oil and gas Science and technology_Rev IFP, 2003, Vols. 58, pp:115-127.

11. corvette-web-central. [Online] http://www.corvette-web-central.com/Corvettemods.html.

12. **Tan, Y.** *Automotive diesel turbocharger investigation.* s.l. : University of Bath, 2007. PhD thesis.

13. Diesel Power Automotive. [Online] dieselpower.automotive.com.

14. **Watson, N and Jonata, M S.** *Turbocharging internal combustion engines.* s.l. : MacMillan, 1982.

15. *Radial and mixed flow turbine option for high boost turbochargers.* **Baines, N.** 2002. 7th international conference on turbochargers and turbochanging.

16. *Supercharging performance of a gasoline engine with a supercharger.* **Chang, S L, Dong, H W and Seo, W C.** s.l. : KSME International Journal, 1997, Vols. 11, No.5, pp:556-564.

17. *Design of an exhaust manifold to improve transient performance of a high-speed turbocharged diesel engine.* **Galindo, J, et al.** s.l. : Experimental Thermal and fluid Science, 2004, Vols. 28, pp:863-875.

18. *Comparison of passive and active methods of improving transient performance of turbocharged diesel engine.* **Glikes, O and Mishra, R.** s.l. : University of Huddersfield, 2006. School of computing and Engineering Researchers' Conference.

19. *Alternative turbocharger systems for the automotive diesel engine.* **Walsham, B E.** s.l. : IMecH, 1990, Vol. C405\036.

20. **Barkhage, R.** *Evaluation of a variable nozzle turbine turbocharger on a diesel engine under steady and transient conditions.* s.l. : PhD thesis. Hanover University, 2002.

21. **Toussaint, M and Podevin, P.** *Guide-Vanes upstream the impeller of centrifugal compressor.* s.l. : Conservatoire National des Arts et Métiers (CNAM), chaire de turbomachines.

22. Borgwarner. [Online] http://www.borgwarner.com.

23. tjcraft. [Online] http://www.tjcraft.net/english/HTML/78.html.

24. **Japikse, D and Baines, N C.** *Introduction to turbomachinery.* s.l. : Concepts ETI, 1997.

25. *An optimum set of loss models for performance prediction of centrifugal compressors.* **Oh, H W, Yoon, E S and Chung, M K.** s.l. : IMecH Proc Instn Mech Engrs. Part A, 1997, Vol. 112.

26. *Design and Numerical Investigation of Advanced Radial Inlet for a Centrifugal Compressor Stage.* **Kim, Y and Koch, J.** 2004, IMECE, pp. IMECE 2004-60538.

27. **Japikse, D.** *Centrifugal compressor design and performance.* Wilder, Vermont 05088, USA : Concept ETI, Inc, 1996.

28. *Potential of flow pre-whirl at the compressor inlet of automotive engine turbochargers to enlarge surge margin and overcome packaging limitations.* **Galindo, J.** 2006, International Journal of Heat and Fluid.

29. *The inlet flow structure of a centrifugal compressor stage and its influence on the compressor performance.* **Engeda, A, Kim, Y and Augnier, R.** 2003, ASME, Journal of FLuid Engineering, pp. Vol, 125. pp:779-785.

30. *The effect of distortion on the performance characteristics of centrifugal compressor.* **Ariga, I, et al.** 1983, ASME Journal for power, pp. Vol, 105. 199-211.

31. *The Influence of Inlet Flow Distortion on the Performance of a Centrifugal Compressor and the Development of Improved Inlet Using Numerical Simulations.* **Kim, Y, et al.** 2001, IMecH, Journal of Power and Energy, pp. Vol. 215, Part A, pp: 323-338.

32. *Review of centrifugal compressor's application and development. Journal of turbomachinery.* **Krain, H.** 2005, ASME, pp. Vol.127 . pp:25-34.

33. **Boyce, M P.** *Centrifugal Compressors a Basic Guide.* Oklahoma : PennWell Corporation, 2003.

34. *Typical performance characteristics of gas turbine radial compressors.* **Rodgers, C.** 1964, Trans ASME.Journal Engng Power, pp. 161-175.

35. **Abdullah, A H.** *The application of high inlet swirl angles for broad operating range turbocharger compressor.* University of Bath : phd thesis, 1996.

36. *Experimental study of centrifugal pumps impellers.* **Acosta, A J and Bowermann, R D.** 1957, Ibid, p. Vol 79.

37. *A Preliminary design performance prediction techniques for centrifugal compressors.* **Whitfield, A.** 1990, IMecH, pp. 131-144.

38. *Mean streamline aerodynamic performance analysis of centrifugal compressors.* **Augnier, R H.** 360-366, s.l. : Journal of turbomachinery, 1995, Vol. 117.

39. *A review of preliminary design and performance prediction technique for centrifugal compressors, Part 2: Performance prediction.* **Whitfield, A.** London : Mechanical Engineering Publications, 1989. Conference on developements in industrial compressors. p. 390/034.

40. **Gravdahl, J T.** *Modeling and control of surge and rotating stall in compressors.* Norway : PhD thesis, Norwegian University of Science and technology, 1998.

41. *Study of incidence loss models in radial and mixed flow turbomachinery.* **Whitfield, A and Wallace, F J.** 1973, IMechE, pp. 122-128.

42. **Galvas, M R.** *Fortran program for predicting off-design perdormance of centrifugal compressors.* s.l. : NASA TN D 7484, 1973.

43. **Augnier, R H.** *Fluid Mechanics thermodynamics of turbomachinery.* New York : ASME press, 2000.

44. *Modélisation de compresseur centrifuges de suralimentation.* **Hammoud, J A, Frelin, M and Garrigou, T A.** 1997. SIA. pp. 57-63.

45. *A method for calculating the flow in a centrifugal impeller when entropy gradients are present.* **Jansen, W.** 1979. Royal society conference on internal aerodynamics, turbomachinery.

46. **Abdullah, A H.** *Notes on prediction of centrifugal compressors.* Malaysia : Faculty of Mechanical Engineering, 2006.

47. *Prédiction des performances statiques d'une turbine de suralimentation avec et sans distributeur.* **Liazid, A, Bencherif, L and Izidi, L.** s.l. : Revue Entropie, 2002.

48. *Loss mechanisms in turbomachines.* **Denton, J T.** 621-656, s.l. : ASME journal of turbomachinery, 1993, Vol. 115.

49. **Rodgers, C.** *Mainline performance prediction for radial inflow turbines.* s.l. : VKI Lecture series, 1987.

50. *Losses in vaneless diffusers on centrifugal compressors and pumps.* **Johnston, J P and Dean, R C.** No.1, s.l. : ASME J. Engng Power, 1966, Vol. 88.

51. *Experimental and numerical investigation of the performance of a 240 kW centrifugal compressor with different diffusers.* **Abraham, E.** 2003, Experimental Thermal Fluid Science, pp. 55-72.

52. *Low solidity tandem-cascade diffusers for wide flow range centrifugal blowers.* **Senoo, Y, Hayami, H and Ueki, H.** 1983, ASME , pp. Paper No. 83-GT-3.

53. *Influence of inlet flow conditions and geometries of centrifugal vane less diffusers on critical flow angle for reverse flow.* **Senoo, Y and Kinoshita, Y.** pp: 98-103, s.l. : Trans ASME journal Fluids Eng, 1977, Vol. 99.

54. *Limits of rotating stall and stall of vaneless diffusers of compressors.* **Senoo, Y and Kinoshita, Y.** New York : ASME, 1978, ASME, pp. Paper No 78-GT-19.

55. *Rotating non-uniform flow in radial compressors.* **Van den Braembussche, R A, Fringe, P and Roustan, M.** Brussels, Belgium : s.n., 1980. centrifugal compressors, Flow phenomena and Performance (AGARD CP-282-12).

56. **Stanitz, J D.** *One dimensional compressible flow in vaneless diffusers of radial and mixed flow centrifugal compressors, including effects of friction, heat transfer and area change.* s.l. : NACA TN 2610, Lewis Flight propulsion lab, 1952.

57. *Pressure recovery in a turbocharger compressor volute. Journal of power and energy Part A.* **Eynon, P A and Whitfield, A.** 2000, IMecH, p. Vol. 214. No:6.

58. **Ayder, E.** *Experimental and numerical analysis of the flow in centrifugal compressor and pump volutes.* Rhode Saint Genese, Belgium : PhD. Von Karman Institute of FLuid Dynamics, 1993.

59. **Reunanen, A.** *Experimental and numerical analysis of different volutes in centrifugal compressor.* Lapeenranta University of Technomogy : PhD thesis, 2001.

60. *Investigation of the circumferential static pressure non-uniformity caused by a centrifugal compressor discharger volute.* **Sorokes, J M, Borer, J C and Koch, J M.** 1998, ASME, pp. Paper No. 98-GT-326.

61. **Van den Braembussche, R A.** *Flow and Loss Mechanisms in Volutes of Centrifugal Pumps. In Design and Analysis of High Speed Pumps.* Neuilly sur Seine, France : Educational notes RTO-EN-AVT-143, 2006.

62. *Development and Design of a Centrifugal Compressor Volute.* **Xu, C and Müller, M.** 2005, International journal of Rotating Machinery , pp. Vol.3. pp:190-196.

63. **Stiefel, W.** *Experience in development of radial compressors.* s.l. : In VKI Lecture Series 50, 1972.

64. **Cumpsty, N.** *Compressor aerodynamics.* s.l. : John Wiley & Sons, 1989.

65. *Performance investigation of large capacity centrifugal compressors.* **Mishina, I and Gyoubu, I.** 1978, ASME, pp. Paper No. 78-GT-3.

66. *The influence of shape and location of the tongue of spiral casing on the performance of single stage radial pumps.* **Lipski, W.** Budapest Akadamia Kiado : s.n., 1979. Sixth conference of FLuid Machinery. pp. 673-682.

67. *Numerical Analysis and Optimization of the Volute in a Centrifugal Compressor.* **Ji, C, Wang, Y and Yao, L.** Hangzhou, China : s.n., 2007. International conference of Power Engineering. pp. 32-27.

68. **Dean, R C.** *The fluid dynamic design of advanced centrifugal compressors.* Lowa state University : Lecture notes presented at ASME Turbomachinery Institure, 1973.

69. *Effect of modification to tongue and impeller geometry on unsteady flow, pressure fluctuation and noise in a centrifugal pump.* **Dong, R, Chu, S and Katz, J.** 1997, Journal of urbomachinery, pp. 506-515.

70. *Flow visualisation studies and the effect of tongue area on the performance of volute casings of centrifugal machines.* **Yadav, R and yahya, S M.** 1980, International journal of Mechanical Science, pp. Vol, 22. No:10, 651-660.

71. *Compressor surge and stall.* **Pampreen, R C.** 1993.

72. *Compressor Surge and Stall Propagation.* **Emmons, H W, Pearson, C E and Grant, H P.** 1952, ASME , pp. Paper No. 53-A-65.

73. *An Experimental Study of Surge in Centrifugal Compressors.* **Toyoma, K, Runstadler, P W and Dean, R C.** 1977, ASME Journal of FLuids Engineering, pp. 115-131.

74. *The analysis of surge.* **Stenz, R H.** Texas : Turbomachinery Laboratory A&M University, 1980. Ninth Turbomachinery Symposium. pp. 57-61.

75. *Surge and Rotating stall in axial flow compressors, Part I: Theoretical compression system model.* **Greitzer, E M.** 1976a, Journal of Engineering for Power, pp. 190-198.

76. *Surge and Rotating Stall in Axial Flow Compressors. Part II: Experimental Results and Comparison With Theory.* **Greitzer, E M.** 1976b, ASME Journal of Engineering for Power, pp. 199-211.

77. *The stability of pumping systems.* **Greitzer, E M.** 1981, ASME Journal of Fluids Engineering, pp. Vol, 103. 193-242.

78. **Willems, F P T.** *Modeling and Bounded Feedback Stabilization of Centrifugal Compressor Surge.* Technische Universiteit Eindhoven : PhD thesis, 2000.

79. **Helvoirt, J V.** *Centrifugal Compressor Surge Modeling and Identification for Control.* 2007.

80. *Distinctions between different types of stall in centrifugal compressor stage.* **Kammer, N and Rautenberg, M.** 1985, ASME, pp. paper 85-GT-195.

81. *Rotating stall and surge control: A survey.* **De Jager, B.** 1995, 34th IEEE Conference on Decision and Control, pp. Vol,2. pp:1857-1862.

82. *Distinction between two types of self exited gas oscillations in vaneless radial diffusers.* **Abdelhamid, A N and Bertrand, J.** s.l. : Canadian Aeronautics and space journal, 1980, Canadian Aeronautics and space journal, pp. 105-117.

83. *Steady fluid flow in a radial vaneless diffuser.* **Jansen, W.** pp:607-619, s.l. : ASME Journal of Basic Engineering, 1964, Vol. 86(4).

84. *A theoretical model for rotating stall in vaneless diffusers of a centrifugal compressor.* **Frigne, P and Van den Braembussche, R.** Paper No.82-GT-188, s.l. : ASME Journal of Engineering for Gas Turbines and Power, 1985.

85. *Analysis of the flow in vaneless diffusers with large width-to-radius ratios.* **Dou, H S and Mizuki, S.** pp: 193-201, s.l. : ASME Journal of turbomachinery, 1998, Vol. 120(1).

86. *Two-Dimensional Rotating Stall Analysis in a wide vaneless diffuser.* **Ljevar, S, Lange, H. C. and Van Steenhoven, A. A.** 2006, Journal of Rotating Machinery.

87. **Ljevar, S.** *Rotating Stall in Wide Vaneless Diffusers.* Norway : PhD thesis Norwegian university of Science and technology, 2007.

88. *Rotating Stall in Centrifugal Compressor Vaneless Diffuser: Experimental Analysis of Geometrical Parameters Influence on Phenomenon Evolution.* **Ferrara, G, Ferrari, L and Baldassarre, L.** 433-442, s.l. : Internationla Journal of Rotating Machinery, 2004, Vol. 10(6).

89. *Analysis of Geometries' Effects on Rotating Stall in Vaneless Diffuser withWavelet Neural Networks.* **Gao, C, Gu, C and Wang, T.** s.l. : Journal of Rotating Machinery, 2007, Vol. 07.

90. *Passive control of rotating stall in vaneless diffuser with radial grooves: detailed numerical study.* **Gao, C, Gu, C and Wang, T.** Orlando, USA : s.n., 2009. ASME turbo Expo.

91. *Study of vaneless diffuser rotating stall based on two-dimensional inviscid flow analysis.* **Tsujimoto, Y, Yoshida, Y and Mori, Y.** pp: 123-127, s.l. : Journal of fluid engineering, 1996, Vol. 118(1).

92. *A discussion of the factors affecting surge in centrifugal compressors.* **Elder, R and Gill, M.** 1984, ASME, pp. 84-GT-194.

93. *Application of map width enhancement devices to turbocharger compressor stages.* **Fischer, F B.** 1988, SAE paper 880794.

94. *Numercial simulation of impeller-volute interaction in centrifugal compressors.* **Hillewaert, K and Van den Braembussche, R.** s.l. : ASME Journal of turbomachinery, 1999, Vol. 121, pp. 603-608.

95. *The dynamics of surge in compression systems. Sadhana.* **Vishwanatha, A N and Ramesh, O N.** 2007, Sâdhâna, pp. Vol. 32, pp.43-49.

96. *Surge Dynamics in a Free-Spool Centrifugal Compressor System.* **Fink, D A, Cumpsty, N A and Greitzer, E M.** 1991, ASME, pp. Paper No. 91-GT-31.

97. *Time to surge concept and surge control for acceleration performance.* **Leufven, O and Eriksson, L.** Seoul, Korea : The International Federation of Automatic Control, 2008. 17th international World Congress.

98. *. Impeller rotating stall as a trigger for the transition from mild to deep surge in a subsonic centrifugal compressor.* **Ribi, B and Gyamathy, G.** 1993. ASME. International gas turbine and aero engine congress.

99. **Stein, A.** *Computational analysis of stall and separation control in centrifugal compressors.* Georgia : PhD thesis, Georgia Institute of Technology, 2000.

100. *Experimental and theoretical study of surge in a small centrifugal compressor.* **Hansen, K E, Jörgensen, P and Larsen, P S.** 1981, Journal of Fluid Engineering, pp. Vol. 103. pp 391-394.

101. *Modeling techniques for predicting compressor performance during surge and rotating stall.* **El Metwally, E S, Abo Rayan, M and Mostapha, N H.** 1996, ASME, p. Vol. 238.

102. **Chesse, P.** *Determination des limites d'exploitation des diesel de forte puissance incidence des circuits de liaison moteur turbocompresseur instabilities et pompage des compresseur.* Nantes, France : PhD thesis, Ecole Centrale de Nantes, 1995.

103. *Influence of pre whirl centrifugal impeller performance.* **Gopalakrishnan, G and Rangaswamy, C.** 1974, Journal of the institution of engineers, India, pp. 1-4. Vol, 55.

104. *The use of compressor inlet pre-whirl for the control of small gas turbines.* **Shouman, A R and Anderson, J R.** 1964, Transactions ASME, pp. Vol, 86.

105. *Impeller Stalling as Influenced by Diffusion Limitations.* **Rodgers, C.** 1977, Transactions ASME , pp. 84-97.

106. *Centrifugal compressor inlet guide vanes for increased surge margin.* **Rodgers, C.** 1990, ASME, pp. Paper No. 90-GT-158.

107. *Experimental and theoretical performance of a radial flow turbocharger compressor with inlet pre-whirl.* **Whitfield, A, Wallace, F R and Ateky, C.** s.l. : IMecHE, 1975, Vols. 189, 43/75.

108. *Effect of prewhirl on the performance of centrifugal compresors.* **Najjar, Y S H and Akeel, S A M S.** 2002, International Journal of turbomachinery, pp. 397-401.

109. *Application of aerodynamically induced prewhirl to small turbocharger compressor.* **Kyrtatos, N and Watson, N.** 1980, ASME J Eng Power, pp. 934-950.

110. *The performance of a centrifugal compressor with high inlet pre swirl.* **Whitfield, A and Abdullah, A H.** 1998, ASME, pp. Paper No. 97-GT-182.

111. *Effects of variable inlet guide vanes on small centrifugal compressor performance.* **Ishino, M, Iwakiri, Y and Bessho, A.** 1999, ASME, pp. Paper 99-GT-157.

112. *Turbocharger compressor flow range improvement for future heavy duty diesel engines.* **Nikpour, B.** 2004. Thiesel conference on thermo-and fluid dynamics processes in diesel engines.

113. *Surge limit definition in a specific test bench for the characterization of automotive turbochargers.* **Galindo, J, Serrano, J R and C, Guardiola.** s.l. : Experimental Thermal and Fluid Science, 2006, Vols. Vol. 30. pp. 449-462.

114. *A discussion of the factors affecting surge in centrifugal compressors.* **Elder, S and Gill, A.** 1985, ASME Paper 84-GT-194.

115. **Uchida, H.** *Trends of turbochargin Technologies.* s.l. : R&D review Toyota, 2006. Vol 41, No.3.

116. *Performance analysis of a centrifugal compressor with variable inlet guide vanes.* **Xiao, J, Chuangang, G and Shu, X.** 2007, Frontiers of energy and power engineering in China, pp. 473-476. Vol, 1. Number 4.

117. *Performance prediction of an industrial centrifugal compressor inlet guide vane system.* **Coppinger, M and Swain, E.** 2000, IMechE, pp. 153-164.

118. **Steinke, R J and Crouse, J E.** *Preliminary analysis of the effectiveness of variable geometry guide vanes to control rotor-inlet flow conditions.* Cleceland, Ohio, USA : Lewis Research Center, 1967.

119. *Influence of various compressor inlet designs on compressor performance.* **Schulte, H, et al.** 2004. Proceeding of Thiesel Engine Conference. pp. 103-116.

120. **Kindl, H M.** *US2006/0042588A1* 2006.

121. **Rudolf, W, Leopold, E and Peter, N.** *DE102005019896* Bayerische Motoren Werke AG, 2006.

122. *Smart Inlet Guide Vanes for Active Flow Vectoring in an Axial Compressor.* **Willimas, D R and Cornelius, D.** San Francisco, California : s.n., 2006. 3rd AIAA flow control conference.

123. **Wimmer, R and Steindl, W.** *DE10250302* Bayerische Motoren Werke AG, 2004.

124. **Barker, D L.** *WO 2005/100798* Integral Powertrain, 2005.

125. **Mcdonald, G.** *GB.2391265* Imra Europe S.A.UK Research Centre, 2004.

126. www.Integral.com . [Online]

127. *Variable Area Turbocharger for High Output Diesel Engines.* **Bereyni, S G and Raffa, C J.** 1979. SAE paper No. 790064.

128. *Improvements in Performance Characteristics of Single-Stage andMultistage Centrifugal Compressors by Simultaneous Adjustments of Inlet Guide Vanes and Diffuser Vanes.* **Simon, H, Wallmann, T and Mönk, T.** s.l. : Trans ASME Journal of turbomachinery, 1987, Vol. 109, pp. 41-47.

129. *Centrifugal Compressor Development for a Variable Area Turbocharger.* **Harp, J L and Oatway, T P.** 1979, SAE paper No. 790066.

130. **Chapman, K S, Keshavaraz, A and Honegger, U.** *Numerical investigation of a turbocharger compressor with variable diffuser vane setting angle.* Kansas state : National Gas Machinery Laboratory,Kansas state University , 2003.

131. **Chapman, K S, Keshavarz, A and Honegger, U.** *Variable Geometry Turbocharger.* Virginia : Pipeline research Council International, Inc, 2007.

132. *Development of a centrifugal compressor with a variable geometry split-ring pipe diffuser.* **Salvage, J W.** s.l. : ASME, 1999, Vol. 121, pp. 295-304.

133. *The Effect of Variable Geometry on the Operating Range and Surge Margin of a Centrifugal Compressor.* **Whitfield, A, Wallace, F J and Atkey, R C.** 1976, ASME, pp. Paper No. 76-GT-98.

134. *The Effect of Vaneless DiffuserGeometry on the Surge Margin of Turbocharger Compressors.* **Whitfield, A and Sutton, A J.** 203, s.l. : IMechE, 1989, Vol. Journal of Automobile Engineering, pp. 91-98.

135. *The development of turbocharger compressors with improved surge margin.* **Whitfield, A, Wallace, F J and Sutton, A J.** s.l. : IMecH, 1991, pp. 9-12.

136. **Nestiel, K.** *US 6872050* York International Corporation, 2002.

137. *Study flow characteristics inducer bleed slot centrifugal compressor.* **Eynon, P A, Whitfield, A and Firth, M R.** 96-GT-262, s.l. : ASME International gas turbine annual aero engine, 1996.

138. *Improvements in Surge Margin for Centrifugal Compressors.* **Jansen, W, Carter, A F and Swarden, M C.** s.l. : AGARD CPP-282, 1980.

139. *Casing Modification for Increasing the Surge Margin of a Centrifugal Compressor in an Automotive Turbine Engine.* **Amann, C A.** pp:329-336, s.l. : Journal of Engineering Power, 1975, Vol. 97.

140. *The improvement of operating range in small, high speed, centrifugal compressor using casing treatments.* **Magdougal, I and Elder, R L.** 1982, IMecH, p. Paper C32/82.

141. *Numerical and experimental investigations of a centrifugal compressor with an inducer casing bleed system.* **Hunziker, R, Dickman, H P and Emmrich, R.** 2001, ImecH, pp. Vol, 215. Part A.

142. *The development of effective casing treatment for turbocharger compressors.* **Yamaguchi, N, et al.** 2002. IMecH seventh international conference.

143. **Nikpour, B.** *US 7229243 B2* 2007.

144. *An Examination of theMethods Used to Vary the Output of Centrifugal Compressors With Particular Reference to Part-Load Efficiency.* **Williams, R P.** London : s.n., 1989. IMecH European Conference: Developement of industrial compressors. pp. 37-48.

145. *Effects of geometry on the performance of radial vaneless diffuser.* **Yingkang, Z and Sjolander, S.** s.l. : Journal of Turbomachinery, Vol. 109, pp. 550-556.

146. *Experimental study of pinch vaneless diffuser of centrifugal compressor.* **Turunen-Saaresti, T, Grônman, A J and Jatinen, A.** Orlando : ASME Turbo EXPO, 2009. GT2009-60162.

147. *A new passive device to suppress several instabilities in turbomachines by use of J-grooves.* **Kurokawa, J, et al.** 1998.

148. *Experimental Investigation of Centrifugal Compressor Stabilization Techniques.* **Shoch, G J.** 2003, ASME, p. Vol. 125.

149. **Anthony, B.** *EP 1473463* Holset Engineering Co. Limited Huddershfield, 2006.

150. www.tecplot.com. [Online]

151. *Detection Of Surge Precursors In Locomotive Turbocharger.* **Menon, S, Furman, A and Krock, M.** s.l. : IEEE, 2006.

152. *Turbocharger Unstable Operation Diagnosis Using Vibroacoustic Measurements.* **Aretakis, N, et al.** s.l. : ASME, 2004, Vols. Vol. 126. pp: 840-847.

153. *Etude expérimentale du pompage des compresseurs centrifuges.* **Toussaint, M and De la Vallée, T.** Bucarest, Romanie : s.n., 2005. International conference Energy Environment CIEM.

154. **Devenport, W J.** *Laser Doppler Annemometry.* 2006.

155. *Laser Anemometry Measurement and Computation for transonic flow condition in annular cascade of high turning core turbine vanes.* **Coldman, L J.** 1993, Nasa technical paper.

156. *Laser Anemometry and Partical sizing.* **Darin, L E and Phil, M A D.** Manchester, U.K : s.n., 1985. International Conference on Laser Anemometry-Advances and Application.

157. *Sizing criteria for laser anemometry particles.* **Dring, R P.** 1982, Journal of Fluid Engineering, p. Vol 104/15.

158. *BSA Flow Software version 4.10: Reference guide.* 2006.

159. **Durst, F, Melling, A and Whitelaw, J H.** *Principles and Practice of Laser- Doppler Anemometry, 2nd Edition,.* London : Academic press, 1981.

160. *Describing the uncertainties in experimental results.* **Moffat, J M.** 1988, Experimental thermal and fluid science, pp. 3-17.

161. *Describing uncertainties in single sample experiments.* **Kline, S K and McClintock, F A.** 1953, IMecH, pp. 3-8.

162. **Kirkup, L.** *Calculating and expressing uncertainty in measurement.* New South Wales, Australia : Departement of applied physics faculty of science, , 2007.

163. **2045, VDI.** *Acceptance and performance tests on turbo compressors and displacement compressors.* s.l. : Duesseldorf, 1993.

164. **Burn, K and Nored, M G.** *Application guideline for centrifugal compressor surge control systems.* s.l. : Gas Machinery Council Southwest Research Institute, 2008.

165. **Dixon, S L.** *Fluid Mechanics thermodynamics of turbomachinery.* s.l. : Elsevier, Forth edition, 1998.

166. *Flow measurement behind inlet guide vane centrifugal compressor.* **Kasen, L and Rautenberg, M.** s.l. : International gas turbine and eroengine congress, ASME, 1998. 86.

167. *Passive control of rotating stall in a parallel-wall vaneless diffuser by radial grooves.* **Kurokawa, J, Saha, S L and Matsui, J.** 2000, ASME Journal of fuids engineering, pp. Vol, 122. 90-96.

168. *Effect of casing treatment and variable axial guide vanes on a turbocharger compressor performance.* **Mohtar, H, Chesse, P and Chalet, D.** Orlando : ASME Turbo Expo, 2009.

169. **Augnier, R H.** *Mean streamline aerodynamic performance analysis of centrifugal compressors.* 1995. pp. 360-366. Vol. 117.

170. www.sensortechnics.com . [Online]

171. www.acam-usa.com . [Online]